CHARGE-CHANGING COLLISIONS OF ENERGETIC HELIUM PROJECTILES PENETRATING THROUGH GASES

AKIO ITOH

1979

Department of Nuclear Engineering
Faculty of Engineering
Kyoto University

CHARGE-CHANGING COLLISIONS OF ENERGETIC HELIUM PROJECTILES PENETRATING THROUGH GASES

AKIO ITOH

1979

Department of Nuclear Engineering
Faculty of Engineering
Kyoto University

PREFACE

The phenomenon of capture of electrons by high speed alpha particles was first observed by Henderson in 1923, and this experimental evidence was examined in greater detail by Rutherford a year later. Since then, many experimental and theoretical investigations on charge-changing collisions have been performed. In recent years, particularly, research works have been extensively made along with the remarkable development of accelerators and their associated instruments.

One of the purposes for these active investigations may be responsible for the practical requirements, especially in the field of the controlled thermonuclear fusion research. Due to the complexity of the phenomena, however, systematic and full understanding of collision mechanisms have not been made hitherto. This is the case even for the light projectile ions such as hydrogen or helium.

This monograph is a thesis for the doctorate in engineering of Kyoto University. In this thesis, detailed investigations are devoted to the electron loss and capture processes of 0.7-2.0 MeV helium particles penetrating through eight kinds of target gases H_2, He, N_2, O_2, CO_2, CH_4, C_2H_6 and C_3H_8. Main purpose of this work is to study the medium dependences of charge-changing cross sections and of equilibrium charge distributions, and is to verify the applicability of the additive rule by a newly developed procedure.

AKNOWLEDGEMENTS

The author is greatly indebted to Professor F. Fukuzawa for the guidance, useful advices and constructive suggestions concerning all problems that arose during this investigation. Particular appreciation is also due to Professor M. Sakisaka for the valuable discussions and continuous encouragement. The author would like to express his deepest gratitude to Dr. M. Asari for the significant and useful suggestions throughout the course of this study.

Dr. M. Tomita and Dr. Y. Kido are also gratefully acknowledged for constructive discussions. Without their efforts, this work could not be completed.

The members of the author's group, Messers K. Ohnishi, K. Tsumaki, T. Ogawa, Y. Kanamori and Y. Haruyama, have been very helpful in performing the experiment. Appreciations are also given to Dr. N. Kobayashi and Dr. N. Maeda for the meaningful discussions.

All the experiments have been practised by using the 4 MV Van de Graaff accelerator of Kyoto University.
The associated instuments have also been used.
Therefore, his cooperative efforts of Mr. K. Norizawa in maintaining these apparatus are highly appreciated.

During preparation of this thesis, was held the *XI International Conference on the Physics of Electronic and Atomic Collisions* on 29th August – 4th September in Kyoto, where the author could have a chance to discuss with some foreign investi gators, whose data are referred in the present study, on charge-changing collisions. It is a great pleasure to express his sincere gratitude to Dr. P. Hvelplund, Dr. H.B. Gilbody,

Dr. S.C. Mukherjee, Dr. N.C. Sill and Dr. V.S. Nikolaev for their valuable suggestions.

Finally, the author wishes deeply to thank for his mother, wife, sister and brothers, including his eldest brother Seiji, who have given much support and supreme encouragement to continue learning and investigations.

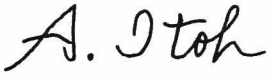

Akio Itoh

Kyoto
October 1979

CONTENTS

CHAPTER I

INTRODUCTION

When fast charged particles pass through a matter, not only do the incident particles excite (excitation process) or ionize (ionization process) the atoms or molecules in the matter, also the projectiles lose or capture some electrons in the collisions with the target substance (charge-changing process).
The investigations of these collision phenomena are quite significant for the fundamental understanding of the complicated mechanisms of atomic collisions.

In recent years, the specific efforts have been devoted to the controlled thermonuclear fusion research. One of the problems to be settled in the fusion research is the behaviours of impurity heavy ions in a magnetically confined high temperature plasma, which play an important role in the plasma cooling; the plasma would be cooled by the radiation process due to the massive impurity ions, and the neutralized particles resulted from the charge transfer process, escaping from the plasma, would produce the impure heavy atoms again in colliding with the reactor first-wall. Therefore, the systematic data of atomic collision processes such as excitation, dissociation, sputtering and charge-changing are demanded in order to understand the plasma in the reactors. Furthermore, for the study of influence of the radiations on the living bodies, there has been increasingly the need of understanding of these interactions at

the atomic or molecular levels.

In the past years, a large number of experimental and theoretical investigations have been made for these collision processes. The author and his co-workers have also made the experiments on the excitation, dissociation and charge-changing processes of various projectiles as well as protons in various target gases[1-3]. Due to the complexity of the phenomena, however, details of these collision mechanisms are in general not understood even at the present time other than the relatively simple cases.

The phenomena of charge-changing reactions have been awared for long in connection with the studies of the penetration of alpha-rays or fission fragments through matters.
According to the remarkable development of accelerators and their associated instruments in the field of atomic physics, a lot of investigations have been performed in recent years.
As the reviews of charge-changing data, Allison[4], Tawara and Russek[5] summarized the data of light projectiles such as hydrogen and helium, and the data of heavy ions are summarized in the review article by Betz[6]. The experimental results published in this last decade have not been summarized yet.
The projectile energies were, however, restricted to the lower range in most of these experiments, and there are only a few works in the higher energies. As to the projectile of helium, experimental charge-changing cross sections in the energy over 0.5 MeV are very few, and these values are not so reliable.

Theoretical treatments of the charge-changing process are

very cumbersome because of the possibility that the multiple electron loss or capture would occur on a single encounter as well as single electron transfer. Quantum mechanical calculations of the electron transfer cross sections have been made only for the simple collision processes of light projectiles (hydrogen or helium) in the target atom such as hydrogen, helium or hydrogen-like heavy ions. As regards the further complicated processes involving heavy ion projectiles, heavy target atoms or molecules, any exact calculations have not been carried out. For such a complicated phenomena, there are only qualitative descriptions which are usually based on physically reasonable but relatively arbitrary assumptions. In order to develop the theory of charge-changing collisions, it is necessary to accumulate systematically the experimental data.

This work is the experimental investigation of charge changing processes of helium projectiles in the energy range 0.7-2.0 MeV penetrating through various gases H_2, He, N_2, O_2, CO_2, CH_4, C_2H_6 and C_3H_8. The experiments have been performed by using 4-MV Van de Graaff accelerator of Kyoto University. Combinations of projectiles and target gases investigated in this work are given by open circles in the following list, where combinations denoted by x were not performed.

	Projectile											
Energy	0.7 MeV			1.0 MeV			1.5 MeV			2.0 MeV		
Charge	0	1	2	0	1	2	0	1	2	0	1	2
Target												
H_2	o	o	o	o	o	o	o	o	o	x	o	o
He	o	o	o	o	o	o	o	o	o	x	o	o
N_2	o	o	o	o	o	o	o	o	o	x	o	o
O_2	o	o	o	o	o	o	o	o	o	x	o	o
CO_2	o	o	o	o	o	o	o	o	o	x	o	o
CH_4	o	o	o	o	o	o	o	o	o	x	o	o
C_2H_6	o	o	o	o	x	x	o	o	o	x	x	x
C_3H_8	o	o	o	o	o	o	o	o	o	x	o	o

The following four basic features are involved in this study.

1] Experimental method.

The following problems must be solved in the charge-changing experiment.

i) How do we prepare the projectile beams with a monoenergy and with a pure single charge-state ?

ii) How do we localize the gaseous target in the collision chamber ?

iii) How do we derive the accurate charge-changing cross sections ?

Experimental technique for the problems i) and ii) are described in detail in this work. For the derivation of the cross sections, an *integration method* is newly developed in this work. In addition to this new method, some approximate methods are described including the slope method which is the roughest approximation and has been frequently used by previous investi gators. The cross sections derived from these methods are compared mutually to some extent.

2] Study of the cross sections.

The experimental and theoretical data by other investigators , which can be compared with the present data in the energy range from 0.7 to 2.0 MeV, are restricted to the target gases H_2, He and N_2 and the present cross sections for gases O_2, CO_2, CH_4, C_2H_6 and C_3H_8 are the original data. Present cross sections are also compared with the classical calculations and with the quantum mechanical ones. In particular, an extention of the theory of Bohr[24] is attempted, i.e., the charge-changing formulae derived by Bohr are modified so as to be applicable to all the single electron transfer cross sections of the helium projectiles. Furthermore, the quantum mechanical calculations are developed for the single electron loss processes (He^0 and He^+ projectiles in H and He target atoms) by assuming that the loss processes can be treated as the free electron scattering processes. This calculation model is same as the binary encounter approximation.

3] Verification of the additive rule.

As already mentioned above, theoretical treatments of the

process invloving multi-atomic molecules are very cumbersome and there is no reports on these collision processes. Nevertheless, these complicated processes would be largely simplified if a tractable method called *additive rule* (Bragg rule) could be applied. The additive rule was first stated by Bragg and Kleeman[7] in 1905 for the stopping powers of compound molecules. According to this rule, a compound molecule is assumed to appear as an assembly of individual atoms if the velocities of the projectile are much faster than the orbital velocities of the electrons forming the molecular bonds, whereby the molecular forces can be neglected. In this case, a cross section for the molecule is given by adding up the corresponding cross sections for the single atoms constituting the molecule.

It has been reported experimentally that the rule appears to hold reasonably well for a description of the energy loss process of projectiles in molecular targets[8]. In recent years, however, experimental results showing the deviation from the additive rule have been reported in the energy loss process[9,10]. As for the charge-changing collision, there are only a few experimental reports which refer to the additive rule. According to their reports, the additive rule holds for the proton and hydrogen projectiles[11,12], but not for the complex heavy ions of iodine[13]. These results show that the atomic structure of the projectile takes an important role for determination whether the chemical binding effects of the target molecules could be neglected or not.

In this thesis, is studied the applicability of this rule

for the helium charge-changing process with use of the experimental cross sections for gases H_2, hydro-carbon, O_2 and CO_2 molecules. For testing the rule, is proposed a new and simple method in this work. By applying the additive rule, cross sections for a carbon atom are estimated. This new method largely reduces the influence of experimental uncertainties of the cross sections in the estimation of carbon cross sections as compared with the *subtraction method* in which the carbon cross sections are estimated from two experimental cross sections, e.g., $\sigma(C) = \sigma(CO_2) - \sigma(O_2)$.

4] Study of the equilibrium charge state distributions.

Together with the cross sections, the equilibrium charge state distributions of helium beam in all the gaseous substances used in this experiment are studied in detail.

The data of equilibrium charge fractions is very important information for us to produce multi-charged ions in the heavy ion accelerators. Solid carbon-foils have been commonly used as charge-strippers. However, carbon foils are very fragile under low energy bombardment, so that much efforts have been directed towards a replacement for foils for many years. Recent works on the equilibrium fractions suggest that the average charge of heavy ions passing through a gas stripper composed of very high molecular weight shifts toward higher value much more than in usual gas materials[14,15]. In order to understand further deeply the medium dependence, it is necessary to examine systematically the average charges of various projectiles in various gases.

In chapter II, the experimental methods and procedure are presented. In chapter III, mathematical descriptions of charge fractions, some examples of the derivation of cross sections and, in particular, the data analysis of the present work are given in detail. In chapter IV, theoretical survey of the charge-changing processes is described. As a classical descriptions of the process, the first and extensive theory presented by Bohr[24] is reviewed and the modifications of the Bohr's theory is developed. Detailed descriptions of the quantum theoretical calculations carried out by the author is given; electron capture cross sections are calculated according to the Schiff's formula[16], and the loss cross sections are calculated on the basis of the free-electron-scattering model. Chapter V, VI and VII give the detailed discussions about the present experimental results for cross sections, additive rule and equilibrium fractions, respectively. The conclusive remarks are stated in chapter VIII.

Glossary of Symbols

The following list contains the symbols most frequently used in this article.

a_o	Bohr radius ($h^2/m_e e^2$ = 5.29 x 10^{-9} cm)
e	Magnitude of electron charge
E	Projectile energy
F_q	Equilibrium fraction of charge-state q
$\phi_{qq'}$	Nonequilibrium charge fraction of state q' when the charge state of the initial beam is q
I	Ionization potential
m_e	Electron mass
N_q	Number of particles in charge-state q detected by PSD
ν	Principal quantum number
ρ	Target gas density in number/cm^3
$\bar{q}$	Average equilibrium charge of ions
s	Number of electrons carried by the projectile before a single charge-changing collision
$\sigma_{qq'}$	Cross section for a charge changing process $q \rightarrow q'$ of the projectile in a single encounter, in cm^2/molecule
u	Orbital velocity of an electron
v	Projectile velocity
v_o	Bohr velocity (e^2/h = 2.188 x 10^8 cm/sec)
x	Target thickness in molecules/cm^2
Z	Atomic number of projectile
Z_T	Atomic number of target atom

CHAPTER II

EXPERIMENTAL METHOD

2-1. Introduction

In this chapter, the experimental set-up used for the charge-changing collisions of 0.7-2.0 MeV helium beams are described. In Fig. 2-1, is shown the experimental arrangement which consists of three fundamental parts; beam preparation system, target chamber, and detection system. Details of these parts are presented in the following three sections.

2-2. Beam Preparation

In the charge-changing experiments, it is sometimes necessary to vary the initial charge state of incident beams in order to obtain the various charge-changing cross sections. In cases of He^+ and He^{2+} incidences, the ion beams obtained from an accelerator are often used as incident beams. As for the incident beam of neutral helium He^0, ion beams from the accelerator are partly neutralized by an appropriate neutralizer set before a collision chamber, and by taking away the charged particles in the beam by an electrostatic or a magnetic deflector only the neutral particles are led into the collision chamber. In the present experiment, these usual methods are suitable for the cases of He^0 incidence, but not for the ion beam incidences

because of the following practical reasons. The first is that the amount of doubly charged helium ion He^{2+} produced in an ion source is very little since a PIG-type ion source is used. The second is that an ion beam which is initially in a pure charge state becomes to be mixed with unnecessary different charge state particles as a result of charge-changing collisions with the residual gas until the beam enters the collision chamber.

In this work, therefore, only the singly charged helium ion He^{+} was extracted from the 4-MV Van de Graaff accelerator, and the desired charge state beams were produced by the following method.

i) Preparation of He^{+} and He^{2+} beams.

He^{+} beam mixed with different charge state components during collisions with residual gas after the accelerator was led into the deflection chamber consisting of electrostatic deflectors. Both of the knife-edged entrance and exit slits (C1, C2) of the chamber are 0.1 x0.1 mm^2-hole, and the deflector plates (E1) are 10 cm-long and 1 cm-gap distance. The beam collimated by the entrance slit were separated into three trajectories according to charge states of particles in the beam by applying the voltage to the deflector. The applied voltage was changed in satisfying the condition, qV_d/V_o = 1.25 (kV/MV), according to the incident energy and to the desired charge state ions. The deflection angle was about $7x10^{-3}$ rad. In this relation, V_d(kV) is the applied voltage of the electrostatic

deflector, V_0(MV) is the terminal voltage of the Van de Graaff accelerator, and q is the desired charge state of the ions; q = 1 for He^+, q = 2 for He^{2+}. This condition was most suitable in order to pass only the desired charge state ion beam through the fixed exit slit of the deflection chamber.
A single charge state beam from the deflection chamber was led into the following apparatus.

ii) Preparation of He^0 beam.

In this case, a neutralizer cell just after the deflection chamber was filled with nitrogen gas of about 5 x 10^{-3} Torr. This cell is 20 cm-long and the exit aperture (A1) is 5 mm-diam. and 10 cm-long. He^+ beam selected by the above procedure i) was passed through this neutralizer cell, and then the charged components in the beam were electrostatically deflected by the deflector (E2) in front of the target chamber. The distance from the exit aperture (A1) of the neutralizer cell to the entrance aperture (A3) of the target chamber is about 100 cm.

2-3. Target Chamber and Vacuum System

Vacuum system takes an important role in the charge-changing experiment. At first, it should be necessary to reduce the background gas pressure as low as possible. Second, due to the windowless target chamber, it should be necessary to limit the increase of the pressure in the portions other than the target chamber when the target gas pressure increases.

Both of these factors largely influence the cross section derivations in the data analysis. In this work, therefore, the double-differentially pumping was employed.
Apertures A2 – A5 are all 2 mm-diam. and 10 mm-long and had threaded inner surfaces in order to decrease the edge scattering. Each of these apertures could give a pressure gradient of approximately $1:10^3$. In actual case, for example, when the gas pressure in the target chamber(III) was 0.1 Torr, those in portions II and IV were less than 1×10^{-4} Torr, while those in the portions I and V did not change practically from the background pressure of about 2×10^{-6} Torr.

The target thickness x in the charge-changing process is given by,

$$x = \int_0^{L_0} \rho(L)\mathrm{d}L \qquad (2.1)$$

where the lower limit of the integration is, $L = 0$, the position where the desired charge state beam was selected and the upper limit $L = L_0$ is a distance from $L = 0$ to the position of the detector, $\rho(L)$ is the gas density at the distance L in the beam line. In practical case, the formula (2.1) can be approximated by

$$x = \sum_i \rho_i L_i = \rho_{\mathrm{I}} L_{\mathrm{I}} + \rho_{\mathrm{II}} L_{\mathrm{II}} + \cdots + \rho_{\mathrm{V}} L_{\mathrm{V}} \qquad (2.2)$$

where ρ_i is the measured gas density in the i-th beam transport duct, and L_i is the length of the duct. The target thickness

is, therefore, calculated from the formula (2.2) by using the data of ρ_i and L_i. In this work, gas pressure and lengths in all these portions were measured, and the target thickness was finally approximated by $x \simeq \rho L_{eff}$, where ρ and L_{eff} are the gas density and an effective chamber length of the target chamber, respectively. This approximation is based on the following reasons.

1) As mentioned above, the pressure in the portions other than the target chamber was significantly low.
2) In the derivation of cross sections, only substantial quantities of fractions resulted from collisions with pure target gas are used by subtracting the unnecessary fractions $\phi(x_0)$ resulted from the collisions with residual gas (detail of the derivation method of cross sections will be described in the next chapter).

These two evidences indicate that the effects due to the residual gas of the order of magnitude $\sim 10^{-6}$ Torr are not the matter in practice. The problem is the effect of target gas flowing out of the entrance or exit apertures of the target chamber rather than the residual gas effects. By the rough estimation of the gas-flowing out of a cylindrical slit of 2 mm-diam and 10 mm-long, it is shown that the gas density relative to that in the target cell is about 0.1 at the surface of aperture and below 10^{-3} at the place a few millimeter apart from the surface. Then, by taking account of these results, the effective length of the target chamber was estimated 17 cm, which is the sum of the actual chamber length 16 cm and two half-lengths of entrance

and exit apertures. The errors due to this treatment was estimated to be less than a few percent in the cross section derivation.

Finally, the target thickness at the room temperature, the following formula was obtained after calculating the relations between gas density (molecules/cm^3) and gas pressure P (Torr),

$$x = 3.35 \times 10^{16} PL_{eff} = 6.70 \times 10^{17} \text{ (molecules/cm}^2\text{)} \quad (2.3)$$

Target gases used in this experiment are H_2, He, N_2, O_2, CO_2, CH_4, C_2H_6 and C_3H_8. Pressure measurements were performed by an ionization gauge and a Pirani gauge, both of these gauges are calibrated for N_2 gas. As the relative sensitivities of the ionization gauge for other gases, the values tabulated in the Table II-1 were used[71]. The gas pressure was changed from about 1×10^{-5} Torr to the range where the equilibrium charge fractions could be seen.

2-4. Detection System

The particles with various charge states emerging from the target chamber were spatially separated by an electrostatic deflector (E3), and were detected by a position-sensitive-detector (PSD). The electronics of the detection system is shown in Fig. 2-2. An example of energy signal spectrum from the PSD is shown in Fig. 2-3. The edge-scattering could be almost completely got rid of by an appropriate adjustment of all the

slits in the beam transports. Position-signal from the PSD is proportional to both the projectile energy and a particle detected position, and examples of position spectra are shown in Fig. 2-4. These spectra were obtained for 0.7 MeV He^0, He^+ and He^{2+} incidences on oxygen gas at 3.5×10^{-3} Torr. In this experiment, the number of incident particles was about 400 cps and, therefore, the counting loss or pile-up of the detection system could be neglected.

In actual experimental conditions, it was sometimes difficult to distinguish the low pulse height signal (He^0) from the background noise in the position spectra. Therefore, the following coincidence technique was used. The energy output from the PSD was discriminated within the range between two arrows (see Fig. 2-3) by the single channel analyzer (SCA). An output pulse from the SCA was led into the pulse generator which produces an suitable pulse as a coincidence input. The timing between the energy and position pulse was taken by using the delay circuit. The coincidence technique made it possible to distinguish the neutral helium particles from the background in the lower pulse range, leaving only random coincidenced signals. The errors in the charge fraction calculations due to the random coincidence were, however, negligibly small because the total beam counts per experimental run were very large; in the range from 5×10^4 to 20×10^4. In this case, the number of particles with the smallest charge fraction were larger than about 100.

The charge fractions ϕ_q is calculated by the formula,

$$\phi_q = N_q \,/\, \sum_q N_q = N_q \,/\, N_{tot} \qquad (2.\ 3)$$

where N_q is the number of particles in charge state q, N_{tot} is the total beam counts. Statistical errors of the fractions are determined by

$$\Delta\phi_q/\phi_q = (N_q^{-1} + N_{tot}^{-1})^{1/2} \qquad (2.\ 4)$$

CHAPTER III

DATA ANALYSIS

3-1. Nonequilibrium Charge Fractions

In this section, mathematical descriptions of the variation of charge fractions with target thickness are given and several methods of derivation of charge-changing cross sections are also given (more detailed methematical descriptions of charge fractions are given in the articles by Allison[4], Betz[6] or Nikolaev[17]).

When a particle collides with atom or molecule in a target substance, the particle may lose or capture one or more electrons from the target particle. The charge-changing cross section $\sigma_{qq'}$ represents a cross section for the process where the incident particle of charge state q changes into another state q' on a single encounter. The variation of the charge fraction of the incident beam with charge q penetrating through gaseous target of thickness x is described by a differential equations,

$$d\phi_{qq'}(x)/dx = \sum_k \phi_{qk}(x)\sigma_{kq'}$$

$$\sigma_{qq} \equiv - \sum_{q' \neq q} \sigma_{qq'} \qquad (3.1)$$

where $\phi_{qk}(x)$ denotes the fraction of the particles with charge k.

For the two components beam fraction ($q = 1,2$), exact solution of Eq.(3.1) can be obtained simply in the following form.

$$\phi_{12}(x) = \sigma_{12}/\sigma + (\phi_{12}(x_0) - \sigma_{12}/\sigma)exp\{-\sigma(x-x_0)\}$$

$$\phi_{21}(x) = \sigma_{21}/\sigma + (\phi_{21}(x_0) - \sigma_{21}/\sigma)exp\{-\sigma(x-x_0)\}$$

$$\phi_{11}(x) = 1 - \phi_{12}(x), \quad \phi_{22}(x) = 1 - \phi_{21}(x) \qquad (3.2)$$

where the quantity $\phi(x_0)$ is the fraction at the target thickness x_0, and σ is the sum of two cross sections; $\sigma \equiv \sigma_{12} + \sigma_{21}$. Eq. (3.2) reduces to a well-known formula as presented by Allison if taken $x_0 = 0$.

As for the three components beam fractions, the direct solution of Eq. (3.1) is very cumbersome. For example, the exact solution given by Allison is not tractable in practice. Therefore, the practical interest is how to obtain an approximate solution of Eq. (3.1). In the following subsections, the two representative approximations(slope method, iteration method) which have been often used by other investigators and a direct integration method which is newly proposed in this study are described. All of these approximations are able to be used in the relatively low gas pressure region which is so-called single collision region.

3-1-1. Slope Method

In this approximation, the background gas thickness, which will be denoted by x_0 as corresponding to background gas pressure, is approximated to be zero, and the charge fractions at the thickness x_0 is approximated by

$$\phi_{qq'}(x_0)\Big|_{x_0=0} = \delta_{qq'} \begin{cases} =1 & \text{for } q'=q \\ =0 & \text{for } q'\neq q \end{cases} \tag{3.3}$$

Eq. (3.3) is substituted into the right hand side of Eq. (3.1) and one obtains

$$d\phi_{qq'}(x)/dx = \sum_k \delta_{qk}\sigma_{kq'} = \sigma_{qq'} \tag{3.4}$$

consequently,

$$\phi_{qq'}(x) = \delta_{qq'} + \sigma_{qq'}x \tag{3.5}$$

As pointed out by Datz *et al*[18], the slope method can be used only if the following experimental conditions are satisfied:
i) A pure charge state has to be selected for the incident beam (Eq.(3.3)).
ii) The total amount of any residual gas must be so small that its effect on the incident beam is negligible even for the smallest target thickness.
In actual experiments, it is sometimes difficult to satisfy the above conditions. Therefore, some modifications should be

necessary to the simplest slope method Eq. (3.5)

3-1-2. Iteration Method

The slope method is modified into the following form by taking account of the actual experimental cases; $x_0 \neq 0$, and $\phi_{qq'}(x_0) = \delta_{qq'}$. Instead of $\delta_{qq'}$, quantities $\phi_{qq'}(x_0)$ must be substituted into the right hand side of Eq. (3.1),

$$d\phi_{qq'}(x)/dx = \sum_k \phi_{qk}(x_0)\sigma_{kq'} \tag{3.6}$$

and the solution of this equation is

$$\phi_{qq'}(x) = \phi_{qq'}(x_0) + \sum_k \phi_{qk}(x_0)\sigma_{kq'}[x - x_0] \tag{3.7}$$

Eq. (3.7) will be called the first-order-approximation in the following. By substituting this solution into the right hand side of Eq. (3.1)

$$d\phi_{qq'}(x)/dx = \sum_k \{\phi_{qk}(x_0) + \sum_{k'} \phi_{qk'}(x_0)\sigma_{k'k}[x - x_0]\}\sigma_{kq'} \tag{3.8}$$

By solving this equation, the second-order-approximation is obtained in the form,

$$\phi_{qq'}(x) = \phi_{qq'}(x_0) + \sum_k \phi_{qk}(x_0)\sigma_{kq'}[x - x_0] + (1/2)\sum_k \sum_{k'} \phi_{qk'}(x_0)\sigma_{k'k}\sigma_{kq'}[x - x_0]^2 \tag{3.9}$$

The higher-order-approximations can be obtained by iterating this procedure. However, they will have very complicated forms. Therefore, it is necessary to express charge fraction by another form in order to derive the charge-changing cross sections more easily.

3-1-3. Direct Integration Method

In this method, the Eq. (3.1) is integrated directly from the thickness x_0 to x, and one obtains

$$\phi_{qq'}(x) - \phi_{qq'}(x_0) = \sum_k \{\int_{x_0}^{x} \phi_{qk}(x)dx\}\sigma_{kq'} \qquad (3.10)$$

By applying the mean value theorem to the integral in the Eq. (3.10), the solution in the direct integration method is obtained in the following formula,

$$\phi_{qq'}(x) - \phi_{qq'}(x_0) = \sum_k \phi_{qk}(\bar{x})\sigma_{kq'}[x - x_0] \qquad (3.11)$$

$$(x_0 \leq \bar{x} \leq x)$$

The integration method does not contain any approximations, and , therefore, the formula (3.11) can be applied in principle to all the target thickness region.

As the simplest case, the Eq. (3.11) was applied to the range where all charge fractions change linearly with the target thickness. In this region, the quantity $\phi_{qk}(\bar{x})$ in Eq. (3.11)

can be approximated by $(\phi_{qk}(x_0) + \phi_{qk}(x))/2$. when $\phi_{qk}(x)$ in the bracket of this formula is expressed by the first-order-approximation Eq. (3.7), Eq. (3.11) reduces to the following formula.

$$\phi_{qq'}(x) - \phi_{qq'}(x_0) = \sum_k \phi_{qk}(x_0)\sigma_{kq'}[x - x_0] +$$

$$+ (1/2) \sum_k \sum_{k'} \phi_{qk'}(x_0)\sigma_{k'k}\sigma_{kq'}[x - x_0]^2 \qquad (3.12)$$

This is just the same as the second-order-approximation Eq.(3.9). In other words, this result shows that the strict solution (3.11) obtained in the direct integration method contains the approximate solutions obtained in the iteration method. It is easy to see that the Eq. (3.11) is much simpler than the second-order-approximation Eq. (3.9). From this reason, using the solutions (3.10) or (3.11) is the best way for the derivation of charge-changing cross sections.

3-2. Equilibrium Charge Fractions

As the pressure of target gas becomes higher, the balance between electron loss and capture processes will be established after undergoing several times encounters and all the charge fractions will not change any more. In this case, the left hand side of Eq. (3.1) becomes zero, so that

$$\sum_q F_q \sigma_{qq'} = 0 \qquad (3.13)$$

where F_q is defined as the equilibrium charge fractions with charge q.

In the case of helium beam, Eq. (3.13) gives the following relations.

$$\begin{aligned} F_0\sigma_{00} + F_1\sigma_{10} + F_2\sigma_{20} &= 0 \\ F_0\sigma_{01} + F_1\sigma_{11} + F_2\sigma_{21} &= 0 \\ F_0\sigma_{02} + F_1\sigma_{12} + F_2\sigma_{22} &= 0 \end{aligned} \tag{3.14}$$

From the above equations, three equilibrium fractions can be expressed in terms of cross sections in the forms

$$\begin{aligned} F_0 &= (\sigma_{21}\sigma_{10} + \sigma_{12}\sigma_{20} + \sigma_{10}\sigma_{20})/D \\ F_1 &= (\sigma_{20}\sigma_{01} + \sigma_{02}\sigma_{21} + \sigma_{01}\sigma_{21})/D \\ F_2 &= (\sigma_{10}\sigma_{02} + \sigma_{01}\sigma_{12} + \sigma_{02}\sigma_{12})/D \end{aligned} \tag{3.15}$$

with

$$\begin{aligned} D = {} & \sigma_{12}(\sigma_{01} + \sigma_{02} + \sigma_{20}) + \sigma_{10}(\sigma_{20} + \sigma_{21} + \sigma_{02}) + \\ & + \sigma_{21}(\sigma_{01} + \sigma_{02}) + \sigma_{20}\sigma_{01} \end{aligned} \tag{3.16}$$

In the high incident energy region, neutral fraction F_0 of the helium beam is, in general, very small and by neglecting the neurtral parts in Eq. (3.13) the equilibrium fractions F_1 and F_2 can be approximated by

$$F_1 = \sigma_{21}/(\sigma_{12} + \sigma_{21})$$

$$F_2 = \sigma_{12}/(\sigma_{12} + \sigma_{21}) \qquad (3.17)$$

Equilibrium fractions can then be computed numerically according to Eqs. (3.15) or (3.17) if the cross sections are known.
As increases the atomic number of incident particle, it becomes difficult to obtain all the charge changing cross sections necessary to the calculation of equilibrium fractions.
Therefore, some approximations have been proposed for the expressions of equilibrium charge fractions[6,19]. It has been shown experimentally that the equilibrium charge distributions can be represented by a Gaussian type. According to this expression,

$$F_q = (2\pi d^2)^{-1/2} \exp[-(q - \bar{q})^2/2d^2] \qquad (3.18)$$

where $\bar{q}$ is the average equilibrium charge, which is given by

$$\bar{q} = \sum_q qF_q \qquad (3.19)$$

and d is the half width of the distributions,

$$d = \{\sum_q (q - \bar{q})^2 F_q\}^{1/2} \qquad (3.20)$$

The equilibrium charge fractions are expressed in terms of two quantities $\bar{q}$ and d instead of cross sections.

Therefore, if the theoretical expressions are given to $\bar{q}$ and d, unknown equilibrium fractions of heavy projectiles will be predicted theoretically. Many investigators have proposed the theoretical expressions of $\bar{q}$ and d. For instance, Dmitriev and Nikolaev[20] derived the following semi-empirical formulae for these quantities by using the experimental data up to that time.

$$\bar{q}/Z = log(v/mZ^{\alpha_1})/log(nZ^{\alpha_2}), \quad (0.3 \leqq \bar{q}/Z \leqq 0.9) \tag{3.21}$$

$$d = d_o Z^k, \quad k = \{1 - \alpha_2/ln(nZ^{\alpha_2})\}/2 \tag{3.22}$$

where v is the projectile velocity in unit of 10^8 cm/sec. The parameters α_1, α_2, m, n and d_o in Eqs. (3.21) and (3.22), which are experimentally determined, are presented for projectiles with atomic number $Z < 10$ in the following list.

List of parameters for the semiempirical formula Eqs.(3.21) and (3.22) given by Dmitriev and Nikolaev[20].

Medium	α_1	α_2	m	n	k	d_o
H_2	0.4	0.3	1.2	4.0	0.43	
He	0.4	0.3	1.3	4.5	0.43	0.35
N_2	0.4	0.3	0.9	7.0	0.45	0.32
solid	0.1	0.6	1.2	5.0	0.40	0.38

3-3. Data Treatment and Analysis

Measured charge fractions of helium beam (growth curves) are shown in Fig. 3-1(1)-(30) as a function of target thickness in unit of Torr·cm. All the fractions $\phi_{qq'}$, with $q' \neq q$ at lowest gas thickness are smaller than several percent. Charge fractions change gradually with increasing the target thickness, and finally settle down at constant values of each charge fraction called equilibrium charge fractions. It can be seen that these constant fractions are determined solely by the incident helium energy, and independent of the kind of charge state of the incident beam.

In these figures, the data in the pressure region monitored by the ionization gauge and those in the pressure region monitored by the Pirani gauge are connected suitably by shifting the latter data to the former one because of the lack of relative sensitivities of the Pirani gauge for the gases used in the experiment.

All the charge fractions in the lower target thickness are found to change linearly with thickness x. An example of the linear variations of charge fractions (1.5 MeV He^+ on He) are shown in Fig. 3-2 by plotting them in linear-linear scale. Therefore, the charge fractions in the linear range may be approximated sufficiently by the mathematical expressions containing x to a first order as described in section 3-1.

In this work, however, the following three methods are used for the derivation of charge-changing cross sections.

α) The first-order-approximation Eq. (3.7) in the iteration method.

β) The following further approximation of Eq. (3.7), that is,

$$\phi_{qq'}(x) = \phi_{qq'}(x_0) + \phi_{qq}(x_0)\sigma_{qq'}[x - x_0] \qquad (3.7)'$$

This formula was obtained by neglecting $\phi_{qk}(x_0)$ with $k \neq q$ in the second term of the right hand side of Eq. (3.7).

γ) The strict solution Eq. (3.11) in the direct integration method.

In the cases of the former two methods α) and β), only the linear part of fractions were used under the condition that the incident fraction $\phi_{qq}(x)$ is larger than 0.8. The third method γ) can be applied for all the part of growth curves in principle, but in this work the fractions which begin to lose its linearity were taken as the upper limit of the integration.

In all cases of above three methods, charge fractions at the lowest target thickness x_0 in corresponding growth curves were used as $\phi_{qq'}(x_0)$ in Eqs. (3.7), (3.7)' and (3.11). Therefore, the quantities, $\phi_{qq'}(x) - \phi_{qq'}(x_0)$, represent the substantial changes only due to the change of target gas under considerations.

The method β) is the simplest of above three methods. In this case the charge-changing cross sections $\sigma_{qq'}$ can be obtained directly by the slope, $\phi_{qq}(x_0)\sigma_{qq'}$, of growth curves. The straight lines in Fig. 3-2 were determined by least-square fitting procedure. In the method α) and γ), three unknown cross sections are contained in each fraction equation.

Therefore, it is necessary to solve a series of simultaneous equations in order to obtain the cross sections. For instance, Eq. (3.7) is written for the case of He^+ incidene as follows.

$$\phi_{10}(x) = \phi_{10}(x_0) + \{\phi_{10}(x_0)\sigma_{00} + \phi_{11}(x_0)\sigma_{10} + \phi_{12}(x_0)\sigma_{20}\}[x - x_0]$$

$$\phi_{11}(x) = \phi_{11}(x_0) + \{\phi_{10}(x_0)\sigma_{01} + \phi_{11}(x_0)\sigma_{11} + \phi_{12}(x_0)\sigma_{21}\}[x - x_0]$$

$$\phi_{12}(x) = \phi_{12}(x_0) + \{\phi_{10}(x_0)\sigma_{02} + \phi_{11}(x_0)\sigma_{12} + \phi_{12}(x_0)\sigma_{22}\}[x - x_0] \tag{3.23}$$

In these formulae, σ_{00}, σ_{11} and σ_{22} are not independent qunatities (e.g. $\sigma_{11} = -(\sigma_{10} + \sigma_{12})$), but are treated as independent ones for convenience.

Similar equations are obtained for He^0 or He^{2+} incidences. The slope, $\sum_k \phi_{qk}(x_0)\sigma_{kq}$, of each growth curve of $\phi_{qq'}(x)$ can be determined by the least-square-fitting, and is denoted by $Q_{qq'}$ in the following. The qunatities $Q_{qq'}$, $\phi_{qq'}(x_0)$ and $\sigma_{qq'}$ form the following matrix equation,

$$Q = \Phi\sigma \tag{3.24}$$

or

$$\begin{pmatrix} Q_{00} & Q_{01} & Q_{02} \\ Q_{10} & Q_{11} & Q_{12} \\ Q_{20} & Q_{21} & Q_{22} \end{pmatrix} = \begin{pmatrix} \phi_{00} & \phi_{01} & \phi_{02} \\ \phi_{10} & \phi_{11} & \phi_{12} \\ \phi_{20} & \phi_{21} & \phi_{22} \end{pmatrix} \cdot \begin{pmatrix} \sigma_{00} & \sigma_{01} & \sigma_{02} \\ \sigma_{10} & \sigma_{11} & \sigma_{12} \\ \sigma_{20} & \sigma_{21} & \sigma_{22} \end{pmatrix} \tag{3.25}$$

The cross sections can then be calculated by

$$\sigma = \Phi^{-1} Q$$

In the case of direct integration method γ), similar equation to Eq. (3.24) is derived[22]. Cross sections derived by these three methods were found to be in good agreement with one another within experimental errors.

For 2 MeV incidence, the following formulae are used for fractions.

$$\phi_{12}(x) = \phi_{12}(x_0) + (\phi_{11}(x_0)\sigma_{12} - \phi_{12}(x_0)\sigma_{21})[x - x_0]$$

$$\phi_{21}(x) = \phi_{21}(x_0) + (\phi_{22}(x_0)\sigma_{21} - \phi_{21}(x_0)\sigma_{12})[x - x_0] \qquad (3.26)$$

because the dominant fractions are only charged components ϕ_1 and ϕ_2. By similar procedures as mentioned above, the cross sections σ_{12} and σ_{21} were derived. Cross sections σ_{01} and σ_{02} were not obtained since the experiments on He^0 projectile were not made in this work.

In addition to this method, the following one was used, too. In Eq. (3.2), which is the strict solution of two-components differential equations, the quantities σ_{21}/σ and σ_{12}/σ are exactly equivalent to the equilibrium charge fractions F_1 and F_2, respectively, given by Eq. (3.17). Therefore, Eq. (3.2) can be rewritten in the following form by using the experimentally-obtained equilibrium fractions F_1 and F_2,

$$\phi_{qq'}(x) = F_{q'} + (\phi_{qq'}(x_0) - F_{q'})exp[-\sigma(x - x_0)] \qquad (3.27)$$

where the unknown quantity is only $\sigma(= \sigma_{12} + \sigma_{21})$, and it is

calculated by fitting the above formula to the growth curves. Next, with the relations $\sigma_{12} = \sigma F_2$ and $\sigma_{21} = \sigma F_1$, the each cross section can be derived. Cross sections obtained by this method were in good agreement with those obtained by using the Eq. (3.26).

Experimental uncertainties of the obtained cross sections are caused by the followings;

i) pressure fluctuations,

ii) uncertainties of relative sensitivities of the ionization gauge (Table II-1),

iii) estimation of the effective length of the collision chamber, and

iv) counting statistics of the detection system.

Counting statistics $\Delta\phi_{qq'}$ are the order of magnitude as the error bars in the figures of growth curves, and must be taken into account only for the cases of ϕ_{20} or ϕ_{10}.
As mentioned previously, the obtained cross sections agreed within errors in all the derivation methods α)-γ).
From this fact, estimation of errors were carried out for the method β) as in the following. Eq. (3.23) is rewritten by

$$\{\phi_{qq'}(x) - \phi_{qq'}(x_0)\}/\phi_{qq}(x_0) = \sigma_{qq'}[x - x_0] \qquad (3.28)$$

which will be denoted by $m_i = \sigma x_i$, i stands for the run-number of experimental data. By using the least square technique, the cross section is calculated by

$$\sigma = \sum_i x_i m_i \; / \; \sum_i x_i^2 \tag{3.29}$$

and the uncertainty $\Delta\sigma$ of the cross section is determined by

$$(\Delta\sigma)^2 = \sum_i \{(\frac{\delta\sigma}{\delta m_i}\Delta m_i)^2 + (\frac{\delta\sigma}{\delta x_i}\Delta x_i)^2$$

$$= \sum_i \{(\frac{x_i}{\sum_i x_i^2})^2 + k^2[\frac{(m_i x_i)\sum_i x_i^2 - 2x_i^2(\sum_i m_i x_i)}{(\sum_i x_i^2)^2}]^2\} \tag{3.30}$$

where $\Delta x_i = k x_i$ corresponds to the uncertainty of target thickness caused by the uncertainty k of relative sensitivity, which are listed in Table II-1, and Δm_i is the errors determined by the right hand side of the Eq. (3.24), and square of it is written by

$$(\Delta m_i)^2 = \{(\Delta\phi_{qq'}(x))^2 + (\Delta\phi_{qq'}(x_0))^2\}/\{\phi_{qq'}(x_0)\}^2 +$$

$$+ \{[\phi_{qq'}(x) - \phi_{qq'}(x_0)]^2/[\phi_{qq'}(x_0)]^2\}\{\Delta\phi_{qq'}(x_0)\}^2 \tag{3.31}$$

Actual calculations were made only for the first term of this formula since the counting statistics $\Delta\phi_{qq'}(x_0)$ in the second term are almost zero in practice.

Solid curves presented in the growth curves in Fig. 3-1(1) -(30) are the calculated fractions by using the cross sections derived by the above procedures.

For 2 MeV incidence, computations were made by the formula (3.2), which is strict solution of the two-components differential equations. For 0.7-1.5 MeV incidences, charge fractions were computed by applying the Runge-Kutta integration method to the original differential equation (3.1). All the numerical computations of growth curves have been performed on the *FACOM M-190* of Kyoto University. The program code is presented in the last pages of this thesis.

In the stage of the computations, the uncertainties of the cross sections were not taken into consideration. Therefore, in some cases, calculated values deviated somewhat largely from the experimental data, especially in high pressure region. In order to check the agreement between them, the author computed the growth curves by using the cross sections containing uncertainties of 10 percent and found that the computed values were in agreement with experimental data very well.

CHAPTER IV

THEORETICAL STUDIES

4-1. Introduction

The processes involved in the capture and loss of electrons between the projectile and the target atoms or molecules are in general so intricate as to make precise and comprehensive description. Even at the present time the quantum mechanical calculations of the cahrge-changing cross sections have been carried out only for the simplest cases, such as for hydrogen or helium ions passing through atomic hydrogen or helium, and relatively good agreement could be obtained between theory and experimental results. As for a heavy target atom with many electrons, there are few quantum theoretical calculations even for the lightest ions like hydrogen or helium[23], needless to say for heavy ions. Nevertheless, it is expected to be able to get over-all pictures of charge transfer process to some extent from a classical point of view. In fact, from the classical and statistical arguments Bohr[24] presented the theoretical pictures of the charge transfer process.

Afterwards, Bell[19], Bohr and Lindhard[25], Gluckstern[26], Nikolaev[17,27] and Dmitriev[28,29] modified the Bohr's theory particularly for the heavy ion incidence so as to make close the theoretical values to the experimental ones.
However, it is not too much to say that their arguments are

nothing but the *'modifications'* of the first extensive theory of Bohr. The major part of the theoretical treatments given by Bohr and by other authors has been based on Physically reasonable but relatively arbitrary assumptions and,accordingly, the applications of these theories are limited to the restricted region of the basic collision parameters Z, Z_T and v. Furthermore, all of these theories have been limited to a single electron capture and loss. Therefore, it is impossible to apply these calculations to the processes where the multiple electron transfer takes place on a single encounter.

In this chapter, the over-all pictures of charge-changing process of light projectiles are described on the basis of Bohr's theory. Next, the quantum mechanical calculations are given for the following processes;

$$He^0 + A \rightarrow He^+ + A + e$$
$$He^+ + A \rightarrow He^{2+} + A + e$$
$$He^{2+} + A \rightarrow He^+ + A^+$$

where A stands for the target atoms H and He.
Descriptions for the heavy projectiles, which are given in articles by Betz[6] or Nikolaev[17], are excluded from this thesis.

4-2. Classical Theory

4-2-1. Theory of Bohr

Elastic collisions between two particles with no electron can be described by a Rutherford scattering. The cross sec-

tion of the collision process where incident particle, with mass m_1, charge e_1 and velocity v, transfers a kinetic energy in the range $(T,\ T + dT)$ to the target tarticle with m_1 and e_2 is given by reforming the Rutherford scattering formula in the form,

$$d\sigma = \frac{2\pi(e_1 e_2)^2}{m_2 v^2} \frac{dT}{T^2} \qquad (4.1)$$

By using this formula, Bohr treated the electron loss and capture processes as follows.

1) Loss process.

Electron loss process is, simply speaking, the ionization process of projectile particle and it reduces to the two body problem. In the rest frame of the projectile, the process is assumed as that the atomic nucleus and electrons of the target particle collide with the projectile independently and ionize it. This condition is fulfilled when the incident particle is light atom. In this model, the cross section for the process where one of electrons in the target particle gives to an electron in the projectile an energy larger than the binding energy I of the latter electron, is obtained by integrating the Eq. (4.1) from I to T_m, the largest possible energy transfer in a free collision,

$$\sim \frac{2\pi e^4}{m_e v^2} \left(\frac{1}{I} - \frac{1}{T_m}\right) \sim \frac{2\pi e^4}{m_e v^2} \frac{1}{I} \qquad (4.2)$$

In a similar way, the cross section for the process where the

target nucleus $Z_T e$ gives the energy larger than I is given by

$$\sim \frac{2\pi Z_T^2 e^4}{m_e v^2} \frac{1}{I} \qquad (4.\ 3)$$

Therefore, the total cross section for one-electron-ionization of the projectile, that is electron loss cross section, is given by summing these two contributions,

$$\sigma_l \simeq \frac{2\pi e^4}{m_e v^2}(Z_T^2 + Z_T)\frac{1}{I} = 4\pi a_o^2 (Z_T^2 + Z_T) Z^{-2} (v_o/v)^2 \qquad (4.\ 4)$$

where $a_o = h^2/m_e$ is the Bohr radius, $v_o = e^2/h$ is the Bohr velocity. In the final form of Eq. (4.4), the quantity $m_e Z^2 v_o/2$ is substituted into the binding energy I.
Contrary to the case of light target, when the target atoms are not light, the firmly bound electrons and nucleus in the target would no longer act independently on the electrons of the projectile even in the close encounters. Then, the so-called free electron collision approximation mentioned above can not be applied. In this case, by taking account of the screening effects of electrons surrounding the nucleus, Bohr assumed that the target particle will act on the projectile as a core, and he found

$$\sigma_l \simeq \pi a_o^2 Z_T^{2/3} Z^{-1} (v_o/v) \qquad (4.\ 5)$$

As for the case of very heavy target atoms, most of the firmly bound electrons are within the Bohr radious a_o. Since the strong electric field is present in this region, the light projectile ion penetrating through there loses its electrons substantially. Then the loss cross section is of the order of geometrical cross section,

$$\sigma_l \sim \pi a_o^2 \tag{4. 6}$$

The formula (4.6) indicates that the loss cross sections for the very heavy target atoms are completely independent of Z, Z_T and v.

2) Capture process.

As regards electron capture, Bohr stated that the process is more difficult to estimate because at least three particles take part in the transfer of energy and momentum.
By applying the statistical considerations, he represented the capture cross section of alpha particle in heavy substances in the form,

$$\sigma_c \sim \sigma \cdot f \cdot n \tag{4. 7}$$

σ: the cross section for a collision where the ion transfers an energy of the order of $m_e v^2/2$ to an electron with an orbital velocity u, and is obtained by using Eq. (4.1) in the form

$$\sigma \simeq 4\pi a_o^2 Z^2 (v_o/v)^4 \tag{4. 8}$$

f: the electron capture probability of the ion after the collision, and is assumed to be of the same order of magnitude as the fraction of velocity space corresponding to the orbital velocity Zv_o of the ion relative to the incident velocity, that is

$$f \sim (Zv_o/v)^3 \tag{4. 9}$$

n: the number of electrons in a target atom with orbital velocities close to v, and is given on the basis of the statistical model, in the form

$$n \simeq Z_T^{1/3} (v/v_o) \tag{4.10}$$

Consequently, the single electron capture cross section by a bare atom is expressed by

$$\sigma \simeq 4\pi a_o^2 Z^5 Z_T^{1/3} (v_o/v)^6 \tag{4.11}$$

4-2-2. Modification of Bohr's Theory

In the above section, are presented the whole descriptions of Bohr's theory for the light incident particles, where only

the ground state of orbital velocity $u = Zv_o$ is taken into consideration as the bound state of the projectile. Therefore, the above formulae can be applied only for the following cases;

σ_{10}, σ_{01} for hydrogen projectile

σ_{21}, σ_{12} for helium projectile

As for helium projectile, there are still two cross sections σ_{01} and σ_{10} as the single electron transfers.

In this section, the modifications of Bohr's formulae are presented so as to be applied for the cross sections σ_{01}, σ_{10}, too. As the orbital velocity of electron under consideration, u itself should be used instead of Zv_o of the ground state. Then, the author obtained the following modified formulae.

Instead of Eq. (4.4),

$$\sigma_{q,q+1} = s4\pi a_o^2 (Z_T^2 + Z_T)(v_o^2/vu)^2, \quad \text{for light } Z_T \tag{4.12}$$

Instead of Eq. (4.5),

$$\sigma_{q,q+1} = s\pi a_o^2 Z_T^{2/3} (v_o^2/vu), \quad \text{for intermediate } Z_T \tag{4.13}$$

Instead of Eq. (4.11),

$$\sigma_{q,q-1} = 4\pi a_o^2 Z_T^{1/3} Z^2 (v_o u/v^2)^3, \quad \text{for intermediate } Z_T \tag{4.14}$$

Here, s stands for the number of electrons with orbital velocity u carried by the incident particle before an encounter, that is, $s = 2$ for He^0 and $s = 1$ for He^+.

4-3. Quantum Theory (First Born Approximation)

In regard to the charge transfer process of the very simple projectile particle, such as proton or heavy ions with only one electron arround the nuclei, many investigators have devoted considerable effort to the quantum theoretical calculations since published the first theoretical report by Oppenheimer[30] in 1928. Synthetic reviews of these theories are given by Mapleton[31] or by Mott and Massey[32,33].

Representative examples of approximations are Born approximation, impact parameter approximation, impulse approximation or binary encounter approximation, and the applicable range of these theories are in general known empirically. It is known that, in the high incident energy range ($v >> v_o$), all of these approximations give the cross sections with same order of magni tude. Therefore, only the well-known first Born approxi mation (FBA) is described in this section.

The FBA is usually applied to the processes where the projectile velocities are very large and the duration of collision interactions are very short. In this approximation, the cross section for the collision process, where the total system of collisional particles changes into a final state indicated by f from an initial state i, is given by

$$d\sigma_{fi} = \left(\frac{m}{2\pi h^2}\right)^2 \frac{k_f}{k_i} |T_{fi}|^2 \, d\Omega \qquad (4.15)$$

with $T_{fi} = \langle \Psi_f | V | \Psi_i \rangle$

where m is the reduced mass of two particles, k_i and k_f are the wave numbers of the incident particle relative to the target before and after a collision, Ψ_i and Ψ_f represent the wave functions of initial and final states of the system, respectively, V is the interaction potential between particles.

Many authors[16,23,30,31,34-43] have calculated the charge changing cross sections of hydrogen or helium projectiles by using the equation (4.15). Theoretical data for helium projectile will be compared with the present experimental results in the next chapter. The calculated values with the impact parameter approximation by Mukherjee *et al*[61] will also be compared.

In the following sections, the theoretical formulae with which the author carried out the calculations will be described in detail; that is, capture cross sections derived by Schiff[16] and loss cross sections derived by the author.

4-3-1. Capture Cross Sections.

In 1930, Brinkman and Kramers[34] gave the theoretical cross sections for capture of an electron into the ground state of the bare atom with atomic number Z from the target ion of atomic number Z_T carring one electron in the form,

$$\sigma_1(BK) = \frac{2^{18}}{5} \pi a_o^2 Z^5 Z_T^5 (v_o/v)^{12} \qquad (4.16)$$

The formula (4.16) does not include the interaction between

incident and target nuclei, and is called Brinkman-Kramers approximation (BKA). Schiff generalized the Eq. (4.16) for the case where the projectile captures an electron into any excited state with principal quantum number ν in the form,

$$\sigma_{\nu}(BK) = \frac{\pi a_o^2 2^{18} \nu^2 (ZZ_T/\nu)^5 (v/v_o)^8}{5\{(v/v_o)^2 + (Z_T - Z/\nu)^2\}^5 \{(v/v_o)^2 + (Z_T + Z/\nu)^2\}^5} \tag{4.17}$$

In this formula, when we take $v/v_o >> Z_T + Z/\nu$, and leave only the term $(v/v_o)^2$ in the brackets of denominator, the formula reduces to

$$\sigma_{\nu}(BK) \simeq \frac{2^{18}}{5} \pi a_o^2 \nu^{-3} (v_o/v)^{12} = \nu^{-3} \sigma_1(BK) \tag{4.18}$$

where $\sigma_1(BK)$ stands for the ground-state-capture cross section expressed by Eq. (4.16). The formula (4.18) implies that the probability of capture into a state with principal quantum number ν varies as ν^{-3}, which was first demonstrated by Oppenheimer[30].

Because the nucleus-nucleus interactions are neglected in the BK approximation, the generalized formula (4.17) can not be applied directly. For instance, Jackson and Schiff[38] stated that $\sigma_{\nu}(BK)$ of hydrogen ions gives larger values than the experimental ones. From this reason, by taking account of the interaction between nuclei Schiff presented the following total capture cross section for the process $He^{2+} + H \rightarrow He^{+} + H^{+}$.

$$\sigma_{21} = \sigma_1\{1 + (\sigma_2/\sigma_1)(1 + 2.1(\sigma_3/\sigma_2)_{BK})\}, \qquad (4.19)$$

where σ_1 and σ_2 are the cross sections for capture into the ground state ($\nu = 1$) and the first excited state ($\nu = 2$), respectively, and $(\sigma_3/\sigma_2)_{BK}$ represents $\sigma_3(BK)/\sigma_2(BK)$. Exact calculations made by Schiff were, however, only for σ_1 and σ_2, and therefore, the total capture cross section given by Eq. (4.19) was obtained by assuming ν^{-3} law for capture into the states $\nu \geq 3$. In the higher energy range $E > 0.7$ MeV, the relation $\sigma_2/\sigma_1 \simeq (\sigma_2/\sigma_1)_{BK}$ was established by Schiff. By using this relation, the cross section given by Eq. (4.19) can be rewritten by

$$\sigma_{21} = \sigma_1\{1 + (\sigma_2/\sigma_1)_{BK} + 2.1(\sigma_3/\sigma_1)_{BK}\}, \qquad (4.20)$$

where σ_1 is given by

$$\sigma_1 = 2^8(ZZ_T)^7\pi a_o^2(v_o/v)^2\{V^2/5t^5 + 2VW/4t^4 + \\ + (W^2 + 2VX)/3t^3 + 2WX/2t^2 + X^2/t\} \qquad (4.21)$$

with $V = 2\lambda_1^1(Z, Z_T) - 1/ZZ_T$

$W = \lambda_3^1(Z, Z_T)$

$X = (3/4)\lambda_5^1(Z, Z_T)$

$$\lambda_{\nu}^{\mu}(Z, Z_T) = \int_0^1 \frac{x^{\mu}(1 - x)\, dx}{\{-(v/v_o)^2 x^2 + ((v/v_o)^2 + Z^2 - Z_T^2)x + Z_T\}^{\nu/2}}$$

and with $Z = 2$, $Z_T = 1$.

The author calculated Eq. (4.21) in the energy range larger than 1 MeV, since the calculated cross sections are reported only up to the energy 1.0 MeV in the Schiff's paper.

As for the process, $He^+ + He \rightarrow He + He^+$, Schiff reported the cross sections σ_{10} up to the energy 0.7 MeV. Therefore, the author calculated in the energy over 0.7 MeV with the explicit formula given by Schiff,

$$\sigma_{10} = 1.4\sigma = 1.4 \times \frac{3^{24}}{2^{14}} \frac{\pi a_o^2}{5E\{E + (27/8)^2\}^5} \{\frac{3.8443}{E^2} + \frac{0.72252}{E} +$$

$$- \frac{2}{E^{1/2}} \tan^{-1}(\frac{8E^{1/2}}{27}) [\frac{12.975}{E^2} + \frac{5.7587}{E} + 1.9500] +$$

$$+ \frac{4}{E}[\tan^{-1}(\frac{8E^{1/2}}{27})]^2 [\frac{10.947}{E^2} + \frac{7.6885}{E} + 2.6156]\}, \quad (4.22)$$

where E is the projectile energy in the unit of 100 keV.

4-3-2. Loss Cross Sections

The author carried out the quantum theoretical calculations of electron loss of helium projectile in a hydrogen atom and a helium atom as described in the following.

According to Bohr, the electron loss process in the light target atom is treated as the process where a bound electron in the projectile gains the energy larger than its ionization potential as a result of an encounter. Therefore, the collision model may be approximated by an electron scattering by a light target atom. In the case of electron scattering, the quantity T_{fi} in Eq. (4.15) of FBA can be written by

$$T_{fi} = \int exp(-i\vec{k}_f\vec{R})\phi_f^*(\vec{\tau})[-\frac{Z_T e^2}{|\vec{R}|} + \sum_{j=1}^{Z_T}\frac{e^2}{|\vec{R}-\vec{r}_j|}]\phi_i(\vec{\tau}) \times$$

$$\times exp(-i\vec{k}_i\vec{R})\, d^3\vec{R}\, d^3\vec{\tau} \qquad (4.23)$$

where $\vec{R}$ and $\vec{\tau}$ are the radial vectors of the projectile electron and j-th electron in the target atom drawn from the target nucleus (see Fig. 4-1), and $d^3\vec{\tau} = d^3\vec{r}_1 d^3\vec{r}_2 \cdots d^3\vec{r}_{Z_T}$.
After the carrying out the integration over $\vec{R}$, one can get the differential cross section,

$$d\sigma_{fi} = 8\pi(v_o/v)^2 |Z_T\delta_{fi} - \int\{\sum_{j=1}^{Z_T} exp(i\vec{q}\vec{r}_j)\}\phi_f^*(\vec{\tau})\phi_i(\vec{\tau})d^3\vec{\tau}|^2 \frac{dq}{q^3}$$

(4.24)

where $h\vec{q} = h\vec{k}_i - h\vec{k}_f$ stands for the momentum transfer in the collision, and q is the magnitude of the vector $\vec{q}$.
The total differential cross section can be obtained by summing up all the final states of the target particle, that is,

$$d\sigma_{tot} = \sum_f d\sigma_{fi}$$

The author used the hydrogen-like wave functions[32] for the ground state ($i = 0$) of hydrogen and of helium atoms,

$$\phi_0(r) = (\pi a_o^3)^{-1/2} \exp(-r/a_o) \quad \text{for H}$$
$$\phi_0(r_1, r_2) = (Z_T^{*3}/\pi a_o^3) \exp[-Z_T^*(r_1 + r_2)/a_o] \quad \text{for He} \tag{4.25}$$

with $Z_T^* = 27/16 = 1.69$

As regards the elastic part ($f = i$) of the cross sections, the results can be written in a compact form for both H and He,

$$d\sigma_{ela} = 8\pi(v_o/v)^2 Z_T^2 (1 - F(q))^2 \frac{dq}{q^3} \tag{4.26}$$

provided that

$$F(q) = (1 + q^2 a_o^2 / 4 Z_T^{*2})^{-2} \tag{4.27}$$

with $Z_T^* = 1$ for H, $Z_T^* = 1.69$ for He.

Since the calculations for inelastic part ($f \neq i$) is somewhat cumbersome, the methods proposed by Mott[32] for H and by Kuper and Teller[44] for He were used here, and the result is

$$d\sigma_{inel} = 8\pi(v_o/v)^2 Z_T (1 - F(q)^2) \frac{dq}{q^3} \tag{4.28}$$

Consequently, the total differential cross section for the process where the momentum transfer takes place in the range (hq, $\hbar q + hdq$), is given by the following form.

$$d\sigma = 8\pi(v_o/v)^2\{Z_T^2(1 - F(q))^2 + Z_T(1 - F(q)^2)\}\frac{dq}{q^3} \qquad (4.29)$$

The electron loss cross section under consideration can be obtained by integrating the above equation over the momentum space from mu/h, because the "loss" will take place when the incident electron gains the energy larger than $I = mu^2/2$, corresponding to $hq = mu$. The upper limit of the integration of Eq. (4.29) is, according to Mott and Massey, $2mv/h$ for the first term corresponding to the elastic scattering, and mv/h for the second term corresponding to the inelastic scattering, respectively. Finally, the following formula was obtained for electron loss cross section of helium projectile,

$$\sigma_{loss} = 2\pi a_o^2(v_o/Z_T^* v)^2\{Z_T^2[A_e(v/Z_T^* v_o) - A_e(u/2Z_T^* v_o)] +$$

$$+ Z_T[A_i(v/2Z_T^* v_o) - A_i(u/2Z_T^* v_o)]\} \qquad (4.30)$$

with $A_e(x) = 2(1 + x^{-2})^{-1} - (1 + x^{-2})^{-2} + \frac{1}{6}(1 + x^{-2})^{-3}$,

$$A_i(x) = 2\ln(1 + x^{-2})^{-1} - 3(1 + x^{-2})^{-1} + (1 + x^{-2})^{-2} +$$

$$- \frac{1}{6}(1 + x^{-2})^{-3} \qquad (4.31)$$

Eq. (4.30) can be applied when the condition $uv \geq v_o^2$ is ful filled. For the case $v >> u >> 2ZZ_T^* v_o$, the cross section is written by

$$\sigma_{loss} \simeq 4\pi a_o^2 \{Z_T^2 + Z_T - (u/v)^2 [Z_T^2/4 + Z_T]\} (v_o^2/vu)^2 \qquad (4.32)$$

and, furthermore, if one takes $u/v = 0$ in the bracket and takes $u = Zv_o$, the formula reduces to the Bohr's formula (4.4). Therefore, we find that the formula (4.4) derived by Bohr can be applied only for the case $v >> u$.

In chapter V, the formula (4.30) will be applied for the target atoms H and He. However, it must be reminded that this formula was derived on the basis of the free electron scattering model, and then the more strict treatments of the loss process must be referred to Bell *et al*[40,41] or Dmitriev *et al*[43].

In 1963, on the basis of free electron scattering model, Dmitriev *et al*[45] also made the same calculations as the present ones. However, the final formula reported in that paper is clearly incorrect; their expressions would reduce to Eqs. (4.30) and (4.31) if their misprint is corrected.

CHAPTER V

RESULTS AND DISCUSSION: CROSS SECTIONS

5-1. Present Cross Sections

In this chapter, the detailed discussions are presented for the experimentally obtained charge-changing cross sections. Present results of the single and double electron capture and loss cross sections σ_{01}, σ_{02}, σ_{10}, σ_{12}, σ_{20} and σ_{21} are shown in Fig. 5-1(1)-(8) as a function of projectile energy. All the cross sections are plotted in the unit of cm^2/molecule. Experimental errors of the present cross sections were determined from items i)-iv) described in chapter III. In particular, statistical errors of the neutral fractions were large in the higher incident energy region because of the smallness of the fractions. The total uncertainties of the cross sections are 20-30 % for σ_{20} and are smaller than 20 % for cross sections other than σ_{20}.

In the present energy region 0.7-2.0 MeV, the loss cross sections (open symbols) are as a whole larger than the capture ones (closed symbols) for all the target gases used in the present experiment. The loss cross sections change very slowly with projectile energy, while the capture ones decrease very rapidly. Cross sections can be expressed approximately by the form $\sigma = aE^{-p}$, where a and p are the constant values

depending on target gases. The empirical formulae are presented in Table V-1, where E is the incident energy in MeV, and the cross sections are in the unit of $10^{-18}cm^2$/molecule. The solid lines shown in Fig. 5-1 are the computed values by using the empirical formulae in Table V-1. As for the cross section σ_{02}, however, the clear energy dependence is not found for any gases, so that this cross section may be assumed to remain constant in this energy region.

All these cross sections seem to increase as the target substances become heavy; the cross sections for H_2 gas are smallest. About such a medium dependence of the cross sections, the detailed discussion will be given later.

Contrary to the cross sections for gases H_2, He and N_2, the present cross sections for O_2, CO_2, CH_4, C_2H_6 and C_3H_8 are the first data in the helium charge-changing experiments.

5-2. Comparison with Other Cross Sections

5-2-1. Comparison with Other Experiments

Many experimental works have been made for the charge changing process of helium beam up to the present time. Projectile energies used in their experiments were, however, restricted to the relatively lower range and most of them were below 0.5 MeV[46-51]. In the higher energy region, the following works have been reported. As for the capture cross sections σ_{21}, σ_{10} and σ_{20}, Pivovar *et al*[52,53], Nikolaev *et*

al[54,55], Pucket *et al*[56] and Hvelplund *et al*[57] reported the data up to the energy 1.5, 1.3, 1.0 and 7.0 MeV, respectively. As concerns the loss cross sections σ_{12}, σ_{01} and σ_{02}, Pivovar *et al*[53], Dmitriev *et al*[28] and Shah *et al*[58] reported the cross section σ_{12} up to the energy 1.4, 6.0 and 1.0 MeV, respectively, and only a few reports are available for the cross sections σ_{01} and σ_{02} by Hvelplund *et al*[59,60] and by Pivovar *et al*[53].

These investigators used H_2, N_2, He and other noble gases as the target gases, and did not use O_2 or other complicated compounds. Therefore, comparisons with other experimental works will be made only for the gases H_2, He and N_2 in the following.

1) Capture cross sections [Fig. 5-2(1)-(3)].

Present cross sections σ_{21} and σ_{10} are in fairly good agreement with other data within experimental uncertainties, while double electron capture cross section σ_{20} shows a slight deviation from others. This deviation may be due to the large uncertainties of neutral fraction caused by the rapid decrease of double electron capture probability.

2) Loss cross sections [Fig. 5-3(1)-(3)].

Present cross sections σ_{12} are in good agreement with other data for all the target gases, while the cross section σ_{01} are smaller than the data by Hvelplund *et al*[59,60] for the gases H_2 and N_2. As regards the double electron loss cross

section σ_{02}, large uncertainties are present in both cases of present and of Hvelplund *et al*, but both of these cross sections are in the same order of magnitude. In the lower energy region of these figures, the experimental data of σ_{01} by other investigators[48,49,51] are also shown in order to see the reason why the present values of σ_{01} for H_2 and N_2 are smaller than others. As easily can be seen, the agreement of results between them are very poor. In particular for the He target, the discrepancies are the largest and the values by Solov'ev *et al*[49] are larger by two or three times at most than the values by Gilbody *et al*[51]. Therefore, the high energy data by Hvelplund *et al* cannot be trusted simply, although there are no other experimental results to be compared, unfortunately.

One of the cause that the experimental results differ so largely may be attributed to the presence of metastable (or more highly excited) neutral helium in the beam which were produced as a result of neutralization of He^+ beam passing through the neutralizer cell. When the metastable neutral particles are contained in the He^0 beam by a fraction f $(0 \leqq f \leqq 1)$, the formula which was used for the derivation of cross sections must be written by another form. As a simplest example, Eq. (3.7)' should be written by the following modified form.

$$\phi_{01}(x) - \phi_{01}(x_0) = \phi_{00}(x_0)\sigma_{01}^{exp}[x - x_0]$$

$$= \{(1 - f)\phi_{00}(x_0)\sigma_{01} + f\phi_{00}(x_0)\sigma_{01}^{*}\}[x - x_0] \qquad (5.1)$$

where σ_{01}^{exp} is the experimentally determined cross section shown in the figures, σ_{01} and σ_{01}^{*} are the cross sections of ground state and excited state neutral particles, respectively. From Eq. (5.1), the experimental cross section σ_{01}^{exp} can be written by

$$\sigma_{01}^{exp} = (1 - f)\sigma_{01} + f\sigma_{01}^{*} \qquad (5.2)$$

when the relation $\sigma_{01}^{*} = \alpha\sigma_{01}$ is introduced, Eq. (5.2) is written by

$$\sigma_{01}^{exp} = [1 + (\alpha - 1)f]\sigma_{01} \qquad (5.3)$$

Gilbody *et al*[51] reported the single electron loss cross sections of ground state and of metastable particle for various target gases in the energy range from 10 to 350 keV, and showed that the values σ_{01}^{*} are much larger than σ_{01} for any gas. Although the cross sections σ_{01}^{*} have not been reported in the present energy region, it will be reasonable to expect that the helium atom in an excited state will lose its electron easier than the helium atom in the ground state. Then, the author assumed $\sigma_{01}^{*} > \sigma_{01}$, that is, $\alpha > 1$. In this case, the quantity in the bracket in Eq. (5.3) becomes larger than unity, so that the relation $\sigma_{01}^{exp} > \sigma_{01}$ is concluded. This relation implies that the apparent loss cross section σ_{01}^{exp} becomes larger than the cross section σ_{01} when the excited particles are contained in the incident beam.

The present values for H_2 and N_2 are smaller than other experimental values, so that the influence by the metastable helium atoms may be absent or neglegibly small in the present experiment.

Among the experimental results shown in the figures, only the data by Gilbody *et al* (indicated by small open ciecle) are the cross sections of ground state helium atom. It is seen that their cross sections are smallest in all of these results. For the target gases He and N_2 particularly, values by Gilbody *et al* are very smaller than the values by Pivovar *et al* and by Hvelplund *et al*. When the data by Gilbody are extrapolated to the higher energy region, the exptrapolated values seem to be very close to the present cross sections.

In Fig. 5-4, the experimental cross section σ_{01} by Pivovar *et al*, by Hvelplund *et al* and by Gilbody *et al* are shown as a reference for the target gases Ar and Kr. This figure shows that the results by Pivovar *et al*, and by Hvelplund *et al* are significantly inconsistent with each other over 0.4 MeV, and the latter results are larger than the former ones by two times in some cases. The cross sections given by Pivovar *et al* are very close to the results of Gilbody *et al*.

From these considerations, the author concludes that the present values are not so suspicious. Further more precise and numerious experimental works should be performed in order to study the loss cross sections of neutral beam.

5-2-2. Comparison with Theories

As mentioned in the previous chapter IV, the theoretical calculations of charge-changing cross sections of helium have been reported only for simple cases. Theoretical results which can be compared with the present experimental results are listed up in the Table V-2. In this table, the classical calculations denoted by modified-Bohr was described in section 4-1-2, and the quantum mechanical calculations denoted by Itoh of the loss cross sections for hydrogen and helium atoms was described in section 4-2-2. All the calculations in the table are for the target of single atoms, so that the twice of these cross sections will be compared with the experimental ones for the target gases H_2, N_2 and O_2.

1) Capture cross sections [Fig. 5-2(1)-(4)]

i) H_2 gas: σ_{21}

As mentioned previously, the calculated values reported by Schiff[16] are only for the energy up to 1.0 MeV, therefore, the values in the range over 1.0 MeV are calculated in the present study. Theoretical values are somewhat smaller than the present experimental values except for the 2 MeV incidence. Energy dependence of theoretical curve is very close to the present one in the range 0.7-1.5 MeV, but is loose as compared with the present in the range over 1.5 MeV. In this figure, calculated values with the formula given by Brinkman and Kramers is also shown as a comparison. These values are much larger

Table V-2. Summary of theoretical cross sections which can be compared with the present experimental cross sections. Upper and lower part of this table corresponds to quantum mechanical and classical calculations, respectively.

Author (ref.)	Target Atom										Denotations in Figures
	H			He					N , O		
	σ_{21}	σ_{01}	σ_{12}	σ_{21}	σ_{10}	σ_{20}	σ_{01}	σ_{12}	σ_{21}	σ_{10}	σ_{01}	σ_{12}	
Schiff (16)	o				o								S
Mukherjee (61)				o		o							M
Gerasimenko (39)						o							G
Bell (40,41)		o	o				o						Bell
Dmitriev (43)			o					o					Dmit
Itoh (present)		o	o				o	o					Present
Bohr (24)			o					o	o			o	B or B'
Modified-Bohr (present)		o					o			o	o		MB or MB'

than the experimental ones. This is due to the neglect of necleus-nucleus interaction in this approximation.
The large deviation from the experimental values is also seen for the case of proton projectile as reported by Jackson and Schiff[38].

Apart form the absolute values of cross sections, energy dependence given in BKA and by Schiff are $\sigma_{21} \sim E^{-6}$, and $\sigma_{21} \sim E^{-4.5}$, respectively. Present cross sections decrease more rapidly in high energy region than in the lower energy region, indicating that the energy dependence seems to close to BK approximation.

ii) He gas: σ_{21}, σ_{10}, σ_{20}

As for the helium target, calculations with first Born approximation by Schiff and by Gerasimenko and Rosentsveig[39] and those with the impact parameter method by Mukherjee *et al*[61] can be compared with the present data.

Schiff's curve for σ_{10} (denoted by S) is somewhat smaller than the present data and the curve for σ_{21} given by Mukherjee *et al* (denoted by M) is somewhat larger than the present.

Theoretical cross section of double electron capture are larger than the present data over 1.0 MeV for both calculations by Mukherjee *et al* and by Gerasimenko and Rosentsveig.

The following remarks should be stated here. In the calculations by Schiff, exact calculations of σ_{21} for hydrogen target were made only for the capture into the state $\nu = 2$ and 1, where ν is the principal quantum number of the state of helium atom. Then, by assuming the ν^{-3} law for the higher

excited states $\nu \geq 3$, he obtained the total capture cross sections. As for the case of σ_{20} in helium target, only the ground-state capture was evaluated exactly and ν^{-3} law was used for $\nu \geq 2$. In the calculation of σ_{21} for He by Mukherjee *et al*, ground and the first excited state capture were calculated, and their cross sections shown in this figure dose not contain the contributions from the higher excited state capture. Finally, the double electron capture cross section σ_{20} given by Gerasimenko and Rosentsveig are the only ground-state capture. Therefore, it is easy to expect that the reported cross sections by these authors would be somewhat different from the true total capture cross sections. For instance, the cross section σ_{21} and σ_{20} for helium target given by Mukherjee *et al* and by Gerasimenko and Rosentsveig would become larger if the contributions from higher excited-state capture are included. However, the reported theoretical values are relatively in good agreement with the experimental ones. It may be true, therefore, that the higher-state capture process does not contribute so largely to the total capture process.

The author concludes that both the first Born approximation and the impact parameter approximation give almost same cross sections in this energy region, and that it is sufficient to consider only the ground-state and first excited state as the capturing states.

iii) N_2 and O_2 gases: σ_{21}, σ_{10}

As for the heavy target molecules N_2 and O_2, classical calculations with use of the formula given by Bohr and its

modified roumulae (4.13) and (4.14) are compared with the experimental results because of lack of quantum mechanical calculations. Theoretical cross sections σ_{21} (denoted by B) given by the Bohr's formula (4.11) are in very good agreement with the present data for both these target gases, indicating that the Bohr's considerations are very correct. Modified formulae for σ_{10} (denoted by MB) gives somewhat larger values than the experimental ones in two cases of N_2 and O_2. In N_2 gas, the energy dependence of σ_{10} is different between the MB and the present data; the former gives E^{-3}, while the present result is E^{-4}. On the other hand, the energy dependences for O_2 gas agree with each other. In any way, the fact that the cross sections σ_{10} calculated with the modified formula are larger than the experimental ones may indicate the following. In the case where the incident ion is not bare but carries more than one electron, one should take account of interactions between electrons in the projectile and the electron to be captured. Due to the repulsive force between these electrons, the capture cross section σ_{10} would become smaller than that given by the MB formula. Therefore, a simple extension of Bohr's theory cannot be admitted.

2) Loss cross sections; σ_{01}, σ_{12}

In this subsection, present experimental loss cross sections for H_2, He, N_2 and O_2 gases are compared with the FBA (Bell *et al*[40,41], Dmitriev *et al*[43]), the free electron scattering model by present author, Bohr and its modification.

i) H_2, He gases [Fig. 5-5(1)-(2)]

In both gases, quantum theoretical cross sections σ_{12} by Bell *et al* and by Dmitriev *et al* are in good agreement with the present data. But for the higher energy region in H_2 gas, the present results are much smaller than their calculated values. As for the cross section σ_{01}, agreement between the calculations by Bell *et al* and the present data is relatively good for He gas, but is poor for H_2 gas.

When the present data of σ_{01} and σ_{12} are compared with the classical calculations with Bohr or modified Bohr, the calculated results are clearly much larger than the present. The cause of this large deviation is, as mentioned previously, due to the neglect of the effect of screening of nuclear charge by the surrounding electrons of the target atom. As compared with these classical calculations, the cross sections calculated with free electron scattering model are much closer to the experimental values, particularly for the cross section σ_{12}. This is interpreted as follows. In the present calculations with the free electron scattering model, screening effect is taken into considerations by using the wave functions for the target atoms. For the case of σ_{01}, however, the present calculations are still much larger than the experimental data. The discrepancies seen for this case imply that the loss process of projectile carrying one or more electrons should not be treated simply by the free electron scattering model. It is interesting to note that the present calculations in the high energy range approach asymptotically to the calculations by

Bell *et al* using FBA.

In these figures, are shown the classically calculated cross sections with the heavy-target-formula given by Bohr (denoted by B') and its modified one (denoted by MB'). Surprisingly, in this energy region, the heavy-target-formula given in Eq. (4.13) gives far much closer cross sections to the experimental ones than the light-target-formula given by Eq. (4.12). For instance, the cross sections σ_{01} and σ_{12} with the heavy-target-formula are larger than experimental ones by only 30 % in the case of He gas, while the calculated values are still larger than the experimental ones by a factor of about 1.6 in the case of H_2 gas.

ii) N_2, O_2 gases [Fig. 5-3(3)-(4)]

In this case only the classical calculations with Bohr and its modifications can be compared. In the case of cross section σ_{12}, both the experimental and theoretical cross sections agree with one another. As for σ_{01}, the MB cross sections are larger than the experimental ones by 30 % and by 50 % for the target gases N_2 and O_2, respectively.

5-3. Characteristics of Cross Sections

As described in the preceeding sections, comparisons with other experimental and theoretical cross sections can be made only for the target gases H_2, He, N_2 and O_2. As for the other gases of multiatomic molecules such as CO_2, CH_4, C_2H_6 and C_3H_8, there is no other data to be compared. In this sec-

tion, the following characteristics of cross sections are described for all the target gases.

1) Energy dependence.
2) Ratios of cross sections.
3) Atomic number dependence.
4) Medium dependence.

5-3-1. Energy Dependence

The present experimental cross sections are represented with the empirical formulae $\sigma = aE^{-p}$ as given in Table V-1. Fig. 5-6 shows the powers p as a function of total number of electrons in a target molecule. Since the double electron loss cross section σ_{02} does not show a clear energy dependence, the powers for this cross sections are not shown in this figure.

The powers p for the capture cross sections are in the range 3-7, much larger than those for loss cross sections. Particularly, single electron capture cross sections σ_{21} and σ_{10} show the almost same magnitude of p for any gas. The p's for the light targets, H_2 and He, are somewhat larger than those for heavier targets. As for heavy target molecules containing carbon, nitrogen and oxygen atoms, the p's are about 3 which is in agreement with the Bohr's prediction. This indicates that the formula derived by Bohr is correct at least as for the energy dependence.

The powers for the double electron capture cross section σ_{20} are in the range 5-7, which are larger by about two times

than those for single electron catpure.

5-3-2. Ratios of Cross Sections

In Fig. 5-7, are shown the ratios of capture cross sections σ_{20}/σ_{21} and of loss cross sections σ_{01}/σ_{12}. All these values are the average ones over all the projectile energies.

The ratios σ_{20}/σ_{21} of capture cross sections (upper part of the figure) are about 0.04 for H_2 and hydro-carbon molecules and those for other molecules without hydrogen atoms are about two times larger than the former ones. The physical meaning of the factor "2" is not clear in this stage. It is very interesting to note that the double electron capture process does not take place so easier as compared with the single capture process when the projectile ions collide with hydrogen-containing molecules.

The lower part of the figure shows the ratio σ_{01}/σ_{12} of single electron loss cross sections and the values are about 2 for all these gases. According to Eqs. (4.12) or (4.13) derived classically, $\sigma_{01}/\sigma_{12} = 2(u_1/u_0)^2 = 2(4.38/2.95)^2 = 4.4$ for light target, and is $2(u_1/u_0) = 3$ for heavy targets. Values of orbital velocities u_1 and u_0 given in the paper of Lotz[63] were used in the calculations. These theoretical predictions are the same order with, but somewhat larger than the present results. As mentioned in the previous section, the present cross sections σ_{12} agreed with Bohr's formula, but the cross sections σ_{01} were smaller than the values given by

the MB formula. Consequently, the ratios of present cross sections are different from the predictions. This is, however, natural when we recollect that a simple extension of the Bohr's theory cannot be allowed for the projectile with one or more electrons.

Present values σ_{01}/σ_{12} may be regarded to be 2. Then it means that loss probabilities do not depend so largely on the binding energy, $I = mu^2/2$, of an electron to be lost, and are rather proportional to the number of electrons carried by the projectile before a single charge-changing collision. This result indicates that the loss probability of an electron in He^+ is almost equal to that of an electron in He^0 irrespective of their binding energies: $I = 54.4$ eV for He^+, $I = 24.6$ eV for He^0. Quantitative discussion on the loss probability will be given in the section 7-1-1.

5-3-3. Atomic Number (Z_T) Dependence

In this section, dependence of cross sections on atomic number Z_T of target gases H_2, He, N_2 and O_2 are studied. The experimental cross sections for diatomic molecules are divided by 2 in order to compare the cross sections per single atoms. The cross sections in Fig. 5-8(1)-(2) are the relative values to the hydrogen atom.

The loss cross sections show a fairly clear Z_T dependence, and within the experimental errors, the cross sections for these atoms seem to be on a straight line. From these slopes, the

Z_T dependence of loss cross sections is found to be $Z_T^{0.67-1.0}$. This result is very close to the Bohr's prediction, $Z_T^{2/3}$, derived for the intermediate target atoms. Bohr's formula (4.4) gives $(Z_T^2 + Z_T)$ dependence for light target, but it is too much large compared with the experimental results. Therefore, it is concluded that the loss cross sections depend on the target atomic number in the form $Z_T^{2/3}$ whatever the target atom is light or heavy. However, the reason is not clear why the cross sections for an oxygen atom are always equal to or smaller than the cross sections for a nitrogen atom.

Contrary to the loss cross sections, a single dependence is not found for the capture ones; rapid increase in the range $Z_T \leq 2$ and slow increase for the range $Z_T > 2$. Approximately, the slopes in the range from helium to oxygen seem to show the nearly same Z_T dependence as the Bohr's prediction $Z_T^{1/3}$.

5-3-4. Medium Dependence

The experimental cross sections are plotted as a function of total number of electrons in a target molecule in Fig. 5-9 (1)-(2), where the cross sections for hydrogen molecule are taken to be unity. As can be seen in these figures, charge changing cross sections increase with increasing the number of electrons (N). In particular, the single electron loss cross section is almost proportional to the number of electrons in the target gas. The same proportionality was found for

the double electron loss cross sections. On the other hand, the capture cross sections are not always proportional to them. As will be mentioned in the next chapter, the proportionality of the loss cross sections to the number of electrons can be explained very well by applying the additive rule and Z_T dependence to the molecular targets.

CHAPTER VI

RESULTS AND DISCUSSION: ADDITIVE RULE

6-1. Additive Rule

In this chapter, the detailed discussion about the additive rule is presented by using the experimental charge changing cross sections for the gases H_2, CH_4, C_2H_6, C_3H_8, O_2 and CO_2.

The additive rule, as was already mentioned briefly in chapter I, implies that a cross section for a compound molecule consisting of several atoms is a simple sum of cross sections for the individual single atoms. That is, under some specific conditions of ion -molecule collision, the effects of chemical bond of the target molecule can be neglected. In general, the bond energies are of the order of 10 eV, and the orbital velocities of the bond-electrons are below 5×10^8 cm/sec. When the projectile energy is very high and its velocity is much faster than the orbital velocities of the bond-electrons, the molecular forces are negligible and the target molecule appears as an assembly of the individual atoms. This statement is expressed by the following formula.

$$\sigma(A_nB_m) = n\sigma(A) + m\sigma(B), \qquad (6.1)$$

where $\sigma(A_nB_m)$, $\sigma(A)$ and $\sigma(B)$ are the cross sections for a mole-

cule A_nB_m and for a single atoms A and B, respectively.

A few experimental results have been reported for the additive rule in the charge changing process. Hydrogen beam experiments have been made by Toburen *et al*[11] and by Dagnac *et al*[12]. The former workers measured the cross sections σ_{01} and σ_{10} of hydrogen projectile of energy 0.1-2.5 MeV in the target gases O_2, CO_2, H_2, CH_4, C_2H_4, C_2H_6 and C_4H_{10}. They estimated the charge changing cross sections $\sigma_{01}(C)$ and $\sigma_{10}(C)$ for a carbon atom by solving the simultaneous equations of various combinations of the experimental cross sections. Estimated carbon cross sections $\sigma(C)$ were found to agree with one another within experimental errors.

The latter workers made the experiments on 2-60 keV hydrogen charge changing process, and they found that the experimental cross sections for a water molecule $\sigma(H_2O)$ can be reproduced by using the experimental cross sections for H_2 and for O_2, that is,

$$\sigma(H_2O) = \sigma(H_2) + \frac{1}{2}\sigma(O_2) \qquad (6.2)$$

Both of these experimental results show the validity of the additive rule in the collision process of hydrogen projectile.

On the other hand, there is a paper of Wittkower and Betz[13] concerning this rule for the heavy ion projectile. In their experiment, 12 MeV I^{5+} ions were passed through the target gases H_2, N_2, CO_2, N_2O, CH_4 and $(CH_2)_3O$, and the charge changing cross sections $\sigma_{5q}(q = 3\text{-}8)$ were measured.

They reported that it is completely impossible to reproduce the cross sections for the complex molecule from the individual cross sections of constituent atoms of the compound. For instance, the cross sections obtained for $(CH_2)_3O$ are significantly smaller than any possible addition of cross sections for its components, and the single capture or loss cross sections for C differ substantially when determined from formulae $\sigma(CO_2) - \sigma(O_2)$ and $\sigma(CH_4) - 2\sigma(H_2)$. That is to say, the additive rule does not hold for the process of 12 MeV I^{5+} ion projectile.

The additive rule is, therefore, found to be valid for the hydrogen projectile with velocity v = (0.62- 21) x 10^8cm/sec, but not for the iodine ions with velocity v = 4.2 x 10^8 cm/sec. These two experimental evidences are not only contradictory to the simple idea that the rule would be valid if the projectile ions are very fast, but also imply that the electronic structure of the projectile takes a significant role in the collision mechanism. It is, therefore, very important to examine the validity of the rule to what extent of projectile ions, and of projectile energies.

6-2. Estimation of the Cross Sections for a Carbon Atom

6-2-1. Molecular Chain Method

In general, the subtraction method is unsatisfactory for the verification of the additive rule because of the large

influence due to experimental errors of cross sections. Therefore, the author newly developed a molecular chain method as is described below. The hydro-carbon molecules were used as a molecular chain. These molecules can be expressed by the form C_nH_{2n+2}, where n is the total number of carbon atoms in the molecule. The hydrogen molecule H_2 is treated as the case $n = 0$ in the above form. When the additive rule is assumed to hold in the process under consideration, the charge changing cross sections for the molecule C_nH_{2n+2} must be represented by the linear combination of the cross sections for the constituent hydrogen and carbon atoms,

$$\sigma(C_nH_{2n+2}) = n\sigma(C) + (2n + 2)\sigma(H)$$

$$= [\sigma(C) + 2\sigma(H)]n + 2\sigma(H) \qquad (6.3)$$

where $\sigma(C)$ and $\sigma(H)$ are the cross sections for a carbon and a hydrogen atom, respectively. The formula (6.3) indicates that the plot of cross sections $\sigma(C_nH_{2n+2})(n = 0,1,2,3)$ as a function of n will show a straight line with slope, $\sigma(C) + 2\sigma(H)$, and with an intersection, $2\sigma(H)$. The experimental cross sections for these hydro-carbon molecules are shown as a function of n in Fig. 6-1(1)-(6), where the cross sections are the relative values.

Clearly seen in these figures, the fairly good linear relations are obtained for all the cross sections, particularly for loss cross sections. All the straight lines in the

figures are obtained by the least square fitting. These results support the formula (6.3), that is, the additive rule is valid.

The intersections $2\sigma(H)$ may be regarded to be the experimental values $\sigma(H_2)$. From the slopes $[\sigma(C) + 2\sigma(H)]$ of the lines, the cross sections $\sigma(C)$ for a carbon atom were estimated. Results are given in Table VI-1. The carbon cross sections $\sigma(C)$ estimated in this way are the average values of cross sections determined by the subtraction method for all possible combinations of these molecules. Therefore, this new method is more reliable than the subtraction method; $\sigma(CH_4) - 2\sigma(H_2)$.

6-2-2. Subtraction Method

The carbon cross sections can also be estimated from $\sigma(CO_2) - \sigma(O_2)$, and these values are listed in Table VI-1 denoted by asterisk. In both cases of capture and loss cross sections, these values are in fairly good agreement with those derived by the molecular chain method. Agreement between them is very well, in particular, for loss cross sections. As for capture cross sections, the estimated values in the subtraction method are in some cases much different from those estimated in the molecular chain method. For instance, σ_{20}(0.7 MeV) and σ_{10}(1.0 MeV) are the cases (see Table VI-1). This disagreement is explained as follows. As mentioned in chapter V, the capture cross sections decreas rapidly in the present energy region. So that the large experimental errors

of cross sections influence the estimations in the subtraction method.

6-2-3. Cross Sections for a Carbon Atom

Fig. 6-2 show the estimated carbon cross sections. Capture cross sections are from the molecular chain method. Loss cross sections are the average values of two methods; $\sigma_{loss} = (6\sigma_1 + \sigma_2)/(6 + 1)$, where σ_1 and σ_2 represents the cross sections estimated from the present and subtraction method, respectively. The solid lines are the empirical lines determined by the form $\sigma = aE^{-p}$, and the broken lines denoted by B and MB are the calculated values according to Eq. (4.13).

6-3. Semi-Empirical Formula of Cross Sections

In the first step, the empirical formula for the constituent single atoms are used to reproduce the cross sections for CO_2 and hydro-carbon molecules, by assuming the additive rule to hold. The used empirical formulae for H, O and C are presented in Table VI-2. The formula for H and O are the half of the experimental formulae given in Table V-1.

By using these single atomic cross sections, charge changing cross sections for compound molecules were calculated, and the results are shown by dotted curves in Figs. 6-3(1)-(2). Agreement between the experimental and calculated cross sections are very good. Therefore, the validity of the additive rule

is reconfirmed for helium projectile.

In the second step, the semi-empirical formulae for loss cross sections were constructed by using the present experimental findings and the Bohr's theory. As for the capture cross sections, the energy dependence and Z_T dependence are not so clear, so that the general formula for capture cross sections could not be constructed.

As mentioned in chapter V, the following experimental findings are obtained as for single electron loss cross sections.

1). Theoretical cross sections σ_{12} calculated with the heavy target formula (4.5) given by Bohr are in agreement with the present experimental values for the cases of N, O, C and even for He, while for the case of hydrogen atom the formula (4.5) gives the values somewhat larger than the experimental ones by a factor of 1.6.

2). Atomic number dependence of cross sections agrees with the Bohr's prediction $Z_T^{2/3}$.

3). Energy dependence of cross sections can be represented by the Bohr's prediction $E^{-0.5} \propto v^{-1}$ with a good accuracy.

4). Experimental cross sections σ_{01} are about twice of σ_{12} for all the target substances.

These experimental findings suggest that, for the atomic target other than hydrogen atom, the single electron loss cross section σ_{12} can be expressed by the Bohr's formula (4.5) and σ_{01} is $2\sigma_{12}$, that is

$$\sigma_{qq+1} = s\pi a_o^2 Z^{-1} (v_o/v) Z_T^{2/3} \qquad (6.4)$$

where s stands for the number of electrons carried by the projectile before a single encounter. As for the hydrogen atom, the formula (6.4) divided by 1.6 is regarded as the semi-empirical formula for loss cross sections.

By using the formula (6.4) and the additive rule, the cross sections for molecules A_nB_m consisting of heavy atoms, i.e., N_2, O_2 or CO_2 can be written by

$$\sigma_{qq+1}(A_nB_m) = s\pi a_o^2 Z^{-1} (v_o/v) \{nZ_A^{2/3} + mZ_B^{2/3}\} \qquad (6.5)$$

and the cross sections for hydro-carbon molecules C_nH_{2n+2} can be expressed by

$$\sigma_{qq+1}(C_nH_{2n+2}) = s\pi a_o^2 Z^{-1} (v_o/v) \{nZ_C^{2/3} + \frac{1}{1.6}(2n+2) Z_H^{2/3}\} \qquad (6.6)$$

On the other hand, as mentioned in section 5-3-4, the loss cross sections σ_{01}, σ_{12} and σ_{02} are proportional to the total number of electrons (N) in a target molecule. These results can be explained as follows. In Eq. (6.5), the quantities $(nZ_A^{2/3} + mZ_B^{2/3})$ in the bracket are 7.3, 8 and 11.3 for molecules N_2, O_2 and CO_2, respectively, and these values are very close to the half of the total number of electrons in the respective molecules; 7, 8 and 11. As for the case of the formula (6.6),

the quantities in the bracket, $\{nZ_C^{2/3} + (1/1.6)(2n + 2)Z_H^{2/3}\} = 4.55n + 1.25$, are 1.25, 5.8, 10.4 and 14.9 for H_2, CH_4, C_2H_6 and C_3H_8, respectively, and these values are also very close to 1, 5, 9 and 13, the half values of total electrons. Therefore, the quantities in brackets in Eqs. (6.5) and (6.6) can be replaced by $N/2$, and finally the single electron loss cross sections by eight target molecules used in the present work are expressed in terms of N in the following form.

$$\sigma_{qq+1} = s\pi a_o^2 Z^{-1}(v_o/v)N/2 \qquad (6.7)$$

As for the double electron loss cross section σ_{02}, there are no theoretical expressions such like Eq. (6.4). Therefore, the cross sections can be expressed only in the form $\sigma_{02} \sim N = k\pi a_o^2 N$, where k is a constant value independent of target molecules. Finally, the author obtained the following formula which can reproduce the experimental cross sections very well.

$$\sigma_{02} = \frac{1}{44}\pi a_o^2 N \qquad (6.8)$$

It is clear, in Eqs. (6.7) and (6.8), that the loss cross sections σ_{01}, σ_{12} and σ_{02} are proportional to the total number of electrons in a target molecule.

6-4. Conclusion

From the above mentioned considerations, it is concluded that the additive rule is reasonably applicable to the helium charge changing process in the present energy region.
As the theoretical approach to the additive rule, Tuan and Gerjuory[62] calculated the capture cross sections for protons in the collision with H and H_2 with the first Born approximation. They reported that the cross section for hydrogen molecule is not twice the cross section for an atomic hydrogen, and that the interference effect between the atoms in a molecule cannot be neglected. Nevertheless, the experimental results obtained by Toburen *et al*[11], Dagnac *et al*[12] and the present results indicate that the additive rule holds very well for the light projectiles such as hydrogen and helium ions.

Contrary to these light projectiles, the additive rule does not at all hold for the iodine projectile as pointed out by Wittkower and Betz[13]. As mentioned in chapter I, it is known that the additive rule holds well for the energy loss process of heavy ions[8]. The reason why the rule holds reasonably well in the energy loss process may be due to the fact that the process has a statistical characteristics.
However, recent experimental studies have shown the deviations from the additive rule even for hydrogen and helium projectiles. For instance, Park and Zimmerman[9] made the experiment on the stopping cross sections for 40-250 keV H^+ ion passing through H_2, CH_4, C_2H_2, C_2H_4, C_3H_8, $(CH_2)_3$ and C_3H_6, and reported that

the additive rule does not hold in the projectile energies below 150 keV. By using similar carbon-containing molecules as described above, the group of Baylor University made experiments for 0.3-2.4 MeV He^+ ion, and they reported that the rule holds for the molecules with single or double bonds, but not for the molecules with triple bonds.

These experimental results indicate that the validity of the additive rule in energy loss process is dependent on the atomic number of projectiles, incident energies and the nature of chemical bond of target molecules. This will be the case also for the charge changing process. Therefore, in order to investigate the additive rule, the experiments should be made systematically over various projectiles, wide range of incident energies, and various compound molecules.

CHAPTER VII

RESULTS AND DISCUSSION: EQUILIBRIUM CHARGE DISTRIBUTIONS

7-1. Introduction

In this chapter, the equilibrium charge distributions of helium particles are discussed. Many measurements of helium equilibrium distributions have been reported by other investigators, previously. The earlier data in relatively low energy region up to 1958 was summarized in the article by Allison[4]. In the high energy region, Pivovar *et al*[53], Nikolaev *et al*[64], Meckbach *et al*[65], Torres *et al*[66], or Hvelplund *et al*[59] have reported the data for various target gases. However, as in the case of cross section measurements, most of the target gases are restricted to H_2, N_2, He and other noble gases, and no experimental data have been reported for the complex compounds such as used in the present work.

The average equilibrium charge is known in general to be higher in the solid materials than in gaseous materials, and solid carbon foils have been commonly used as the charge strippers in high energy accelerators. There are some interpretations for the reason why the mean charge becomes higher when the projectile passes through the solid than the gas, but it is not clear even at the present time which is the best one. It is,however, uncertain whether the relation $\bar{q}(solid) > \bar{q}(gas)$ is true or not in all the projectile ions or in all the energy

region.

In the following sections, present results of equilibrium charge fractions and of average charges are described in detail by comparing those with other worker's data, and discussion is given to the difference of average charge between solid and gaseous media.

7-2. Equilibrium Charge Distributions

As mentioned in Chapter III, any fractions approach to a definite values, namely the equilibrium fractions, in the high pressure region, independently of the initial charge state of the projectiles. The results of these equilibrium charge fractions are presented in Table VII-1 and in Fig. 7-1(1)-(8). Experimental errors are lower than a few percent for charged fractions F_1 and F_2. The neutral fraction F_0 has somewhat large errors and are in the range within the data symbols. The energy dependence of fractions are quite similar for any target gases. The relation $F_2 > F_1 > F_0$ can be seen in this energy region, except for He and O_2 around 0.7 MeV. The equilibrium fractions can be calculated from six cross sections according to the formula (3.15) and (3.16). Calculated values were, as mentioned in section 3-3, in good agreement with the experimental results.

As the experimental data by other investigators, Pivovar *et al*[53] reported for 0.2-1.5 MeV in H_2, He and N_2, Nikolaev *et al*[64] for 0.67-5.9 MeV in He and N_2, the group of Meckbach and

Torres[65.66] for 60-860 keV in H_2, He and N_2, and Hvelplund *et al*[59] for 1 and 3 MeV in H_2. In these figures, only the data by Pivovar *et al*, and by Meckbach's group are shown since their data are most systematic in respective to the projectile energy. The solid lines are the guide lines of the present data, and agreement with other data are very good for gases H_2, He and N_2.

In Fig. 7-2, the ratios F_0/F_2 and F_1/F_2 for H_2, N_2 and CH_4 are shown. These ratios change linearly with incident energies, and the similar linearities were found for other target gases. Therefore, the ratios can be expressed by the form aE^{-p}. The obtained empirical formulae are given in Table VII-2. The energy dependence of these quantities are $E^{-(5-7)}$ for F_0/F_2 and $E^{-(2.5-3.0)}$ for F_1/F_2.

7-2-1. Application of the Theory of Dmitriev

In 1957, Dmitriev[70] proposed the simple method for calculation of the equilibrium charge fractions. He tried to explain the equilibrium charge fractions in terms of the removal probability of electron which is bound in the projectile particle. Dmitriev's theory is based on the assumption that the removal probability P of the i-th electron with orbital velocity u_i in a projectile with velocity v is a function of only v/u_i, and is not affected by the presence or absence of other electrons in the projectile. Therefore, the probability $P(v/u_i)$ is a universal function and is same for both inner and outer electrons provided that the v/u_i is constant.

In the case of helium projectile, the quantity $P(v/u_0) \equiv P_1$ is the removal probability of one of two electrons in neutral projectile He^0, and $P(v/u_1) \equiv P_2$ corresponds to that of an electron in He^+. By using these quantities, the equilibrium charge fractions can be written in the form,

$$\begin{aligned} F_0 &= (1 - P_1)(1 - P_2) \\ F_1 &= (1 - P_1)P_2 + P_1(1 - P_2) \\ F_2 &= P_1 P_2 \end{aligned} \tag{7. 1}$$

and the average charge $\bar{q}$ is given by

$$\bar{q} = \sum_i qF_q = \sum_i P_i = P_1 + P_2. \tag{7. 2}$$

By solving the formula (7.1), probabilities P_1 and P_2 are obtained in the following forms, respectively.

$$\begin{aligned} P_1 &= \frac{1}{2}\{F_1 + 2F_2 - [(F_1 + 2F_2)^2 - 4F_2]^{1/2}\} \\ P_2 &= \frac{1}{2}\{F_1 + 2F_2 + [(F_1 + 2F_2)^2 - 4F_2]^{1/2}\} \end{aligned} \tag{7. 3}$$

By substituting the experimental values F_1 and F_2 into the formula, the probabilities P_1 and P_2 were obtained. The results are shown in Fig. 7-3(1)-(8), where the probabilities are plotted as a function of projectile velocity. In this energy

region, both of these probabilities are very large and approxi mately $P_1 = P_2$. Therefore, the quantities $(1 - P_1)$ and $(1 - P_2)$ are plotted in these figures instead of P_1 and P_2 in order to see the difference between them more clearly. The values $(1 - P_i)$ stand for the presence probabilities of i-th electron.

According to Dmitriev, the probability P should be a uni versal function, and necessarily P_1 must be equal to P_2 by shifting the abscissa by a factor of $u_1/u_0 = 1.48$. In order to confirm this relation, the shifted values $(1 - P_1)$ are shown by open circles in the figures. As clearly seen, the shifted values are always smaller than $(1 - P_2)$ for most of target gases. But for the gases H_2 and He, the agreement are relatively good. Apart from the magnitude of the pro- babilities, the velocity dependence of $(1 - P_i)$ are very similar each other except for the gases C_2H_6 and C_3H_8.

Meckbach *et al*[65] have calculated P_1 and P_2 for He gas in a similar way, and stated that the shifted values $(1 - P_1)$ are still much smaller than $(1 - P_2)$ in their projectile energies, and that the theory of Dmitriev cannot be supported. In the present case, however, the agreement seems to become good as the incident energy increases and it can be said that the theory is rather a good approximation in the high energy region, al though it is very rough approximation.

Finally, the author emphasizes that the experimental evi dences that both P_1 and P_2 are larger than 90 percent in high energy region explains well the results described in section

5-3-2 that the loss cross sections does not depend so strongly on the binding energy of electrons to be lost.

7-3. Average Equilibrium Charge

Average equilibrium charge $\bar{q}$ is calculated according to the formula $\bar{q} = F_1 + 2F_2$, where F_i is the experimental equilibrium charge fraction. Calculated results are presented in Table VII 1 and in Fig. 7-4, where the $\bar{q}$ for the hydro-carbon molecules are shown in a right hand side of the figure in order to avoid the complexity.

The characteristics of the average charge are as follows.

1) $\bar{q}$ depends largely on target gases.
2) $\bar{q}$ in helium gas is the smallest and is largest in hydrogen gas.
3) $\bar{q}$ in hydro-carbon gases are very close to one another, and particularly the values in CH_4 are almost equal to that in C_3H_8, and both of them are larger than that in N_2 gas.

In order to investigate further more deeply the medium dependence of average charge, the measurements were performed for 1.0 MeV He beam by using the various gases in addition to the previous eight gases. The used gases are Ar and C_nH_{2n+2} (n = 5, 6, 7, 8). The obtained average charges for 1.0 MeV helium projectile are presented in Table VII-3 and in Fig. 7-5. The characteristics are the following.

1) $\bar{q}$ in Ar is the larget.
2) $\bar{q}$ does not differ so much in the gases H_2 and hydro-carbon

gases.

From these experimental results, it is concluded that the $\bar{q}$ of helium particles passing through heavier substances are not alway larger than those in light substances. Particularly, this conclusion is easily understood by viewing the fact that $\bar{q}$ in H_2 is very large. In Fig. 7-4, the average charge of helium ions after penetrating through the carbon-foil[67] are shown by a broken line as a comparison. The average charge in C-foil is smaller than that in H_2, and above 1.5 MeV they are larger than those only in He and O_2. In order to check if this trend is also seen in the lower energy region, the average charge in the energy below 1 MeV are shown in Fig. 7-6, where the presented data are from the papers reported by the group of Meckbach for various gases and from Armstron for carbon foil. In this energy region, the following relation is found: $\bar{q}(C) > \bar{q}(N_2) > \bar{q}(H_2) > \bar{q}(He)$. As for the H_2 gas, the average charge becomes smaller than that in N_2 below 0.6 MeV. These features indicate that as the target substance becomes heavier the average charge increases and becomes closer to the solid carbon data. Briefly speaking, the general trend, $\bar{q}(solid) > \bar{q}(gas)$, is found in the lower energy region, but in the higher region this is not the case. In the case of heavy ion experiment, Ryding *et al*[14] pointed out that the compound perfluorodecalin ($C_{10}F_{18}$) produce a marginal shift toward higher charge states, whose trend is shown in Fig. 7-7, and that the shift becomes very smaller or absent in higher energy region. In the paper of Moak[15], the experimental results of average

charge measured by Clark *et al* are quoted as a private communication, which are presented in the lower part of the figure. Results by Clark *et al* indicate that the average charge in a very heavy molecule called Fomblin YR, molecular weight 6500, is shifted an about a full charge to $\bar{q}$ in solid (C-foil) above that obtained in Ar gas.

A series of these experimental results about the heavy ion projectile show clearly the following relation,

$$\bar{q}(solid) > \bar{q}(heavy\ gas) > \bar{q}(light\ gas).$$

Two theories are available to explain the gas-solid charge state difference, i.e. one is the Bohr-Lindhard theory[25], and the other is Betz-Grodzins theory[68]. The former explanation is that an ion, in solid, can become excited and then be ionized before having time to de-excite because the collisions occur so frequently in a solid. According to this picture, the ion will become more highly stripped in the solid. On the other hand, the latter explanation is that the ion is in highly-excited states in solid, too, by gathering a high degree of compound excitation, but it remains at the same charge it would have in a gas; in this model the ion will be expected to emit a large number of Auger electrons after leaving the solid and finally the ion becomes highly charged.

Recently, Moak[15] suspected a third explanation which is based on the BL-theory. According to his model, the effective capture cross sections in solid become lesser than in gas,

while the effective loss cross sections remain comparable as those in gas, and consequently the charge state distributions will shift to higher levels.

It is, however, not clear which one of these explanations is valid, and what can be said for the case of light projectile such as a helium ion. In the following, the author attempted to give a discussion for the equilibrium charge of the helium ions.

The equilibrium charge distributions are dtermined by the balance between electron loss and capture processes. Therefore, the equilibrium distributions will shift to higher levels when the capture cross sections decrease more rapidly than the loss cross sections. As seen from the empirical formulae in Table V-1, capture cross sections for H_2 decrease most rapidly, while loss cross sections for H_2 decrease with comparable rapidity to other target gases. This results explains the experimental result that the average charge in hydrogen gas is largest in all the target gases. The smallest average charge obtained in helium gas is due to the large capture cross sections. Namely, as can be seen in Fig. 5-8, the loss cross sections follow approximately the $Z_T^{2/3}$ dependendence, while the capture cross sections for He are comparable to those in N_2 or O_2 gas.

In a condition where the equilibrium is established, one may suppose the neutral helium would be partly in excited states. Consequently, the calculated equilibrium fractions from the experimental cross sections obtained in a single col

lision region will be different from the actual experimentally measured values. The process where the excited state of the projectile takes a role is called *density effect*. About the density effects in the case of heavy projectiles, Ryding *et al*[69] or Betz[72] have reported the experimental results, and these processes are described in detail in the review article of Betz[6]. The density effect is expected to appear particularly in the heavy projectile carrying many electrons. The experimental results obtained by the above workers show, however, that the shift of average charge is only $\Delta\bar{q}$ =0.35 at most in the case of 4.5 MeV iodine ions. Then it would be reasonable to assume that the shift of the average charge in the case of light projectile like helium ions would not be so remarkable and would be within experimental errors.

As a final discussion of average charge, the present results are compared with the calculated values with the formula (7.2), and with the semi-empirical formula (3.21), both of two formulae were given by Dmitriev. The results are shown in Fig. 7-8, where the calculated values with Eq. (3.21) are denoted by broken lines, and those with Eq. (7.2) are denoted by solid lines. The broken lines are different from the experimental results particularly in the high energy region. This is, however, natural because the semi-empirical formula (3.21) was derived primarily for the heavy ion projectiles. The solid lines calculated with the experimentally-determined probabilities P_1 and P_2 are, as expected, in good agreement

with the experimental results. In the calculations, extrapolated values of P_1 and P_2, shown in Fig. 7-3, were used in the high energy region. The calculated results with Eq. (7.2) were in good agreement with the experimental data for other target gases, too, not only for H_2, He and N_2 gases.

CHAPTER VIII

CONCLUSIONS

This study is a summary of the author's works on charge changing collisions of helium projectiles in the energy range from 0.7 to 2.0 MeV accumulated mainly since 1976, and part of the experimental evidences have been reported previously (ref. 22, 73, 74).

In the preceeding chapters, the experimental procedures in observing the processes, method of deriving the charge transfer cross sections, the theoretical models relevant to the transfer mechanisms, and the results have been described. In this chapter, the conclusive remarks are made for the present study.

[1] The use of the deflection chamber before the collision chamber is found quite useful and simple method for charge selection of initial beam, which enables us to increase the purity of the initial beam.

[2] In the detection of particles, the method of coincidence between energy and position output from the position-sensitive-detector largely reduce background noise in multi channel pulse height analyzer. Particularly, neutral particles detected in lower pulse region are clearly distinguished. With this method the neutral fractions of charge distributions can be calculated accurately.

[3] In the low pressure region, where the charge fractions change linearly, three methods used for the derivation of cross sections are found to give almost same values if the actual experimental conditions are taken into considerations; residual gas pressure is not zero, and charge fraction $\phi_{qq}(x_0)$ at this pressure is not always equal to 1. Among them, the direct integration method, which is newly developed in this work, gives most reliable cross sections because of exclusion of any approximation, although it is somewhat cumbersome in practice.

[4] Present results of charge changing cross sections and equilibrium charge distributions relevant to the target gases O_2, CO_2, CH_4, C_2H_6 and C_3H_8 are the original data.

[5] Quantum mechanical calculations of loss cross sections of helium projectile in light target atoms such as hydrogen or helium are performed on the basis of the free electron scattering model (binary encounter approximation). The calculated values are in very good agreement with the experimental results, and approach to the values given from the first Born approximation in the high energy region.

[6] The ratios between the double electron capture cross section σ_{20} and the single electron capture cross section σ_{21} are divided into two groups. That is, the ratios are about 0.04 for H_2 and hydro-carbon molecules and about 0.08 for other molecules. This result may indicate that the double electron capture process does not take

place so easily as compared with the single capture process when the projectile ions collide with hydrogen-containing molecules.

[7] Single electron loss cross section σ_{01} are about twice of single loss cross section σ_{12} for all the target gases; indicating that the loss probability of an electron in He^+ is almost equal to that of an electron in He^0 irrespective of their different binding energies. Therefore, single electron loss cross sections are proportional to the number of electrons carried by the projectile before a single charge changing encounter.

[8] Target atomic number dependence of loss cross sections is very clear and is approximated by the Bohr's prediction $Z_T^{2/3}$, while such a clear dependence is not found for the capture cross sections.

[9] The newly developed method for testing the additive rule is more useful than the commonly-used subtraction method and it reduces largely the experimental uncertainties of cross sections.

[10] The additive rule is found to be applicable for both processes of capture and loss in the energy range from 0.7 to 2.0 MeV.

[11] Carbon cross sections $\sigma(C)$, which cannot be obtained by experimentally, have been estimated by the present new method.

[12] The loss cross sections are found to increase linearly with the total number of electrons in a molecule. This pro-

portionality can be explained very well by using the Z_T dependence and the additive rule. However, such a trend is not obserbed for the capture cross sections.
The following simi-empirical formulae are given to the loss cross sections.

$$\sigma_{qq+1} = s\pi a_o^2 Z^{-1} (v_o/v) N/2$$

$$\sigma_{02} = \frac{1}{44} \pi a_o^2$$

where N is the total number of electrons in a molecule.

[13] The equilibrium charge distributions can be explained very well by the theory of Dmitriev[70]. Removal probabilities of single electron from He^0 and He^+ are almost equal and they are larger than 0.9 in the high energy region.
It is concluded that the removal probability is independent of the binding energy of electrons to be lost if the projectile energy is very high.

[14] Average charges $\bar{q}$ in various media have the following relations;

$\bar{q}$: $H_2 > CH_4 \simeq C_3H_8 > C_2H_6 > N_2 > CO_2 > O_2 > He$.

The difference of $\bar{q}$ among the hydrogen-containing molecules are very small.

[15] Average charge in solid media (carbon foil)[67] lies between $\bar{q}(H_2)$ and $\bar{q}(CO_2)$, and the well-known relation $\bar{q}(solid) > \bar{q}(gas)$ cannot be found in the case of helium projectile in this energy region. The relative magnitude between

$\bar{q}(solid)$ and $\bar{q}(gas)$ is largely dependent on the projectile velocities.

Some problems to be solved in the future investigations are summarized in the following.

(α) Estimation of fractions of metastable particles contained in the initial beam.

(β) Identification of the bound state of the projectile into which an electron is captured.

(γ) Applicable range of the additive rule; which should be tested by using the various heavy projectiles and various target gases in the wide range of projectile energies.

(δ) Influence of density effect; that is, the difference between a long-target chamber and a short-target chamber experiments.

REFERENCES

1) A.Itoh, M.Asari and F.Fukuzawa; J. Phys. Soc. Jpn 44 (1978) 1672.

2) A.Itoh, M.Asari and F.Fukuzawa; Mem. Fac. Eng. Kyoto Univ. 39 (1977) 201-214, 321-334.

3) M.Asari, Y.Kido and F.Fukuzawa; J. Phys. Soc. Jpn 42 (1977) 982.

4) S.K.Allison; Rev. Mod. Phys. 30 (1958) 1137.

5) H.Tawara and A.Russek; Rev. Mod. Phys. 45 (1973) 179.

6) H.D.Betz; Rev. Mod. Phys. 44 (1972) 465.

7) W.H.Bragg and L.Kleeman; Philos. Mag. 10 (1905) 318.

8) L.C.Northcliffe and R.F.Schilling; Nucl. Data Tables A7 (1970) 233.

9) J.T.Park and E.J.Zimmerman; Phys. Rev. 131 (1963) 1611.

10) P.D.Bourland and D.Powers; Phys. Rev. B 3 (1971) 3635.

11) L.H.Toburen, M.Y.Nakai and R.A.Langley; Phys. Rev. 171 (1968) 114.

12) R.Dagnac, D.Blanc and D.Molina; J. Phys. B 3 (1970) 1239.

13) A.B.Wittkower and H.D.Betz; J. Phys. B 4 (1971) 1173.

14) G.Ryding, A.B.Wittkower and P.H.Rose; Particle Accelerators 2 (1971) 13.

15) C.D.Moak; IEEE Trans. on Nucl. Sci. vol NS-23 (1976) 1126.

16) H.Schiff; Can. J. Phys. 32 (1954) 393.

17) V.S.Nikolaev; Sov. Phys. -Usp. 8 (1965) 269.

18) S.Datz, H.O.Lutz, L.B.Birdwell, C.D.Moak, H.D.Betz and L.D.Ellsworth; Phys. Rev. A 2 (1970) 430.

19) G.I.Bell; Phys. Rev. 90 (1953) 548.

20) I.S.Dmitriev and V.S.Nikolaev; Sov. Phys. -JETP 20 (1965) 409.

21) V.S.Nikolaev and I.S.Dmitriev; Phys. Lett. 28 A (1968) 277.

22) A.Itoh, M.Asari and F.Fukuzawa; J. Phys. Soc. Jpn 48 (1980) No. 3 (to be published).

23) V.S.Nikolaev; Sov. Phys. -JETP 24 (1967) 847.

24) N.Bohr; K. Dan. Vidensk. Selsk. Mat.-Fys. Medd. 18 (1948) No 8.

25) N.Bohr and J.Lindhard; K. Dan. Vidensk. Selsk. Mat.-Fys. Medd. 28 (1954) 7.

26) R.L.Gluckstern; Phys. Rev. 98 (1955) 1817.

27) V.S.Nikolaev; Sov. Phys. -JETP 6 (1958) 417.

28) I.S.Dmitriev, V.S.Nikolaev, L.N.Fateeva and Ya.A.Teplova; Sov. Phys. -JETP 15 (1962) 11.

29) I.S.Dmitriev, V.S.Nikolaev, L.N.Fateeva and Ya.A.Teplova; Sov. Phys. -JETP 16 (1963) 259.

30) J.R.Oppenheimer; Phys. Rev. 31 (1928) 349.

31) R.A.Mapleton; *Theory of Charge Exchange* (Willey, New York 1971).

32) N.F.Mott and H.S.W.Massey; *The Theory of Atomic Collisions* (Oxford, 1933).

33) N.F.Mott and H.S.W.Massey; *The Theory of Atomic Collisions*, 3rd edition (Oxford, 1965).

34) H.C.Brinkman and H.A.Kramers; Proc. Acad. Sci. Amsterdam 33 (1930) 973.

35) R.A.Mapleton; Phys. Rev. 122 (1961) 528.

36) R.A.Mapleton; Phys. Rev. 126 (1962) 1477.

37) R.A.Mapleton; Phys. Rev. 130 (1963) 1829.

38) J.D.Jackson and H.Schiff; Phys. Rev. 89 (1953) 359.

39) V.I.Gerasimenko and L.N.Rosentsveig; Sov. Phys. -JETP 4 (1957) 509.

40) K.L.Bell, V.Dose and A.E.Kingston; J. Phys. B 2 (1969) 831.

41) K.L.Bell and A.E.Kingston; J. Phys. B 11 (1978) 1259.

42) D.W.Rule; Phys. Rev. A 16 (1977) 19.

43) I.S.Dmitriev, Ya.M.Zhileikin and V.S.Nikolaev; Sov. Phys. -JETP 22 (1966) 352.

44) B.H.Kuper and E.Teller; Phys. Rev. 58 (1940) 602.

45) I.S.Dmitriev and V.S.Nikolaev; Sov. Phys. -JETP 17 (1963) 447.

46) S.K.Allison; Phys. Rev. 109 (1958) 76.

47) S.K.Allison; Phys. Rev. 110 (1958) 670.

48) C.F.Barnet and P.M.Stier; Phys. Rev. 109 (1958) 385.

49) E.S.Solov'ev, R.N.Il'in, V.A.Oparin and N.V.Fedorenko; Sov. Phys. -JETP 18 (1964) 342.

50) F.J.deHeer, I.Schutten and M.Moustafa; Physica 32 (1966) 1793.

51) H.B.Gilbody, K.F.Dunn, R.Browning and C.J.Latimer; J. Phys. B 3 (1970) 1105.

52) L.I.Pivovar, M.T.Novikov and V.M.Tubaev; Sov. Phys. -JETP 15 (1962) 1035.

53) L.I.Pivovar, V.M.Tubaev and M.T.Novikov; Sov. Phys. -JETP 14 (1962) 20.

54) V.S.Nikolaev, I.S.Dmitriev, L.N.Fateeva and Ya.A.Teplova;

Sov. Phys. -JETP 13 (1961) 695.

55) V.S.Nikolaev, L.N.Fateeva, I.S.Dmitriev and Ya.A.Teplova; Sov. Phys. -JETP 14 (1962) 67.

56) J.L.Puckett, G.O.Taylor and D.W.Martin; Phys. Rev. 178 (1969) 271.

57) P.Hvelplund, J.Heinemeier, E.Horsdal Pederson and F.R. Simpson; J. Phys. B 9 (1976) 491.

58) M.B.Shah, T.V. Goffe and H.B.Gilbody; J. Phys. B 10 (1977) L723.

59) P.Hvelplund and E.Horsdal Pederson; Phys. Rev. A 9 (1974) 2434.

60) E.Horsdal Pederson and P.Hvelplund; J. Phys. B 7 (1974) 132

61) S.C.Mukherjee, K.Roy and N.C.Sil1; J.Phys. B 6 (1973) 467.

62) T.F.Tuan and E.Gerjuory; Phys. Rev. 117 (1960) 756.

63) Wolfgang Lotz; J. Opt. Soc. of Am. 58 (1968) 915.

64) V.S.Nikolaev, I.S.Dmitriev, L.N.Fateeva and Ya.A.Teplova; Sov. Phys. -JETP 12 (1961) 627.

65) W.Meckbach and I.B.Nemirovsky; Phys. Rev. 153 (1967) 13.

66) P.Torres, W.Meckbach and A.Valenzuola; Phys. Rev. 183 (1969 216.

67) J.C.Armstrong, J.V.Mullendore, W.R.Harris and J.B.Marion; Proc. Phys. Soc. 86 (1963) 1283.

68) H.D.Betz and L.Grodzins; Phys. Rev. Lett. 25 (1970) 211.

69) G.Ryding, A.Wittkower and P.H.Rose; Phys. Rev. 184 (1969) 9

70) I.S.Dmitriev; Sov. Phys. -JETP 5 (1957) 473.

71) F.Nakao; Vacuum 25 (1975) 431.

72) H.D.Betz; Phys. Rev. Lett. 25 (1970) 903.

73) F.Fukuzawa, M.Tomita, M.Asari, A.Itoh and K.Ohnishi; *Contributions of the Research Group of Atoms and Molecules to Heavy Ions Science* (1979) p171.

74) A.Itoh, M.Asari and F.Fukuzawa; Abstracts of Contributed Papers to *XI International Conference on the Physics of Electronic and Atomic Collisions* (1979) p502.

Table II-1. Relative sensitivities of ionization gauge[71]. Values presented in brackets are uncertaintes in percent.

Molecule	Relative sensitivity	
H_2	0.44	0.05 (0.11)
He	0.19	0.04 (0.21)
N_2	1.00	0.00 (0.00)
O_2	0.87	0.09 (0.10)
CO_2	1.36	0.23 (0.17)
CH_4	1.49	0.19 (0.13)
C_2H_6	2.53	0.26 (0.10)
C_3H_8	3.80	0.40 (0.11)

Table V-1. Empirical formulae of charge-changing cross sections of helium projectile in the energy range 0.7-2.0 MeV for various gases: $\sigma(10^{-18}\ cm^2/molecule)$, E(MeV)

Target Gas	Capture Cross Sections		
	σ_{21}	σ_{10}	σ_{20}
H_2	$(4.8 \pm 0.5)E^{-(4.7 \pm 0.24)}$	$(1.0 \pm 0.1)E^{-(4.3 \pm 0.22)}$	$(0.07 \pm 0.006)E^{-(6.5 \pm 0.65)}$
H_e	$(11.0 \pm 1.1)E^{-(3.5 \pm 0.18)}$	$(2.4 \pm 0.3)E^{-(4.0 \pm 0.20)}$	$(0.20 \pm 0.06)E^{-(6.8 \pm 0.68)}$
N_2	$(38.0 \pm 4.0)E^{-(3.0 \pm 0.15)}$	$(4.6 \pm 0.5)E^{-(4.0 \pm 0.20)}$	$(1.20 \pm 0.36)E^{-(5.9 \pm 0.60)}$
O_2	$(46.0 \pm 4.6)E^{-(3.0 \pm 0.15)}$	$(6.0 \pm 0.6)E^{-(3.0 \pm 0.15)}$	$(0.90 \pm 0.18)E^{-(5.6 \pm 0.56)}$
CO_2	$(54.0 \pm 5.5)E^{-(3.0 \pm 0.15)}$	$(8.5 \pm 0.9)E^{-(2.9 \pm 0.15)}$	$(1.20 \pm 0.24)E^{-(6.0 \pm 0.60)}$
CH_4	$(20.0 \pm 2.1)E^{-(3.4 \pm 0.17)}$	$(2.8 \pm 0.3)E^{-(3.6 \pm 0.18)}$	$(0.35 \pm 0.07)E^{-(5.6 \pm 0.56)}$
C_2H_6	$(30.0 \pm 3.0)E^{-(3.2 \pm 0.16)}$	$(5.0 \pm 0.5)E^{-(3.0 \pm 0.16)}$	$(0.63 \pm 0.13)E^{-(5.1 \pm 0.50)}$
C_3H_8	$(45.0 \pm 4.5)E^{-(3.0 \pm 0.15)}$	$(6.3 \pm 0.6)E^{-(2.8 \pm 0.14)}$	

Table V-1 (continued)

Target Gas	Loss Cross Sections σ_{01}	σ_{12}
H_2	$(53 \pm 5.3)E^{-(0.70 \pm 0.07)}$	$(17.0 \pm 1.7)E^{-(0.70 \pm 0.07)}$
He	$(45 \pm 4.5)E^{-(0.72 \pm 0.07)}$	$(16.5 \pm 1.7)E^{-(0.53 \pm 0.05)}$
N_2	$(215 \pm 22)E^{-(0.40 \pm 0.04)}$	$(100 \pm 10)E^{-(0.39 \pm 0.04)}$
O_2	$(185 \pm 19)E^{-(0.48 \pm 0.05)}$	$(90.0 \pm 9.0)E^{-(0.30 \pm 0.03)}$
CO_2	$(255 \pm 26)E^{-(0.38 \pm 0.04)}$	$(115 \pm 12)E^{-(0.30 \pm 0.03)}$
CH_4	$(160 \pm 16)E^{-(0.61 \pm 0.06)}$	$(68.0 \pm 6.9)E^{-(0.40 \pm 0.04)}$
C_2H_6	$(250 \pm 25)E^{-(0.54 \pm 0.06)}$	$(100 \pm 10)E^{-(0.25 \pm 0.03)}$
C_3H_8	$(370 \pm 37)E^{-(0.37 \pm 0.04)}$	$(155 \pm 16)E^{-(0.43 \pm 0.04)}$

Table VI-1. Estimation of charge-changing cross sections of helium projectile for a carbon atom as a target. Estimations were made from two methods; the cross sections denoted by asterisk are from the ordinary method, and otherwise are from the present new method.

Energy	LOSS			CAPTURE		
	σ_{01}	σ_{02}	σ_{12}	σ_{10}	σ_{21}	σ_{20}
0.7 MeV	58 ± 14	8.7 ± 1.6	27 ± 5.5	2.0 ± 0.8	13 ± 5.6	0.96 ± 0.41
*	79 ± 32	8.6 ± 5.1	34 ± 15	5.5 ± 2.8	21 ± 17	2.5 ± 1.2
1.0 MeV	54 ± 17	9.3 ± 0.7	30 ± 4.1	0.6 ± 0.3	4.6 ± 0.5	0.17 ± 0.04
*	73 ± 29	13 ± 6	26 ± 14	5.2 ± 1.2	3.4 ± 4.8	0.19 ± 0.13
1.5 MeV	63 ± 13	13 ± 1.2	29 ± 1.8	0.39 ± 0.13	2.3 ± 0.6	0.03 ± 0.03
*	55 ± 27	10 ± 4.8	22 ± 5.3	0.37 ± 0.52	8.6 ± 2.7	0.02 ± 0.04
2.0 MeV			29 ± 4		1.61 ± 0.08	
*			19 ± 13		1.4 ± 0.9	

Table VI-2. Empirical cross sections for single atoms of H, O and C: Cross sections are presented in unit of 10^{-18} cm^2/atom, and E is the incident helium energy in unit of MeV.

Target atom	Capture			Loss	
	σ_{21}	σ_{10}	σ_{20}	σ_{01}	σ_{12}
H	$2.4E^{-4.7}$	$0.5E^{-4.3}$	$0.035E^{-6.5}$	$27.0E^{-0.70}$	$9.0E^{-0.70}$
O	$23.0E^{-3.0}$	$3.0E^{-3.0}$	$0.45E^{-5.6}$	$93.0E^{-0.48}$	$45.0E^{-0.30}$
C	$6.0E^{-3.0}$	$0.7E^{-3.0}$	$0.18E^{-4.8}$	$65.0E^{-0.40}$	$30.0E^{-0.30}$

Table VII-1. Experimental values of equilibrium charge fractions and average charges of helium ions.

Target Gas	F_0	F_1	F_2	$\bar{q}$	Energy (MeV)
	0.02	0.410	0.572	1.55	0.7
H_2	0.0025	0.153	0.845	1.84	1.0
	0.0002	0.042	0.96	1.96	1.5
		0.013	0.986	1.99	2.0
	0.075	0.58	0.35	1.28	0.7
He	0.02	0.377	0.603	1.58	1.0
	0.0033	0.171	0.826	1.82	1.5
		0.080	0.92	1.92	2.0
	0.032	0.443	0.526	1.50	0.7
N_2	0.0055	0.246	0.748	1.74	1.0
	0.0004	0.102	0.898	1.90	1.5
		0.052	0.948	1.95	2.0
	0.045	0.505	0.449	1.40	0.7
O_2	0.01	0.311	0.678	1.67	1.0
	0.0016	0.138	0.861	1.86	1.5
		0.066	0.934	1.93	2.0
	0.032	0.473	0.495	1.46	0.7
CO_2	0.0084	0.289	0.703	1.70	1.0
	0.0016	0.122	0.877	1.88	1.5
		0.067	0.933	1.93	2.0

Table VII-1 (continued)

	0.018	0.398	0.584	1.57	0.7
CH_4	0.003	0.185	0.812	1.81	1.0
	0.00053	0.072	0.928	1.93	1.5
		0.039	0.961	1.96	2.0
	0.02	0.398	0.583	1.56	0.7
C_2H_6	0.0005	0.078	0.921	1.92	1.5
	0.019	0.398	0.585	1.57	0.7
C_3H_8	0.0027	0.190	0.810	1.81	1.0
	0.00025	0.072	0.928	1.93	1.5
		0.042	0.958	1.96	2.0

Table VII-2. Empirical formulae of equilibrium ratios F_0/F_2 and F_1/F_2 for various gases, where E is the projectile energy in unit of MeV.

Target Gas	F_0/F_2	F_1/F_2
H_2	$3.0\times10^{-3}E^{-6.72}$	$0.18E^{-3.8}$
He	$3.32\times10^{-2}E^{-5.22}$	$0.63E^{-2.8}$
N_2	$7.35\times10^{-3}E^{-6.04}$	$0.33E^{-2.6}$
O_2	$1.47\times10^{-2}E^{-5.23}$	$0.46E^{-2.6}$
CO_2	$1.20\times10^{-2}E^{-4.68}$	$0.40E^{-2.5}$
CH_4	$3.70\times10^{-3}E^{-5.57}$	$0.25E^{-2.7}$
C_2H_6	$4.93\times10^{-3}E^{-5.44}$	$0.24E^{-2.7}$
C_3H_8	$3.33\times10^{-3}E^{-6.29}$	$0.25E^{-2.7}$

Table VII-3. Experimental values of equilibrium average charges of 1.0 MeV helium ions. Value in gas C_2H_6 is the interpolated one in Fig. 7-1(7).

Target Gas (Molecular Weight)	H_2 (2)	CH_4 (16)	C_2H_6 (30)	C_3H_8 (44)	C_5H_{12} (72)	C_6H_{14} (86)	C_7H_{16} (100)	C_8H_{18} (114)
$\bar{q}$	1.84	1.81	1.77	1.81	1.80	1.78	1.80	1.83
Target Gas (Molecular Weight)	He (4)	Ar (40)	N_2 (28)	O_2 (32)	CO_2 (44)			
$\bar{q}$	1.58	1.88	1.74	1.67	1.70			

Figure Captions

Fig. 2-1. Experimental arrangement for measuring charge changing collisions: C1-C2; collimating slits, A1-A5; apertures, E1-E3; electrostatic deflectors. Dimensions of these slit-system are follows; less than 0.1 x 0.1 mm^2 for C1-C2, 5 mm-diam for A1, 2 mm-diam for A2-A5. Portions of the beam transport ducts surrounded by C1 and C2 is an initial charge-state selection chamber.

Fig. 2-2. Block diagram of the electronics; position-sensitive-detector bias is about 60 V.

Fig. 2-3. An example of energy spectra obtained from the PSD, by using the 1.5 MeV He^+ incidence on methane gas. Discrimination of energy spectra is taken between two arrows, which is variable according to the incident energies.

Fig. 2-4. Examples of position spectra from the PSD, measured by using 0.7 MeV $He^{0,1+,2+}$ incidences on oxygen gas at 3.5×10^{3} Torr.

Fig. 3-1(1)-(30). Variations of charge fractions (growth curves) of 0.7-2.0 MeV helium as a function of target thickness (Torr cm). Projectile energies and target gases are represented in the lower part of figures. Closed circles; He^0 incidences, open circles; He^+ incidences, open triangles; He^{2+} incidences. Solide lines are the calculated fraction-curves according to Runge-Kutta

integration method applied for Eq. (3.1) with use of experimentally obtained charge-changing cross sections.

Fig. 3-2. Example of linear-variations of charge fractions in respective to the target thickness measured by using the 1.5 MeV He^+ incidence on helium gas, all the other fractions have also linear relations.

Fig. 5-1(1)-(8). Present charge-changing cross sections(cm^2/molecule) of helium as a function of projectile energy, in colliding with H_2, He, N_2, O_2, CO_2, CH_4, C_2H_6 and C_3H_8 molecules, respectively. Open symbols represent the loss cross sections and closed symbols represent capture ones; o σ_{01}, Δ σ_{12}, $\square$ σ_{02}, $\bullet$ σ_{21}, $\blacktriangle$ σ_{10}, $\blacksquare$ σ_{20}. Solid lines are the computed values of the empirical formulae obtained by applying the form aE^{-p} to the cross sections (see text.).

Fig. 5-2(1)-(4). Comparisons of capture cross sections for H_2, He N_2 and O_2 with other experimental and theoretical values: Experimental; —o— present, • Pivovar et al (refs. 52,53), + Nikolaev et al (ref. 54,55), x Hvelplund et al (ref. 57). Theoretical; S Schiff (ref. 16), M Mukherjee et al (ref. 61), G Gerasimenko and Rosentsveig (ref. 39), B Bohr (ref. 24), MB present.

Fig. 5-3(1)-(4). Comparisons of loss cross sections for H_2, He, N_2 and O_2 with other experimental and theoretical values: Experimental; o Δ $\square$ present, • Hvelplund et al (refs. 59,60), + Pivovar et al (ref. 53), ▼ Shah et al

(ref. 58), o Gilbody et al (ref. 51), ▲ Solov'ev et al (ref. 49), x Barnet and Stier (ref. 48), ■ Dmitriev et al (ref. 28). Theoretical; Bell Bell et al (ref. 40, 41), D Dmitriev et al (ref. 43), B Bohr (ref. 24).

Fig. 5-5(1)-(2). Comparisons of loss cross sections for H_2 and He with theoretical values; o σ_{01}, Δ σ_{12} are the present experimental cross sections, and curves shown in the figures are explained in the text.

Fig. 5-6. Energy dependence of capture (upper) and loss (lower) cross sections. Powers p in the form $\sigma = aE^{-p}$ are plotted as a function of total number of electrons contained in a molecule; dotted lines represent the predicted values (3 for capture and 0.5 for loss) from the theory of Bohr (ref. 24).

Fig. 5-7. Ratios of cross sections σ_{20}/σ_{21} and σ_{01}/σ_{12} as a function of total number of electrons in a molecule.

Fig. 5-8(1)-(2). Target atomic number Z_T dependence of loss and capture cross sections for Z_T = 1,2,7 and 8. Presented cross sections (cm^2/atom) are plotted relatively to the hydrogen data. In the case of loss cross sections (Fig.5-8(1)), the carbon cross sections (Z_T = 6) estimated by using the additive rule are also shown.

Fig. 5-9(1)-(2). Medium dependence of loss and capture cross sections as a function of total number of electrons in a molecule; open circles correspond to hydrogen-containing molecules C_nH_{2n+2}, closed circles to other molecules He, N_2, O_2 and CO_2, and + for carbon atom(Fig.5-9(1)). .

Fig. 6-1(1)-(6). Relative cross sections σ_{21}, σ_{20}, σ_{10}, σ_{12}, σ_{02} and σ_{01} for the molecules C_nH_{2n+2} (n = 0,1,2,3) as a function of total number of carbon atoms in the molecule.

Fig. 6-2. Carbon cross sections (cm^2/atom) estimated from the present newly developed procedure (see the text). Solid lines are the empirical lines determined by the least square fitting of the cross sections to the form $\sigma = aE^{-p}$.

Fig. 6-3(1)-(2). Comparisons of experimental capture and loss cross sections (o, Δ, $\square$) with calculated ones (denoted by dot-dash curves) from the additive rule. Calculations are made by using empirical formulae of cross sections for constituent single atoms H, C and O.

Fig. 7-1(1)-(8). Equilibrium charge fractions of helium penetrated through H_2, He, N_2, O_2, CH_4, C_2H_6, C_3H_8 and CO_2. o, Δ, $\square$ present, • Pivovar et al (ref. 53), + Torres and Meckbach et al (ref. 65,66). Experimental errors of the present values are within symbols.

Fig. 7-2. Examples of the equilibrium fraction ratios F_0/F_2, F_1/F_2 for the gases H_2, N_2 and CH_4.

Fig. 7-3(1)-(8). Presence probabilities $(1 - P_1)$ for keeping one of electrons in He^0, and $(1 - P_2)$ for a electron in He as a function of ion velocity. Open circles are the shifted values of $(1 - P_1)$.

Fig. 7-4. Average equilibrium charges of helium in various gases Solid curves are the present values and dotted line

represents the average charge of ions penetrating through carbon foil (ref. 67).

Fig. 7-5. Avera charge of helium ions at 1.0 MeV in various gases: o C_nH_{2n+2}(n = 0,1,3,5,6,7,8), ● N_2, ▲ O_2, Δ CO_2, □ He, ■ Ar.

Fig. 7-6. Average charge of helium ions in the energy below 0.8 MeV: All the data are borrowed from others; Torres *et al* for H_2 and N_2, Meckbach *et al* for He, Armstrong *et al* for carbon foil.

Fig. 7-7. Charge state distributions of heavy ions in gases and solid. Upper figure shows equilibrium fractions of 12 MeV iodine ions measured by Ryding *et al*(ref. 14), and lower figure shows charge fractions of 87 MeV krypton ion measured by Clark *et al* quoted in the reference (15).

Fig. 7-8. Comparisons of present average charges with calculated values from the theories of Dmitriev (refs. 20, 70). Solid lines are from ref.70), and dotted lines are from ref. 20).

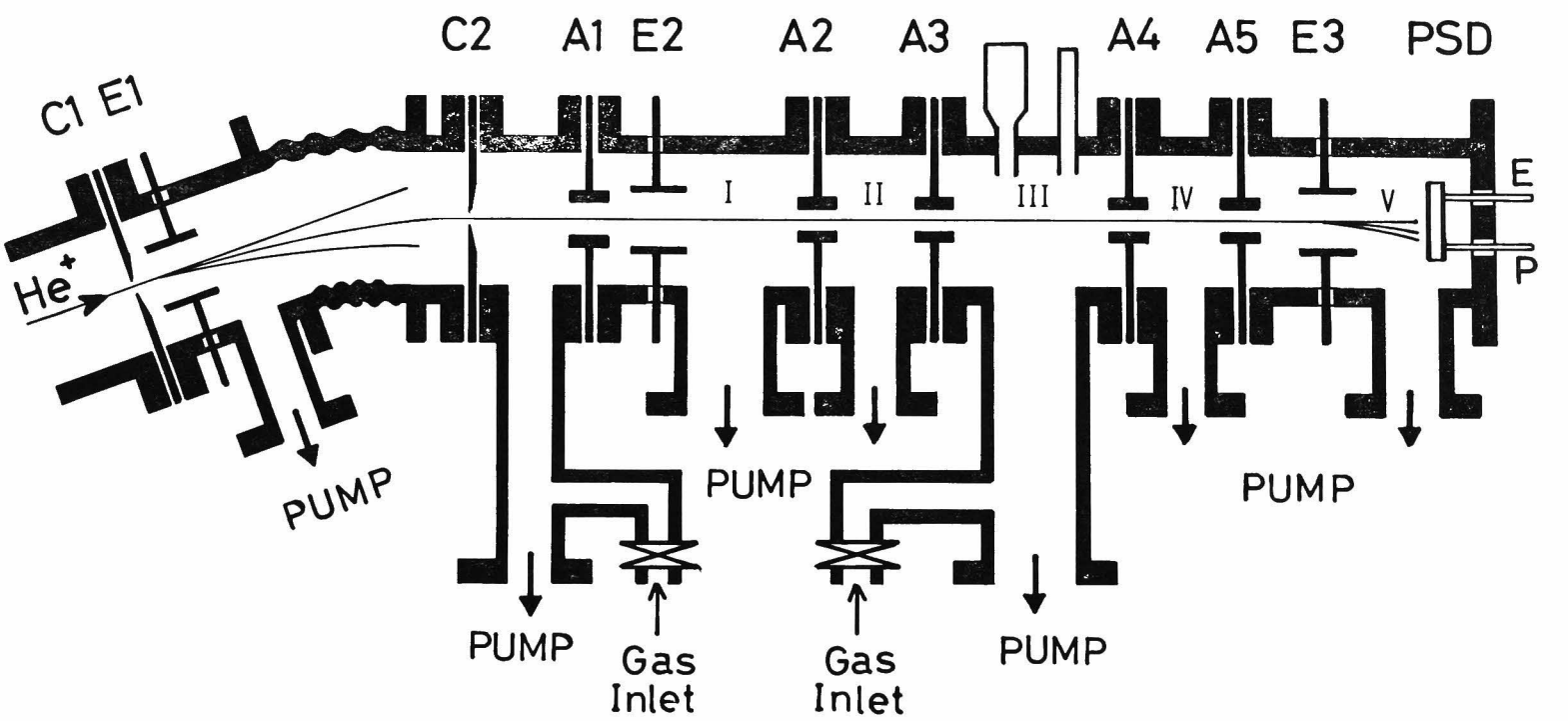
C2
A1
E2
A2
A3
A4
A5
E3
PSD
C1
E1
He+
I
II
III
IV
V
E
P
PUMP
PUMP
PUMP
PUMP
PUMP
Gas
Inlet
Gas
Inlet

FIG. 2-1

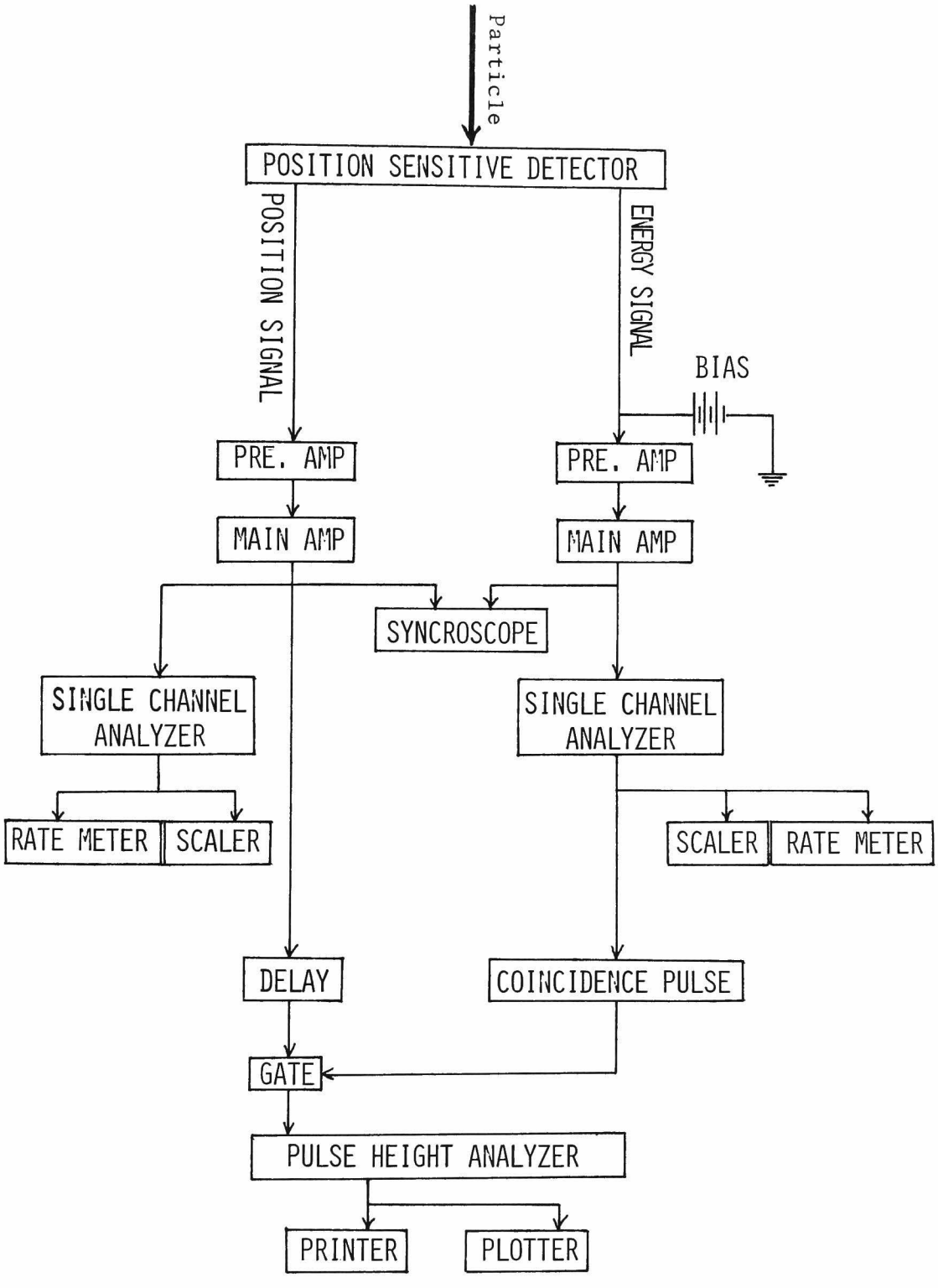
Particle
POSITION SENSITIVE DETECTOR
POSITION SIGNAL
ENERGY SIGNAL
BIAS
PRE. AMP
PRE. AMP
MAIN AMP
MAIN AMP
SYNCROSCOPE
SINGLE CHANNEL ANALYZER
SINGLE CHANNEL ANALYZER
RATE METER
SCALER
SCALER
RATE METER
DELAY
COINCIDENCE PULSE
GATE
PULSE HEIGHT ANALYZER
PRINTER
PLOTTER

FIG. 2-2

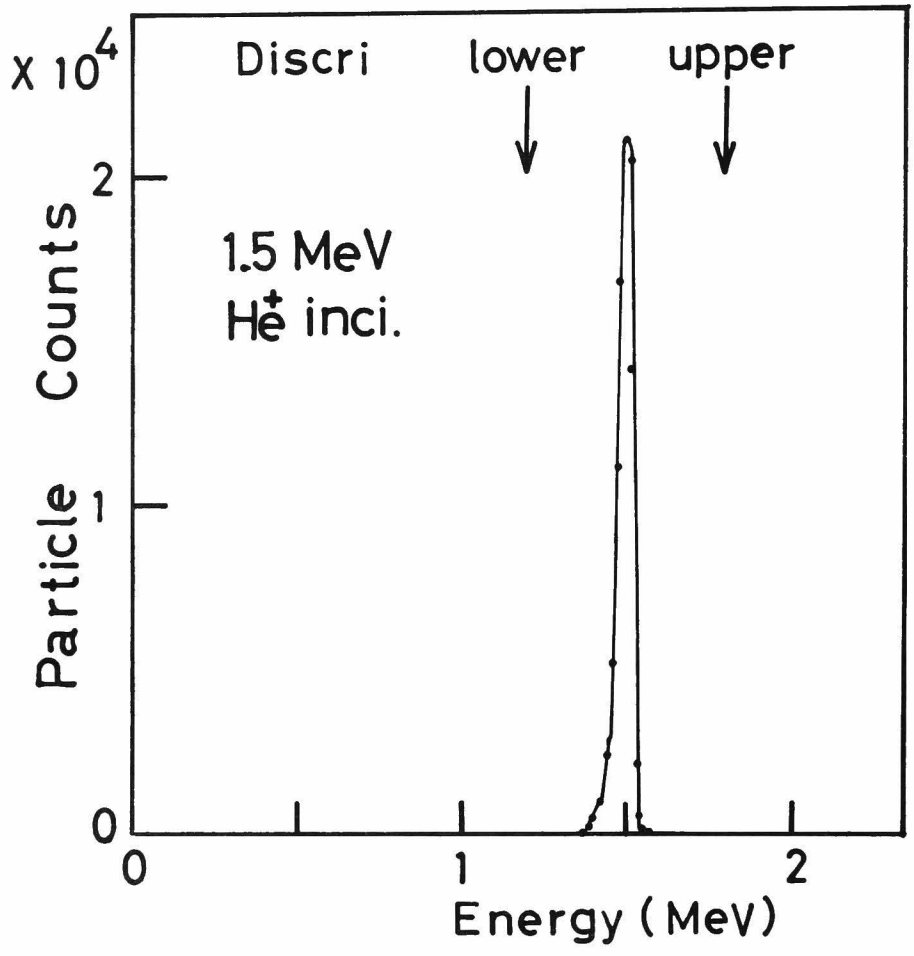
X 10^4
Discri
lower
upper
2
1.5 MeV
He+ inci.
Particle Counts
1
0
0
1
2
Energy (MeV)

FIG. 2-3

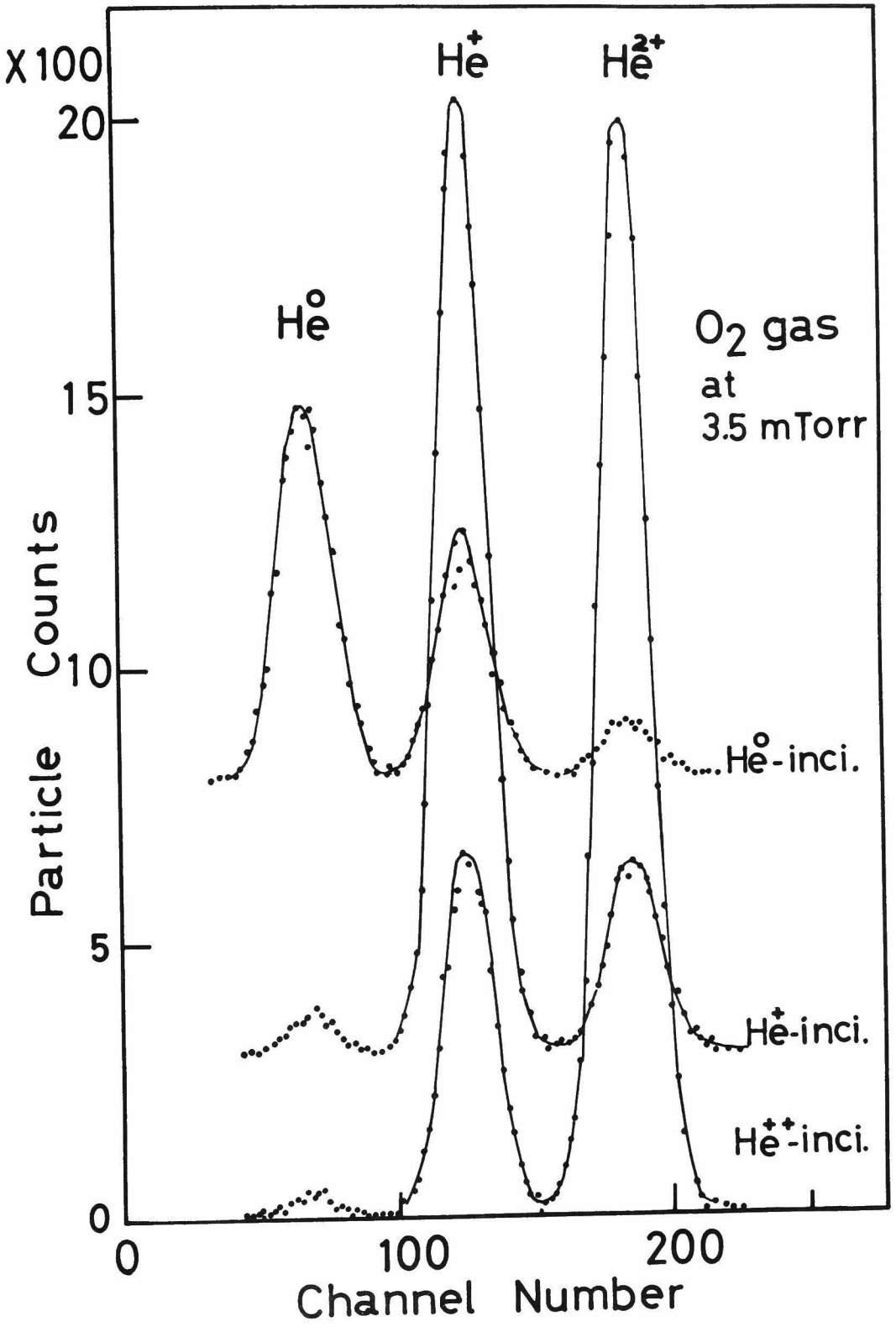
X100
20
15
10
5
0
Particle Counts
He°
He+
He2+
O2 gas
at
3.5 mTorr
He°-inci.
He+-inci.
He++-inci.
0
100
200
Channel Number

FIG. 2-4

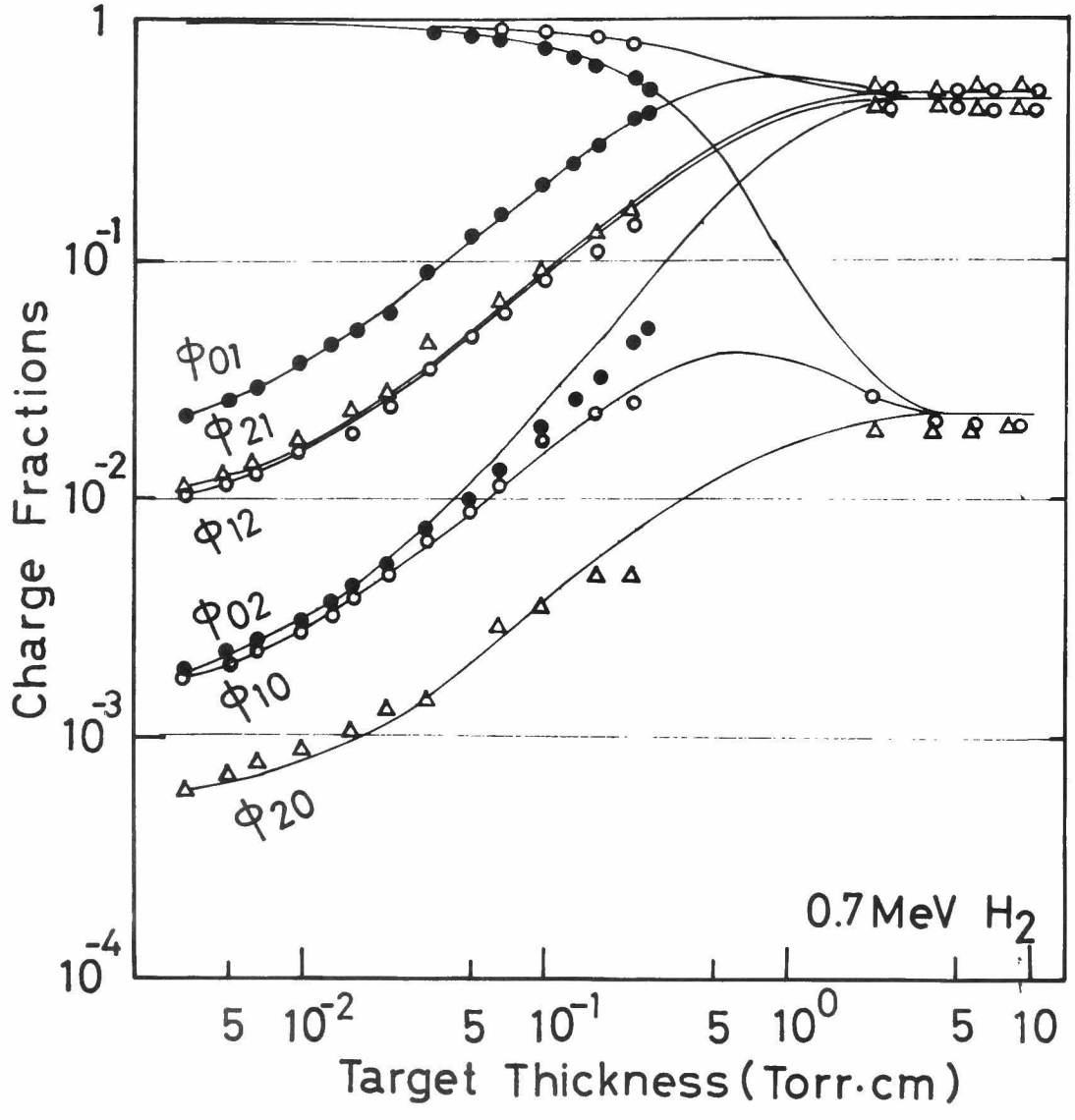
1
10^{-1}
10^{-2}
10^{-3}
10^{-4}
Charge Fractions
ϕ_{01}
ϕ_{21}
ϕ_{12}
ϕ_{02}
ϕ_{10}
ϕ_{20}
0.7MeV H_2
5 10^{-2} 5 10^{-1} 5 10^{0} 5 10
Target Thickness (Torr·cm)

FIG. 3-1(1)

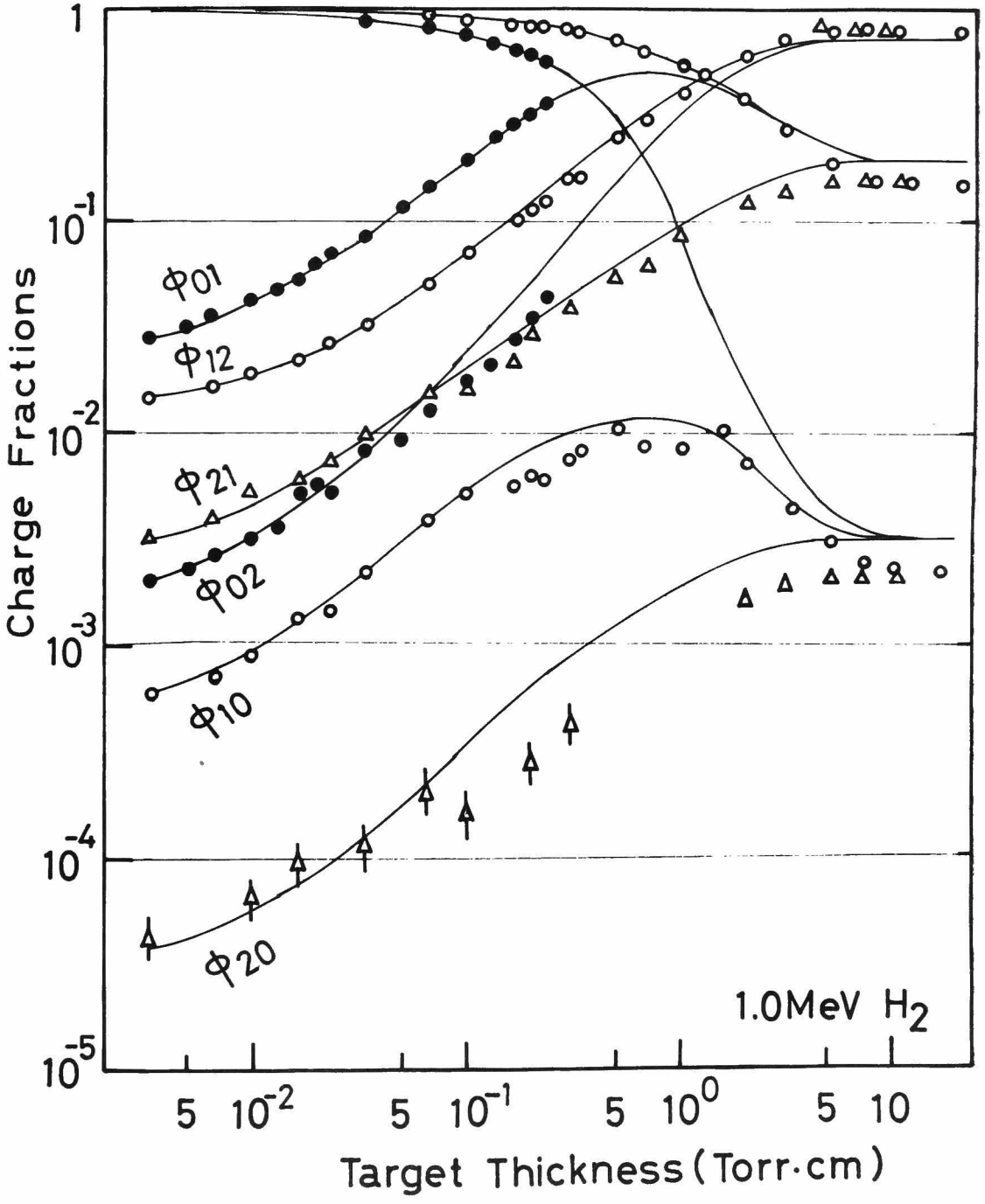
1
10^{-1}
10^{-2}
10^{-3}
10^{-4}
10^{-5}
Charge Fractions
Φ_{01}
Φ_{12}
Φ_{21}
Φ_{02}
Φ_{10}
Φ_{20}
1.0MeV H_2
5 10^{-2}
5 10^{-1}
5 10^{0}
5 10
Target Thickness (Torr·cm)

FIG. 3-1(2)

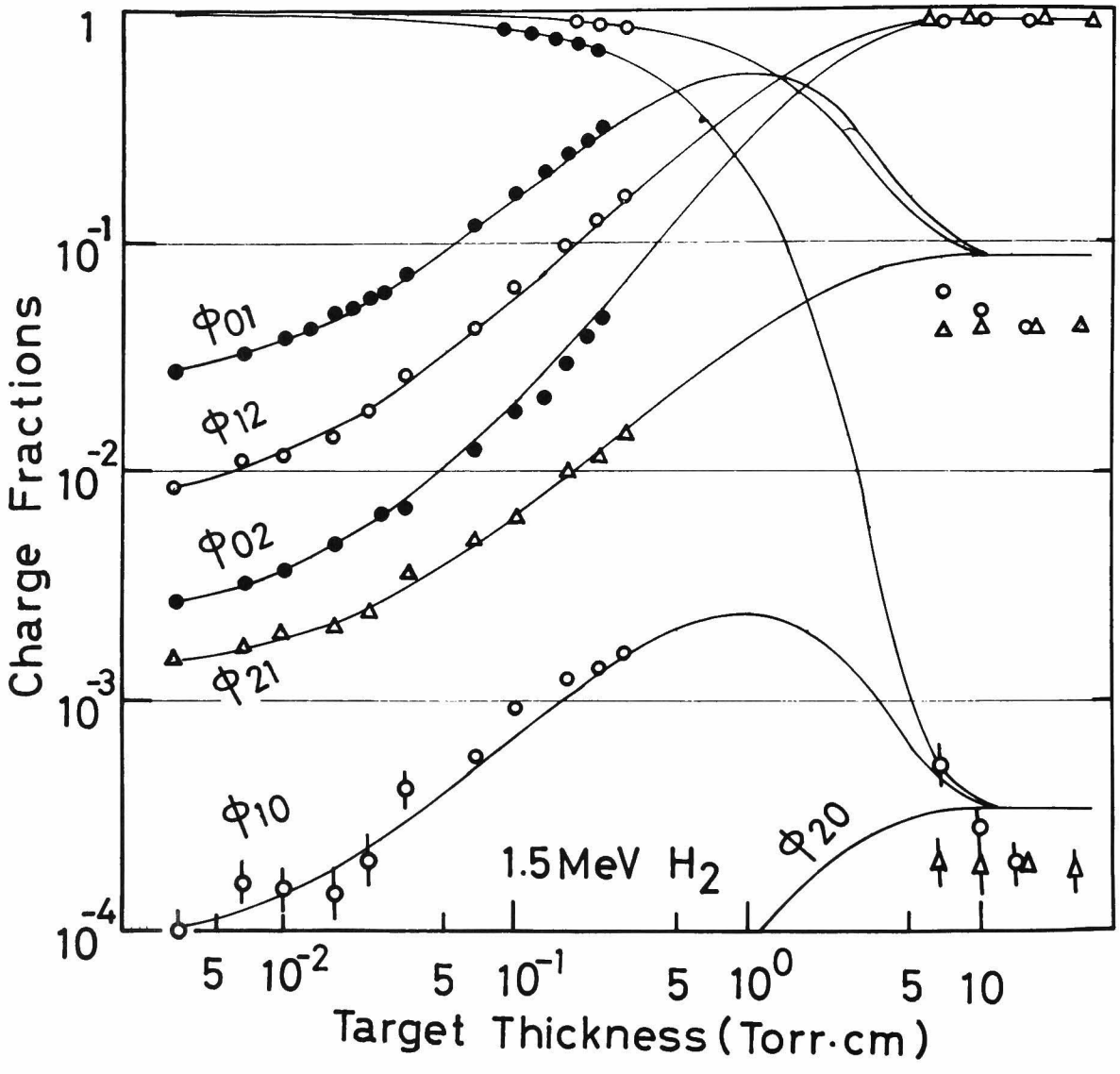
1
10^{-1}
10^{-2}
10^{-3}
10^{-4}
Charge Fractions
ϕ_{01}
ϕ_{12}
ϕ_{02}
ϕ_{21}
ϕ_{10}
ϕ_{20}
1.5MeV H_2
5 10^{-2}
5 10^{-1}
5 10^{0}
5 10
Target Thickness (Torr·cm)

FIG. 3-1(3)

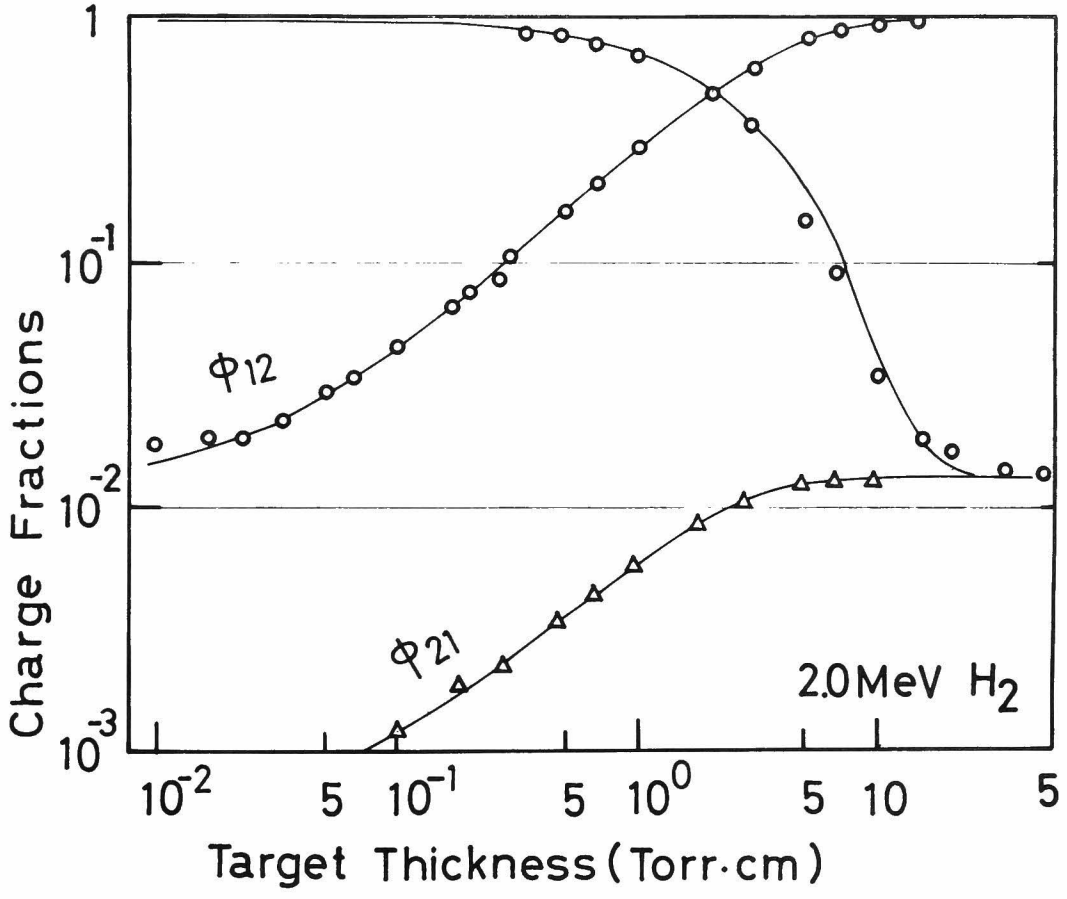
1
10^{-1}
10^{-2}
10^{-3}
Charge Fractions
Φ_{12}
Φ_{21}
2.0MeV H_2
10^{-2}
5
10^{-1}
5
10^{0}
5
10
5
Target Thickness (Torr·cm)

FIG. 3-1(4)

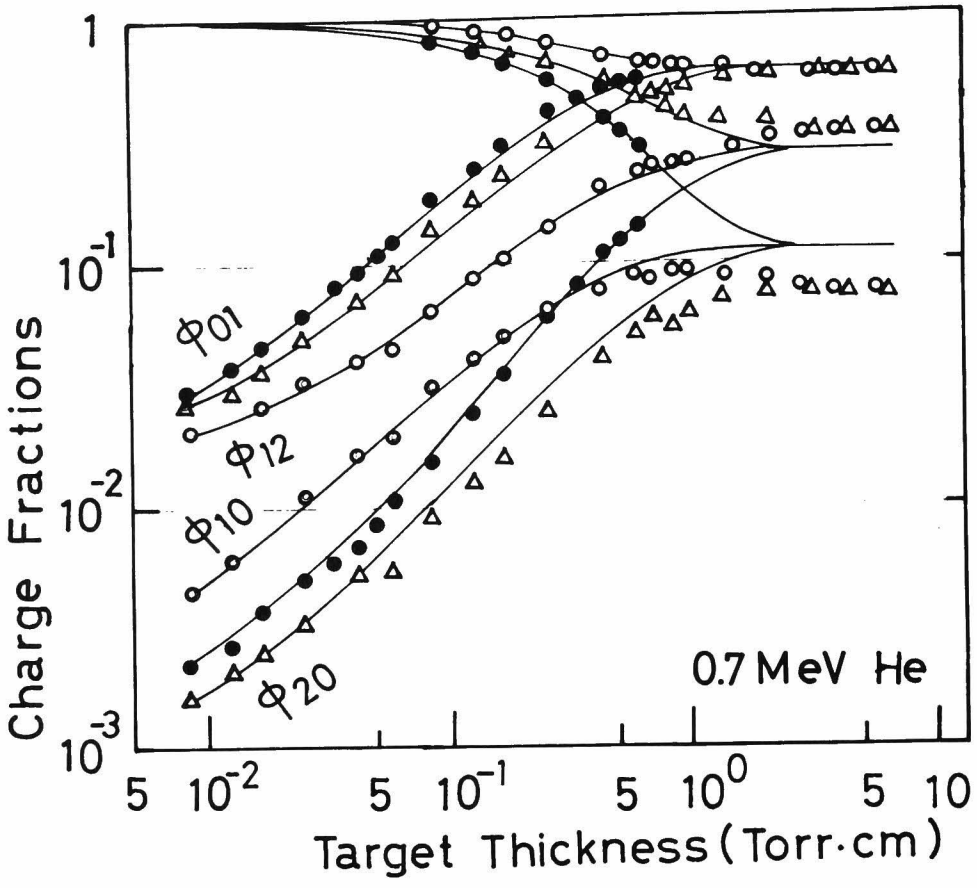
1
10^{-1}
10^{-2}
10^{-3}
Charge Fractions
ϕ_{01}
ϕ_{12}
ϕ_{10}
ϕ_{20}
0.7 MeV He
5 10^{-2}
5 10^{-1}
5 10^{0}
5 10
Target Thickness (Torr·cm)

FIG. 3-1(5)

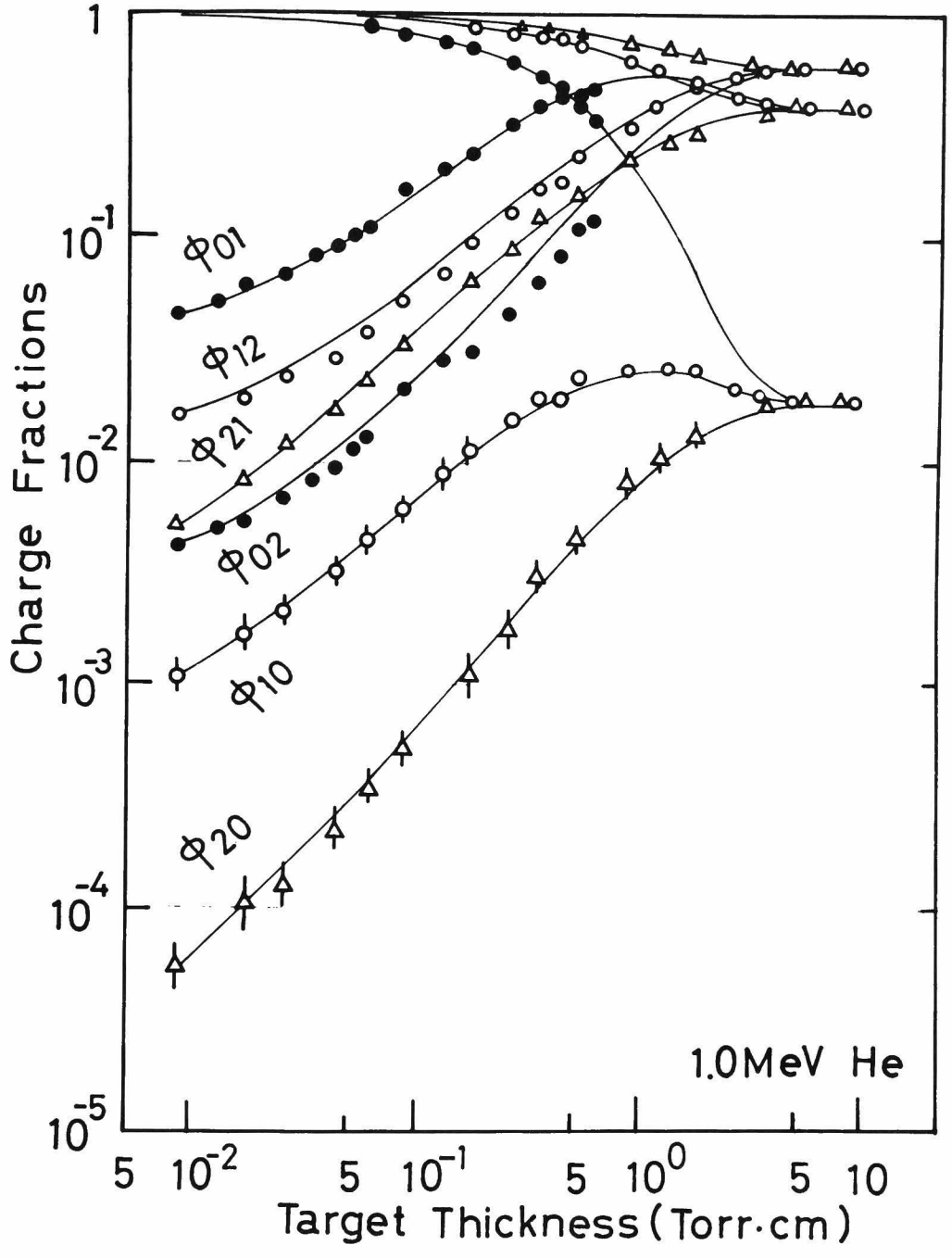
1
10^{-1}
10^{-2}
10^{-3}
10^{-4}
10^{-5}
Charge Fractions
ϕ_{01}
ϕ_{12}
ϕ_{21}
ϕ_{02}
ϕ_{10}
ϕ_{20}
1.0MeV He
5 10^{-2}
5 10^{-1}
5 10^{0}
5 10
Target Thickness (Torr·cm)

FIG. 3-1(6)

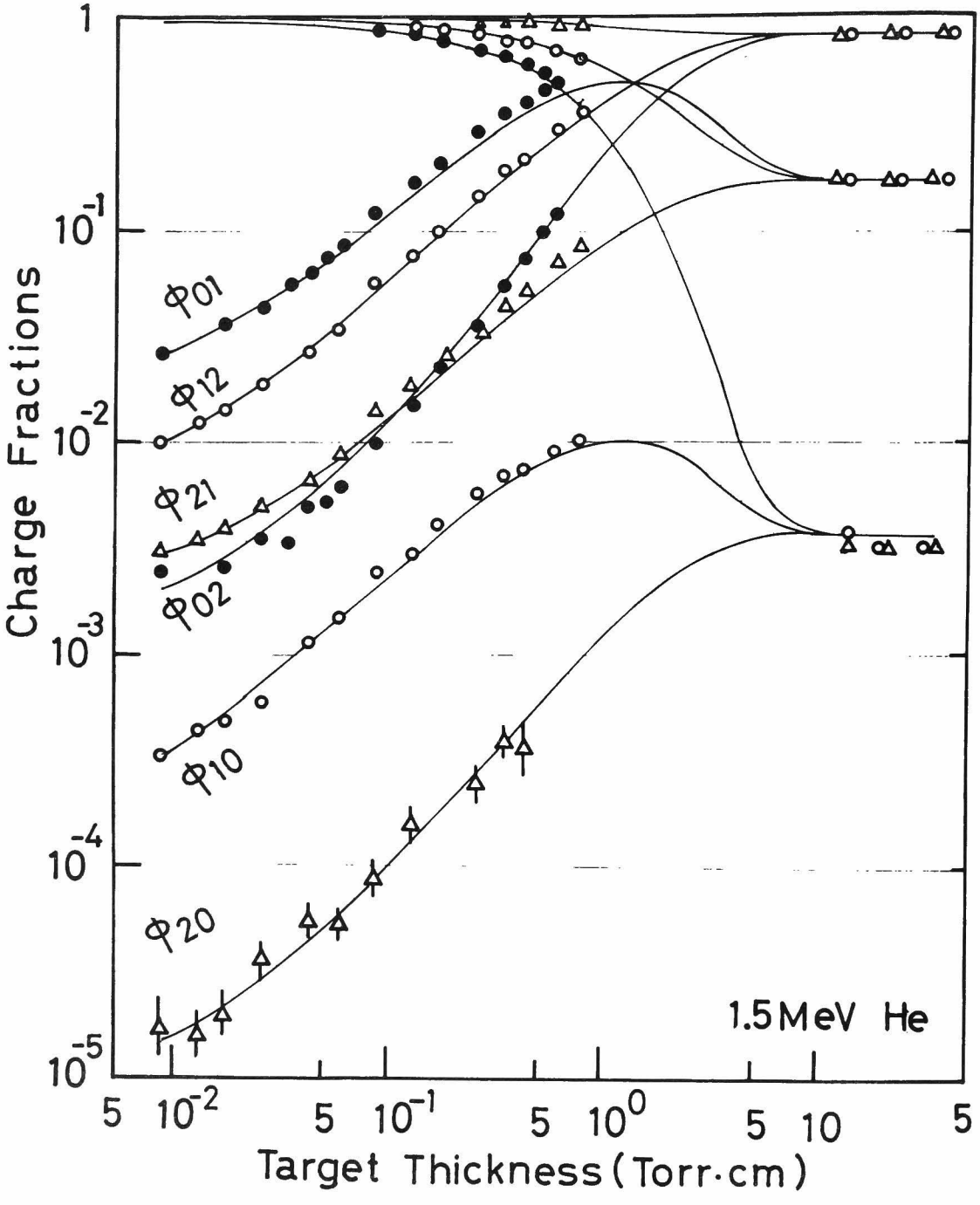
1
10^{-1}
10^{-2}
10^{-3}
10^{-4}
10^{-5}
Charge Fractions
ϕ_{01}
ϕ_{12}
ϕ_{21}
ϕ_{02}
ϕ_{10}
ϕ_{20}
1.5 MeV He
5 10^{-2}
5 10^{-1}
5 10^{0}
5 10
5
Target Thickness (Torr·cm)

FIG. 3-1(7)

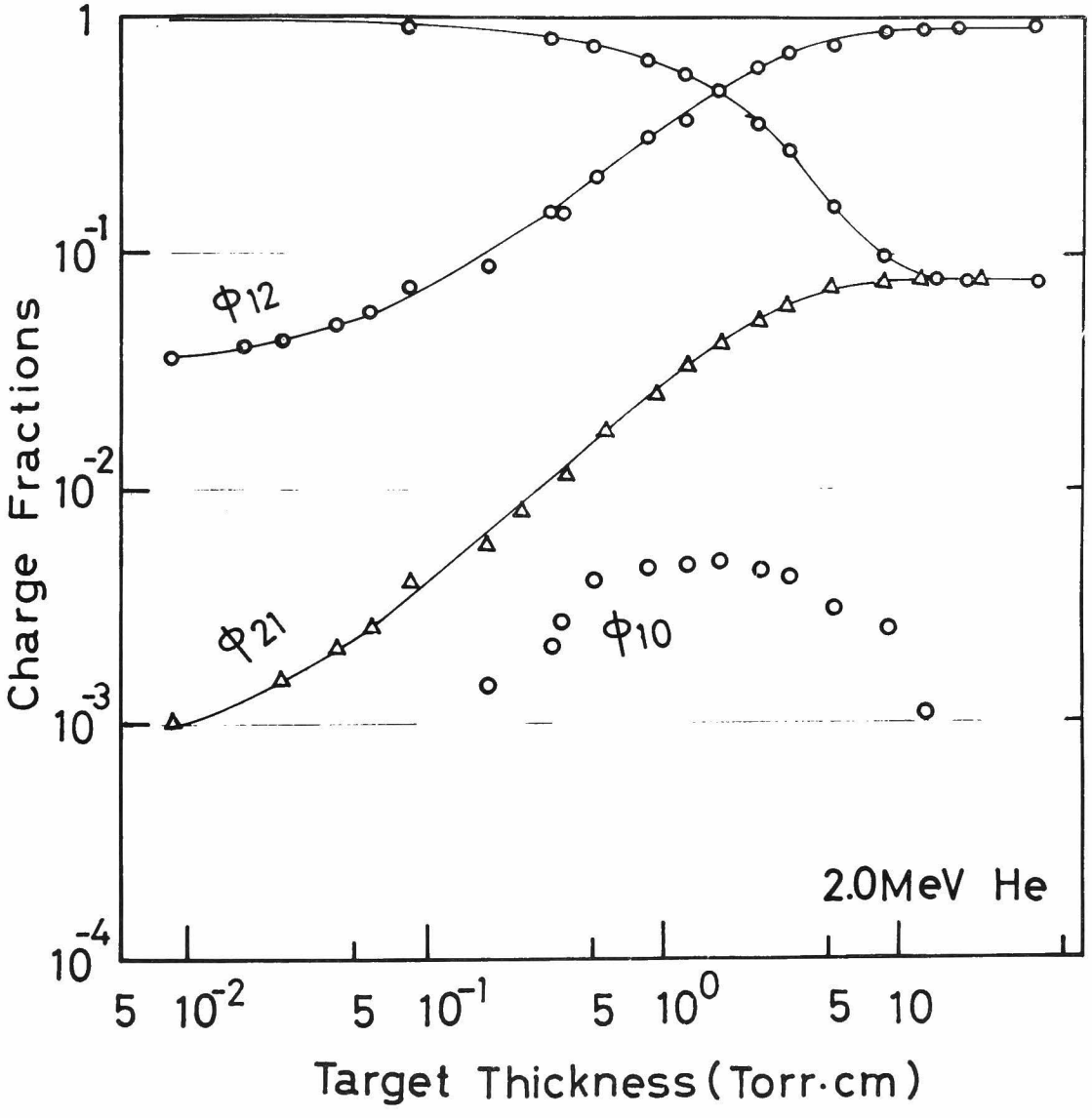
1
10^{-1}
10^{-2}
10^{-3}
10^{-4}
Charge Fractions
ϕ_{12}
ϕ_{21}
ϕ_{10}
2.0MeV He
5 10^{-2}
5 10^{-1}
5 10^{0}
5 10
Target Thickness (Torr·cm)

FIG. 3-1(8)

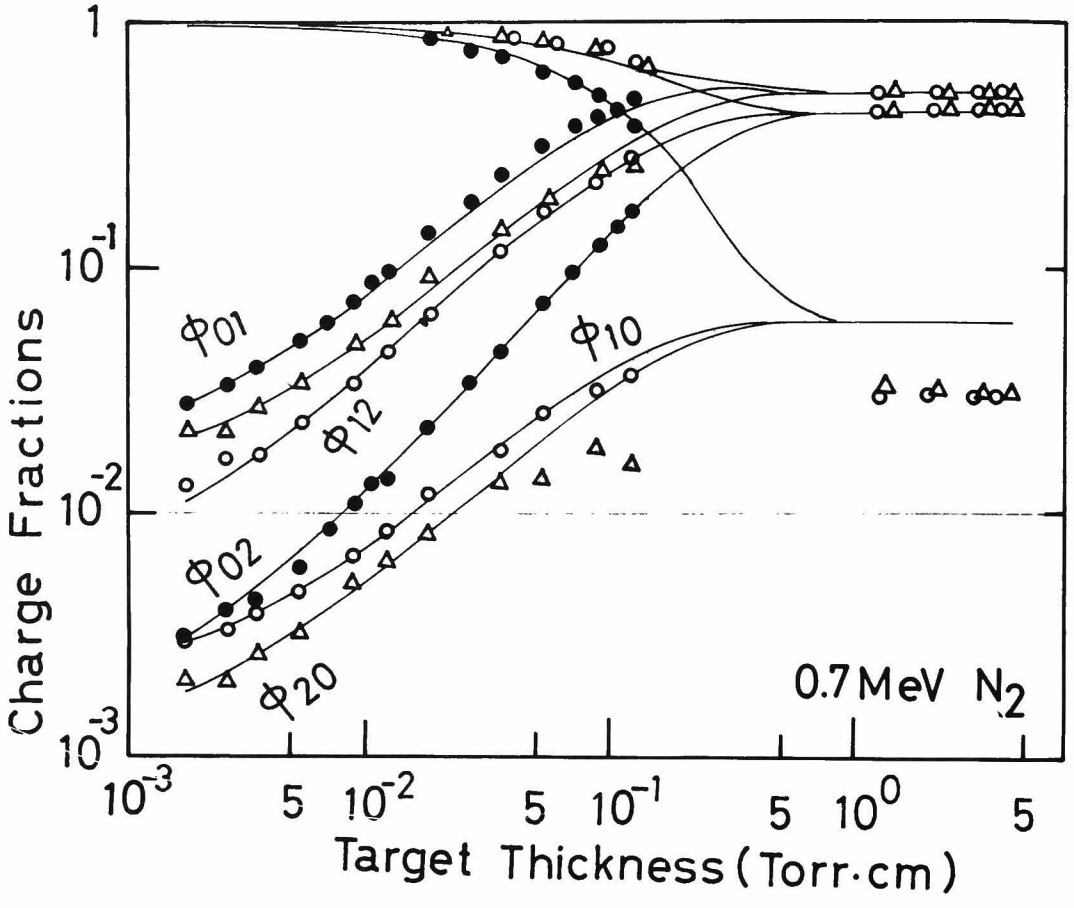
1
10^{-1}
10^{-2}
10^{-3}
Charge Fractions
ϕ_{01}
ϕ_{12}
ϕ_{10}
ϕ_{02}
ϕ_{20}
0.7 MeV N_2
10^{-3}
5 10^{-2}
5 10^{-1}
5 10^{0}
5
Target Thickness (Torr·cm)

FIG. 3-1(9)

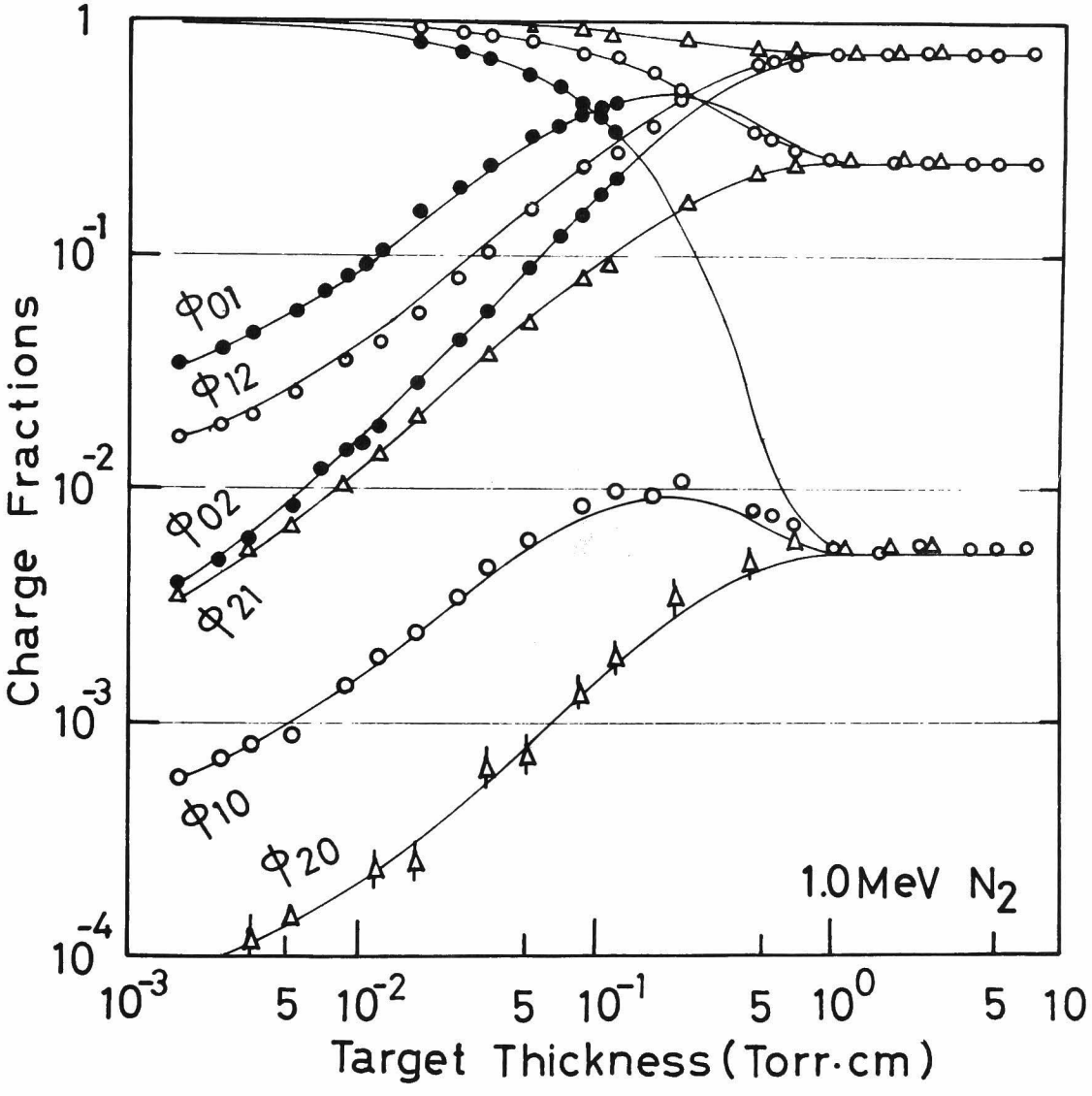
1
10^{-1}
10^{-2}
10^{-3}
10^{-4}
Charge Fractions
ϕ_{01}
ϕ_{12}
ϕ_{02}
ϕ_{21}
ϕ_{10}
ϕ_{20}
1.0MeV N_2
10^{-3}
5 10^{-2}
5 10^{-1}
5 10^{0}
5 10
Target Thickness (Torr·cm)

FIG. 3-1(10)

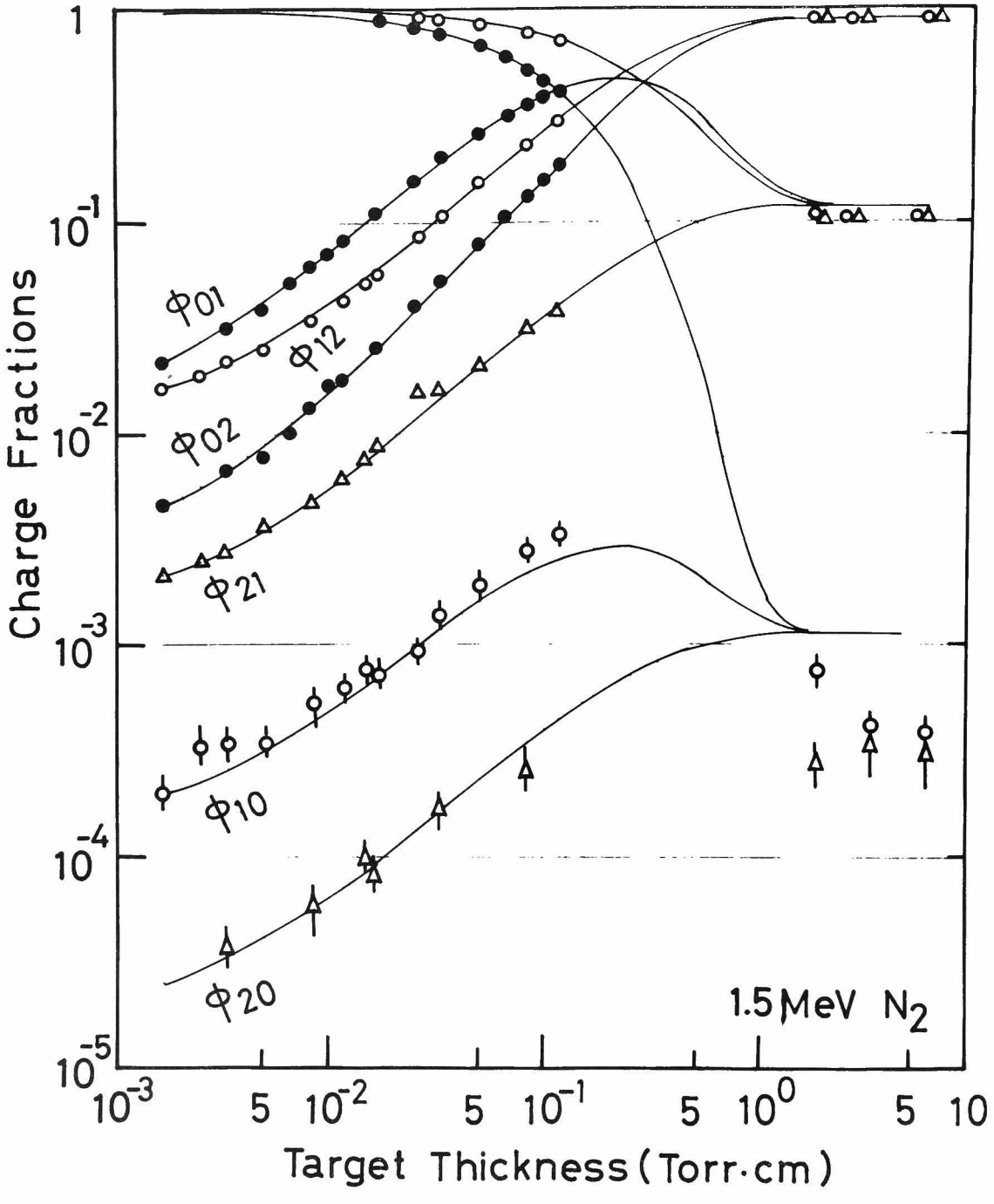
1
10^{-1}
10^{-2}
10^{-3}
10^{-4}
10^{-5}
Charge Fractions
ϕ_{01}
ϕ_{12}
ϕ_{02}
ϕ_{21}
ϕ_{10}
ϕ_{20}
1.5 MeV N_2
10^{-3}
5 10^{-2}
5 10^{-1}
5 10^{0}
5 10
Target Thickness (Torr·cm)

FIG. 3-1(11)

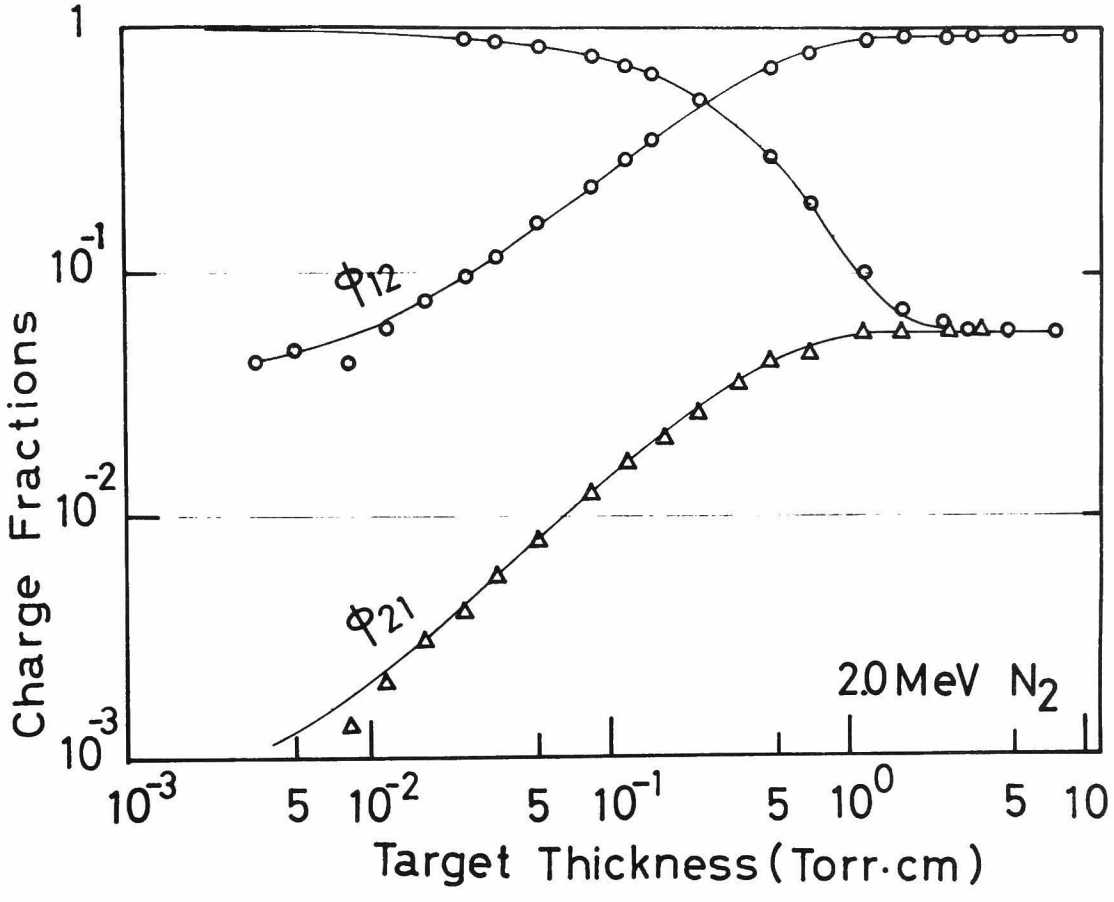
1
10^{-1}
10^{-2}
10^{-3}
Charge Fractions
ϕ_{12}
ϕ_{21}
2.0 MeV N_2
10^{-3}
5 10^{-2}
5 10^{-1}
5 10^{0}
5 10
Target Thickness (Torr·cm)

FIG. 3-1(12)

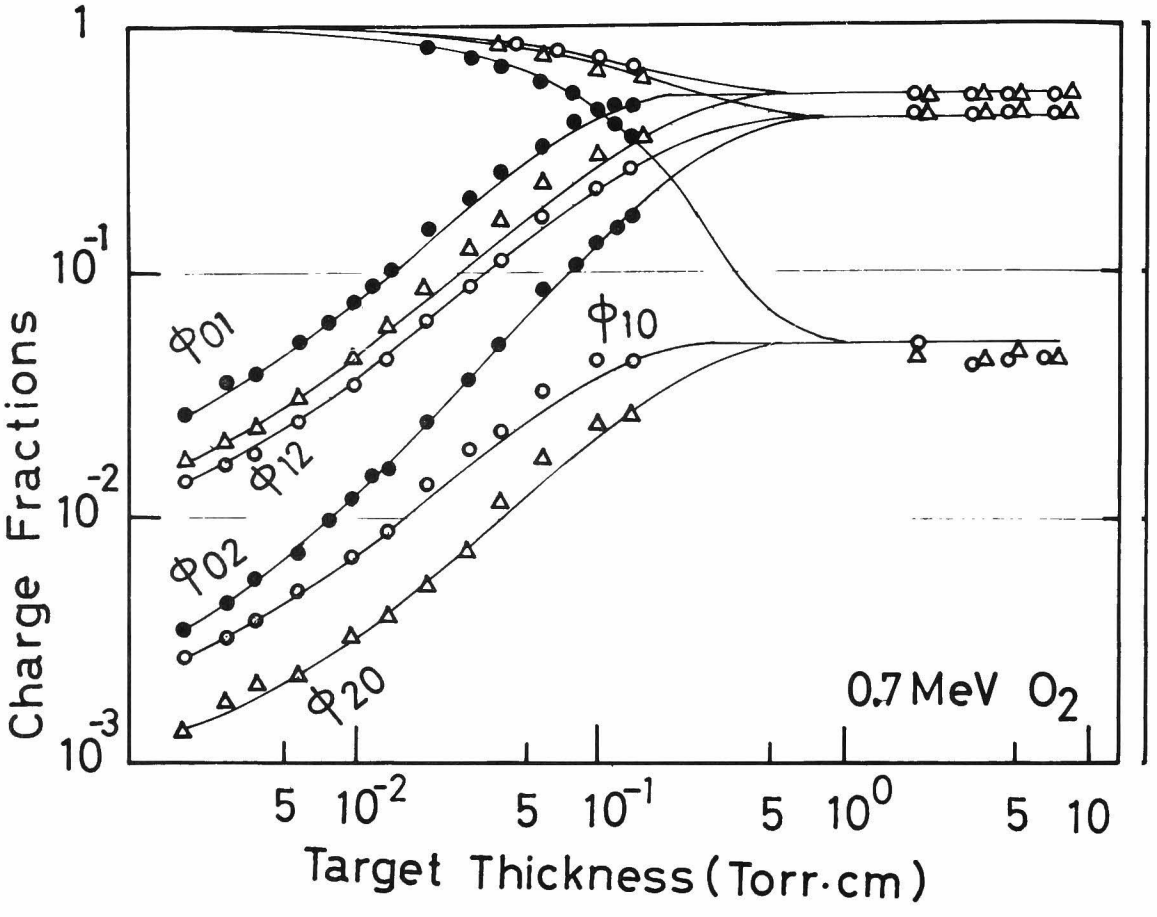
1
10^{-1}
10^{-2}
10^{-3}
Charge Fractions
ϕ_{01}
ϕ_{12}
ϕ_{02}
ϕ_{20}
ϕ_{10}
0.7 MeV O_2
5 10^{-2}
5 10^{-1}
5 10^{0}
5 10
Target Thickness (Torr·cm)

FIG. 3-1(13)

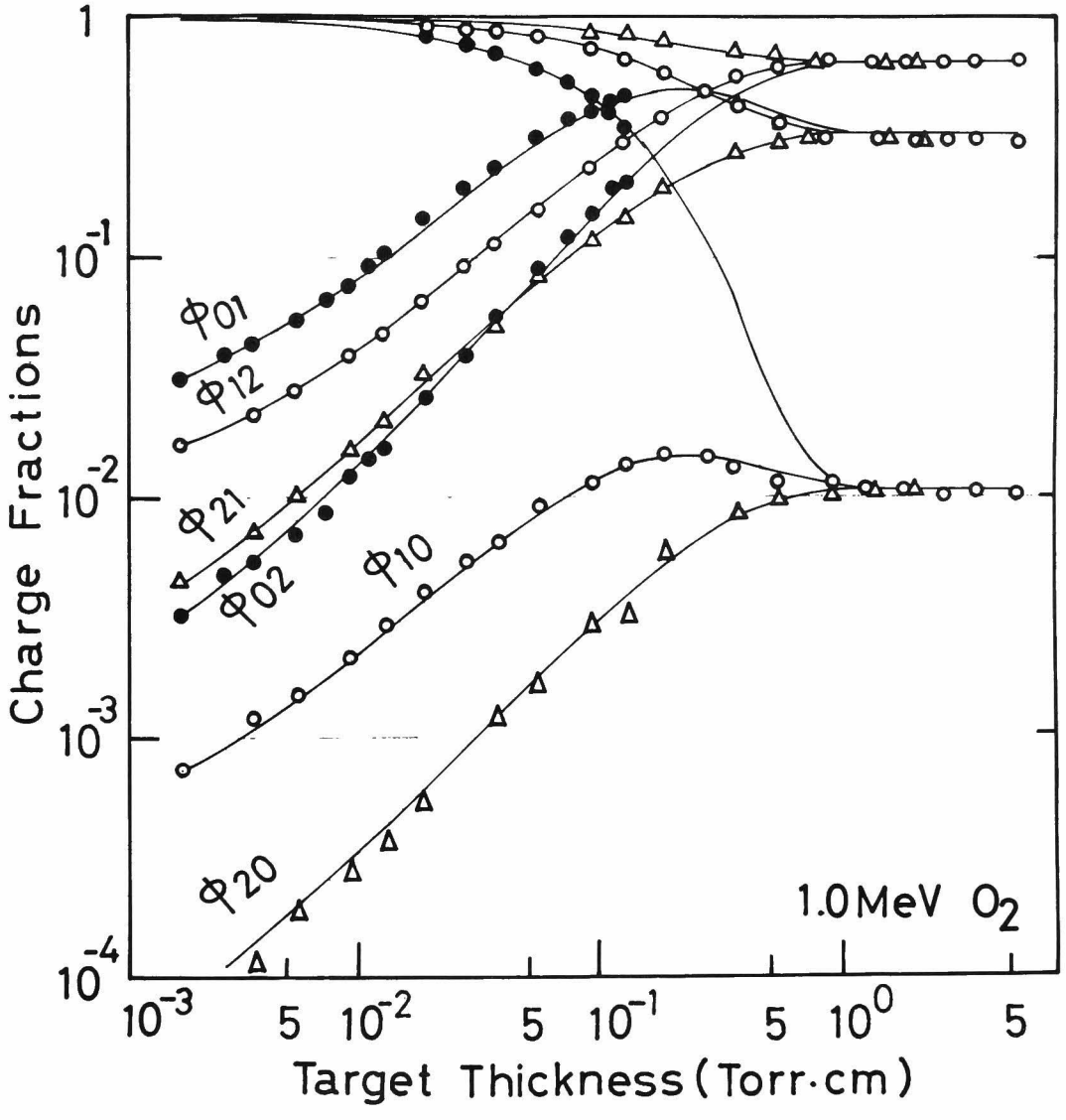
1
10^{-1}
10^{-2}
10^{-3}
10^{-4}
Charge Fractions
ϕ_{01}
ϕ_{12}
ϕ_{21}
ϕ_{02}
ϕ_{10}
ϕ_{20}
1.0MeV O_2
10^{-3}
5 10^{-2}
5 10^{-1}
5 10^{0}
5
Target Thickness (Torr·cm)

FIG. 3-1(14)

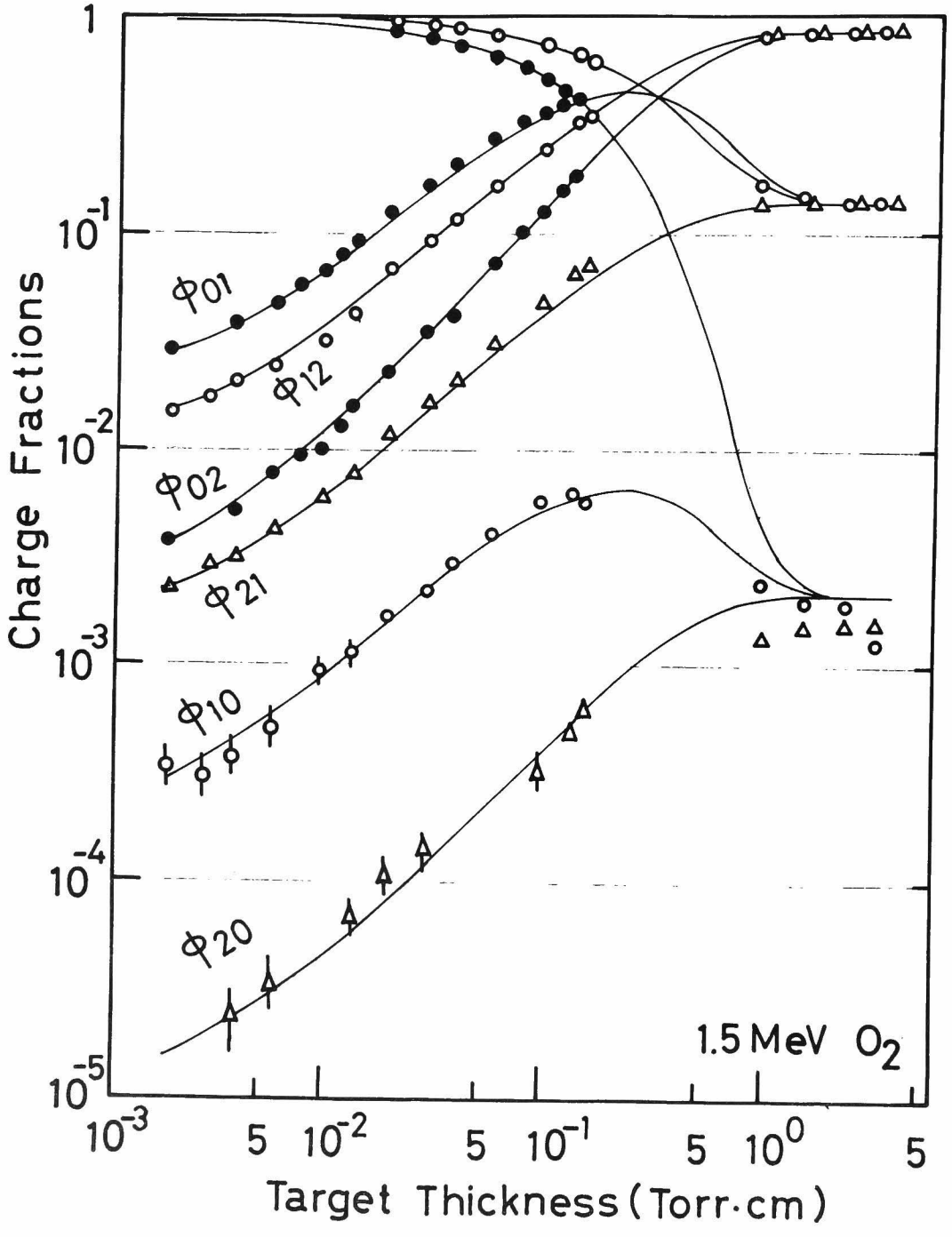
1
10^{-1}
10^{-2}
10^{-3}
10^{-4}
10^{-5}
Charge Fractions
ϕ_{01}
ϕ_{12}
ϕ_{02}
ϕ_{21}
ϕ_{10}
ϕ_{20}
1.5 MeV O_2
10^{-3}
5 10^{-2}
5 10^{-1}
5 10^{0}
5
Target Thickness (Torr·cm)

FIG. 3-1(15)

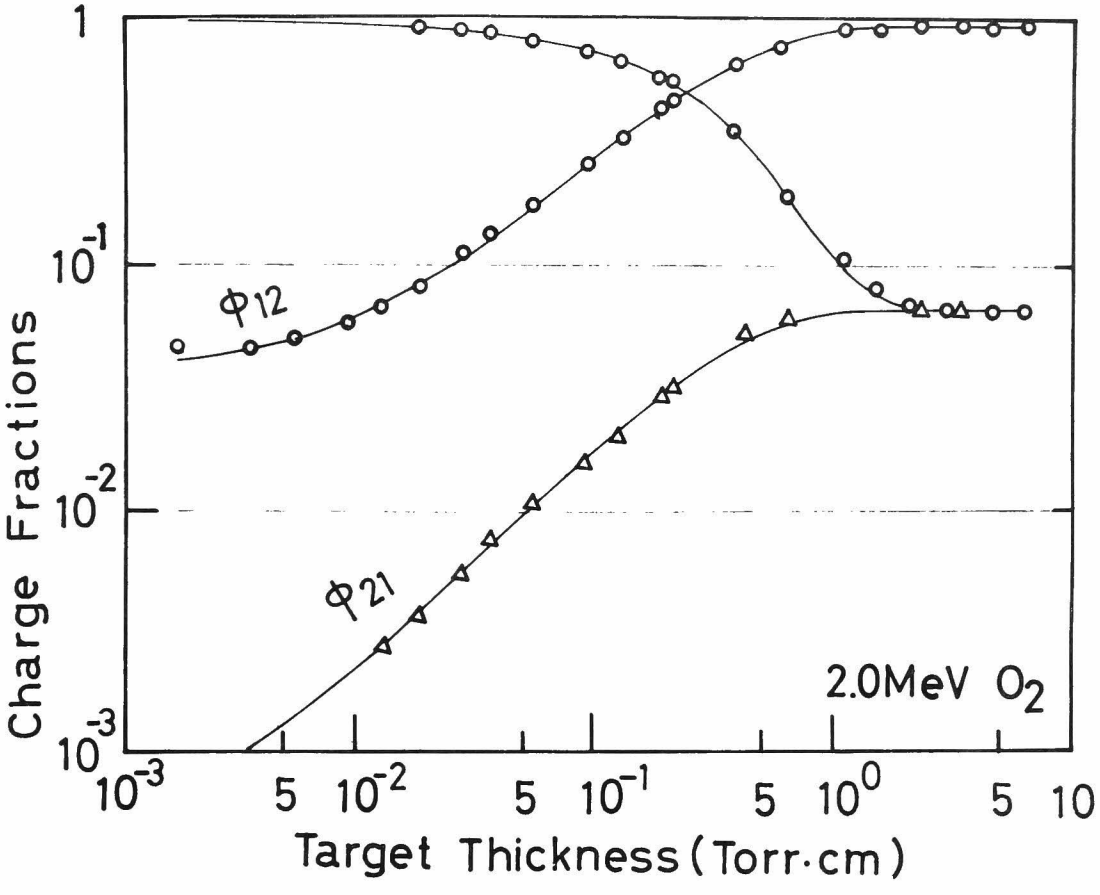
1
10^{-1}
10^{-2}
10^{-3}
Charge Fractions
ϕ_{12}
ϕ_{21}
2.0MeV O_2
10^{-3}
5 10^{-2}
5 10^{-1}
5 10^{0}
5 10
Target Thickness (Torr·cm)

FIG. 3-1(16)

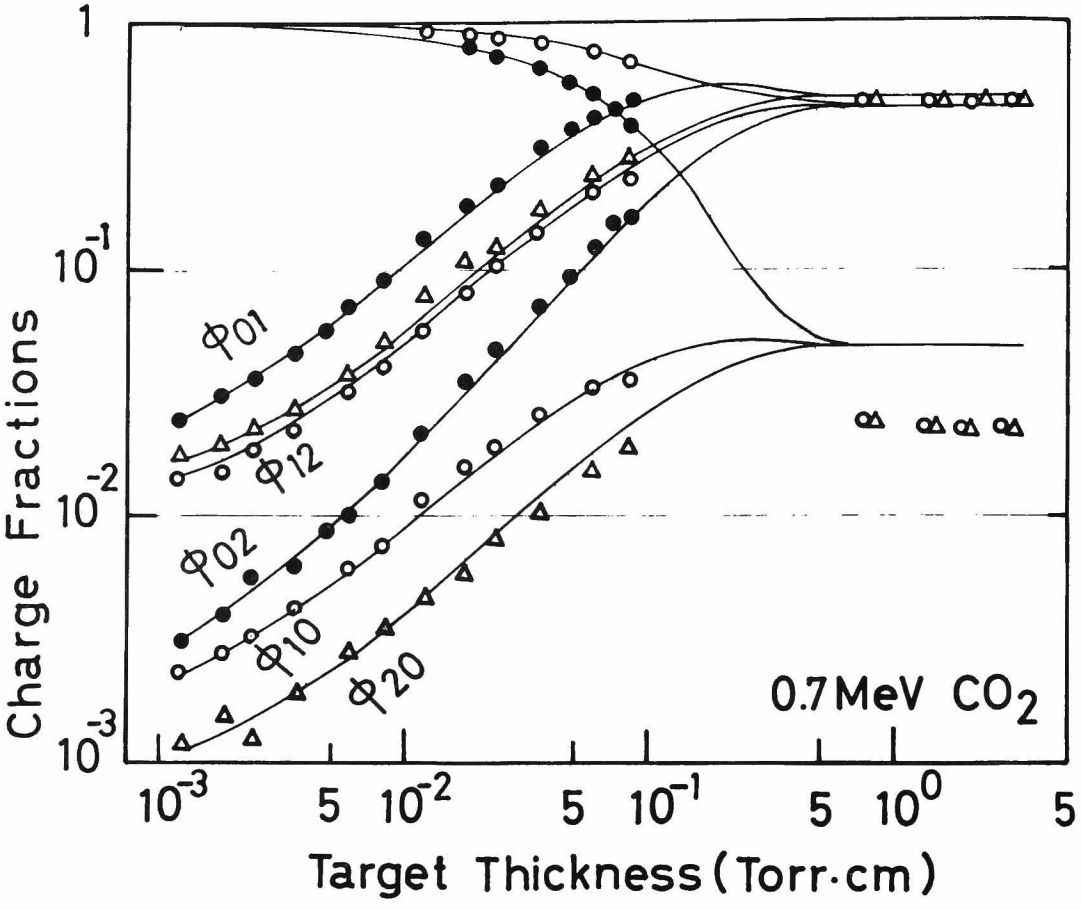
1
10^{-1}
10^{-2}
10^{-3}
Charge Fractions
ϕ_{01}
ϕ_{12}
ϕ_{02}
ϕ_{10}
ϕ_{20}
0.7MeV CO_2
10^{-3}
5 10^{-2}
5 10^{-1}
5 10^{0}
5
Target Thickness (Torr·cm)

FIG. 3-1(17)

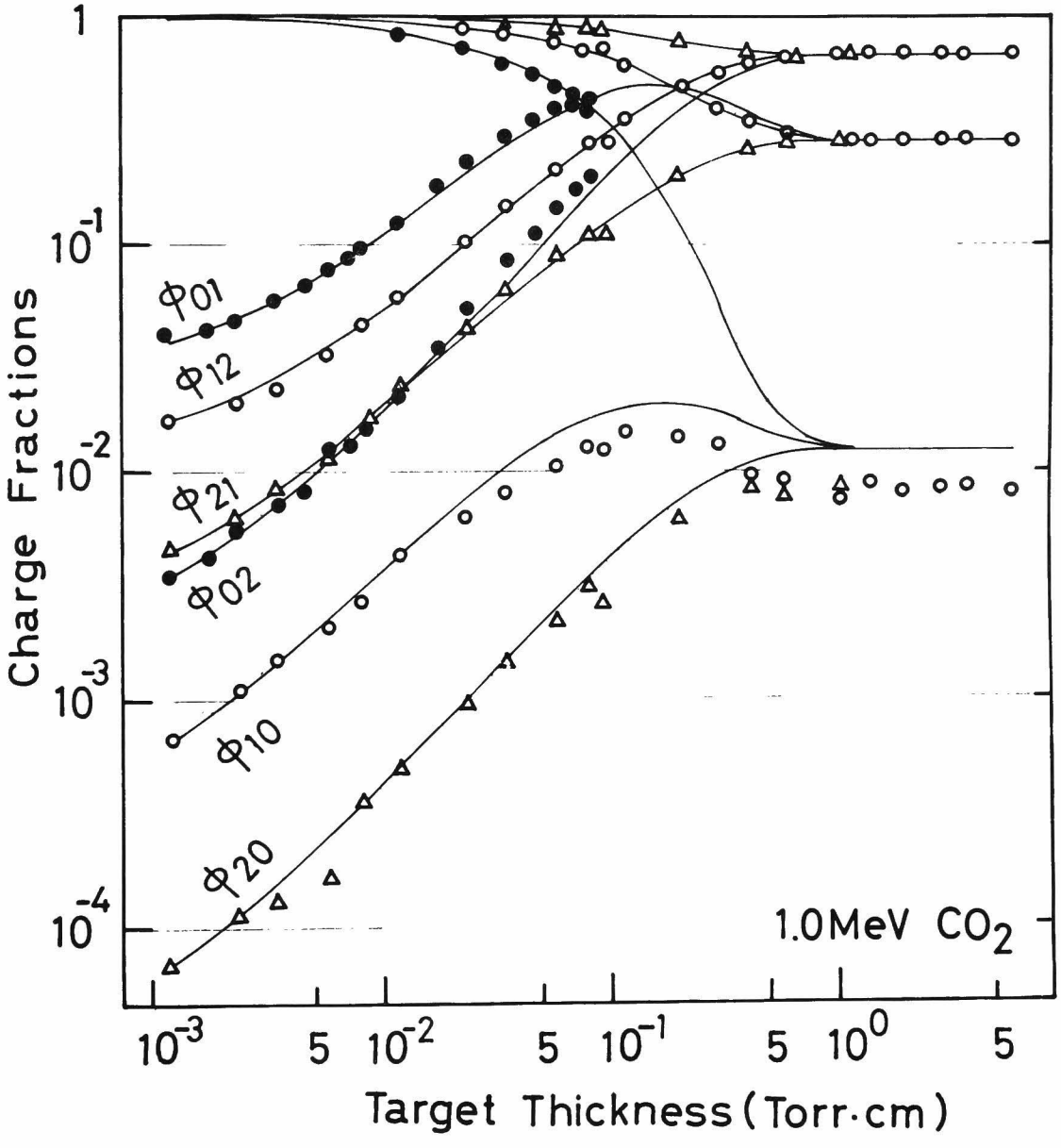
1
10^{-1}
10^{-2}
10^{-3}
10^{-4}
Charge Fractions
ϕ_{01}
ϕ_{12}
ϕ_{21}
ϕ_{02}
ϕ_{10}
ϕ_{20}
1.0MeV CO_2
10^{-3}
5
10^{-2}
5
10^{-1}
5
10^{0}
5
Target Thickness (Torr·cm)

FIG. 3-1(18)

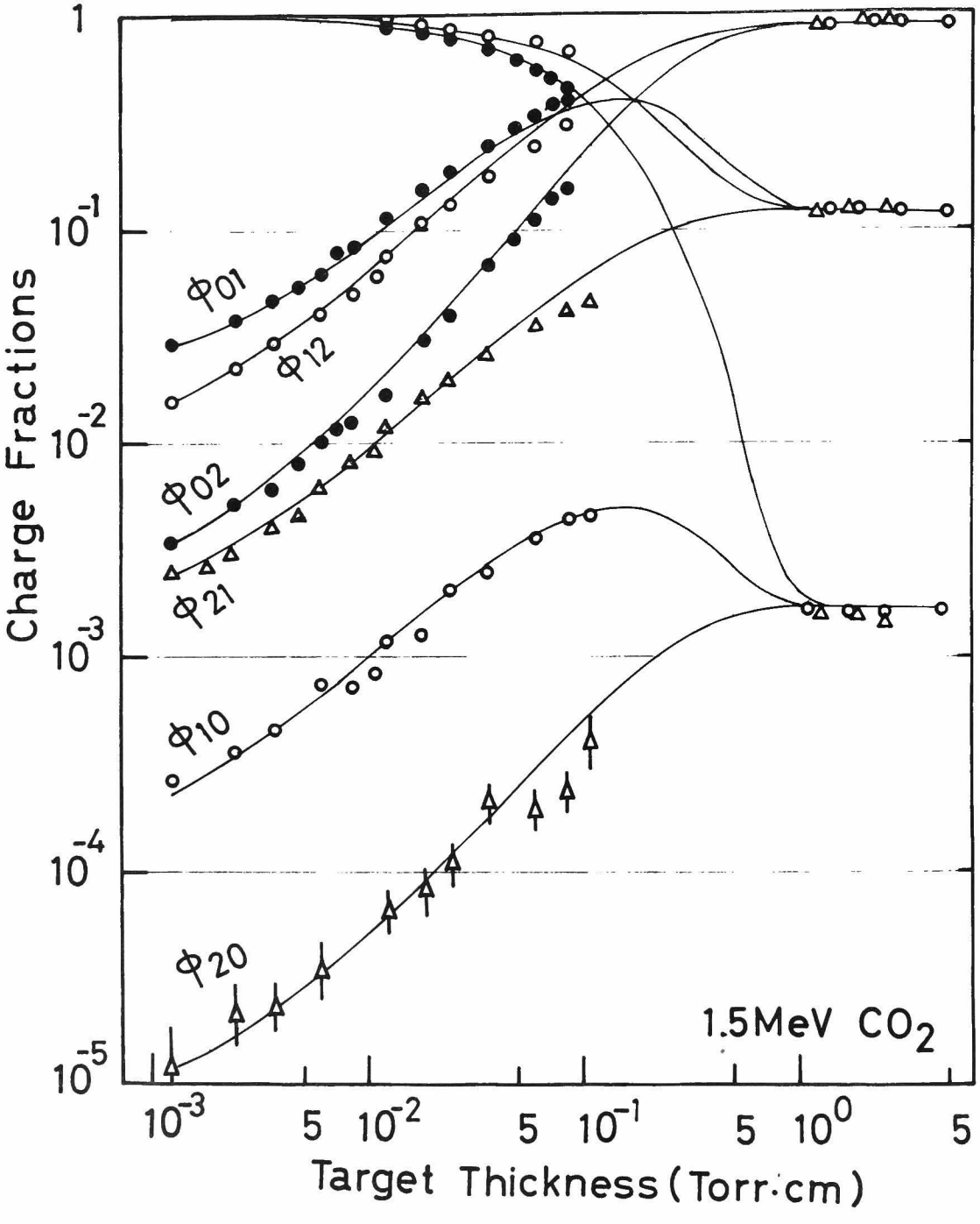
1
10^{-1}
10^{-2}
10^{-3}
10^{-4}
10^{-5}
Charge Fractions
ϕ_{01}
ϕ_{12}
ϕ_{02}
ϕ_{21}
ϕ_{10}
ϕ_{20}
1.5MeV CO_2
10^{-3}
5 10^{-2}
5 10^{-1}
5 10^{0}
5
Target Thickness (Torr·cm)

FIG. 3-1(19)

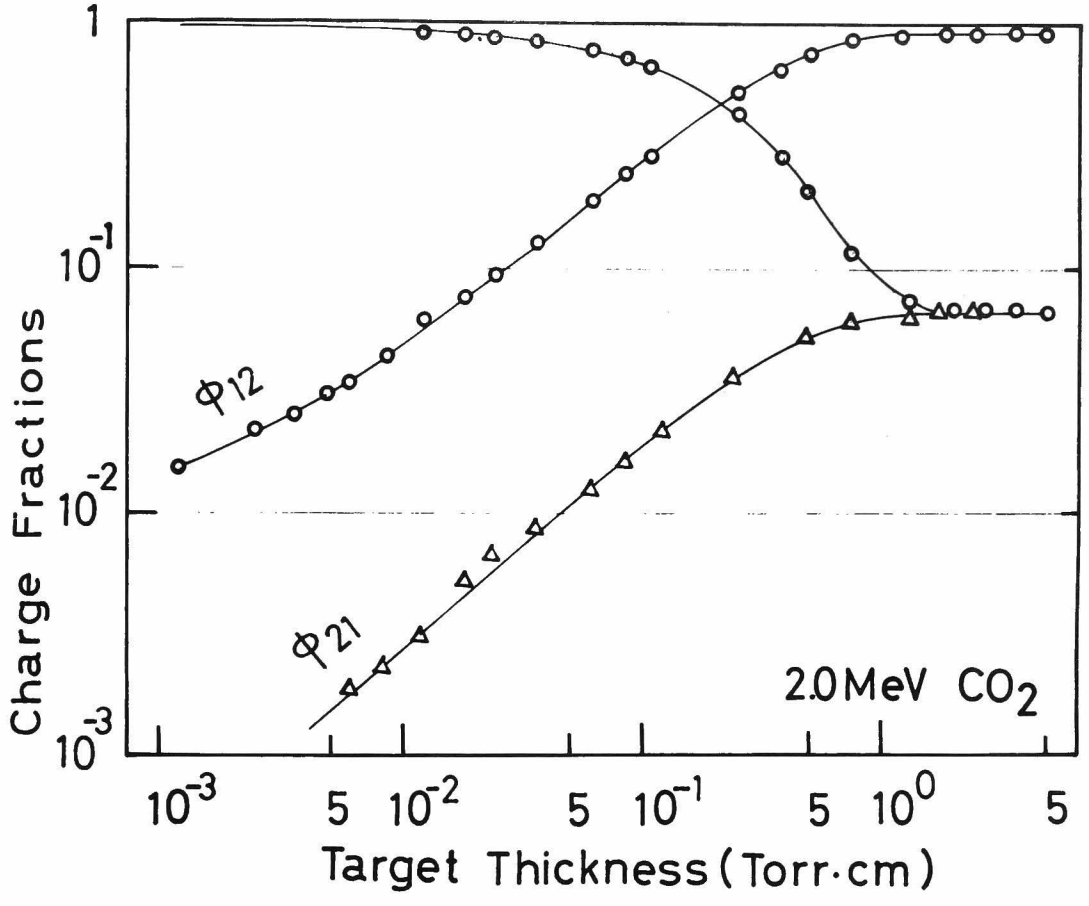
1
10^{-1}
10^{-2}
10^{-3}
Charge Fractions
ϕ_{12}
ϕ_{21}
2.0MeV CO_2
10^{-3}
5 10^{-2}
5 10^{-1}
5 10^{0}
5
Target Thickness (Torr·cm)

FIG. 3-1(20)

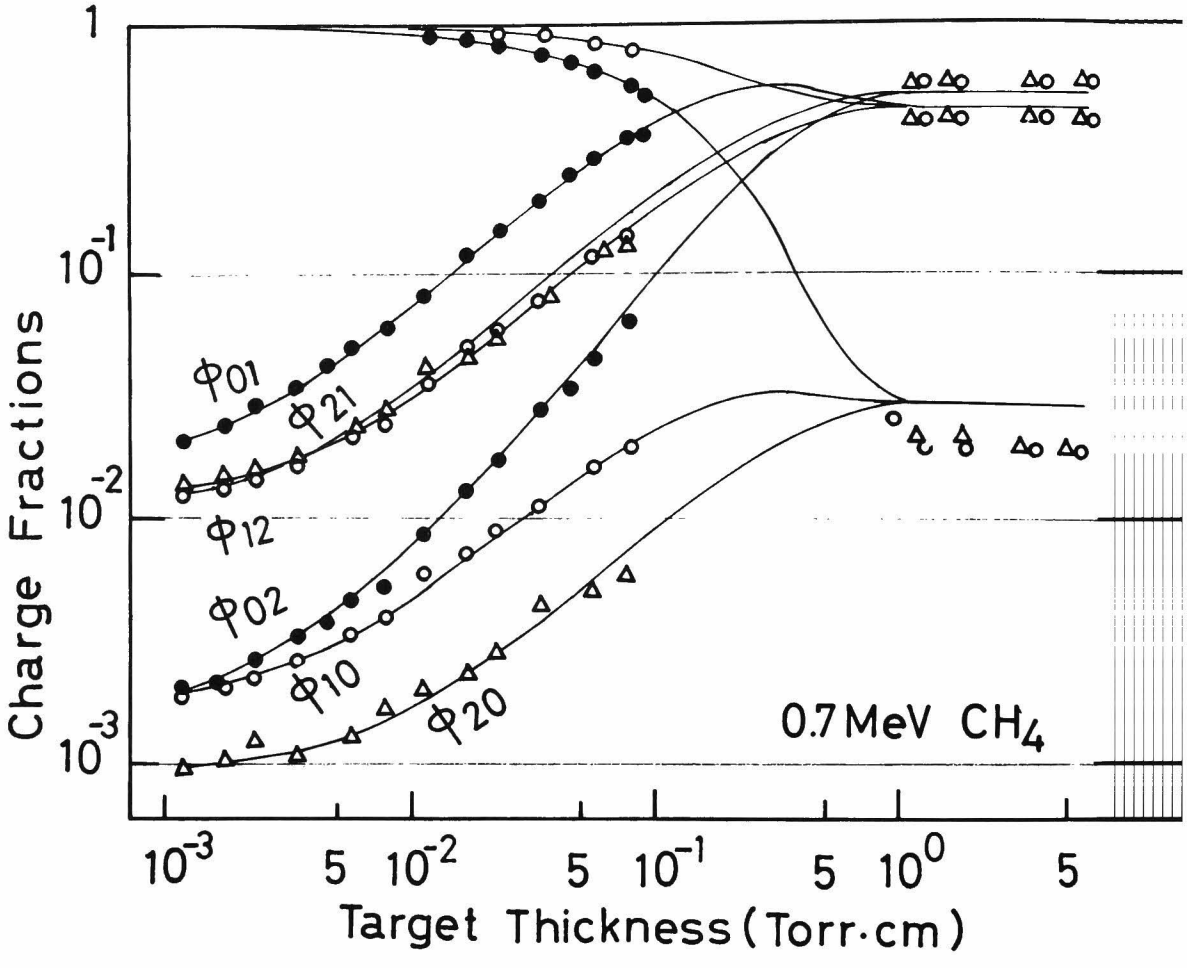
1
10^{-1}
10^{-2}
10^{-3}
Charge Fractions
ϕ_{01}
ϕ_{21}
ϕ_{12}
ϕ_{02}
ϕ_{10}
ϕ_{20}
0.7MeV CH_4
10^{-3}
5 10^{-2}
5 10^{-1}
5 10^{0}
5
Target Thickness (Torr·cm)

FIG. 3-1(21)

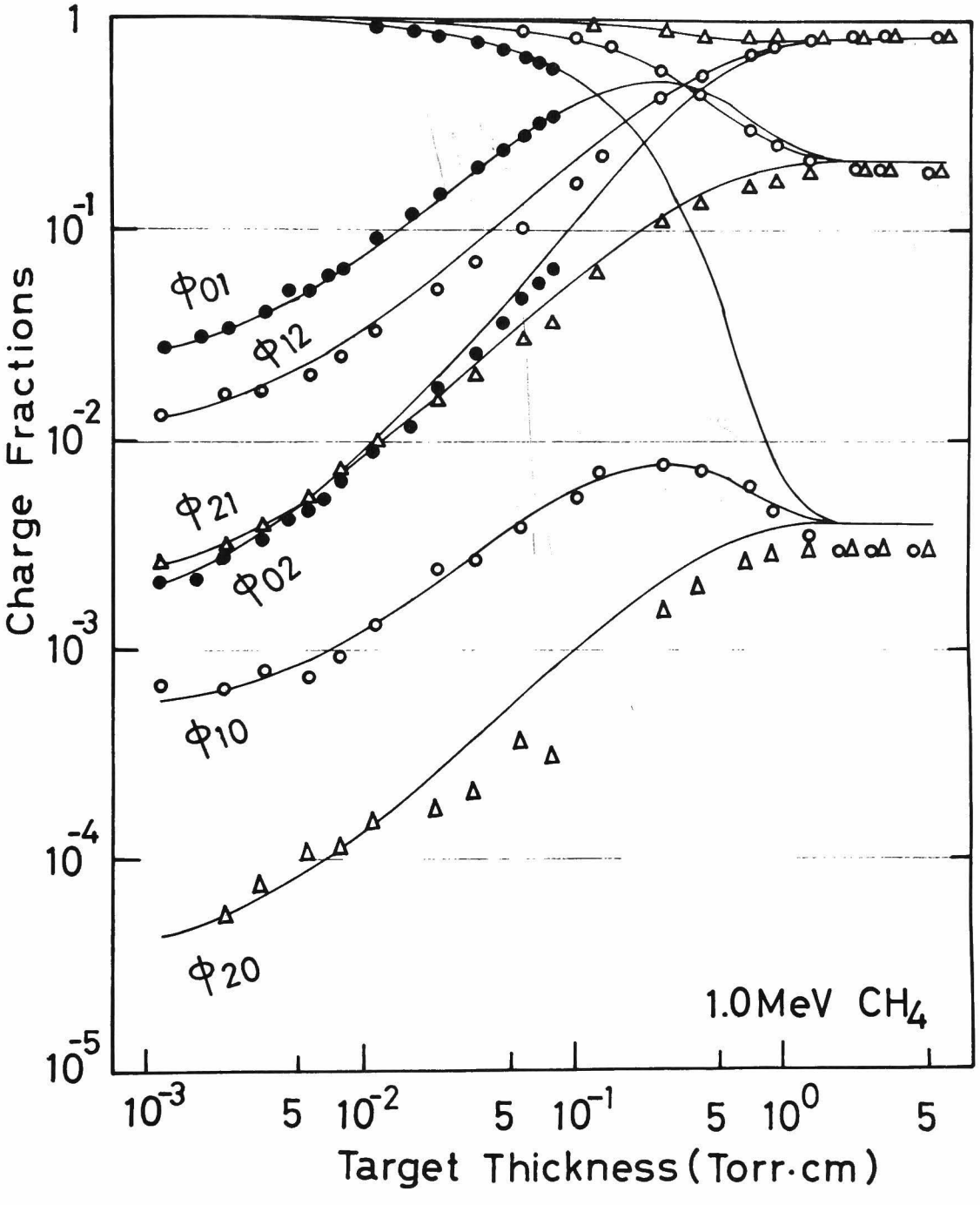
Charge Fractions
1
10^{-1}
10^{-2}
10^{-3}
10^{-4}
10^{-5}
ϕ_{01}
ϕ_{12}
ϕ_{21}
ϕ_{02}
ϕ_{10}
ϕ_{20}
1.0MeV CH_4
10^{-3}
5
10^{-2}
5
10^{-1}
5
10^{0}
5
Target Thickness (Torr·cm)

FIG. 3-1(22)

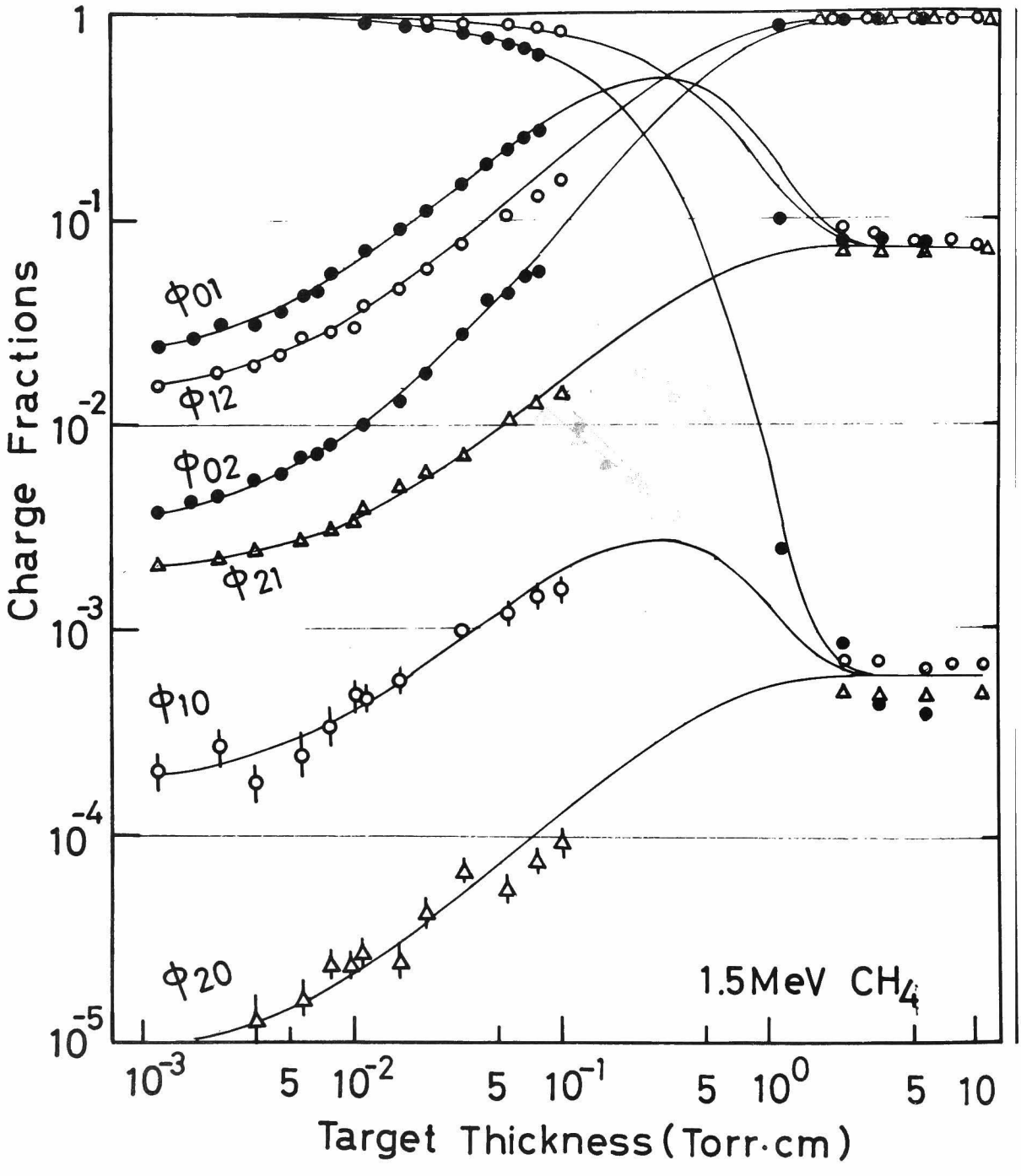
Charge Fractions
1
10^{-1}
10^{-2}
10^{-3}
10^{-4}
10^{-5}
Φ_{01}
Φ_{12}
Φ_{02}
Φ_{21}
Φ_{10}
Φ_{20}
1.5MeV CH_4
10^{-3}
5 10^{-2}
5 10^{-1}
5 10^{0}
5 10
Target Thickness (Torr·cm)

FIG. 3-1(23)

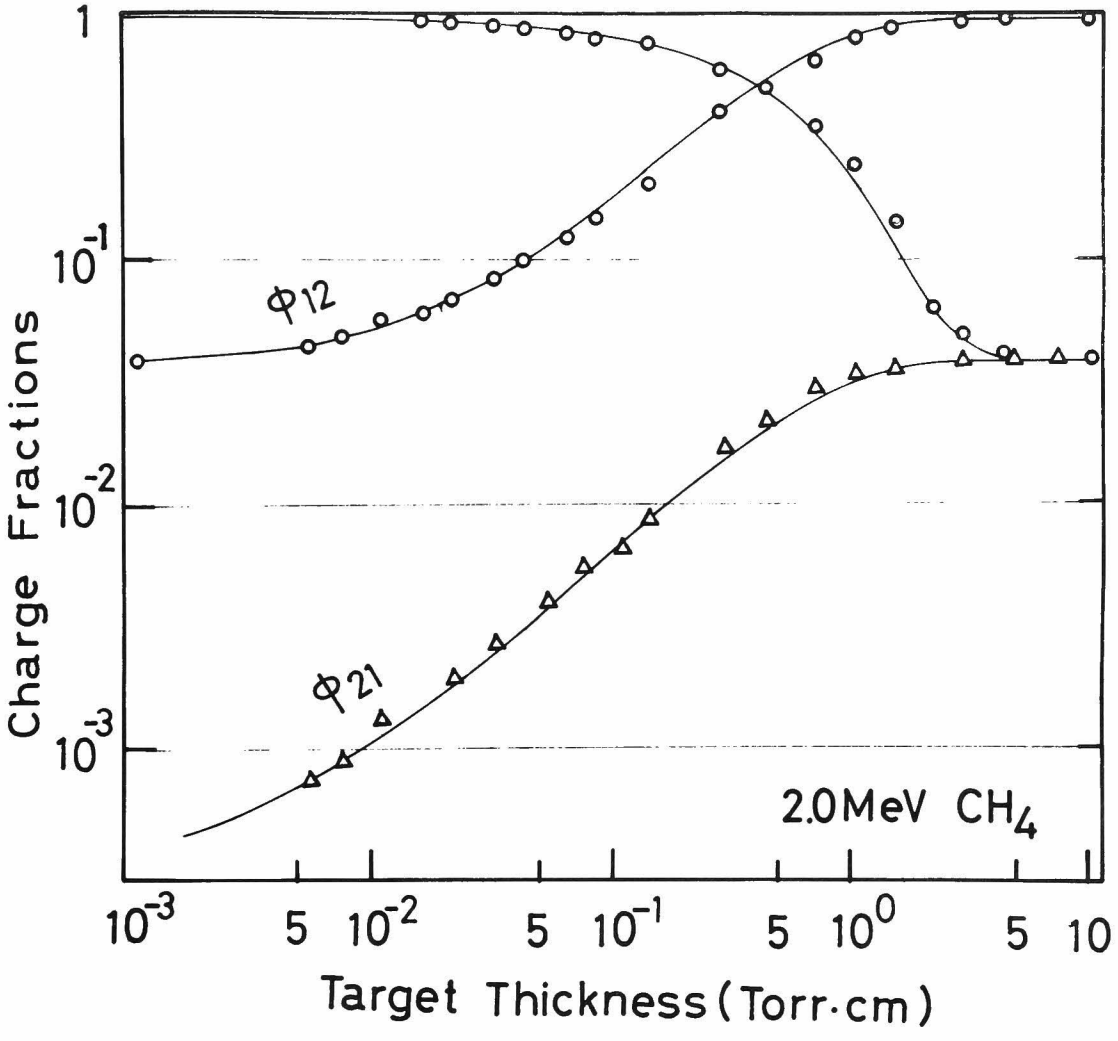
1
10^{-1}
10^{-2}
10^{-3}
Charge Fractions
ϕ_{12}
ϕ_{21}
2.0MeV CH_4
10^{-3}
5 10^{-2}
5 10^{-1}
5 10^{0}
5 10
Target Thickness (Torr·cm)

FIG. 3-1(24)

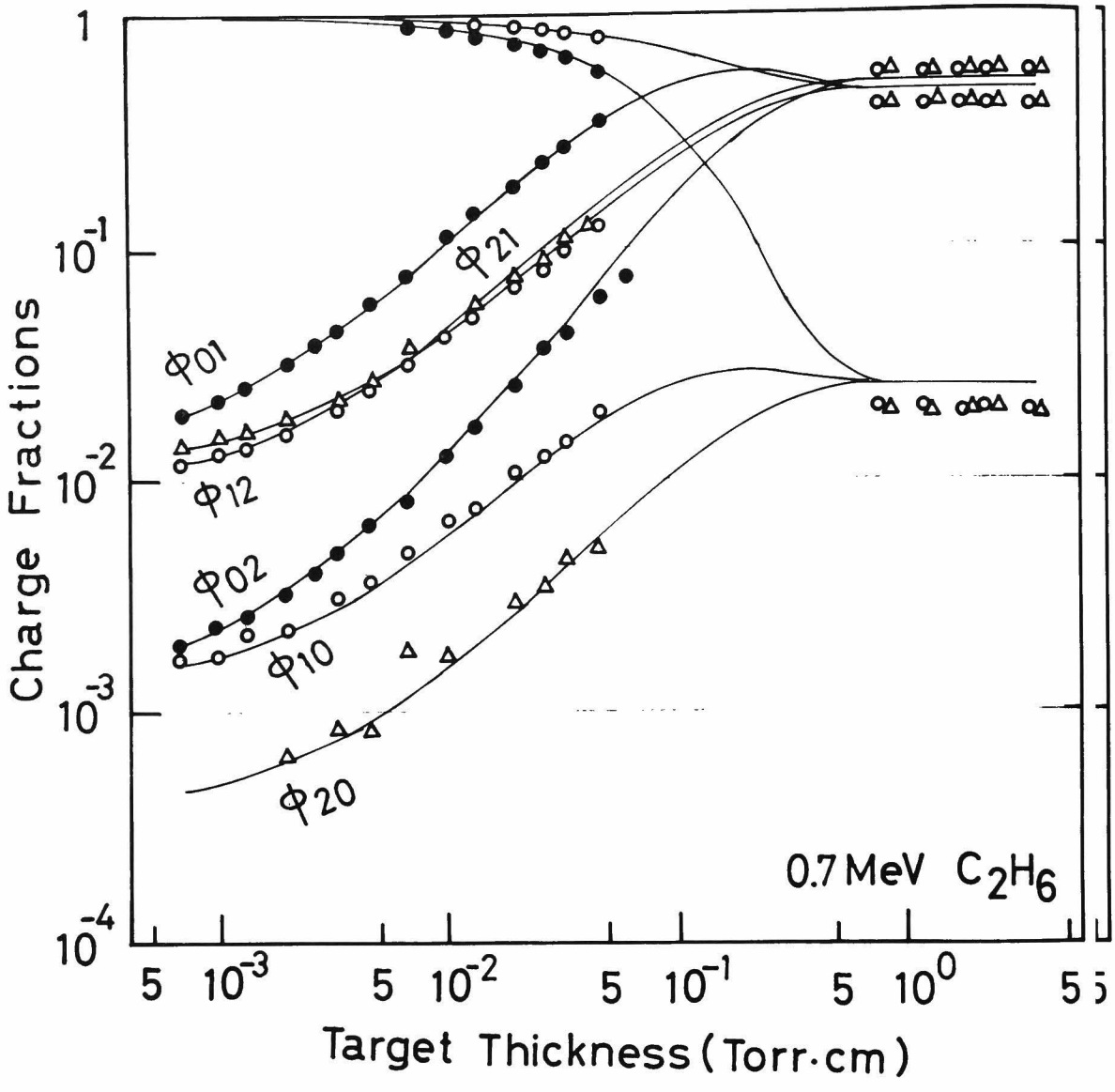
1
10^{-1}
10^{-2}
10^{-3}
10^{-4}
Charge Fractions
ϕ_{01}
ϕ_{21}
ϕ_{12}
ϕ_{02}
ϕ_{10}
ϕ_{20}
0.7 MeV C_2H_6
5 10^{-3}
5 10^{-2}
5 10^{-1}
5 10^{0}
5
Target Thickness (Torr·cm)

FIG. 3-1(25)

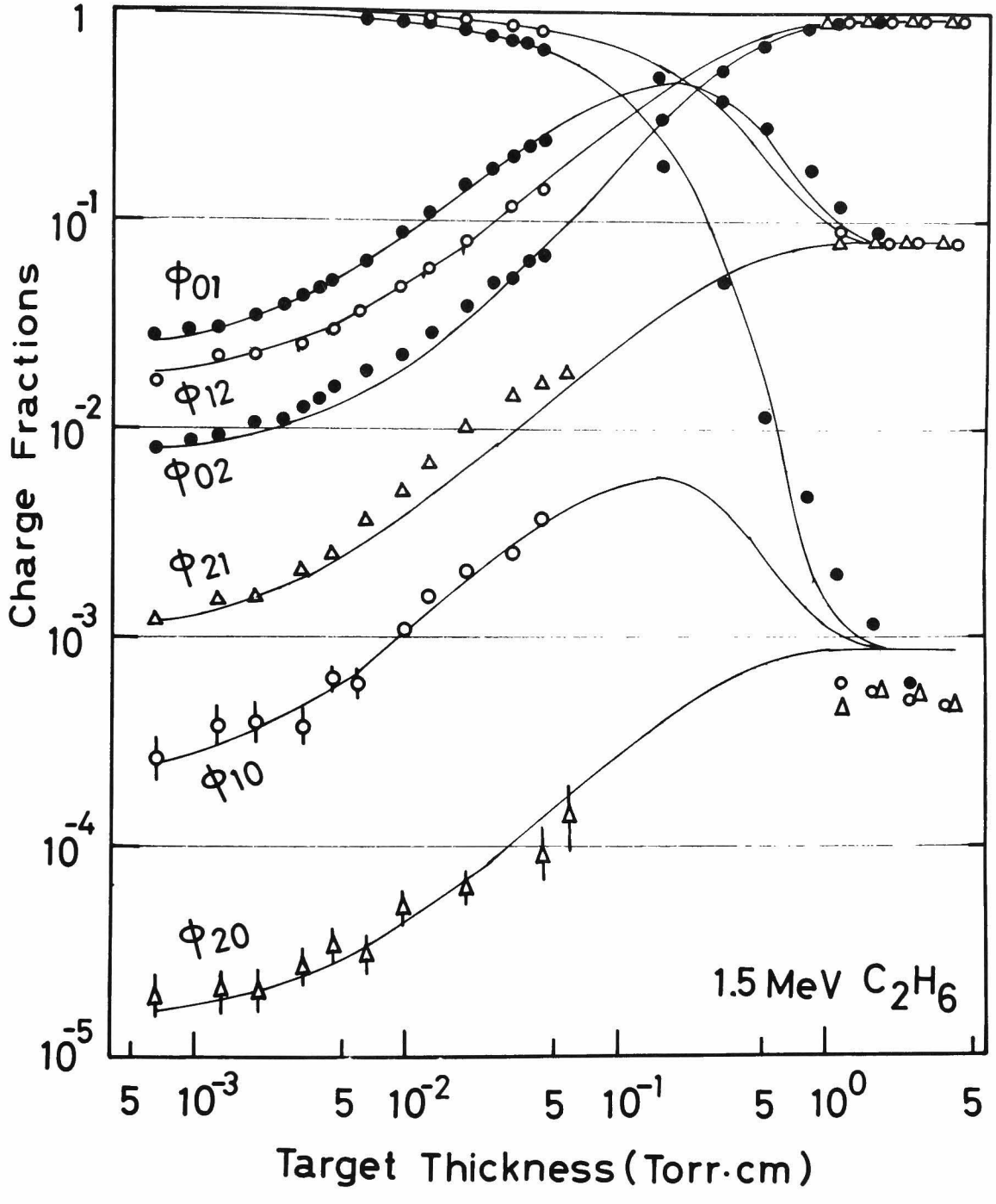
1
10^{-1}
10^{-2}
10^{-3}
10^{-4}
10^{-5}
Charge Fractions
Φ_{01}
Φ_{12}
Φ_{02}
Φ_{21}
Φ_{10}
Φ_{20}
1.5 MeV C_2H_6
5 10^{-3} 5 10^{-2} 5 10^{-1} 5 10^{0} 5
Target Thickness (Torr·cm)

FIG. 3-1(26)

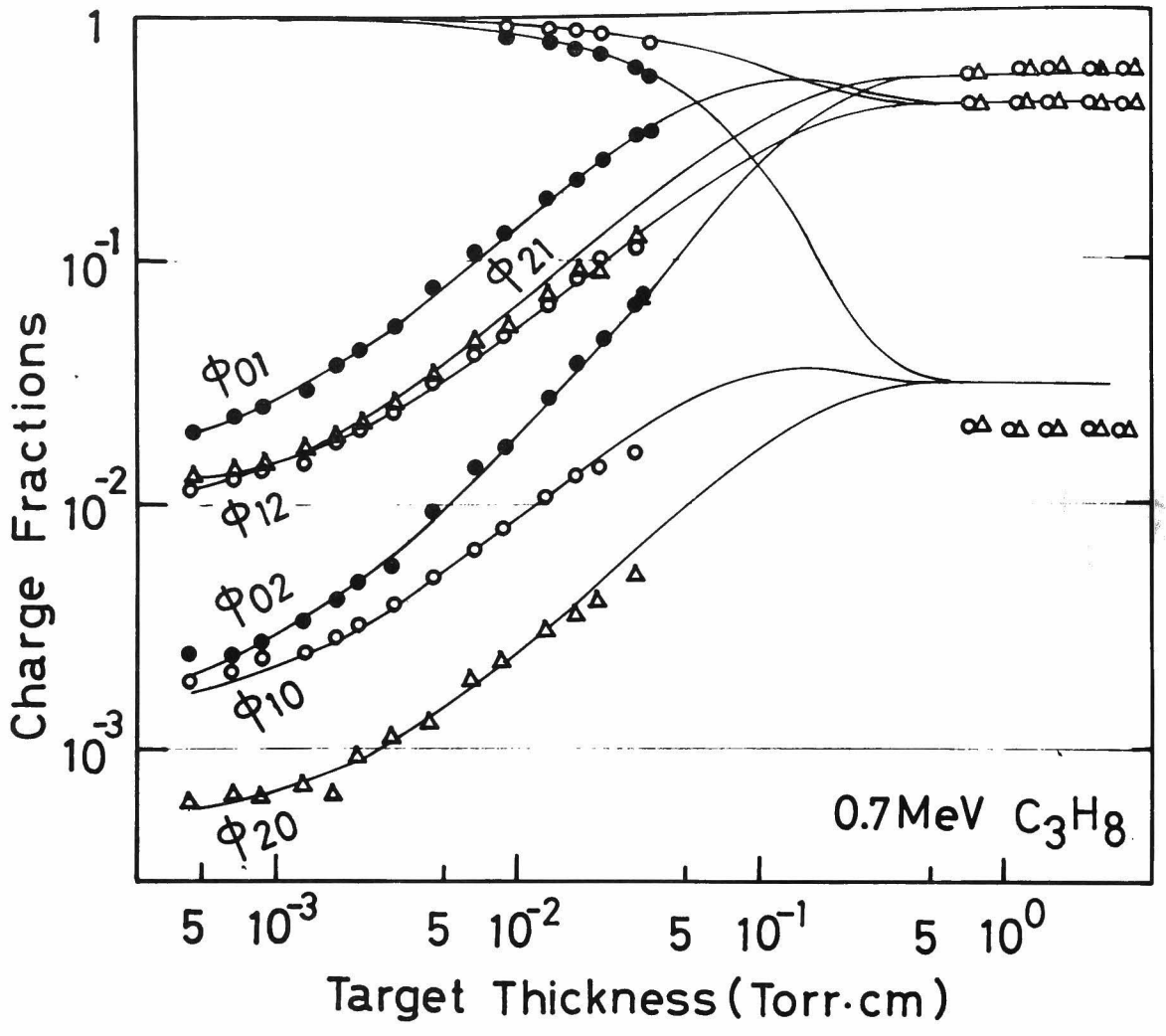
1
10^{-1}
10^{-2}
10^{-3}
Charge Fractions
ϕ_{01}
ϕ_{21}
ϕ_{12}
ϕ_{02}
ϕ_{10}
ϕ_{20}
0.7MeV C_3H_8
5 10^{-3}
5 10^{-2}
5 10^{-1}
5 10^{0}
Target Thickness (Torr·cm)

FIG. 3-1(27)

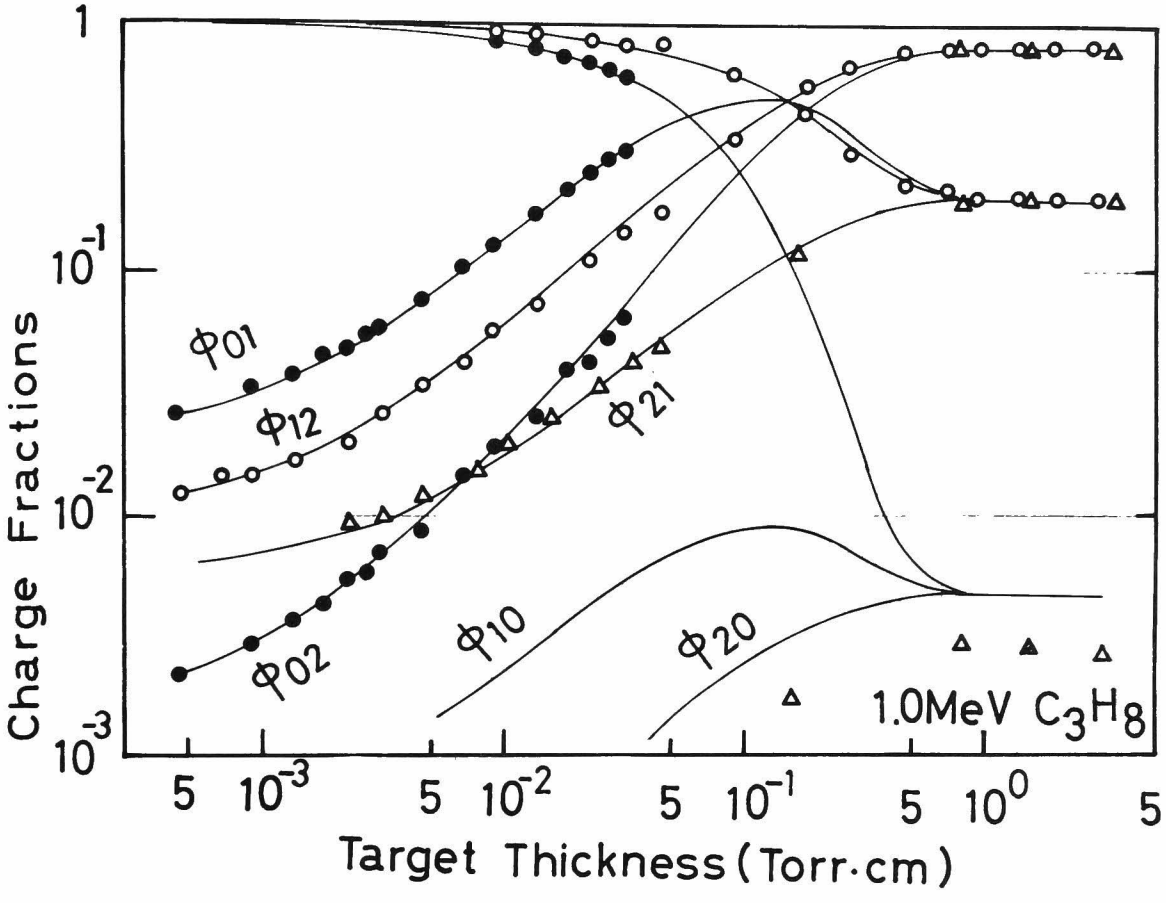
1
10^{-1}
10^{-2}
10^{-3}
Charge Fractions
ϕ_{01}
ϕ_{12}
ϕ_{21}
ϕ_{02}
ϕ_{10}
ϕ_{20}
1.0MeV C_3H_8
5 10^{-3}
5 10^{-2}
5 10^{-1}
5 10^{0}
5
Target Thickness (Torr·cm)

FIG. 3-1(28)

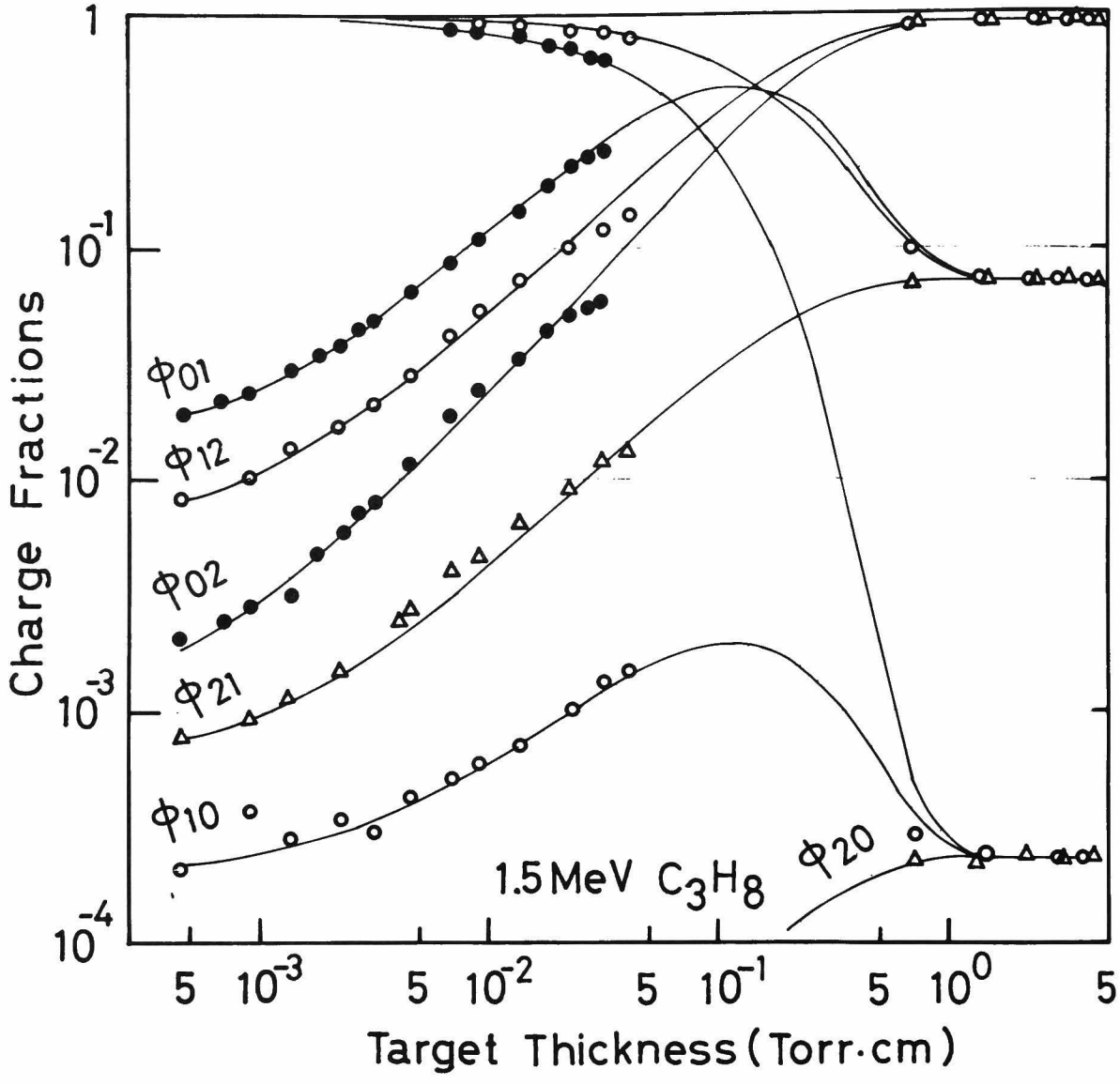
1
10^{-1}
10^{-2}
10^{-3}
10^{-4}
Charge Fractions
Φ_{01}
Φ_{12}
Φ_{02}
Φ_{21}
Φ_{10}
Φ_{20}
1.5MeV C_3H_8
5 10^{-3}
5 10^{-2}
5 10^{-1}
5 10^{0}
5
Target Thickness (Torr·cm)

FIG. 3-1(29)

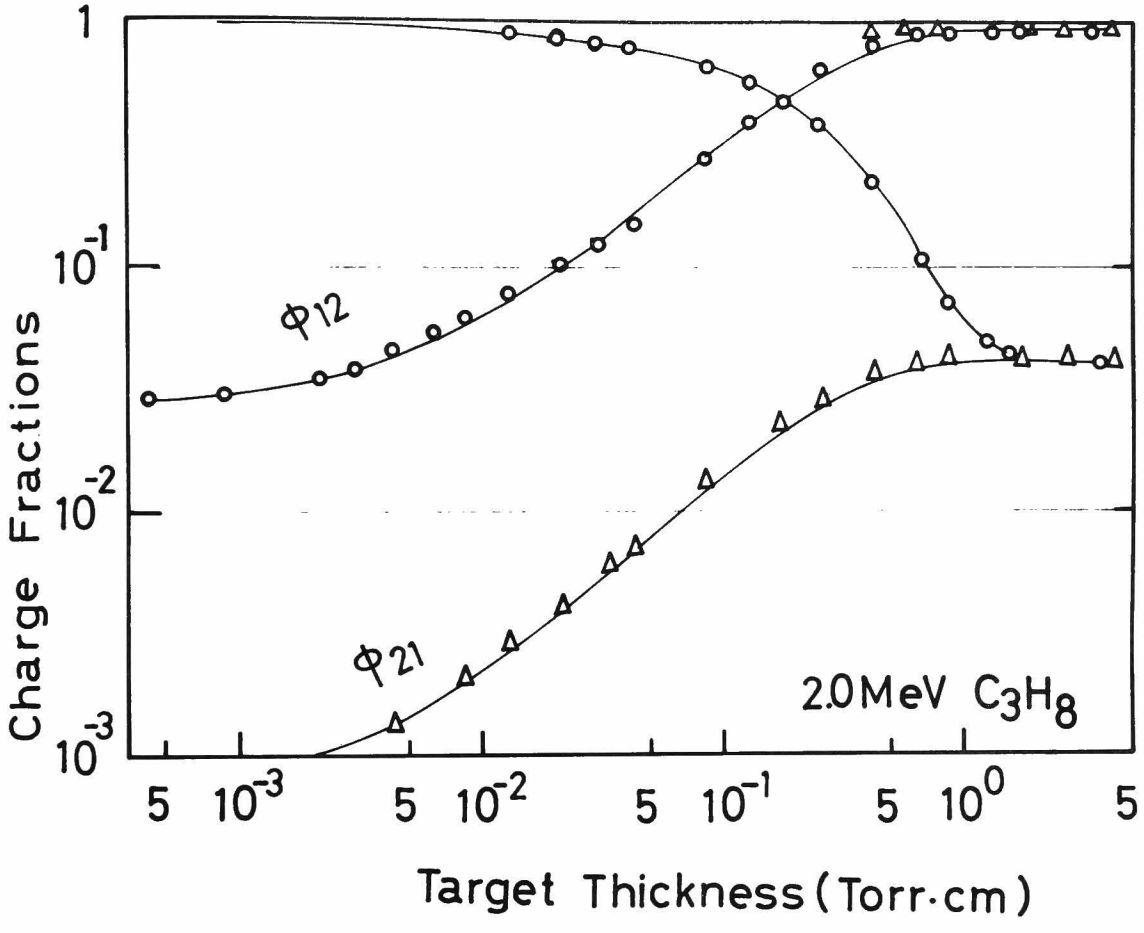
1
10^{-1}
10^{-2}
10^{-3}
Charge Fractions
Φ_{12}
Φ_{21}
2.0MeV C_3H_8
5 10^{-3}
5 10^{-2}
5 10^{-1}
5 10^{0}
5
Target Thickness (Torr·cm)

FIG. 3-1(30)

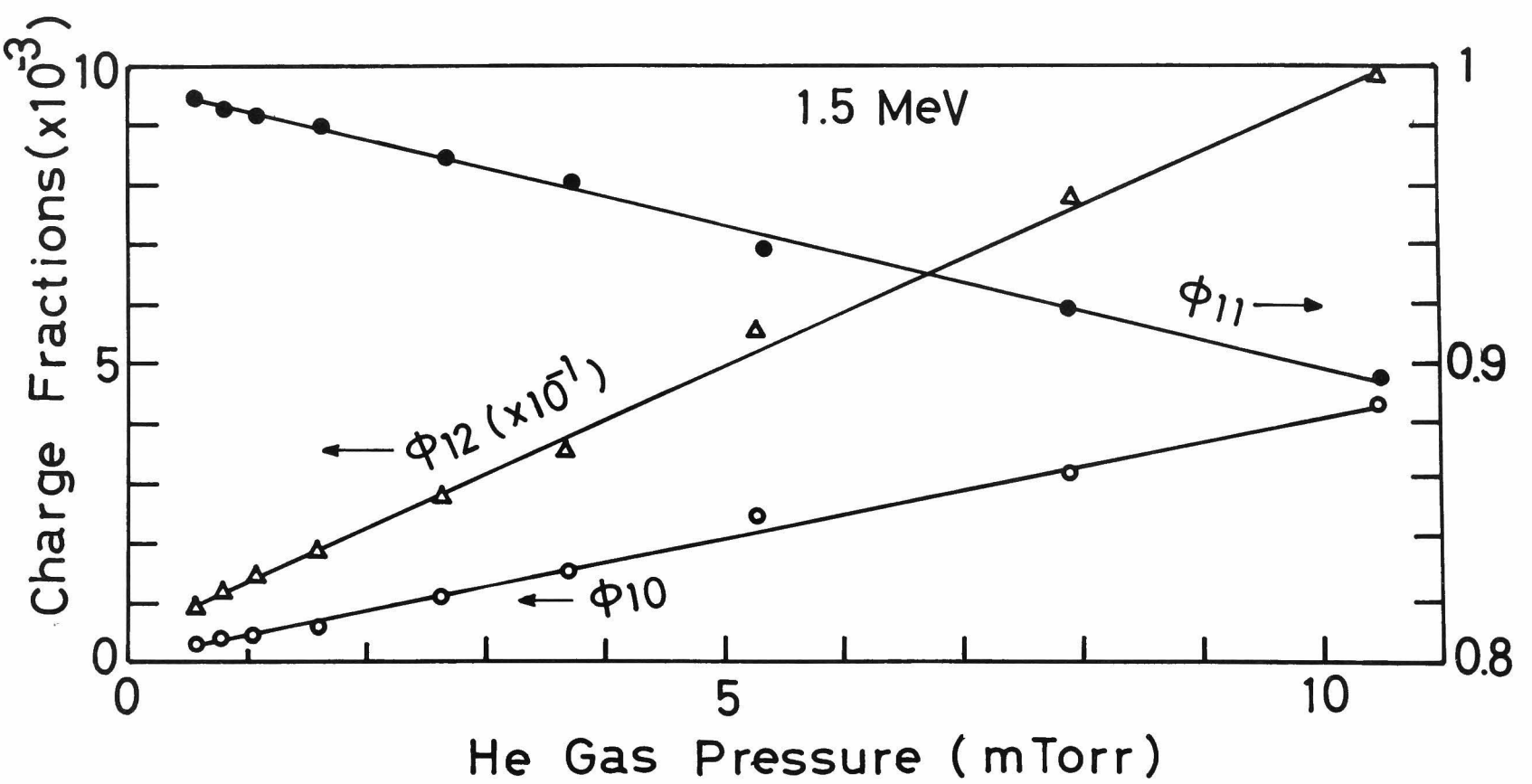
1.5 MeV
Charge Fractions(x10^-3)
10
5
0
1
0.9
0.8
0
5
10
He Gas Pressure (mTorr)
Φ11
Φ12 (x10^-1)
Φ10

FIG. 3-2

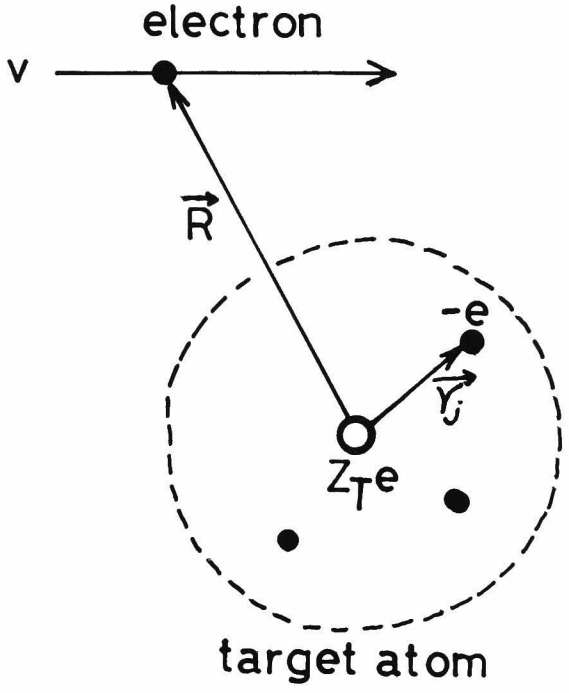

FIG. 4-1. Diagram of free electron scattering. Open circle is the target nucleus and closed circles stand for incident or target electrons.

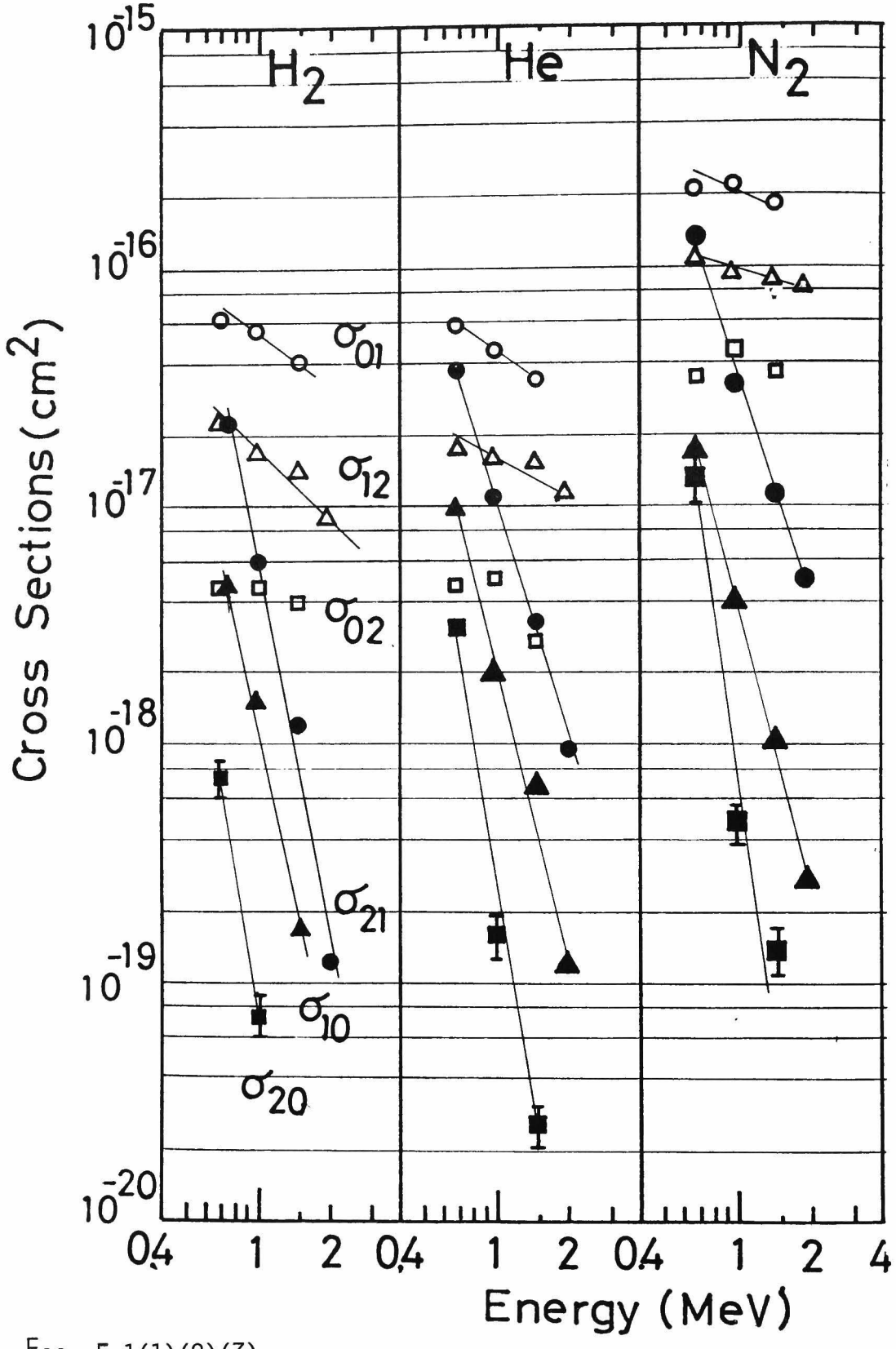
10^{-15}
10^{-16}
10^{-17}
10^{-18}
10^{-19}
10^{-20}
Cross Sections (cm^2)
H_2
He
N_2
σ_{01}
σ_{12}
σ_{02}
σ_{21}
σ_{10}
σ_{20}
0.4
1
2
0.4
1
2
0.4
1
2
4
Energy (MeV)

FIG. 5-1(1)(2)(3)

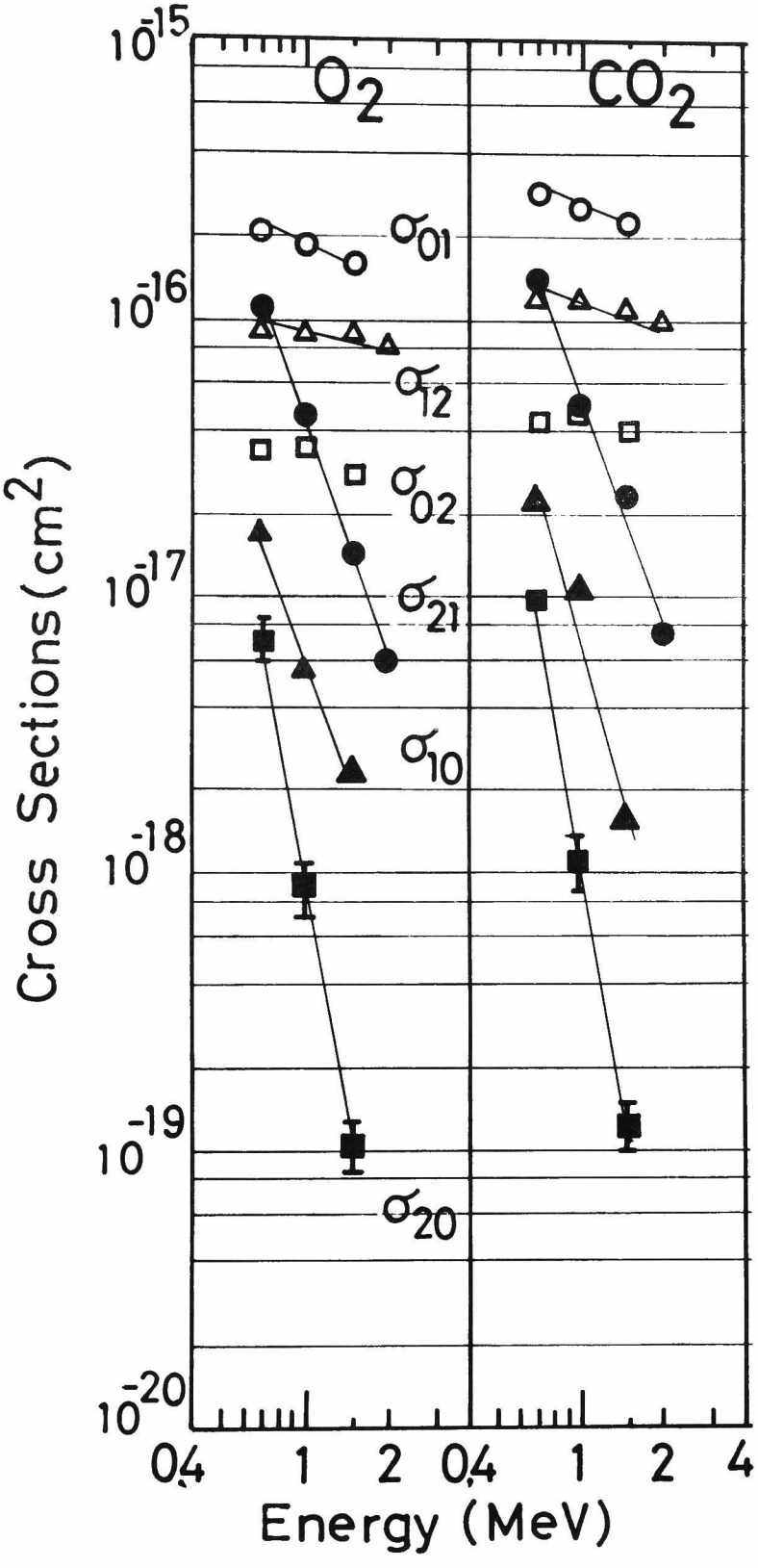
10^{-15}
10^{-16}
10^{-17}
10^{-18}
10^{-19}
10^{-20}
O_2
CO_2
σ_{01}
σ_{12}
σ_{02}
σ_{21}
σ_{10}
σ_{20}
Cross Sections (cm^2)
0.4
1
2
0.4
1
2
4
Energy (MeV)

FIG. 5-1(4)(5)

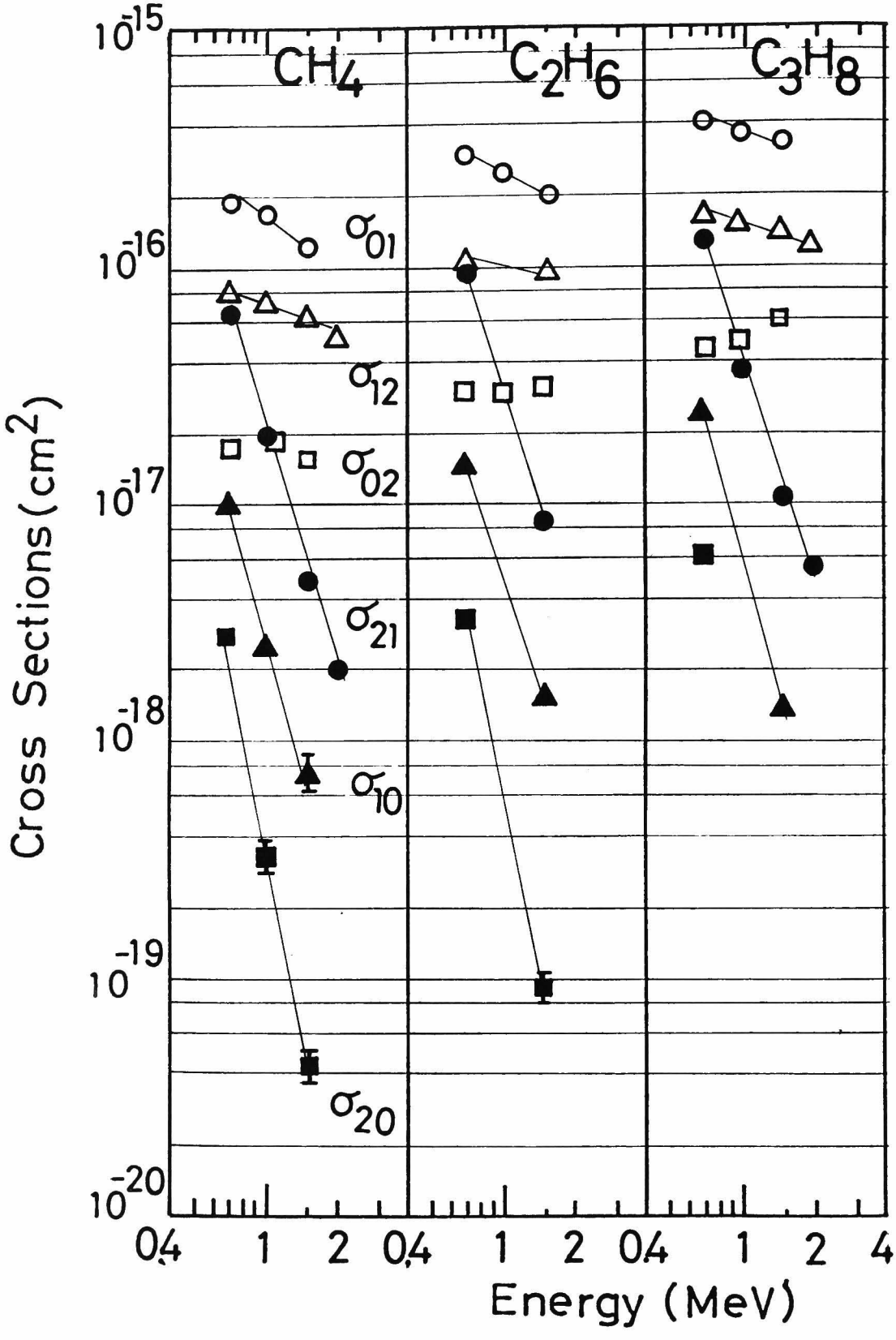
CH_4
C_2H_6
C_3H_8
σ_{01}
σ_{12}
σ_{02}
σ_{21}
σ_{10}
σ_{20}
Cross Sections (cm^2)
10^{-15}
10^{-16}
10^{-17}
10^{-18}
10^{-19}
10^{-20}
0.4
1
2
0.4
1
2
0.4
1
2
4
Energy (MeV)

FIG. 5-1(6)(7)(8)

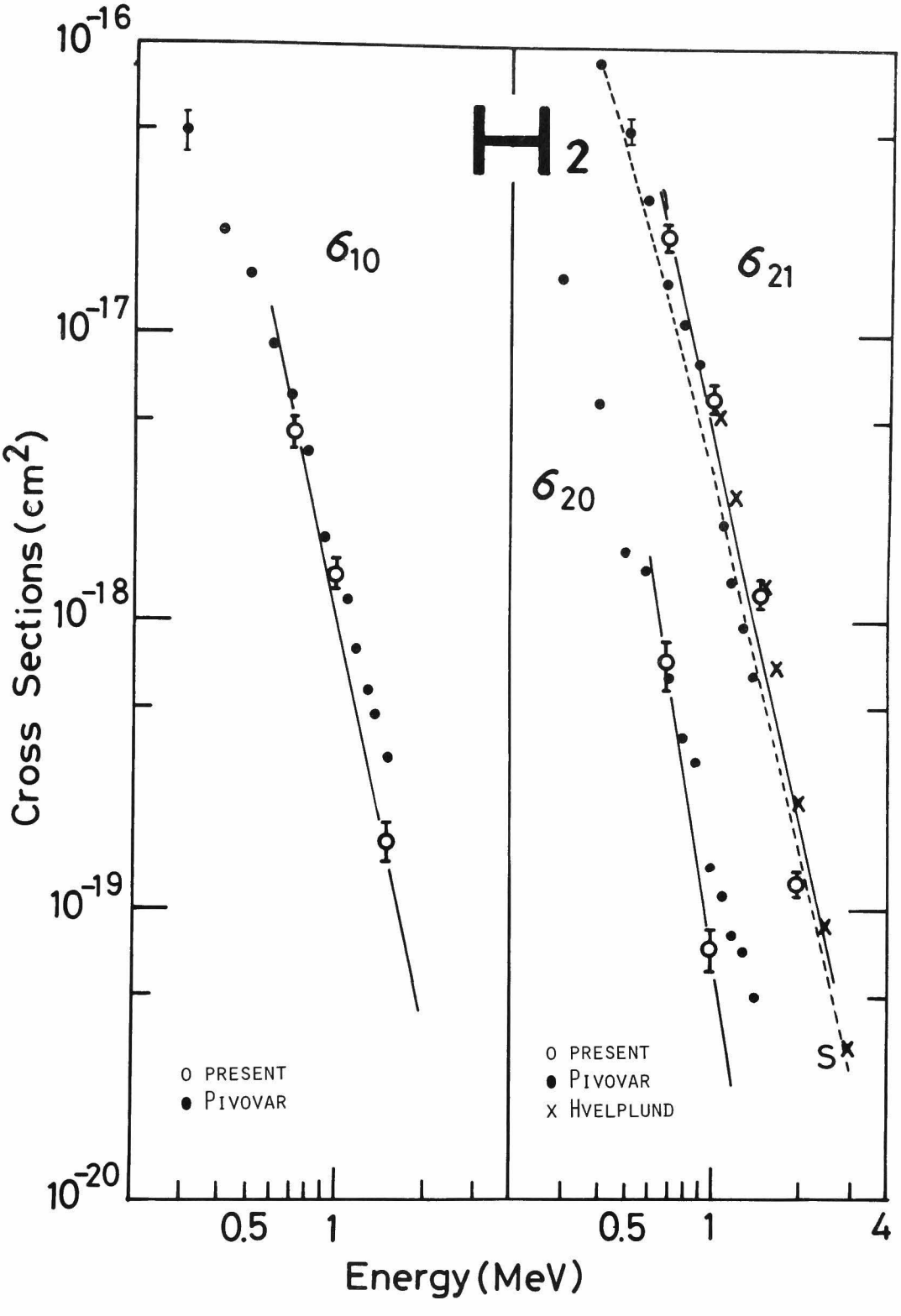
10^{-16}
10^{-17}
10^{-18}
10^{-19}
10^{-20}
Cross Sections (cm^2)
H_2
σ_{10}
σ_{21}
σ_{20}
o PRESENT
• PIVOVAR
o PRESENT
• PIVOVAR
x HVELPLUND
S
0.5
1
0.5
1
4
Energy (MeV)

FIG. 5-2(1)

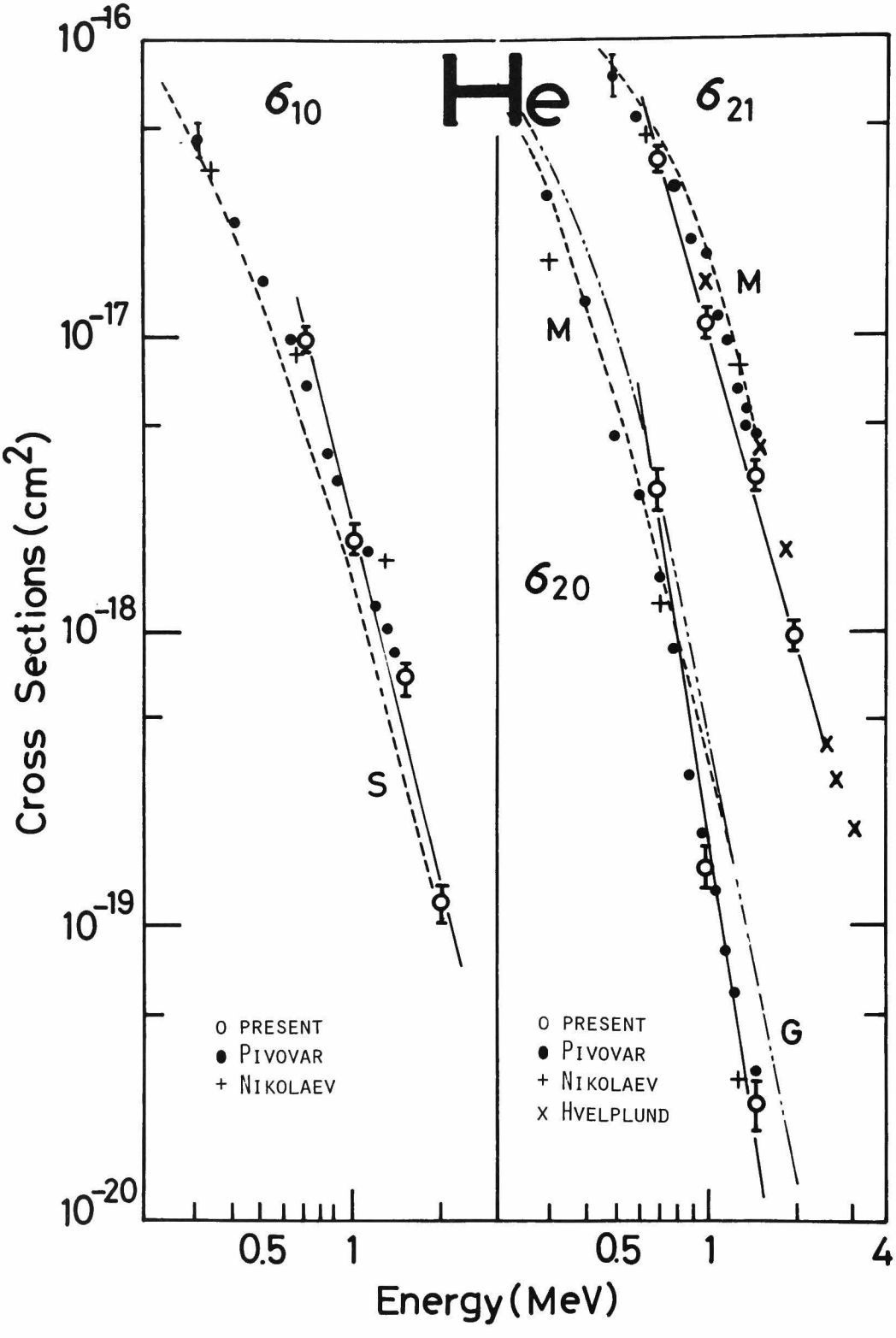
He
σ_{10}
σ_{21}
σ_{20}
S
M
M
G
o PRESENT
● PIVOVAR
+ NIKOLAEV
o PRESENT
● PIVOVAR
+ NIKOLAEV
x HVELPLUND
Cross Sections (cm²)
Energy (MeV)
10^{-16}
10^{-17}
10^{-18}
10^{-19}
10^{-20}
0.5
1
0.5
1
4

FIG. 5-2(2)

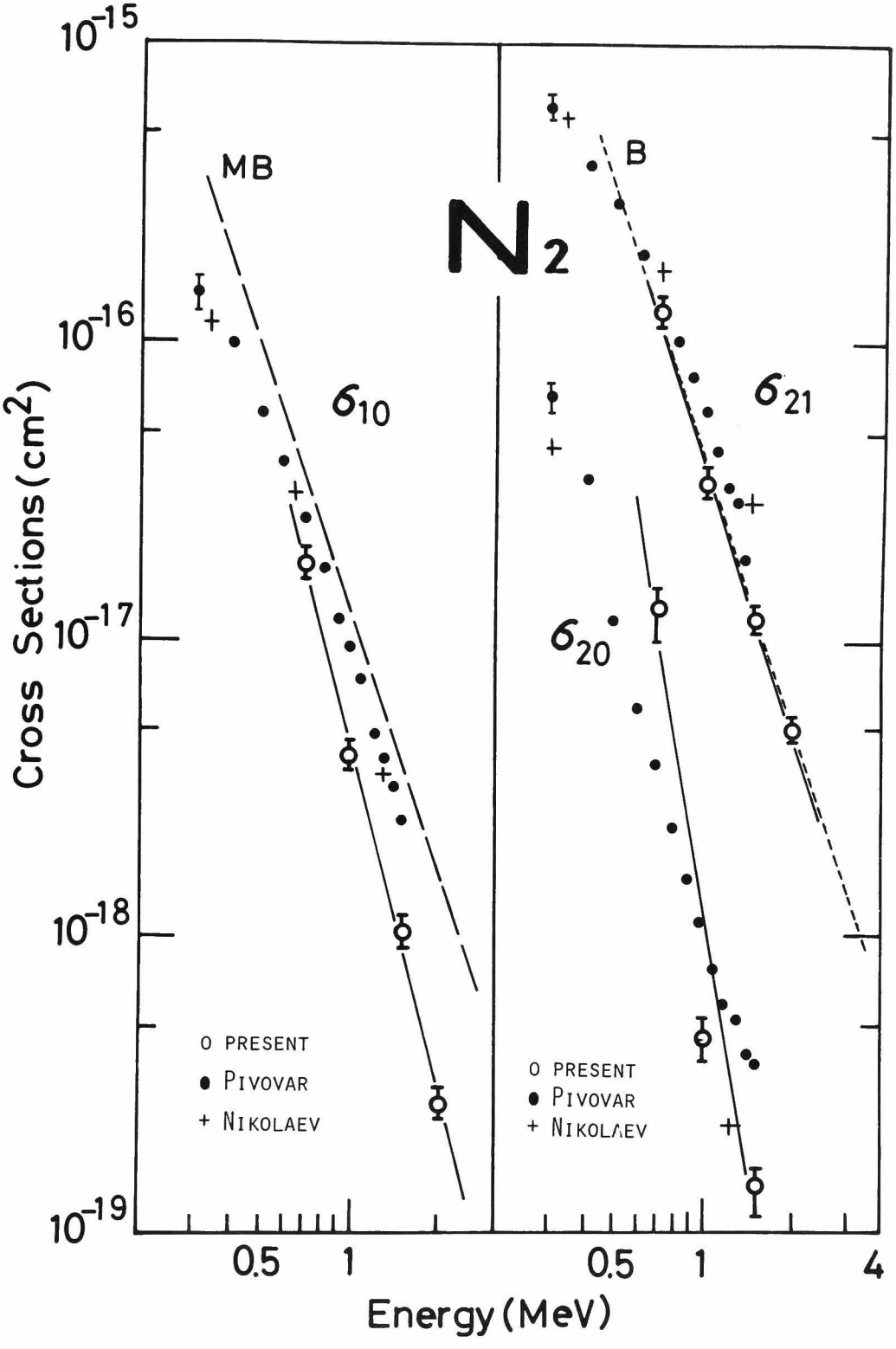
10^{-15}
10^{-16}
10^{-17}
10^{-18}
10^{-19}
Cross Sections (cm^2)
MB
B
N_2
σ_{10}
σ_{21}
σ_{20}
o PRESENT
● PIVOVAR
+ NIKOLAEV
o PRESENT
● PIVOVAR
+ NIKOLAEV
0.5
1
0.5
1
4
Energy (MeV)

FIG. 5-2(3)

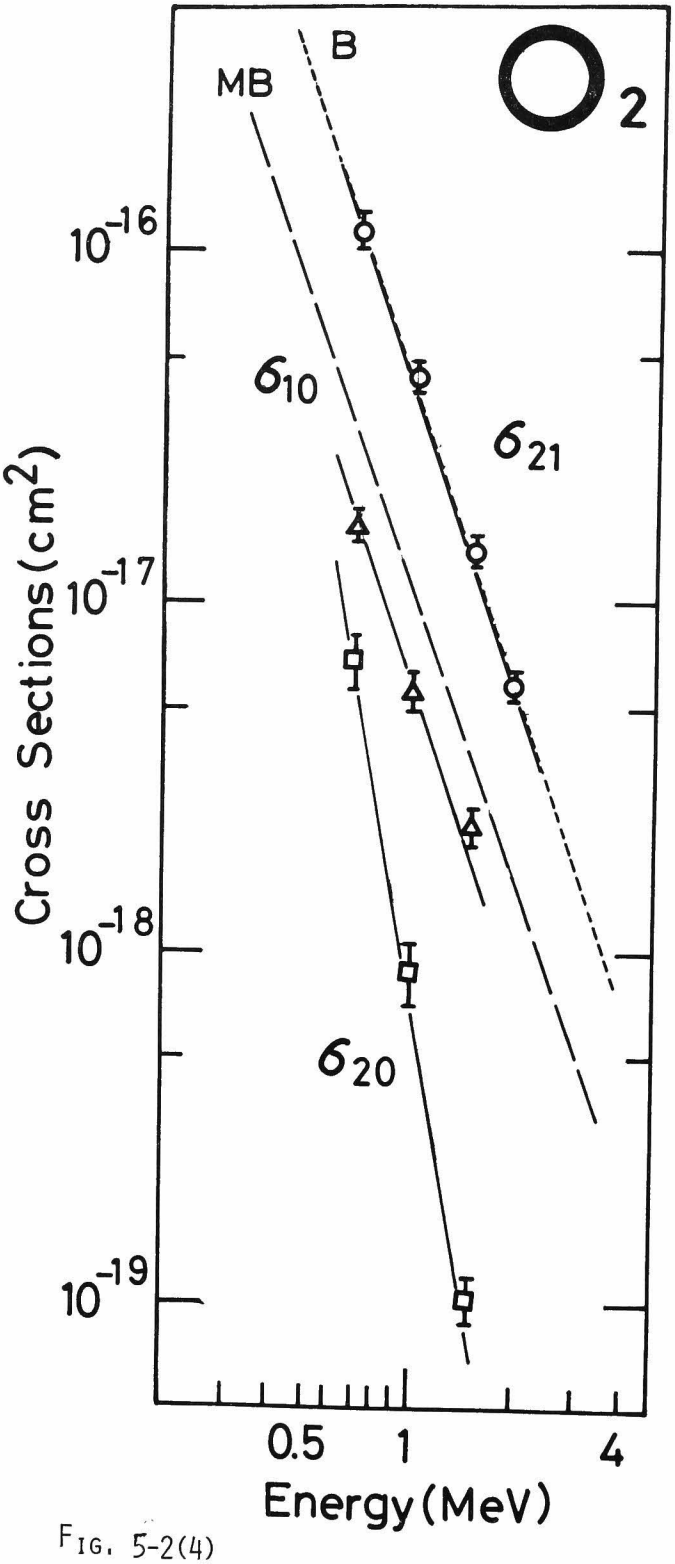
B
MB
O2
10-16
10-17
10-18
10-19
σ10
σ21
σ20
Cross Sections (cm2)
0.5
1
4
Energy (MeV)

FIG. 5-2(4)

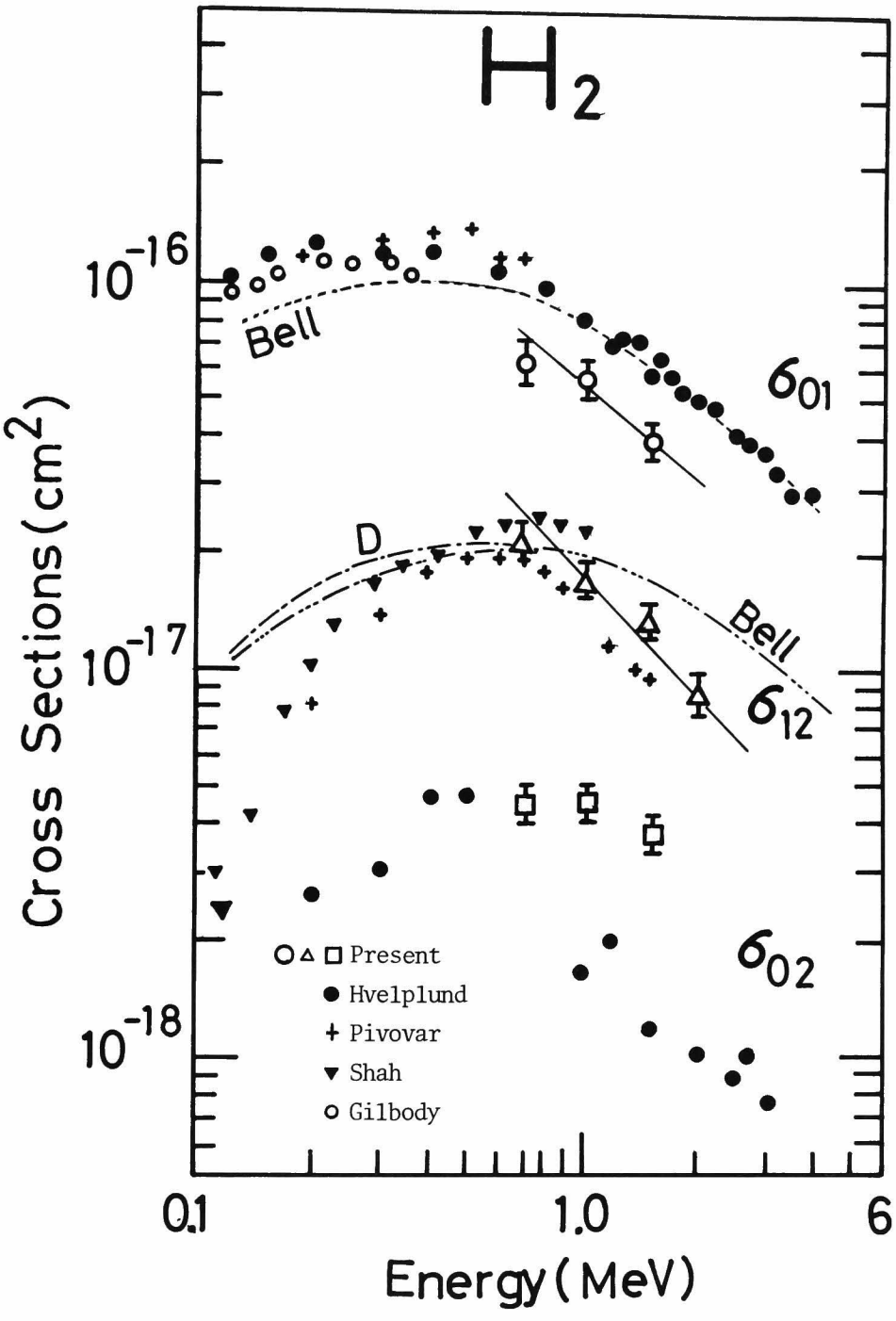
H2
10-16
10-17
10-18
Cross Sections (cm2)
Bell
D
Bell
σ01
σ12
σ02
Present
Hvelplund
Pivovar
Shah
Gilbody
0.1
1.0
6
Energy (MeV)

FIG. 5-3(1)

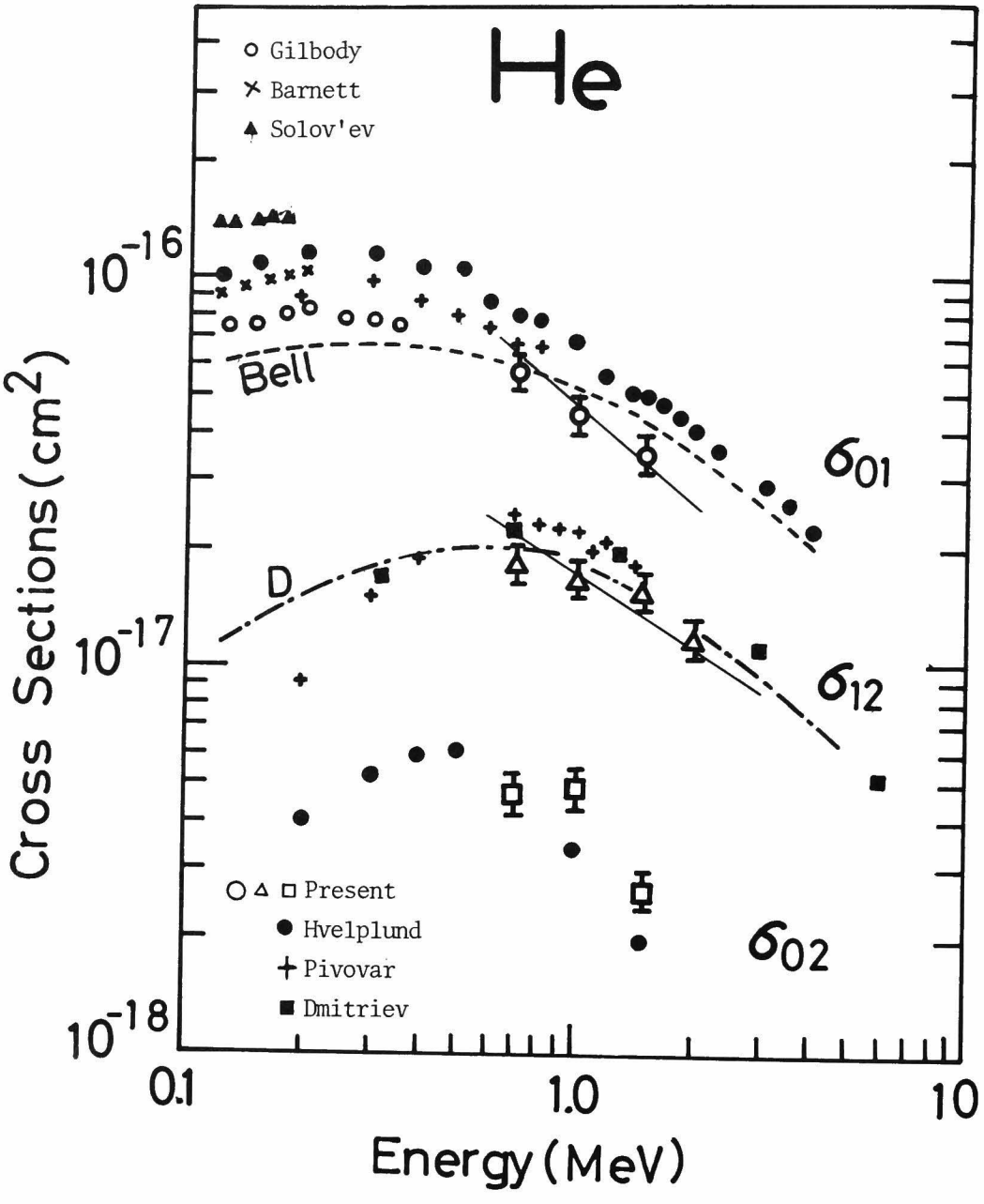
He
Gilbody
Barnett
Solov'ev
Bell
D
σ_{01}
σ_{12}
σ_{02}
Present
Hvelplund
Pivovar
Dmitriev
Cross Sections (cm^2)
10^{-16}
10^{-17}
10^{-18}
0.1
1.0
10
Energy (MeV)

FIG. 5-3(2)

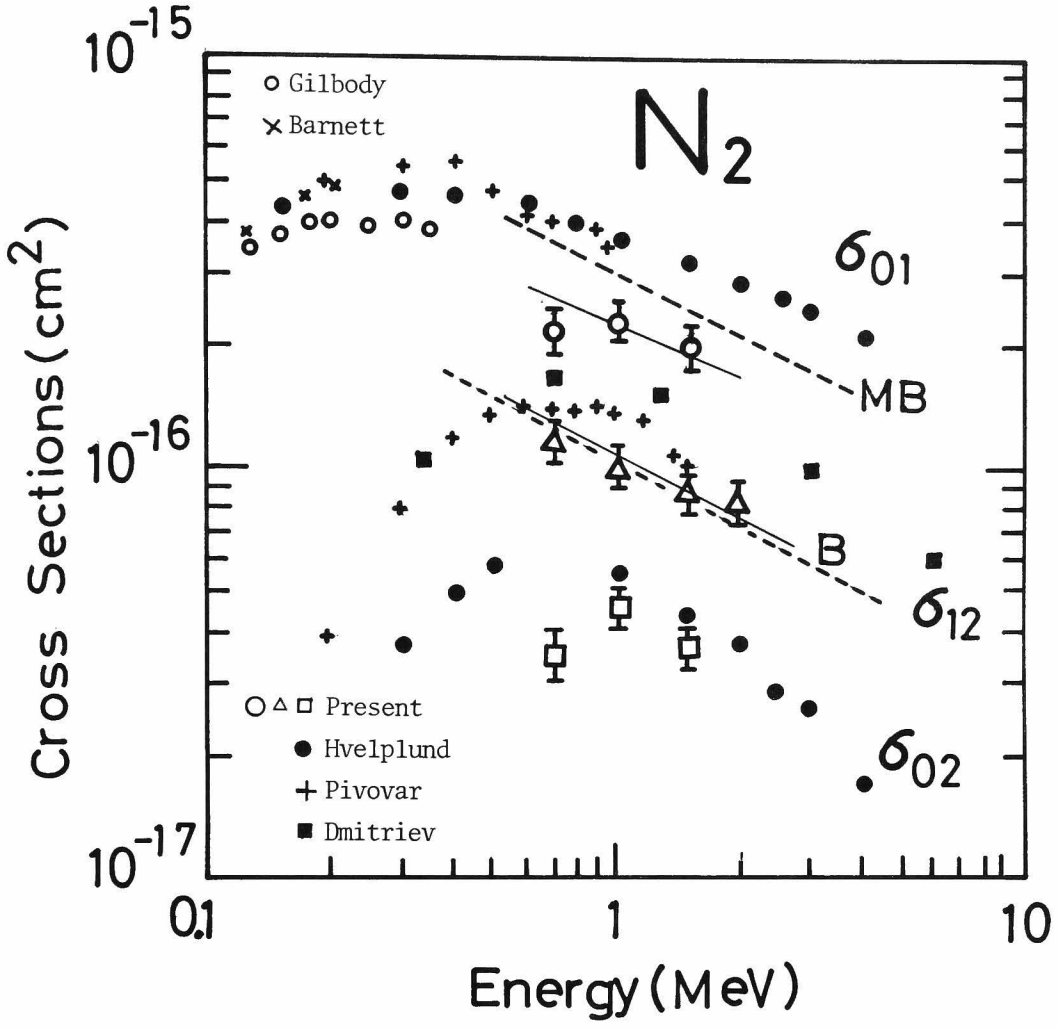
10^{-15}
10^{-16}
10^{-17}
Cross Sections (cm^2)
0.1
1
10
Energy (MeV)
N_2
○ Gilbody
× Barnett
σ_{01}
MB
B
σ_{12}
σ_{02}
○ △ □ Present
● Hvelplund
+ Pivovar
■ Dmitriev

FIG. 5-3(3)

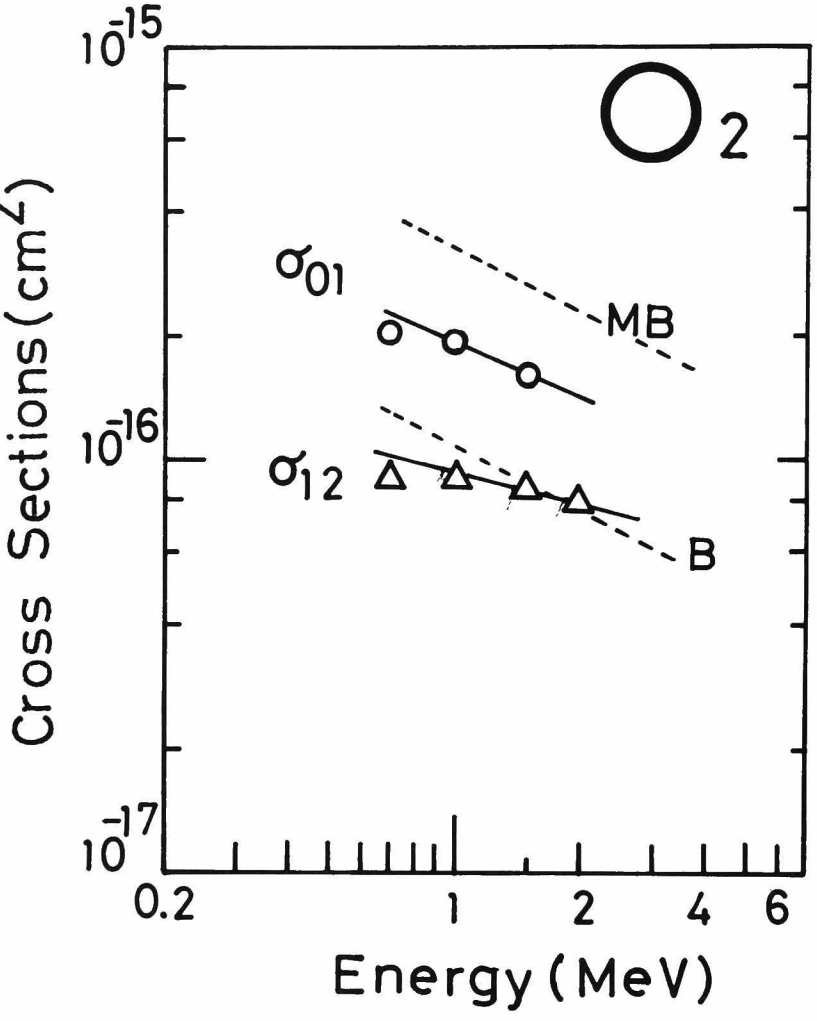
10^{-15}
10^{-16}
10^{-17}
Cross Sections (cm^2)
O_2
σ_{01}
σ_{12}
MB
B
0.2
1
2
4
6
Energy (MeV)

FIG. 5-3(4)

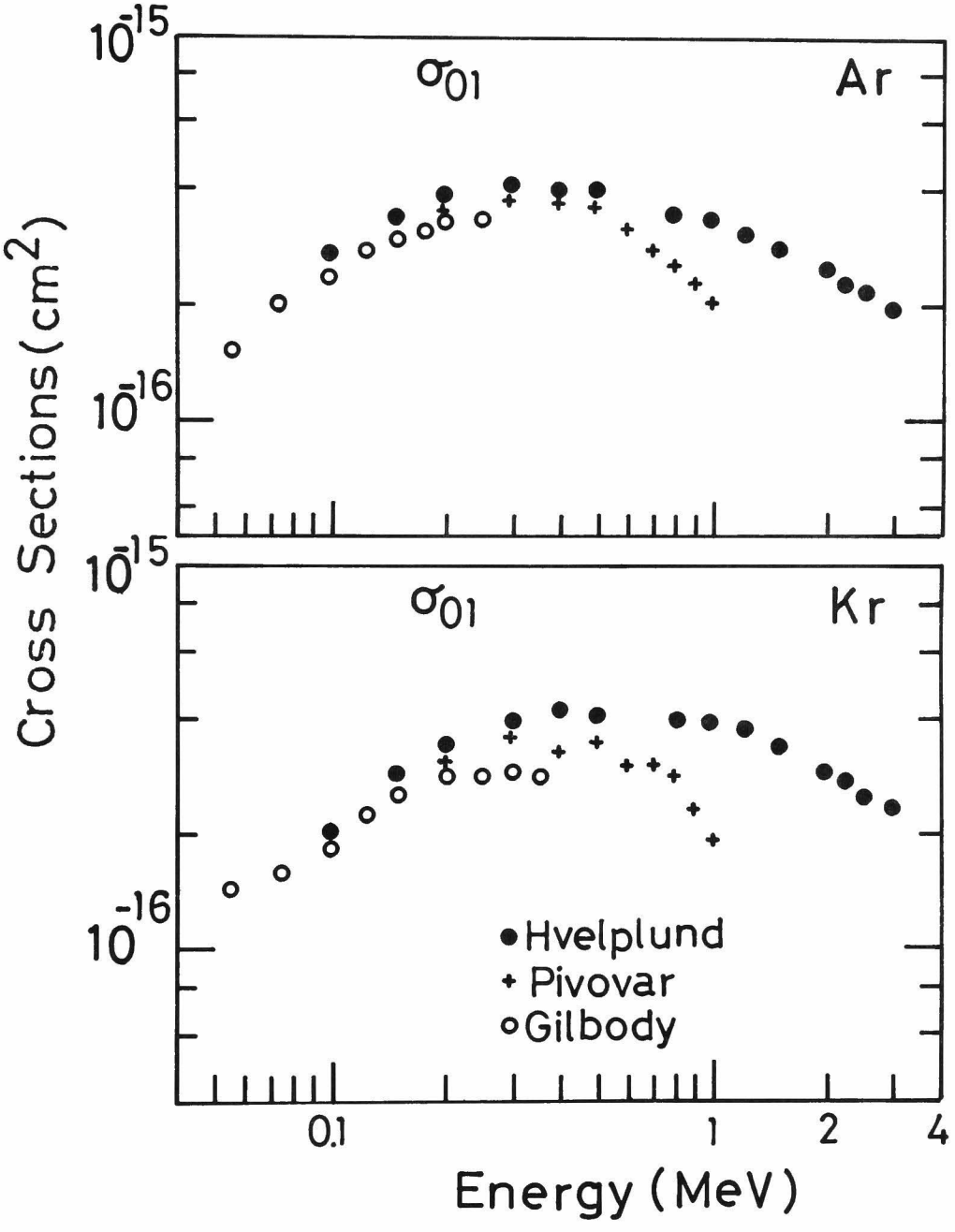

FIG. 5-4. Energy variation of electron loss cross sections for He beam in Ar and Kr; ● Hvelplund *et al*(ref. 59), + Pivovar *et al*(ref. 53), o Gilbody *et al*(ref. 51).

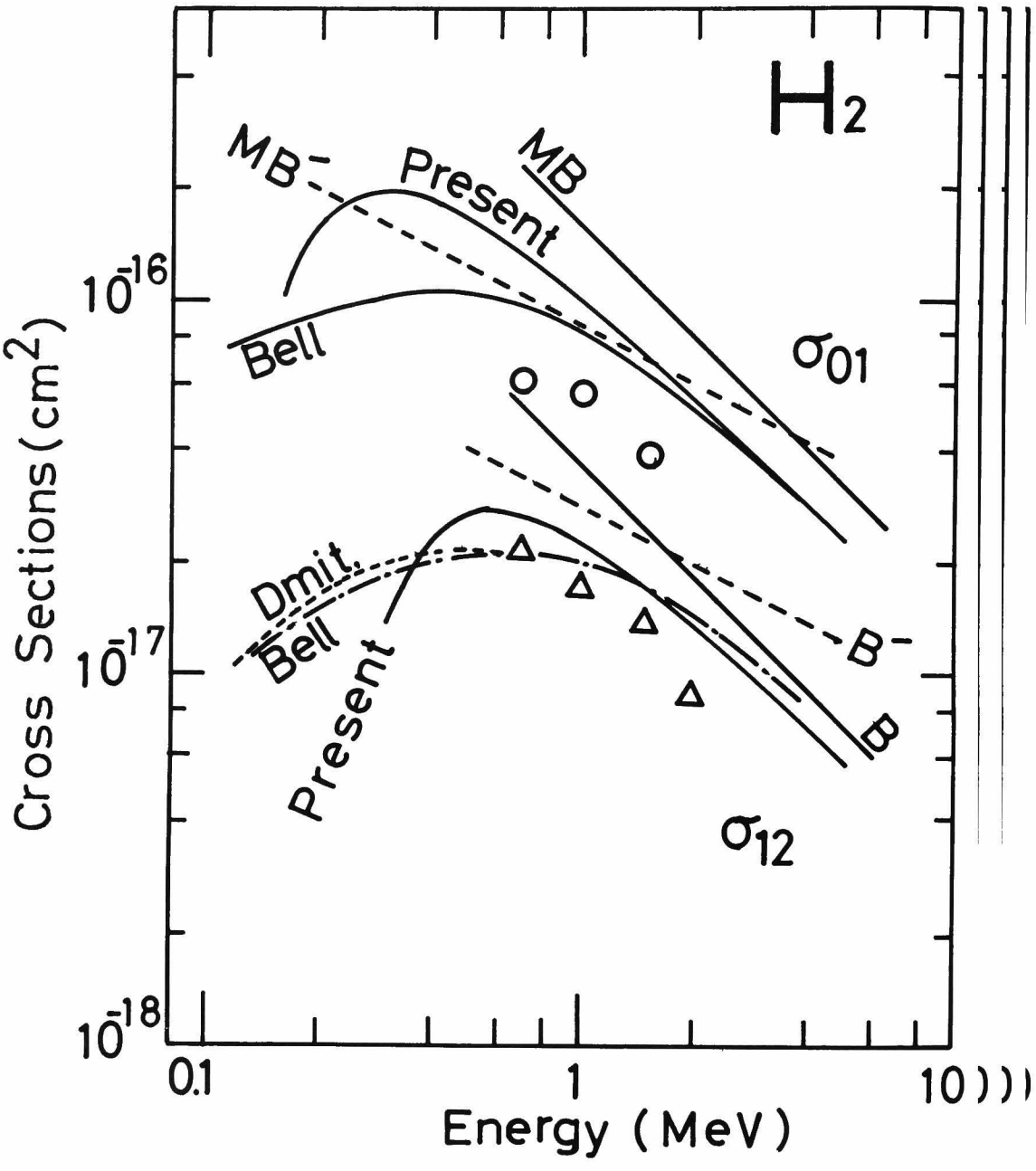
H2
MB
Present
MB
Bell
σ01
Dmit
Bell
Present
B
B
σ12
Cross Sections (cm2)
10-16
10-17
10-18
0.1
1
10
Energy (MeV)

FIG. 5-5(1)

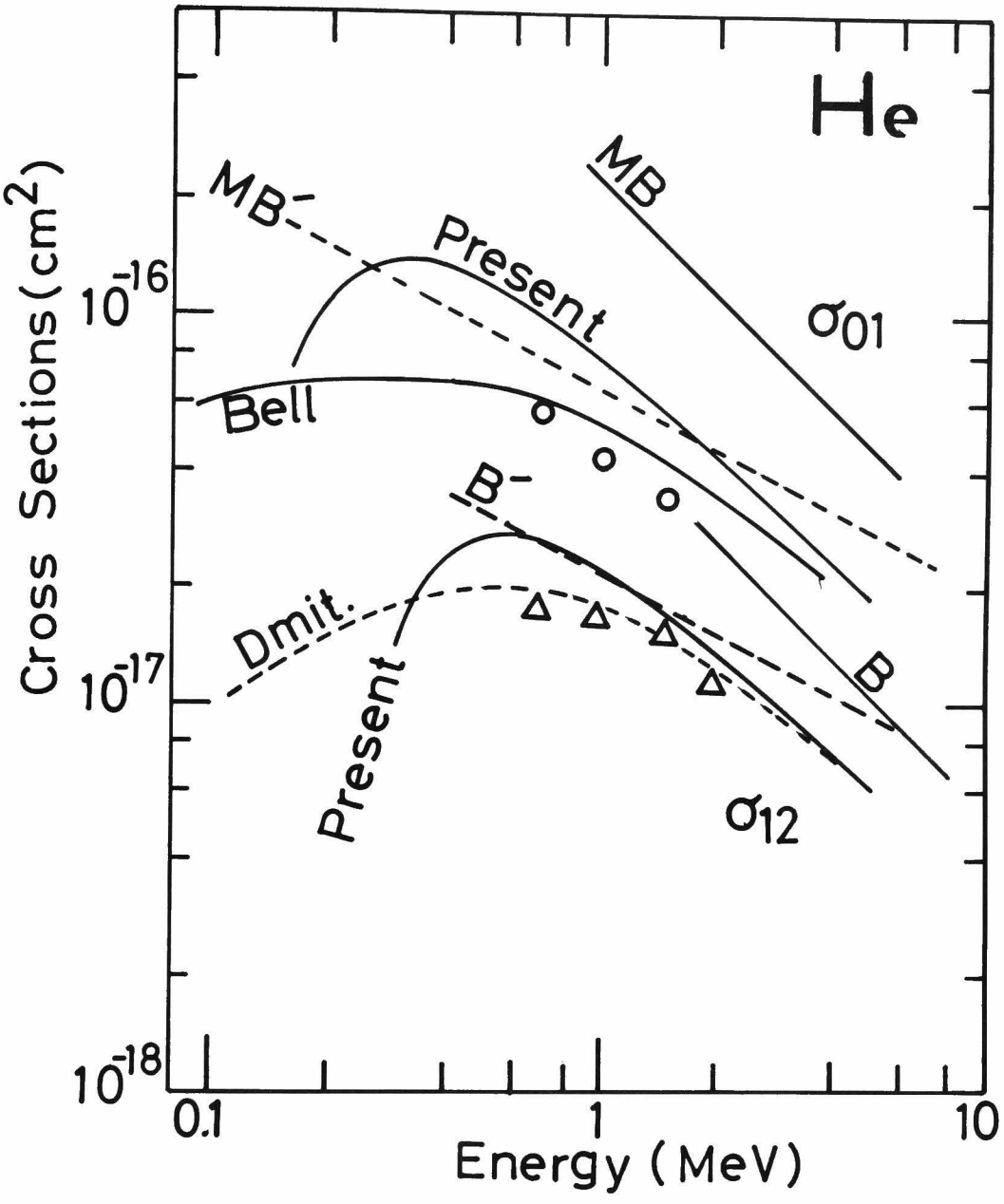
He
MB
MB-
Present
Bell
B-
Dmit.
Present
B
σ_{01}
σ_{12}
Cross Sections (cm^2)
10^{-16}
10^{-17}
10^{-18}
0.1
1
10
Energy (MeV)

FIG. 5-5(2)

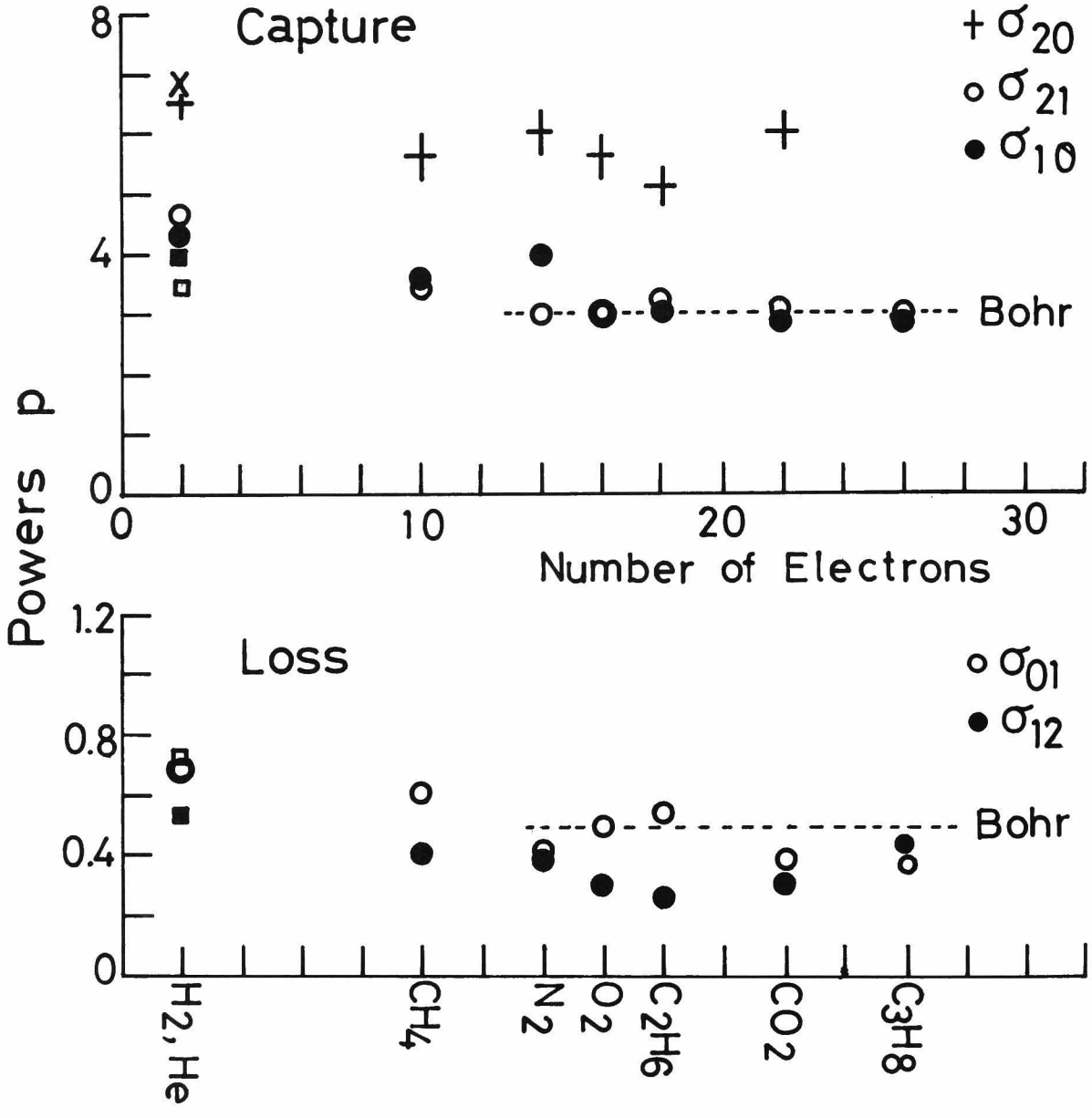
Capture
$+\sigma_{20}$
$\circ\sigma_{21}$
$\bullet\sigma_{10}$
Bohr
Powers p
Number of Electrons
Loss
$\circ\sigma_{01}$
$\bullet\sigma_{12}$
Bohr
H2, He
CH4
N2
O2
C2H6
CO2
C3H8

FIG. 5-6

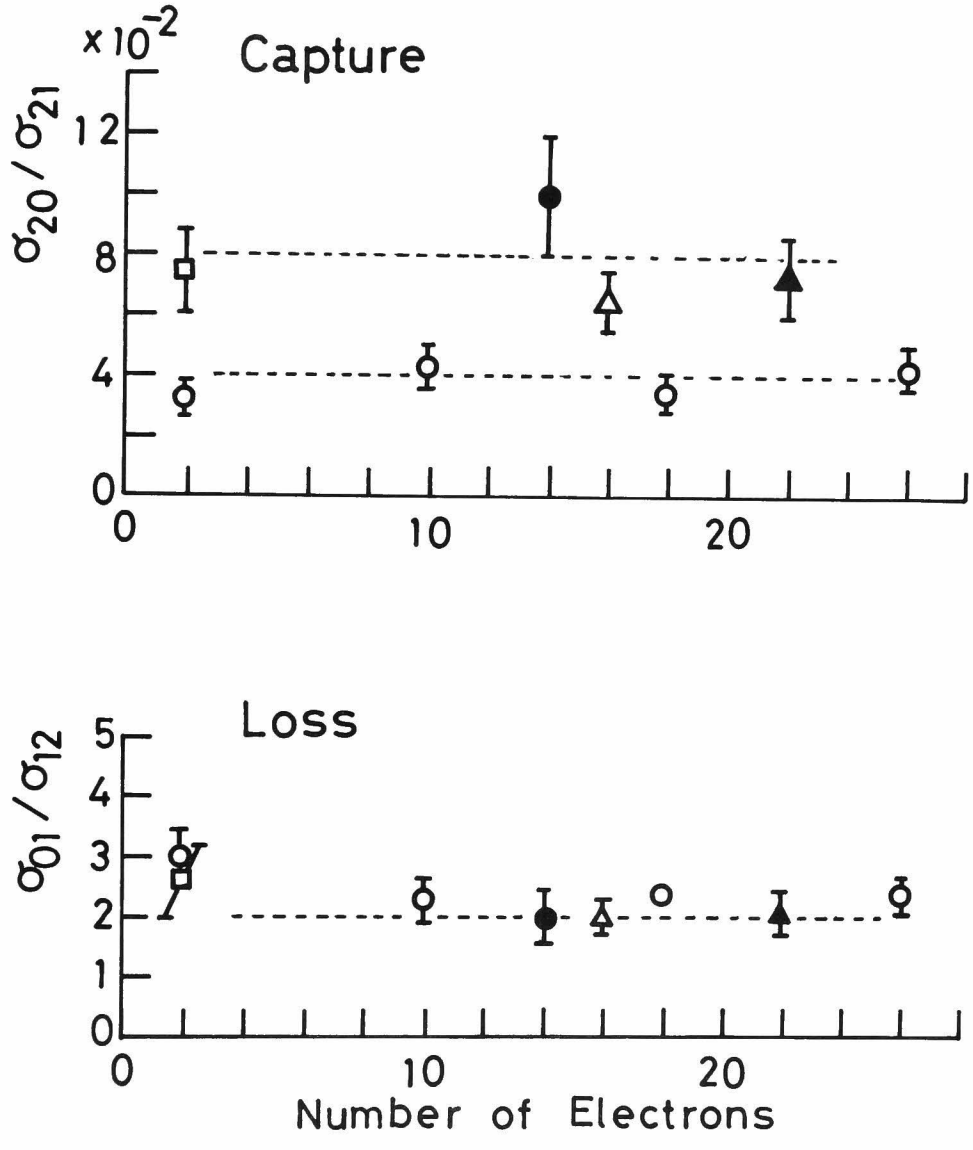
x 10⁻²
Capture
σ20 / σ21
12
8
4
0
0
10
20
Loss
σ01 / σ12
5
4
3
2
1
0
0
10
20
Number of Electrons

FIG. 5-7

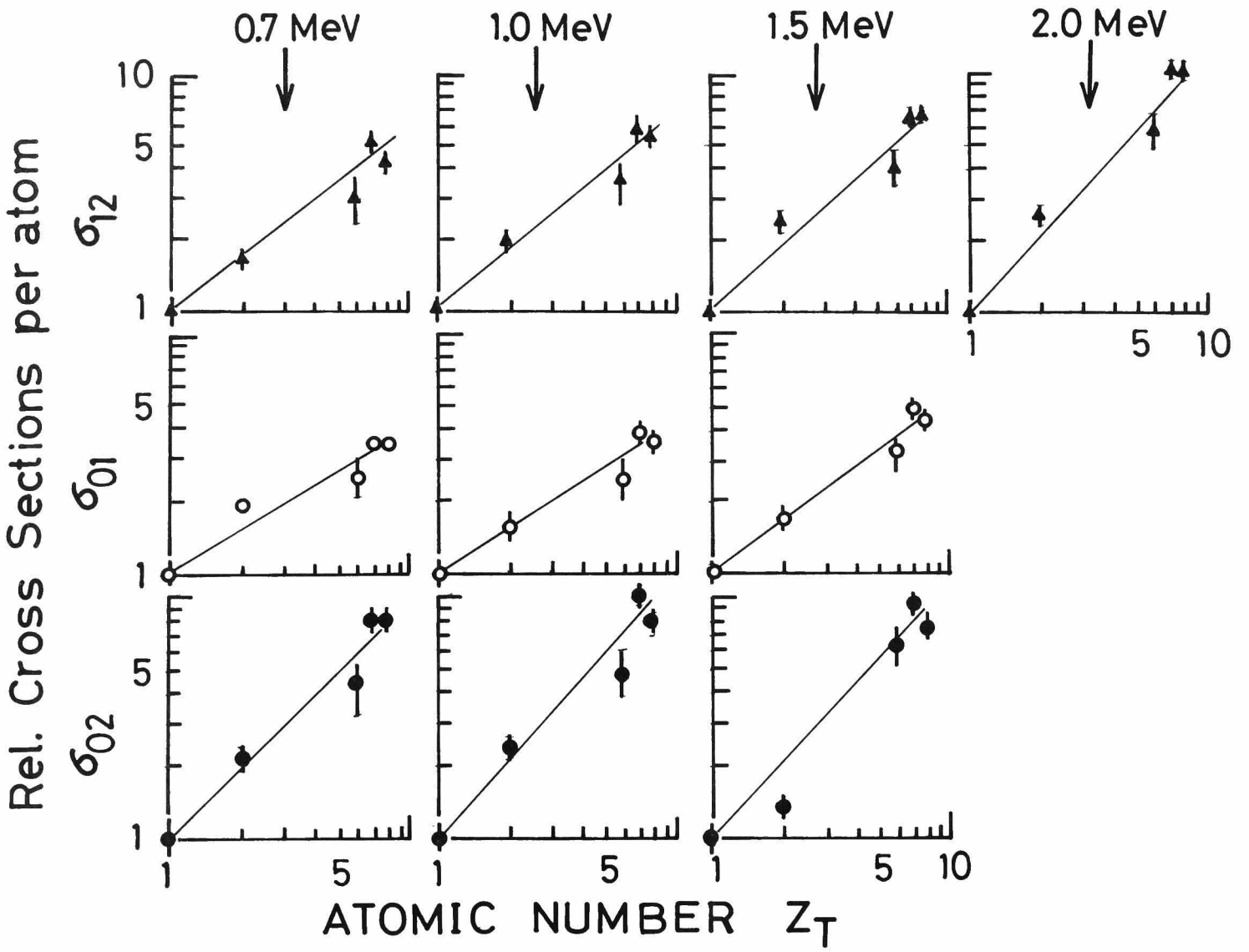
0.7 MeV
1.0 MeV
1.5 MeV
2.0 MeV
Rel. Cross Sections per atom
σ_{12}
σ_{01}
σ_{02}
10
5
1
ATOMIC NUMBER Z_T

FIG. 5-8(1)

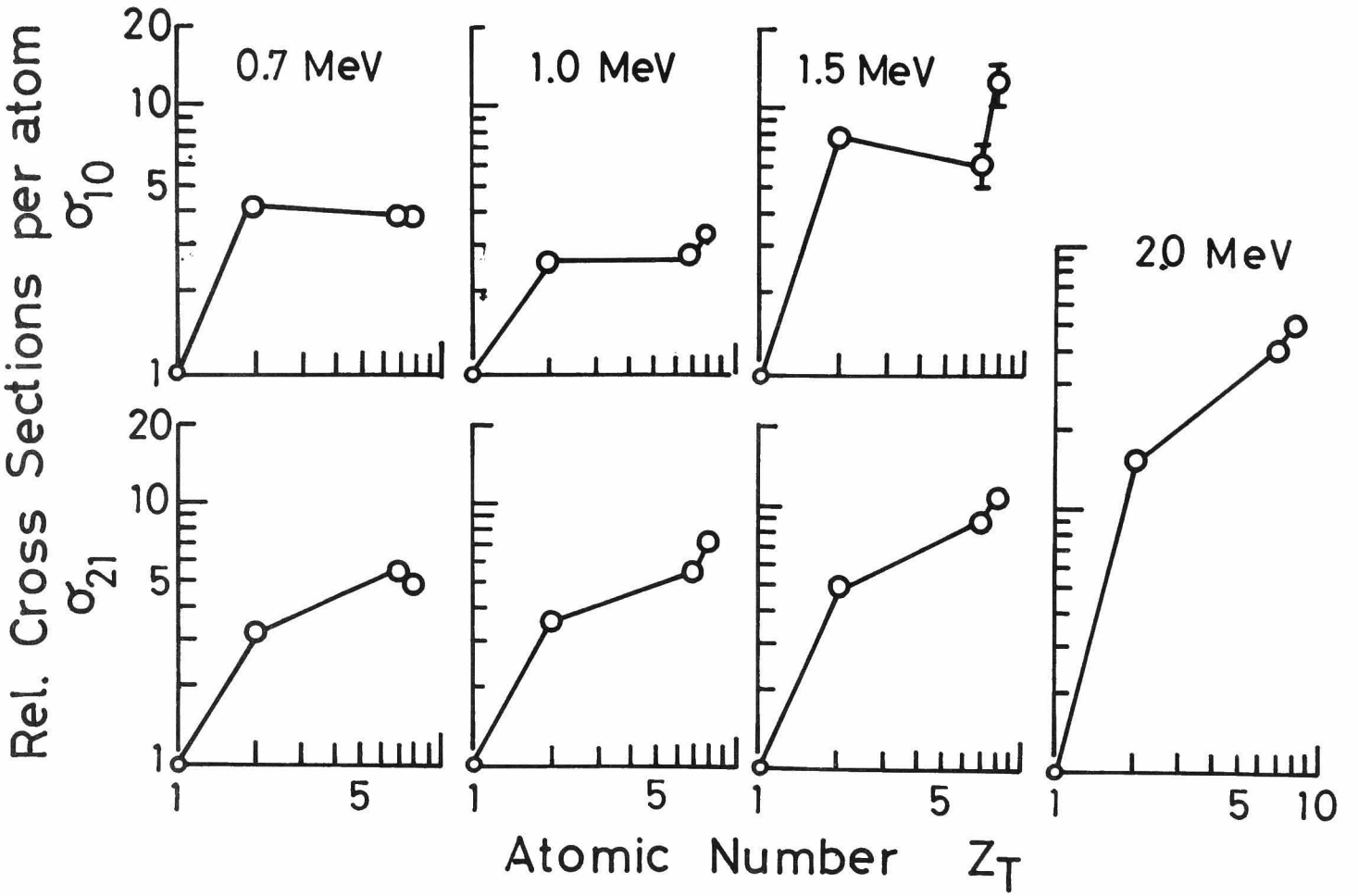
0.7 MeV
1.0 MeV
1.5 MeV
2.0 MeV
Rel. Cross Sections per atom
σ_{10}
σ_{21}
20
10
5
1
1
5
10
Atomic Number Z_T

FIG. 5-8(2)

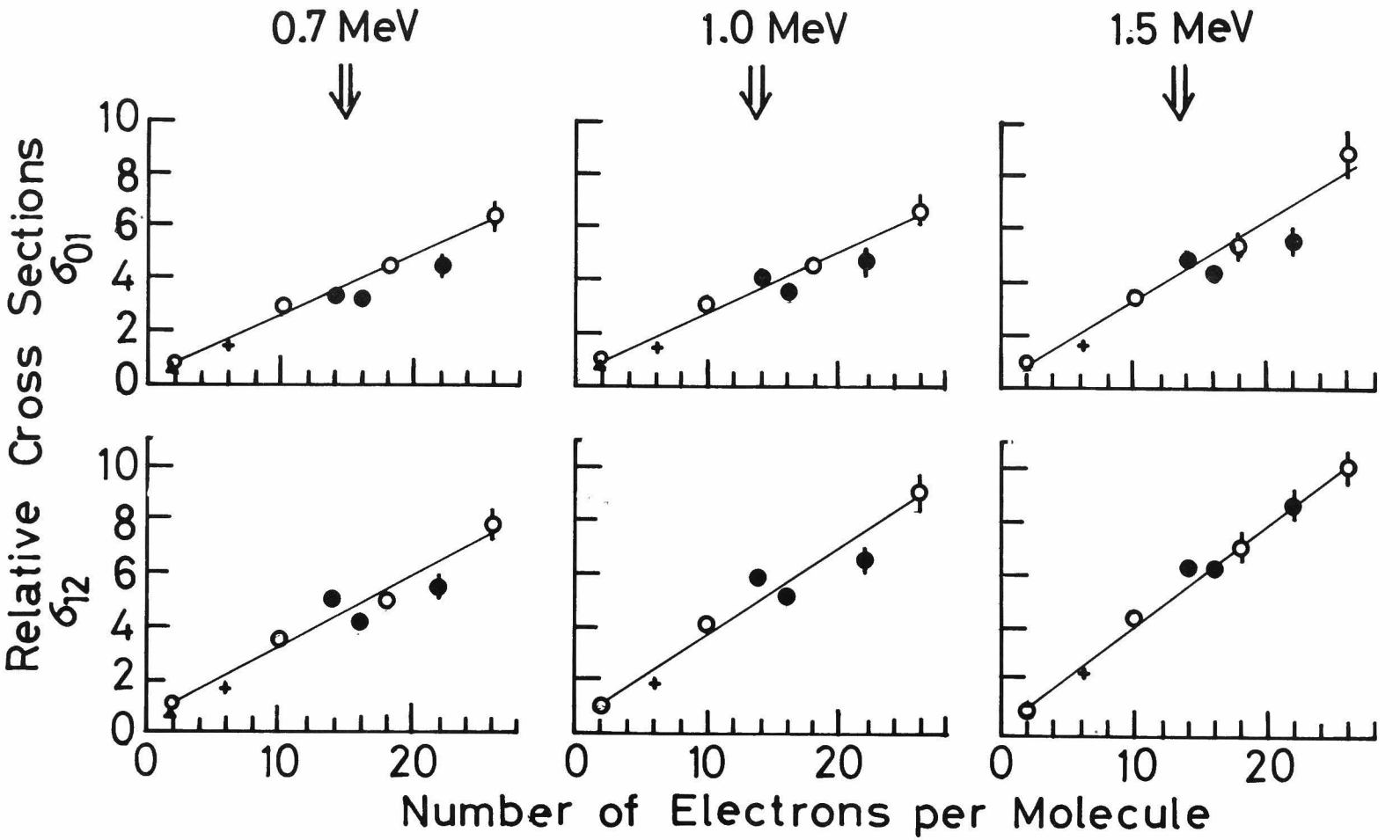
0.7 MeV
1.0 MeV
1.5 MeV
Relative Cross Sections
σ_{01}
σ_{12}
0
2
4
6
8
10
0
10
20
Number of Electrons per Molecule

Fig. 5-9(1)

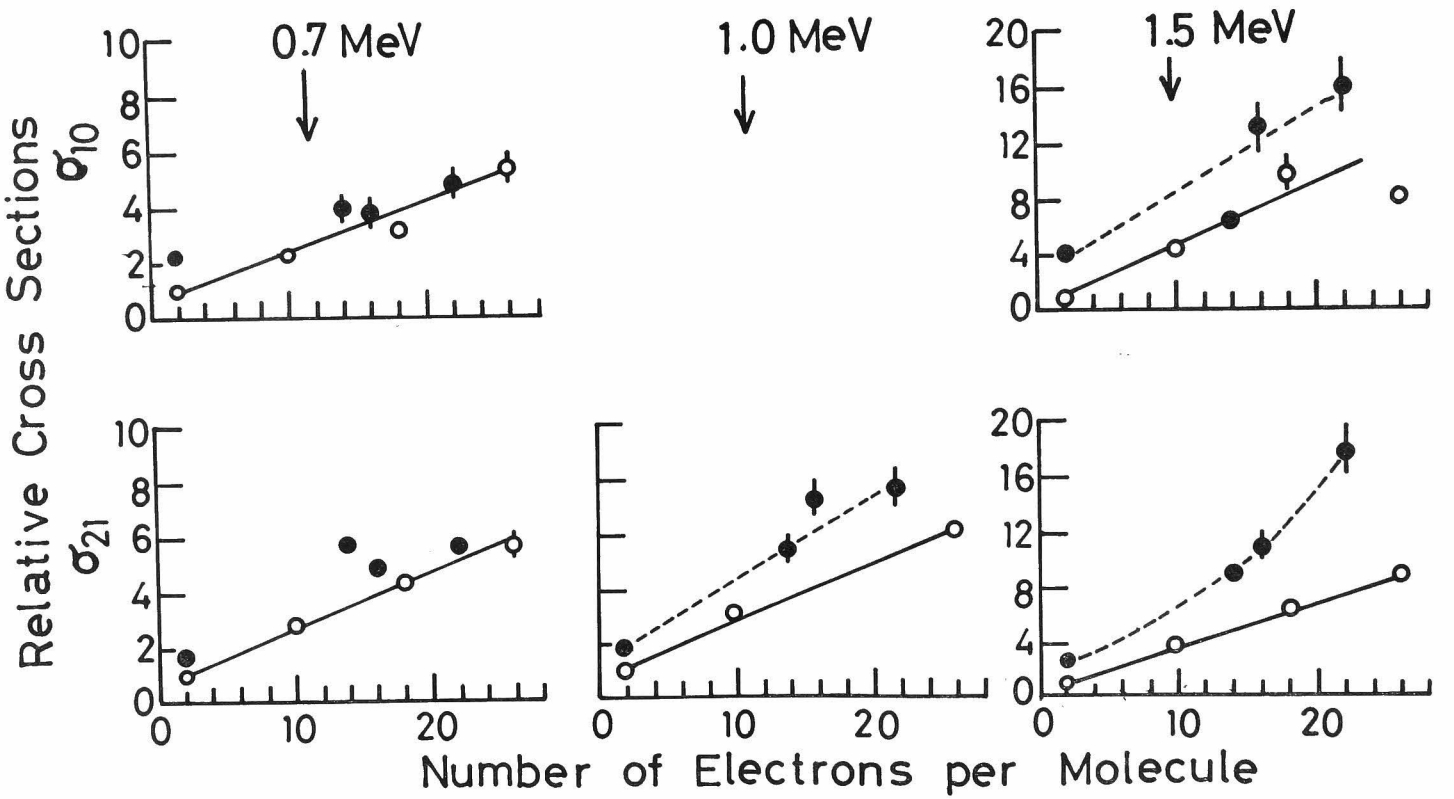
0.7 MeV
1.0 MeV
1.5 MeV
Relative Cross Sections
σ_{10}
σ_{21}
Number of Electrons per Molecule

Fig. 5-9(2)

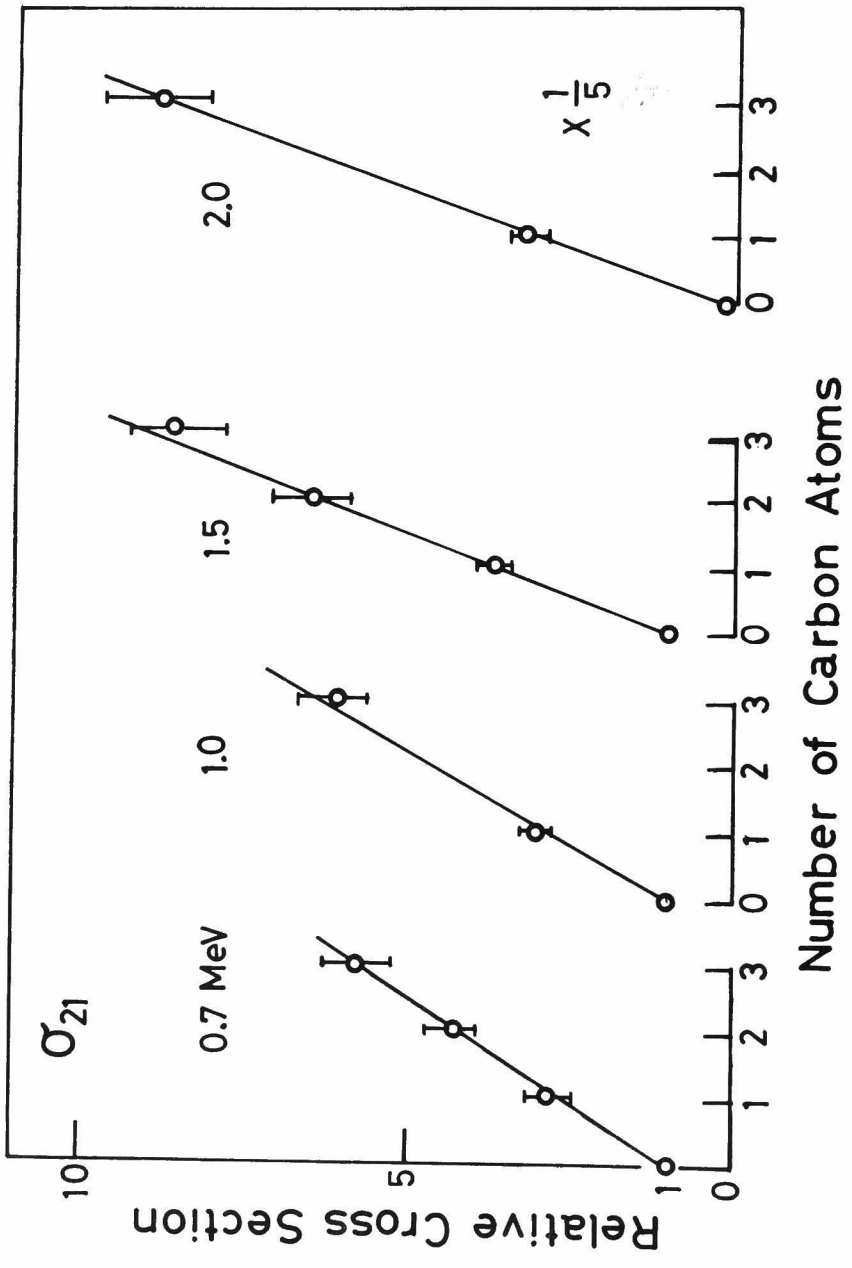
Relative Cross Section
10
5
1
0
σ_{21}
0.7 MeV
1.0
1.5
2.0
$\times\frac{1}{5}$
1 2 3
0 1 2 3
Number of Carbon Atoms

FIG. 6-1(1)

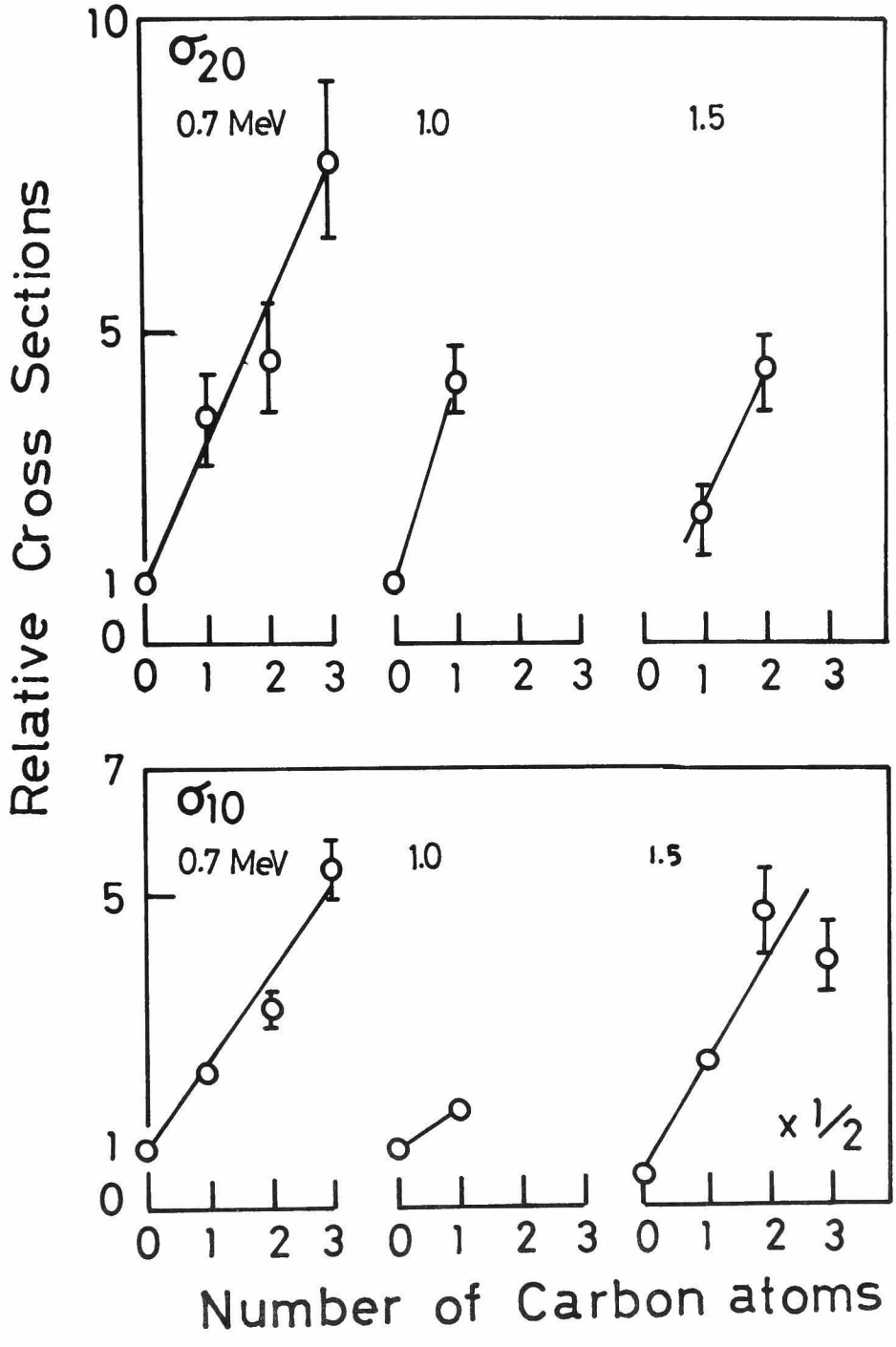
Relative Cross Sections
σ20
0.7 MeV
1.0
1.5
10
5
1
0
σ10
0.7 MeV
1.0
1.5
7
5
1
0
x 1/2
0 1 2 3
Number of Carbon atoms

FIG. 6-1(2)(3)

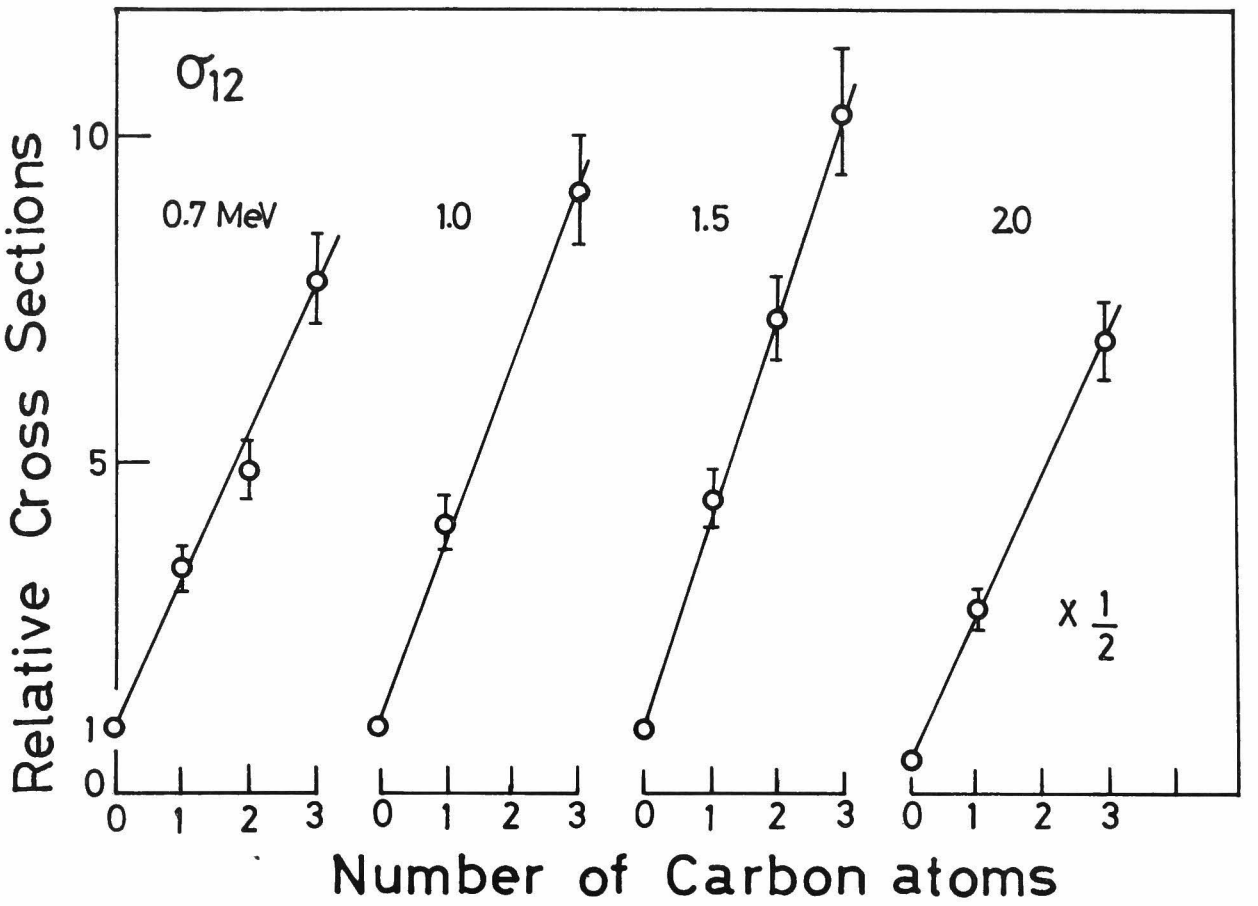
σ12
0.7 MeV
1.0
1.5
2.0
X 1/2
Relative Cross Sections
10
5
1
0
0 1 2 3
Number of Carbon atoms

Fig. 6-1(4)

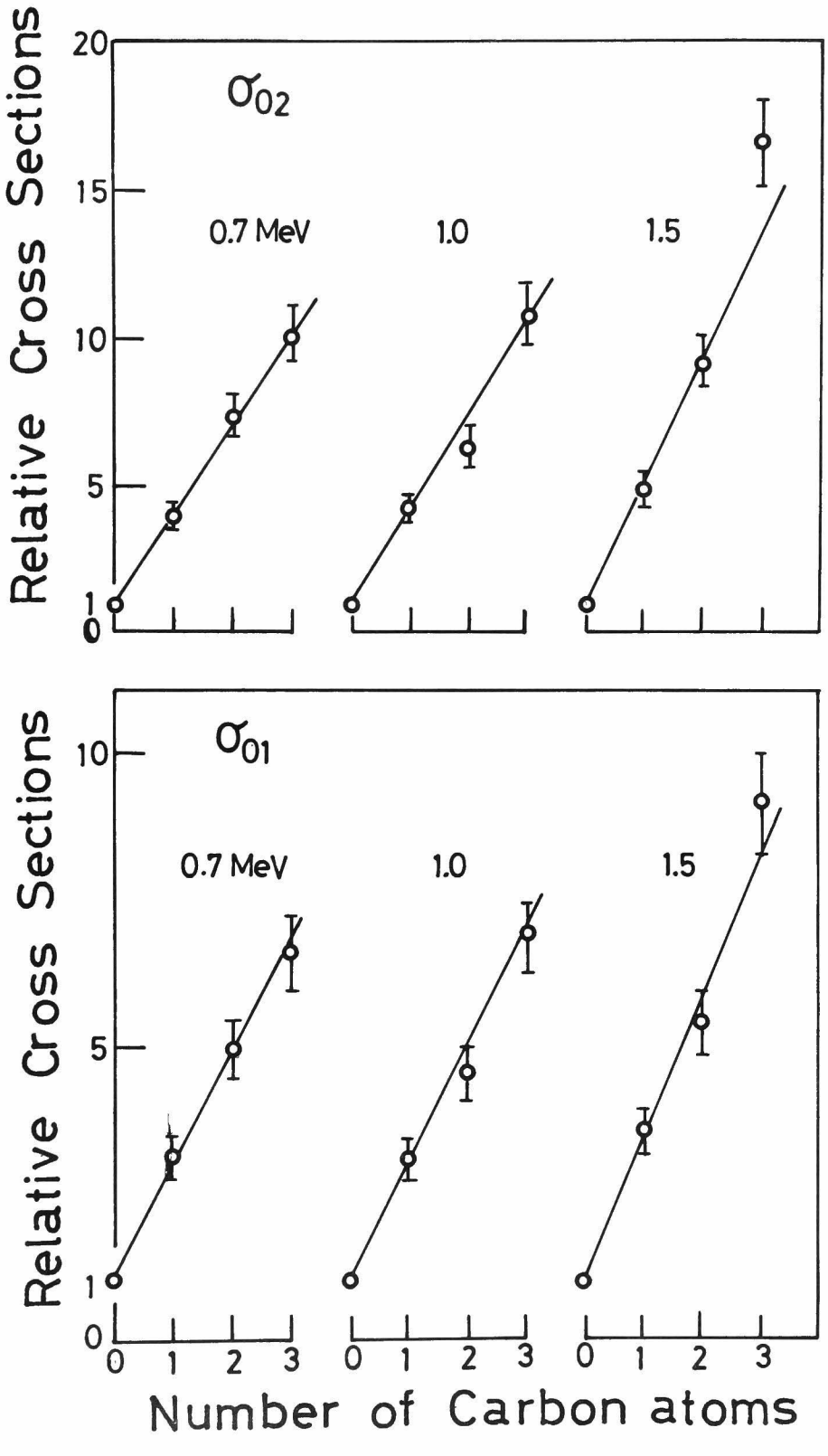
Relative Cross Sections
σ_{02}
0.7 MeV
1.0
1.5
20
15
10
5
1
0
Relative Cross Sections
σ_{01}
0.7 MeV
1.0
1.5
10
5
1
0
0 1 2 3
0 1 2 3
0 1 2 3
Number of Carbon atoms

FIG. 6-1(5)(6)

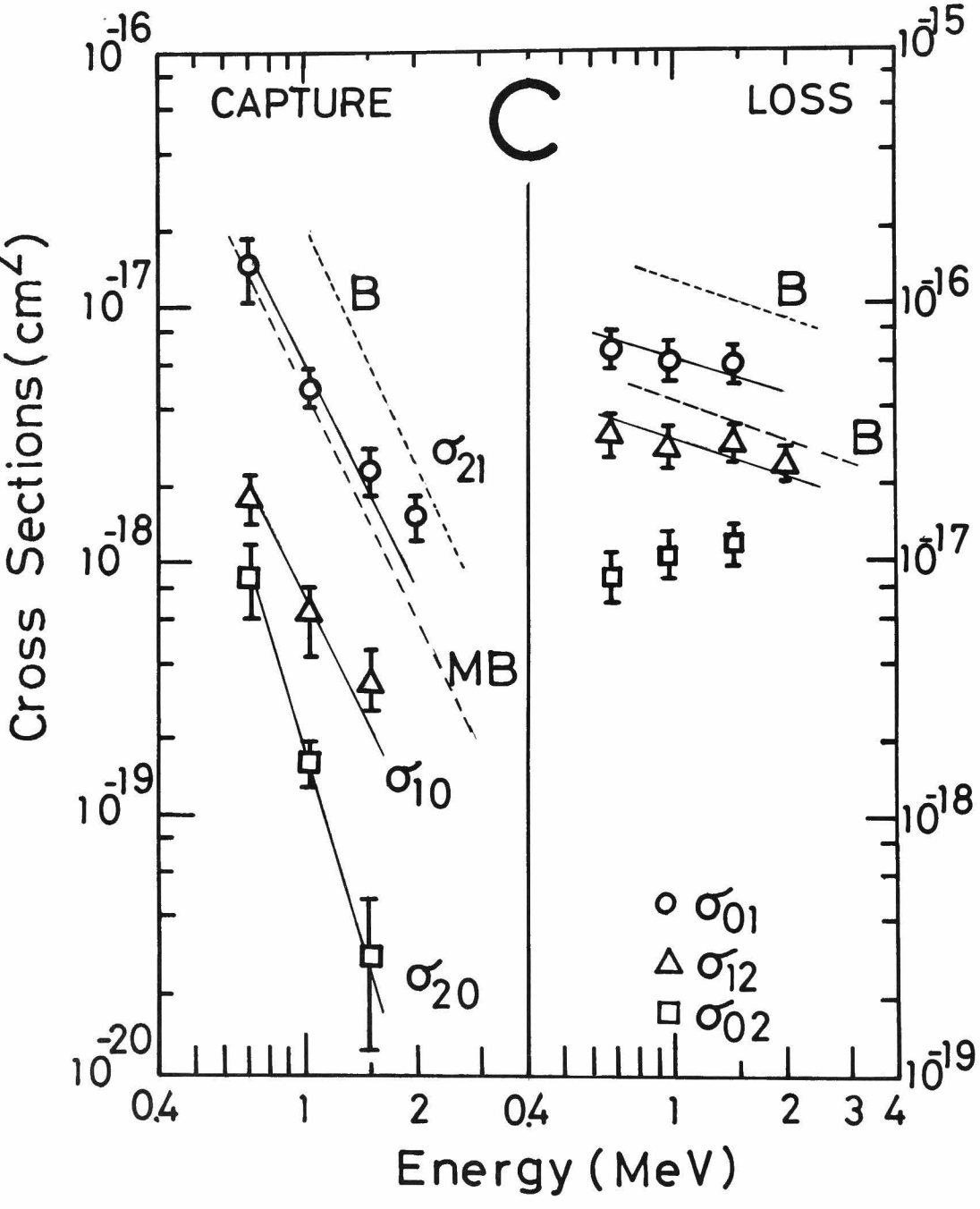
CAPTURE
C
LOSS
B
B
B
MB
σ_{21}
σ_{10}
σ_{20}
σ_{01}
σ_{12}
σ_{02}
Cross Sections (cm^2)
Energy (MeV)
10^{-16}
10^{-17}
10^{-18}
10^{-19}
10^{-20}
10^{-15}
10^{-16}
10^{-17}
10^{-18}
10^{-19}
0.4
1
2
0.4
1
2
3
4

FIG. 6-2

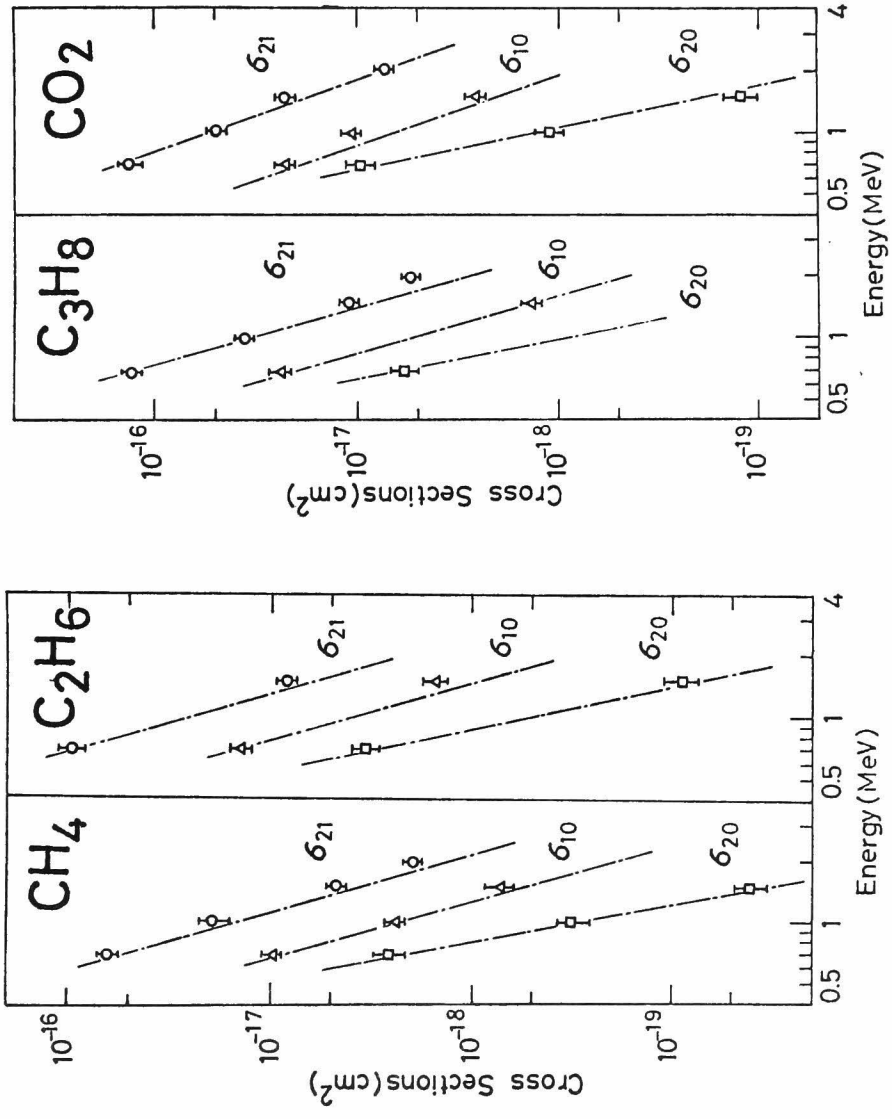
CH4
C2H6
C3H8
CO2
σ21
σ10
σ20
Cross Sections(cm²)
Energy(MeV)
10⁻¹⁶
10⁻¹⁷
10⁻¹⁸
10⁻¹⁹
0.5
1
4

FIG. 6-3(1)

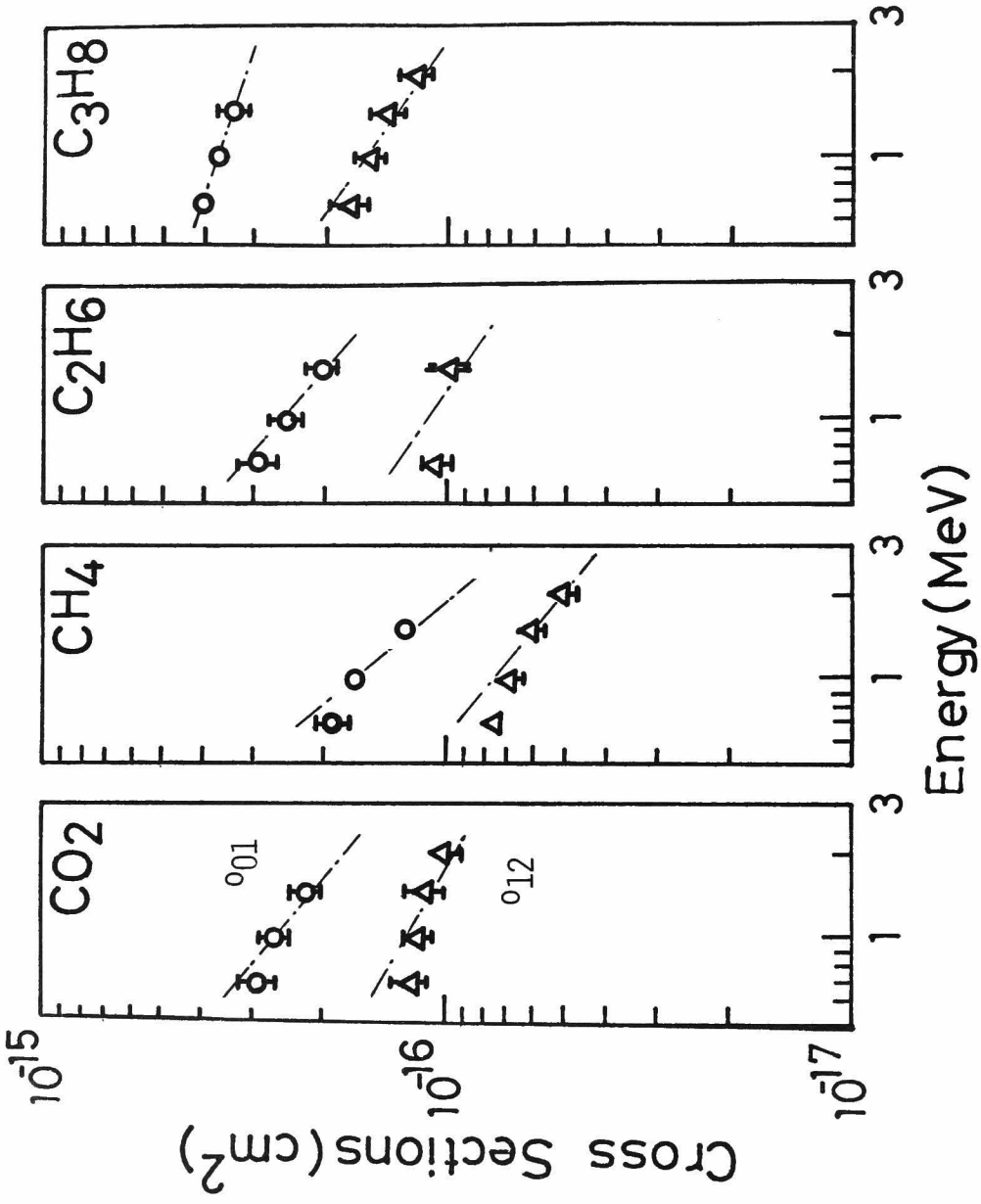
CO2
CH4
C2H6
C3H8
σ01
σ12
10^-15
10^-16
10^-17
Cross Sections (cm^2)
1
3
1
3
1
3
1
3
Energy (MeV)

FIG. 6-3(2)

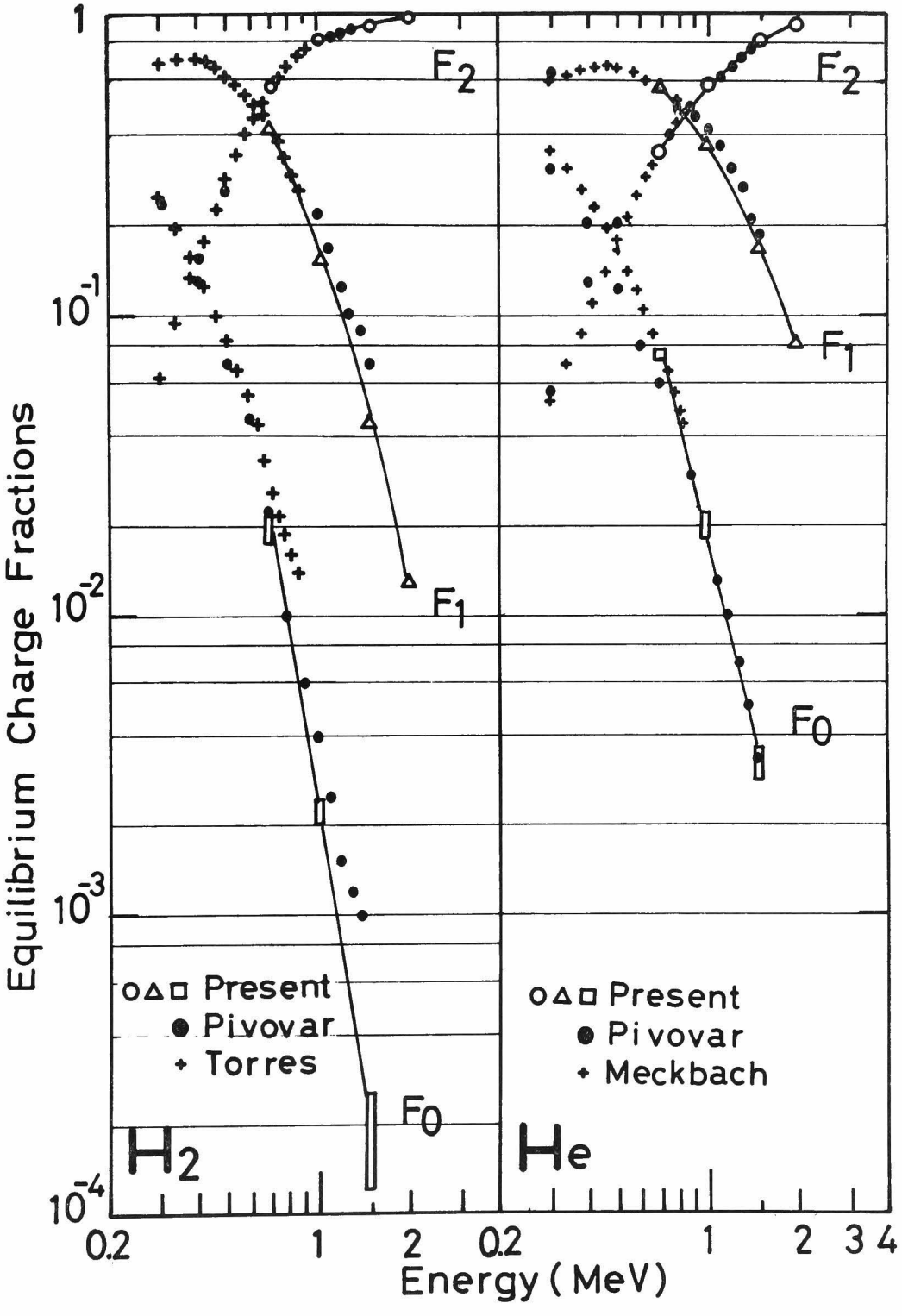
1
10^{-1}
10^{-2}
10^{-3}
10^{-4}
Equilibrium Charge Fractions
F_2
F_1
F_0
o△□ Present
● Pivovar
+ Torres
H_2
o△□ Present
● Pivovar
+ Meckbach
He
0.2
1
2
0.2
1
2
3
4
Energy (MeV)

FIG. 7-1(1)(2)

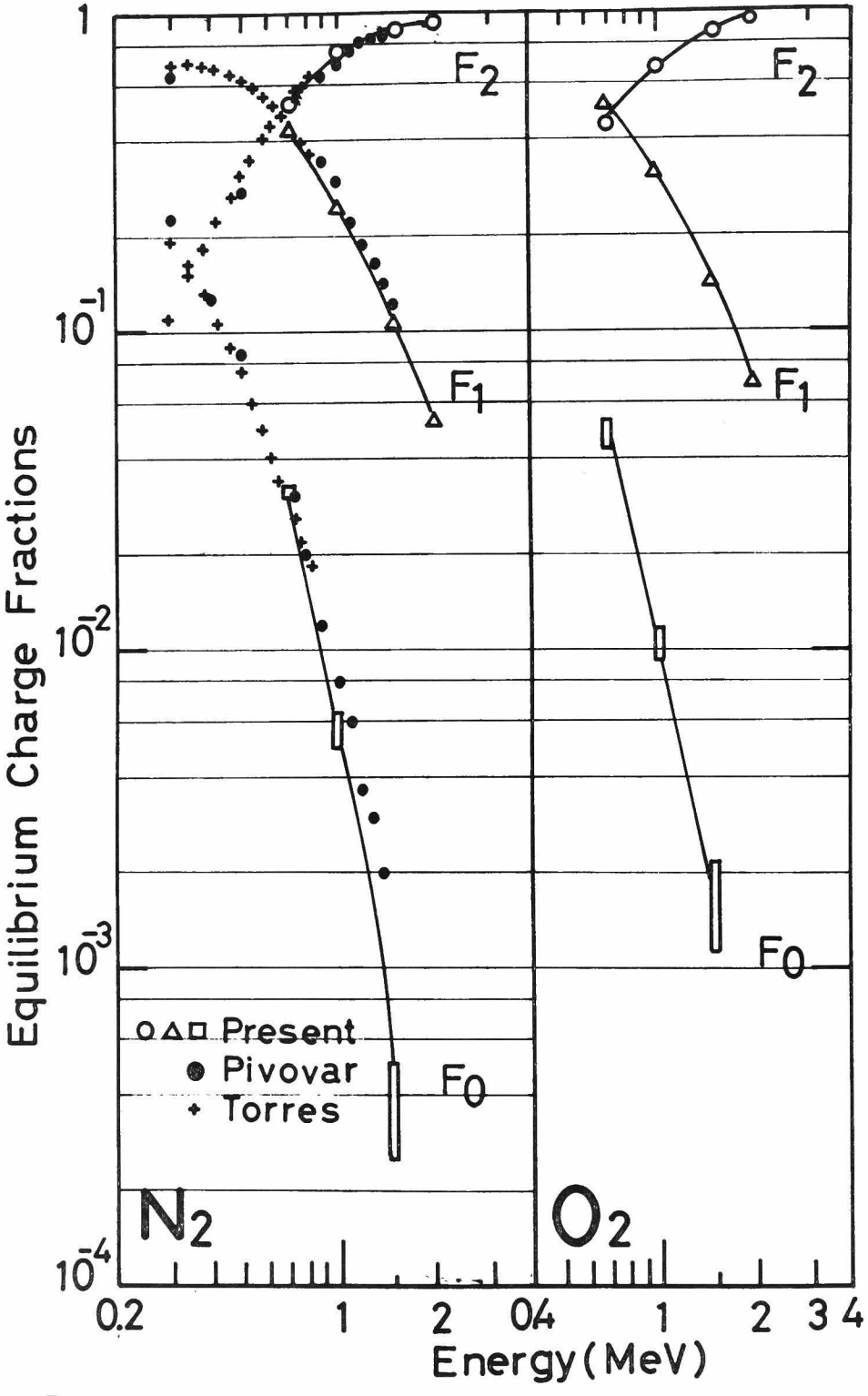
1
10^{-1}
10^{-2}
10^{-3}
10^{-4}
Equilibrium Charge Fractions
F_2
F_1
F_0
F_2
F_1
F_0
○△□ Present
● Pivovar
+ Torres
N_2
O_2
0.2
1
2
0.4
1
2
3
4
Energy (MeV)

FIG. 7-1(3)(4)

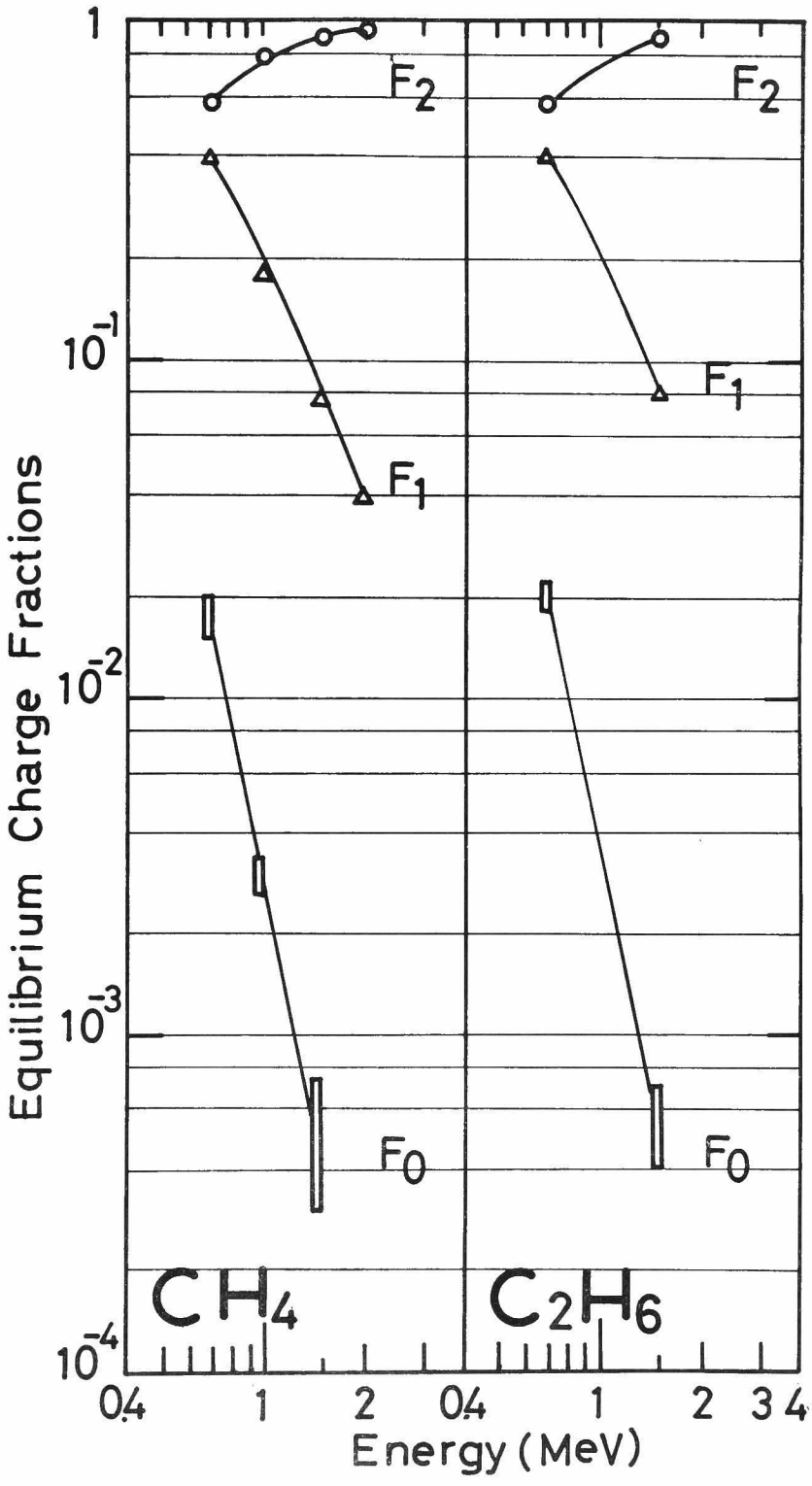
1
10^{-1}
10^{-2}
10^{-3}
10^{-4}
Equilibrium Charge Fractions
F_2
F_1
F_0
CH_4
C_2H_6
0.4
1
2
0.4
1
2
3
4
Energy (MeV)

FIG. 7-1(5)(6)

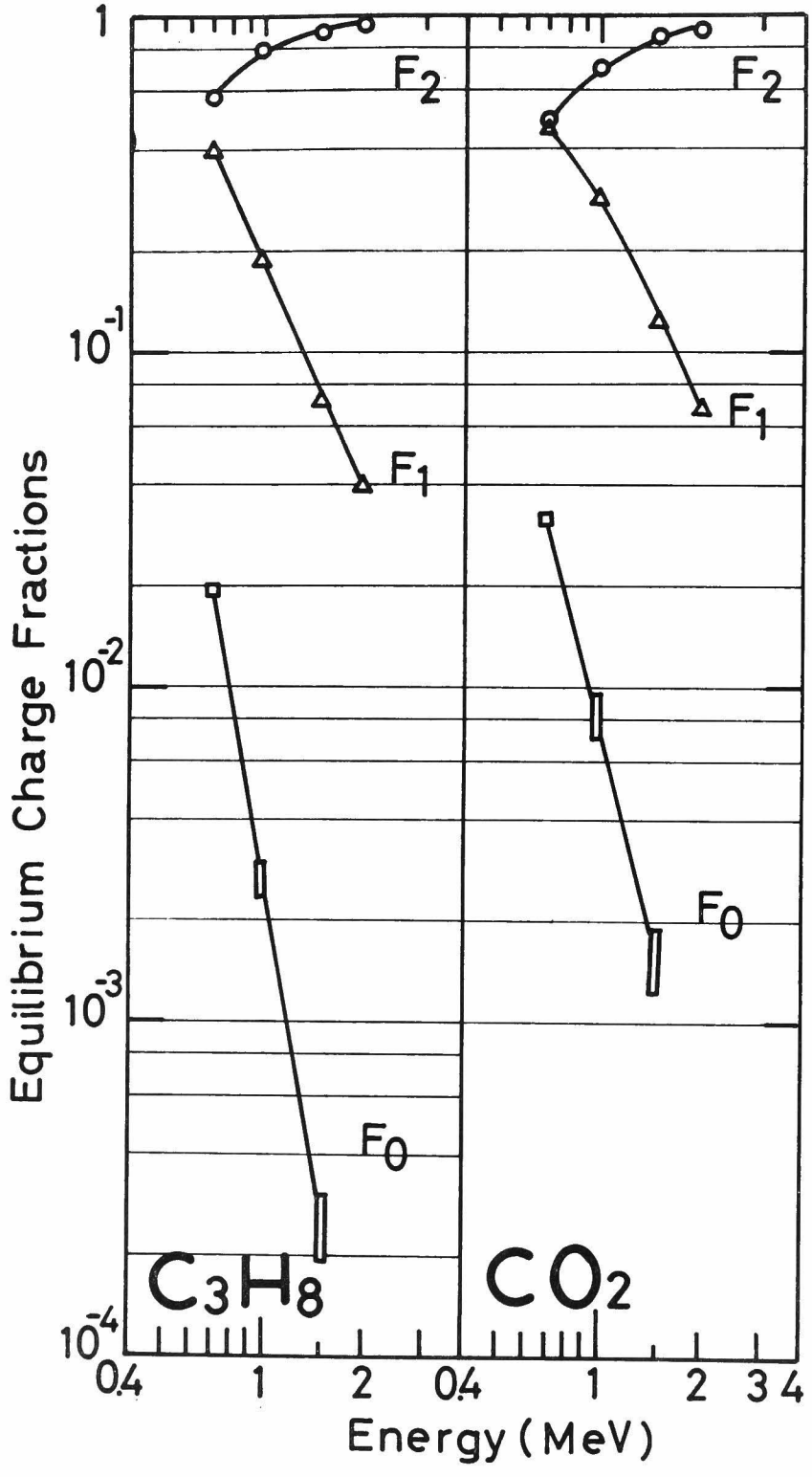
1
10^{-1}
10^{-2}
10^{-3}
10^{-4}
Equilibrium Charge Fractions
F_2
F_1
F_0
C_3H_8
CO_2
0.4
1
2
0.4
1
2
3
4
Energy (MeV)

FIG. 7-1(7)(8)

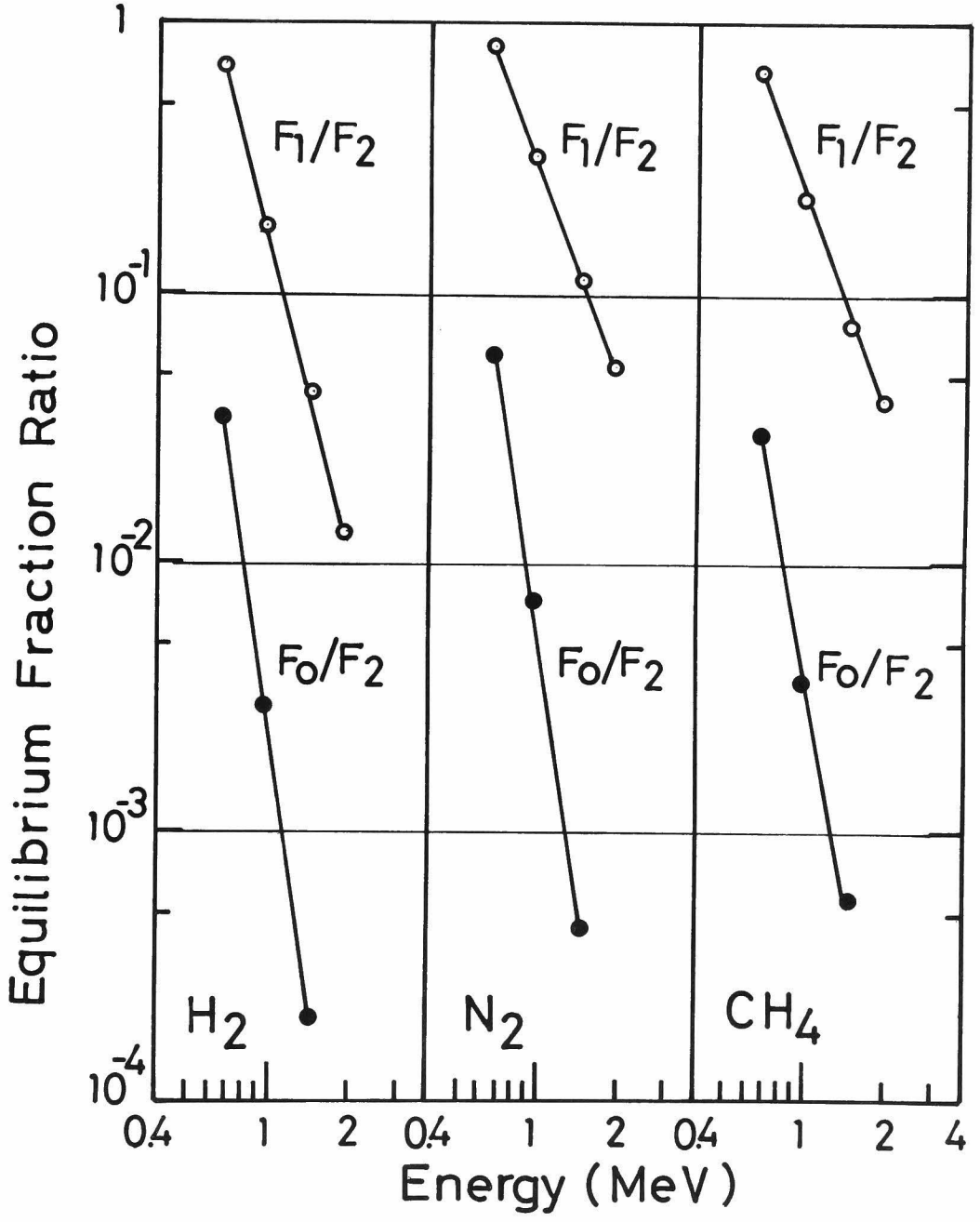
Equilibrium Fraction Ratio
1
10^{-1}
10^{-2}
10^{-3}
10^{-4}
F_1/F_2
F_0/F_2
H_2
N_2
CH_4
0.4
1
2
4
Energy (MeV)

FIG. 7-2

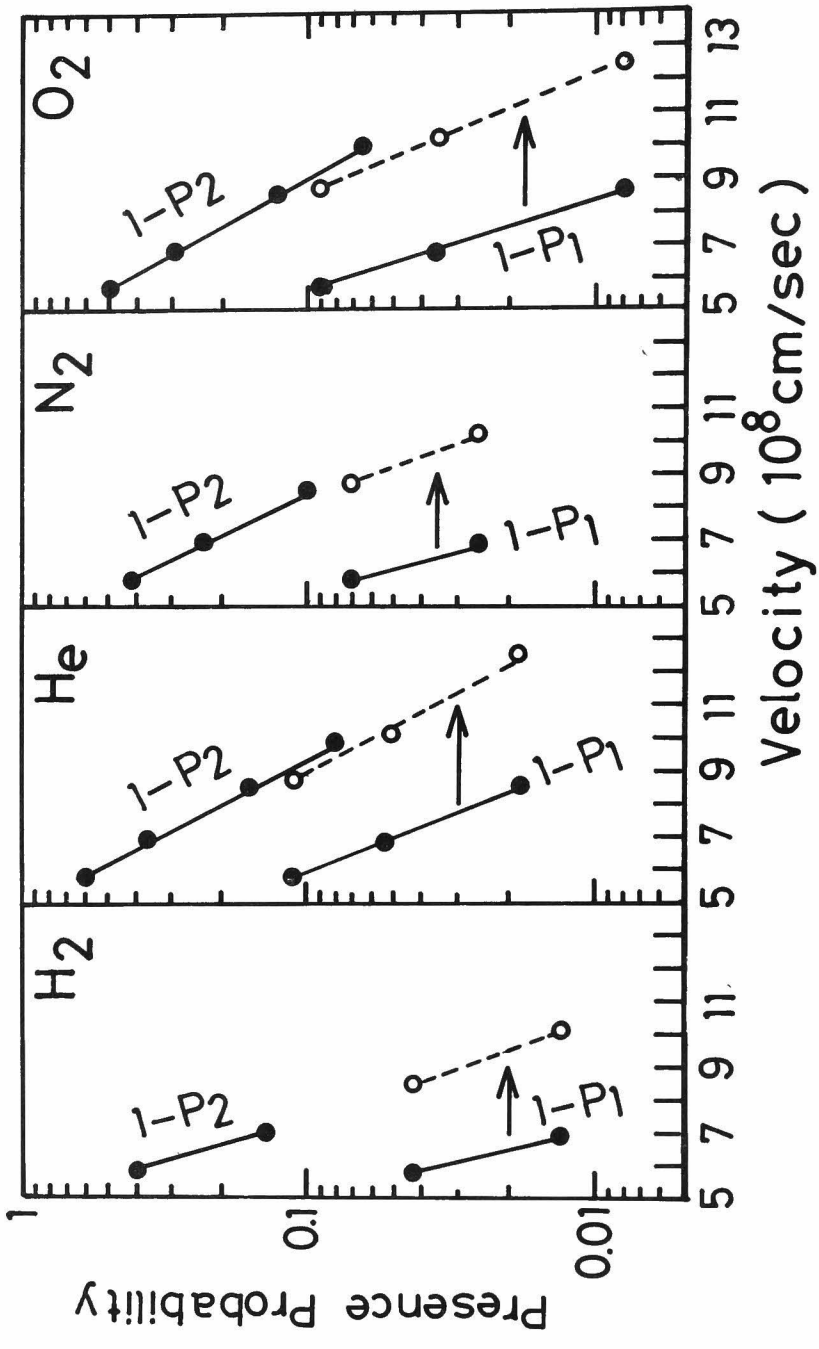
O2
N2
He
H2
1-P2
1-P1
Presence Probability
1
0.1
0.01
5 7 9 11 13
Velocity (10^8 cm/sec)

FIG. 7-3(1)(2)(3)(4)

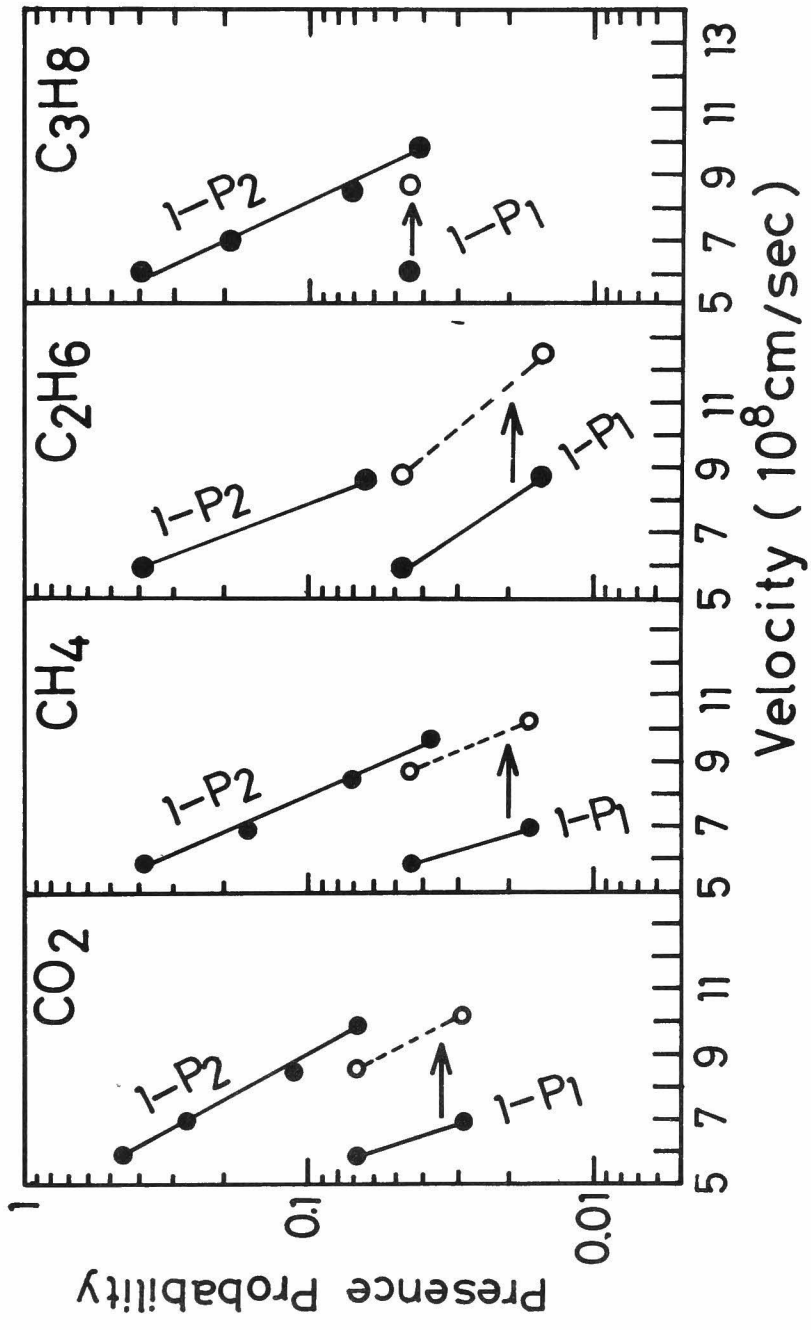
C3H8
C2H6
CH4
CO2
1-P2
1-P1
Presence Probability
1
0.1
0.01
5 7 9 11 5 7 9 11 13
Velocity (10^8cm/sec)

FIG. 7-3(5)(6)(7)(8)

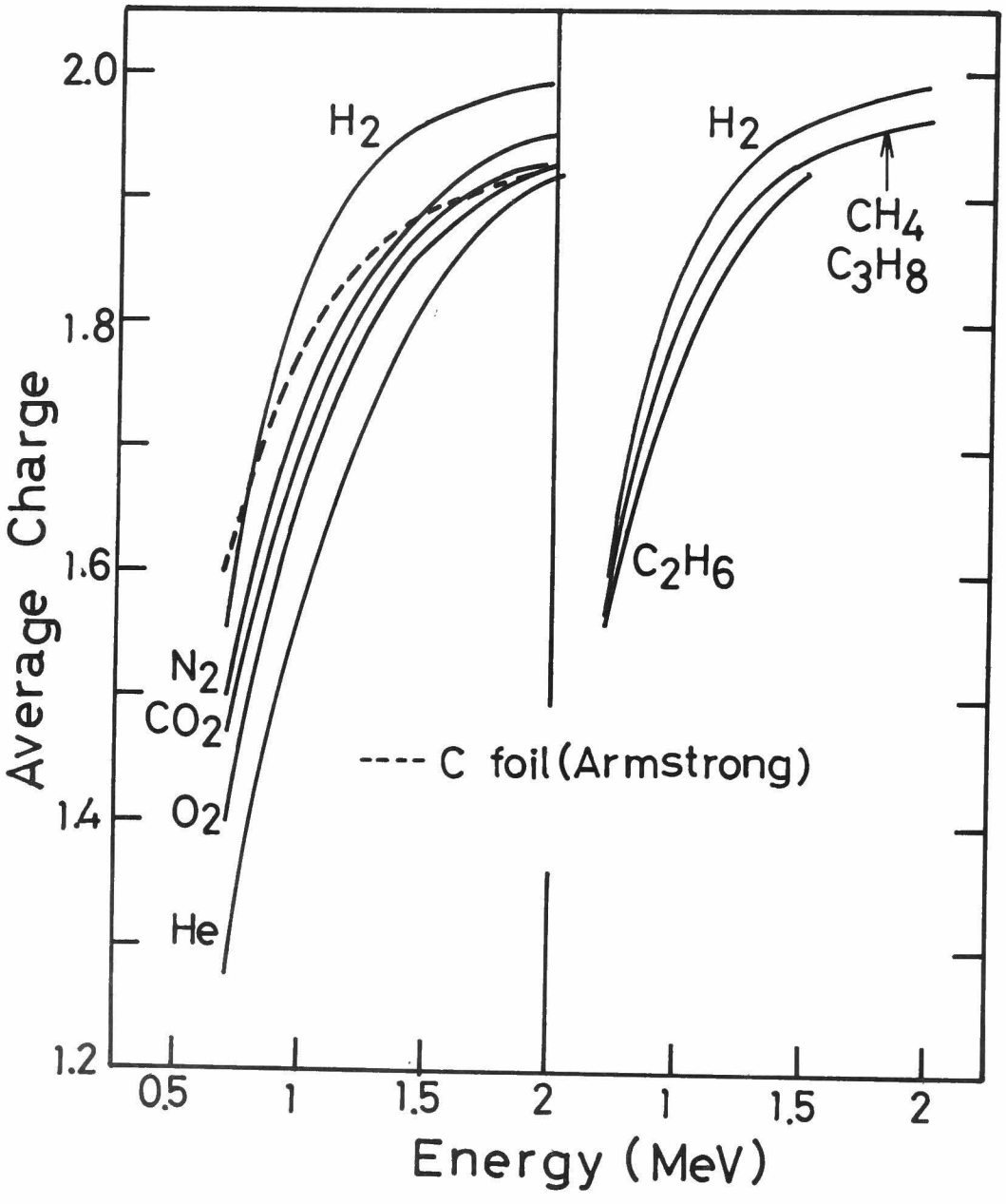
2.0
1.8
1.6
1.4
1.2
Average Charge
H2
H2
CH4
C3H8
C2H6
N2
CO2
O2
He
---- C foil (Armstrong)
0.5
1
1.5
2
1
1.5
2
Energy (MeV)

FIG. 7-4

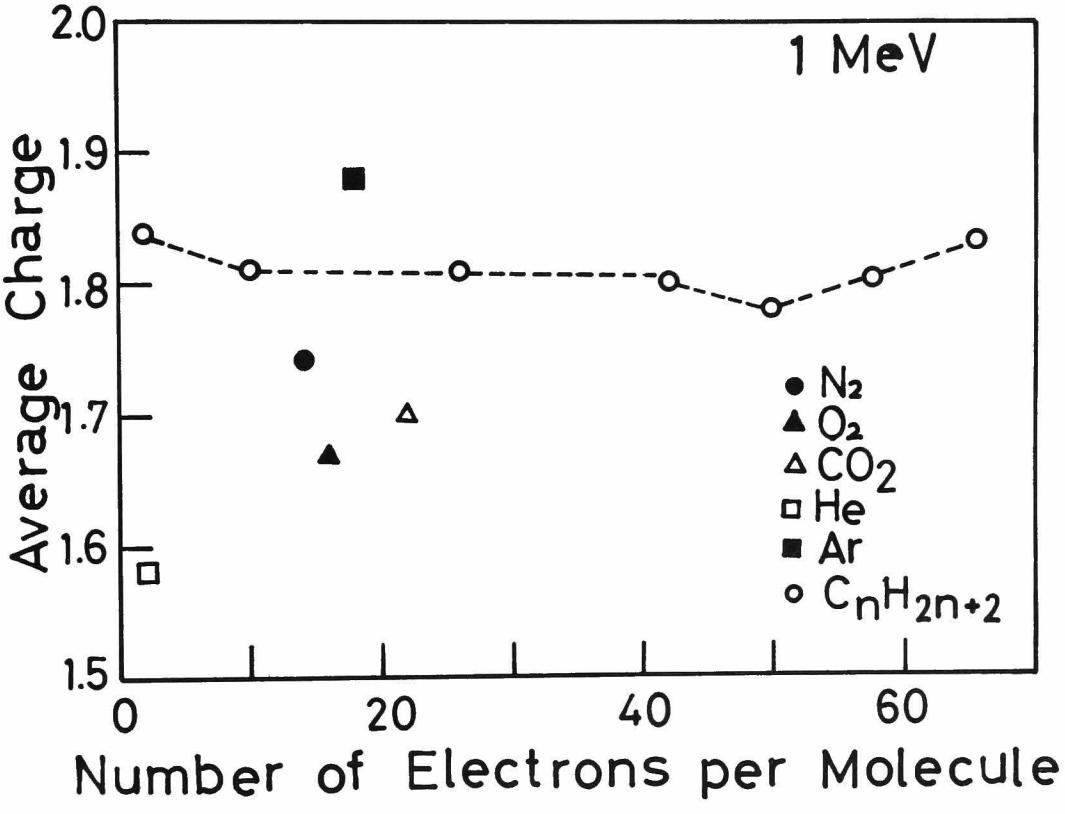
1 MeV
Average Charge
2.0
1.9
1.8
1.7
1.6
1.5
0
20
40
60
Number of Electrons per Molecule
N2
O2
CO2
He
Ar
CnH2n+2

FIG. 7-5

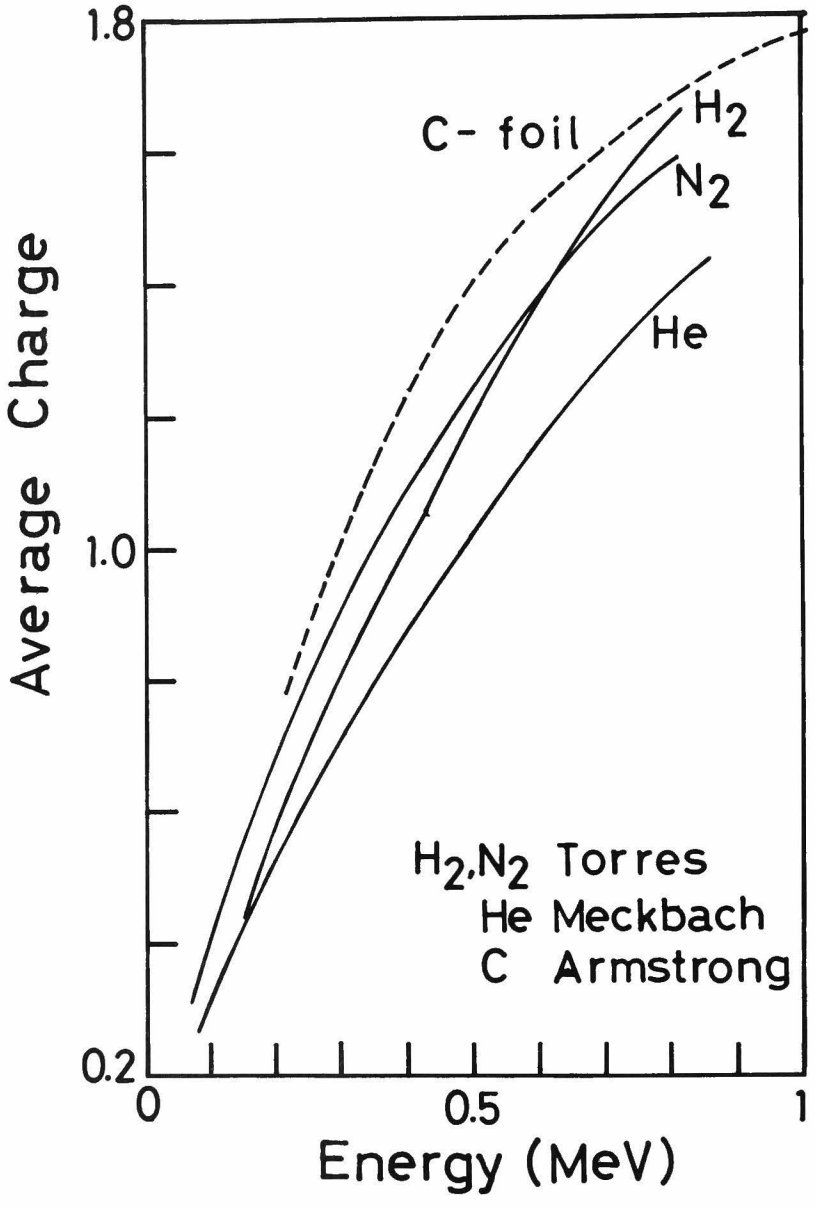
1.8
1.0
0.2
0
0.5
1
Average Charge
Energy (MeV)
C- foil
H_2
N_2
He
H_2,N_2 Torres
He Meckbach
C Armstrong

FIG. 7-6

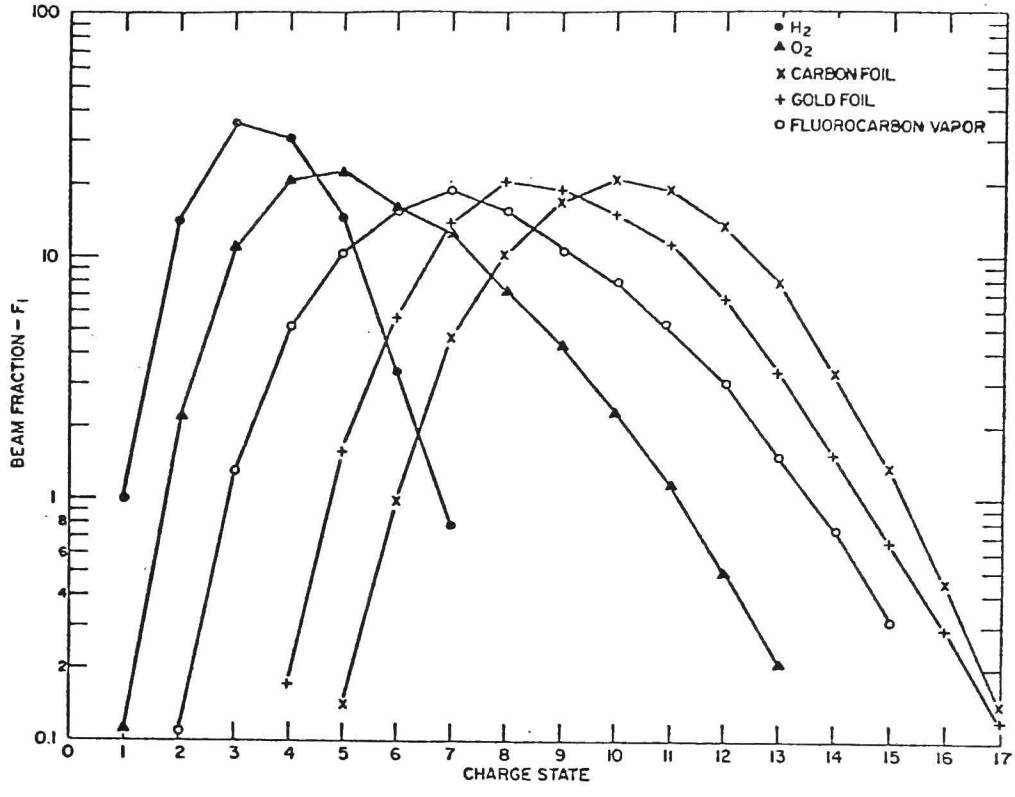
100
10
1
0.1
BEAM FRACTION - F_i
H_2
O_2
CARBON FOIL
GOLD FOIL
FLUOROCARBON VAPOR
0 1 2 3 4 5 6 7 8 9 10 11 12 13 14 15 16 17
CHARGE STATE

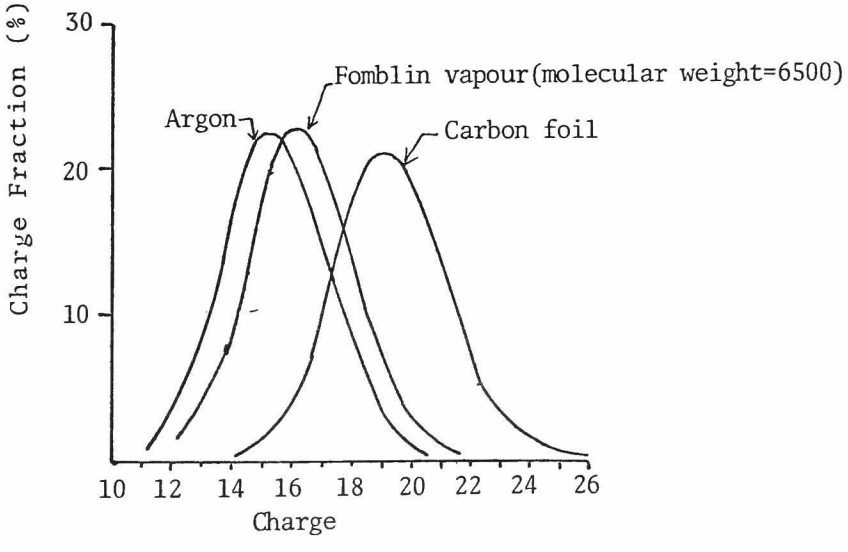
Charge Fraction (%)
30
20
10
Argon
Fomblin vapour(molecular weight=6500)
Carbon foil
10 12 14 16 18 20 22 24 26
Charge

FIG. 7-7

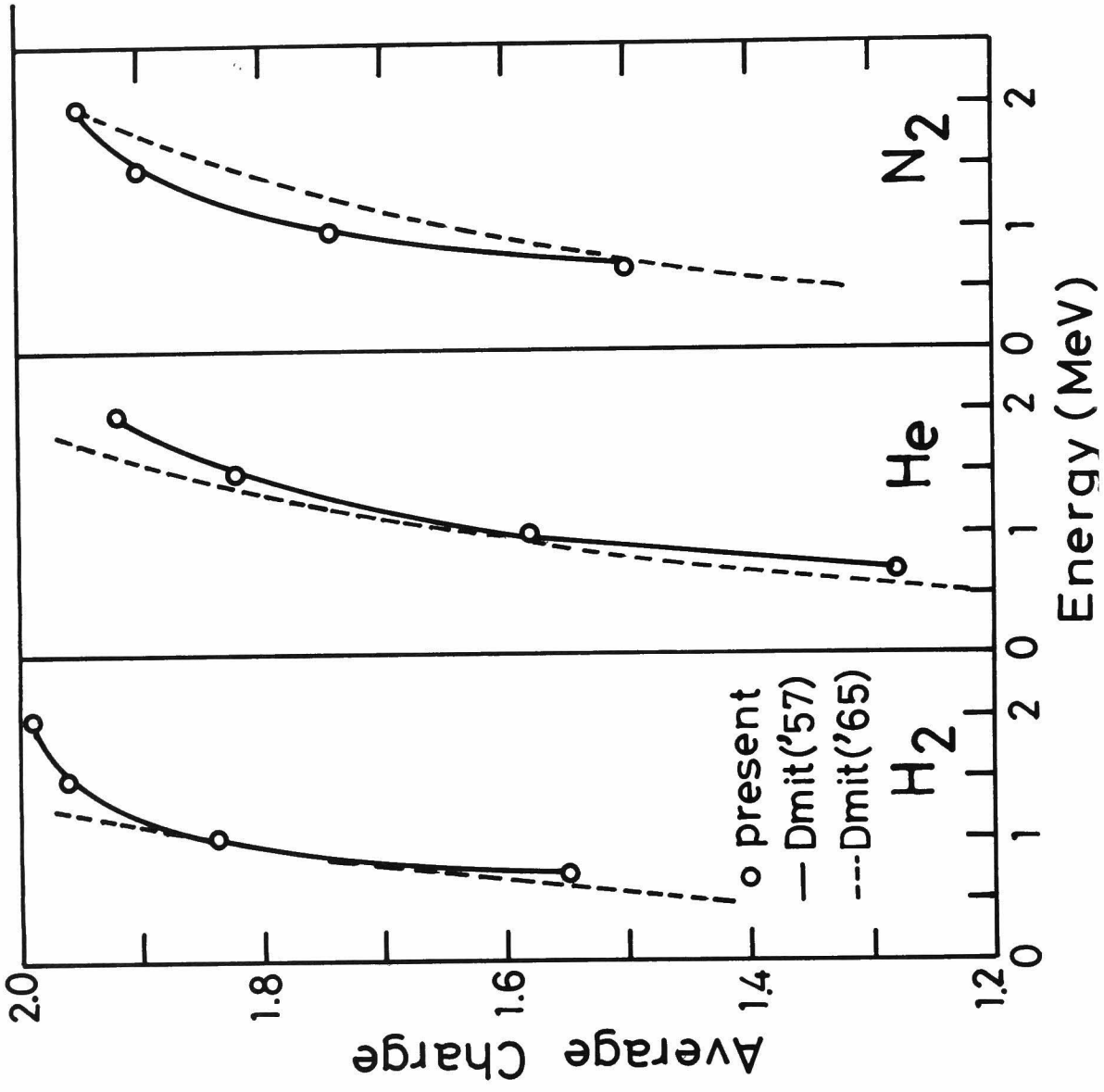
Average Charge
2.0
1.8
1.6
1.4
1.2
o present
— Dmit('57)
---Dmit('65)
H2
He
N2
0
1
2
0
1
2
Energy (MeV)

FIG. 7-8

```
FACOM (S)V/F4 FORTRAN IV (HE)  V04L12                DATE 79.06.27  TIME 16.55.29

                C      CALCULATION OF GROWTH CURVES OF 0.7 - 1.5 MEV HELIUM BEAM
                C      USING THE PRESENT EXPERIMENTALLY DETERMINED CROSS SECTIONS
                C      CALCULATION ARE MADE BY THE RUNGE-KUTTA METHOD
                C      INITIAL PRESSURE   1.00E-04  TORR.
                C      TARGET NUMBER 1 - 8 CORRESPONDS THE GASES OF HE,N,O,CO,CH4,C2H6,C3
ISN 00001              DIMENSION A(8,6),B(8,6),Y(10),E(10),Z(10),W(10),F1(10),F2(10),
                      1F3(10),F4(10),G1(10),G2(10),G3(10),G4(10)
ISN 00002              F(S,T)=-(A(I,1)+A(I,2)+A(I,5))*S+(A(I,3)-A(I,5))*T+A(I,5)
ISN 00003              G(P,6)=(A(I,1)-A(I,6))*P-(A(I,3)+A(I,4)+A(I,6))*6+A(I,6)
ISN 00004              READ(5,10)((A(I,J),J=1,6),I=1,8),((B(I,J),J=1,6),I=1,8)
ISN 00005           10 FORMAT(6E12.4)
ISN 00006           70 DO 300 I=1,8
ISN 00007              C=1.0-B(I,1)-B(I,2)
ISN 00008              B(I,2)=B(I,1)
ISN 00009              B(I,1)=C
ISN 00010              B(I,4)=1.0-B(I,3)-B(I,4)
ISN 00011              AA=0.0
ISN 00012              DO 700 J=1,6
ISN 00013              AA=AA+A(I,J)
ISN 00014          700 CONTINUE
ISN 00015              IF(AA-0.0)300,300,50
ISN 00016           50 X=1.0
ISN 00017              H=0.1
ISN 00018              DO 100 K=1,3
ISN 00019              Y(K)=B(I,2*K-1)
ISN 00020              Z(K)=B(I,2*K)
ISN 00021              W(K)=1.0-Y(K)-Z(K)
ISN 00022          100 CONTINUE
ISN 00023              WRITE(6,400)I,(A(I,J),J=1,6),(B(I,J),J=1,6)
ISN 00024          400 FORMAT(1H0,//,1H0,10HTARGET GAS,I4,10HINPUT DATA,/1H0,6E14.4,
                      1/,1H0,6E14.4//1H0,5X,1HX,10X,3HF00,10X,3HF01,10X,3HF02,10X,3HF10,
                      210X,3HF11,10X,3HF12,10X,3HF20,10X,3HF21,10X,3HF22,//)
ISN 00025              WRITE(6,500)X,(Y(K),Z(K),W(K),K=1,3)
```

```
ISN 00026            J=1
ISN 00027         20 E(J)=10.0**J
ISN 00028            IF(X-E(J))30,55,55
ISN 00029         55 J=J+1
ISN 00030            IF(J-5)11,300,300
ISN 00031         11 H=H*10.0
ISN 00032            GO TO 20
ISN 00033         30 DO 150 II=1,5
ISN 00034            DO 200 K=1,3
ISN 00035            F1(K)=H*F(Y(K),Z(K))
ISN 00036            F2(K)=H*F(Y(K)+F1(K)/2.0,Z(K)+G1(K)/2.0)
ISN 00037            F3(K)=H*F(Y(K)+F2(K)/2.0,Z(K)+G2(K)/2.0)
ISN 00038            F4(K)=H*F(Y(K)+F3(K),Z(K)+G3(K))
ISN 00039            G1(K)=H*G(Y(K),Z(K))
ISN 00040            G2(K)=H*G(Y(K)+F1(K)/2.0,Z(K)+G1(K)/2.0)
ISN 00041            G3(K)=H*G(Y(K)+F2(K)/2.0,Z(K)+G2(K)/2.0)
ISN 00042            G4(K)=H*G(Y(K)+F3(K),Z(K)+G3(K))
ISN 00043            Y(K)=Y(K)+(F1(K)+2.0*F2(K)+2.0*F3(K)+F4(K))/6.0
ISN 00044            Z(K)=Z(K)+(G1(K)+2.0*G2(K)+2.0*G3(K)+G4(K))/6.0
ISN 00045            W(K)=1.0-Y(K)-Z(K)
ISN 00046        200 CONTINUE
ISN 00047            X=X+H
ISN 00048        150 CONTINUE
ISN 00049            WRITE(6,500)X,(Y(K),Z(K),W(K),K=1,3)
ISN 00050            GO TO 20
ISN 00051        500 FORMAT(1HO,10E13.4)
ISN 00052        300 CONTINUE
ISN 00053        350 STOP
ISN 00054            END
```